UC San Diego
UC San Diego Electronic Theses and Dissertations

Title

Conjugated Tri-Pi Systems: Investigations into Hexahapto Metal Complexes of Acyclic Conjugated Trienes and Novel Cycloaromatization Reactions of Nitrogen-Containing Enediynes

Permalink

https://escholarship.org/uc/item/6s68j5n1

Author

Veccharelli, Kate

Publication Date

2017

Peer reviewed|Thesis/dissertation

UNIVERSITY OF CALIFORNIA, SAN DIEGO

Conjugated Tri-Pi Systems: Investigations into Hexahapto Metal Complexes of Acyclic
Conjugated Trienes and Novel Cycloaromatization Reactions of Nitrogen-Containing Enediynes

A dissertation submitted in partial satisfaction of the requirements for the degree Doctor of
Philosophy

in

Chemistry

by

Kate Marie Veccharelli

Committee in charge:

       Professor Joseph M. O'Connor, Chair
       Professor Neal Devaraj
       Professor Charles Perrin
       Professor Jan Talbot
       Professor Yitzak Tor

2017

The Dissertation of Kate Marie Veccharelli is approved, and it is acceptable in quality and form

for publication on microfilm and electronically:

_____

_____

_____

_____

_____

Chair

University of California, San Diego

2017

DEDICATION

This dissertation is dedicated to my husband Patrick.

TABLE OF CONTENTS

Chapter 1. Introduction and Overview of Tri-π-Systems: Facilitating Electrocyclization

Reactions Through Thermal and Metal-Mediated Pathways…………………………1

LIST OF FIGURES

xi

LIST OF TABLES

LIST OF SCHEMES

Chemical Abbreviations

(- indicates covalent substituent)

B: general base

1,4-CHD: 1,4- cyclohexadiene

-^{n}Bu: *n*-butyl, -$CH_2(CH_2)_2CH_3$

-^{t}Bu: *t*-butyl, -$C(CH_3)_3$

Cp: cyclopentadienyl

Cp*: pentamethylcyclopentadienyl

CSA: camphorsulfonic acid

D/ -d: deuterium

DCM: dichloromethane

DMF: N,N-dimethylformamide

-Et: ethyl, -CH_2CH_3

IPA: isopropyl alcohol

L: metal ligand (e.g. AuL)

-Me: methyl, -CH_3

MeCN: acetonitrile

-OAc: acetate, -$OC(O)CH_3$

-OTf: triflate, -$OS(O)_2CF_3$

-Ph: phenyl, -C_6H_5

-nPr: *n*-propyl, -$CH_2CH_2CH_3$

THF: tetrahydrofuran

-TMS: trimethylsilyl

Experimental/ Spectroscopic

$\Delta G°_{rxn}$: standard reaction energy

δ: chemical shift

η^x: x atoms π bound to metal

λ: wavelength

A: conformational energy

APCI: atmospheric pressure chemical

ionization

COSY: correlation spectroscopy

d: doublet

DR: diastereomeric ratio

ESI: electrospray ionization

FT-IR: fourier transform infrared

spectroscopy

hν: ultraviolent radiation

HMBC: heteronuclear multiple-bond

correlation spectroscopy

HMQC: heteronuclear multiplequantum

correlation spectroscopy

HRMS: high resolution mass spectrometry

J: coupling constant

KIE: kinetic isotope effect

m: multiplet

NMR: nuclear magnetic resonance

spectroscopy

p: pentet

q: quartet

RDS: rate determining step

rt: room temperature

s: singlet

t: triplet

TLC: thin layer chromatography

TOF: time of flight

UV: ultraviolet radiation

Parameter Units

(*Conventional SI prefixes were used*)

Å: Angstrom

°C: degree Celsius

h: hour

Hz: Hertzal: calorie

cm-1: wavenumber

eV: electron volt

K: Kelvin

L: liter

M: molar

m: meter

min: minute

mol: mole

ppm: parts per million

s: second

Torr: millimeter of mercury

ACKNOWLEDGEMENTS

First and foremost, I would like to give tremendous thanks to my PhD advisor and mentor Joseph O'Connor, for his instruction and guidance. Joe was an absolute joy to work for and I am forever grateful for him allowing me the freedom to develop into an independent scientist in his laboratory. Joe pushed me when I needed to be pushed and his door was always open to me as I navigated through the trials of my PhD. I would also like to thank my thesis committee: Dr. Neal Devaraj, Dr. Yitzhak Tor, Dr. Jan Talbot and especially Dr. Charles Perrin. Dr. Perrin has been like a second mentor to me and I am forever grateful for his insightful discussions, pointed questions and suggestions in addition to his support throughout my studies here at UCSD. Secondly, I am very appreciative to all of the members of the O'Connor lab past and present: Marissa Aubrey, Stephen Cope, Ryan Holland, Christina Hoong, Pengjin Qin, Han Steger and Pauline Olsen. Thank you for all your guidance, scientific insight, support and most importantly friendship. You all have become like a second family to me.

Thirdly, I would like to take this opportunity to thank all my undergraduate chemistry professors at Western Connecticut State University who were very influential in my decision to pursue a PhD. Many thanks to my undergraduate advisor, Dr. Russ Selzer for the opportunity to work in his lab and gain valuable research experience.

The work presented in this dissertation would not have been possible without the expertise of many individuals across multiple UCSD facilities. I would like to take a moment and thank Dr. Arnold Rheingold, Dr. Curtis Moore and Dr. Milan Gembicky of the UCSD X-Ray Crystallography Facility who acquired all of my X-ray data. Dr. Yongxuan Su of the Mass Spectrometry Facility, who ran countless HRMS for me. Dr. Anthony Mrse of the NMR facility,

who assisted with acquiring data for specialized NMR experiments. I would also like give thanks Norm Olsen in the TEM facility for training me on the TEM.

Next, I would like to thank my friends for supporting me through graduate school. Hope Lipper, Nikki Foote, Michelle Lacoske, Don Johnson, Noelle Johnson, Amelia Ray, Jessica McKay, Libby Webber, Pauline Olsen, Adam Kallel, Jen Michaud, Leo Gallo, Allison Czapracki and Erica Bender. Thank you for keeping me sane though this experience, cheering me on when I wanted to throw in the towel and making graduate school fun.

Last but not least, I would like to express gratitude to my family. My parents Candie and Peter Veccharelli for raising me to be a kind, hardworking and caring person. They have always loved me unconditionally, supported me (even when I wanted to move across the country for graduate school) and have always believed that I could accomplish anything I set my mind to. I would like to thank my brother Dan Veccharelli for sending me cute pictures of my nephews and always making me laugh. A big thank you to my parents-in-law Nancy and John Johnson for their support, love and laughter. I truly feel like I have two sets of parents now. Lastly, I would like to give a very special thanks to the most important person in my life, my husband Patrick Johnson. Patrick has been my anchor through this graduate school experience. He has been there for me through all the ups and downs and I could not have done it without his love and support. I cannot show him enough gratitude for loving me, standing by me and supporting me.

Notes about chapters: Chapter 2, in part, is based on material which appears in "Hexahapto Metal Complexes of Acyclic Conjugated Trienes" O'Connor, J. M.; Baldridge, K. K.; Veccharelli, K. M.; Cope, S.K.; Holland, R.L.; Qin, P., Rheingold, A. L. *Submitted*. The dissertation author is a co-author on this paper.

Chapter 3, contains material which appears in "Enediyne Cycloaromatization with Incorporation of Chlorine from Chloroform and Hydrogen from 1,4-Cyclohexadiene" Qin, P.; O'Connor, J. M.; Baldridge, K. K.; Hitt, D. M.; Cope, S. K.; Veccharelli, K. M.; Holland, R. L.; Raub, A. *In Preparation*. The dissertation author is a co-author on this paper.

Chapter 4, is a full reprint of the publication "Dual Responsive Polymeric Nanoparticles Prepared by Direct Functionalization of Polylactic Acid-based Polymers via Graft-from Ring Opening Metathesis Polymerization" Veccharelli, K. M.; Tong, V. K.; Young, J. L.; Yang, J. Gianneschi, N. C. *Chem. Commun*., **2016**, 52, 567. The dissertation author was the primary investigator and author of this material.

CURRICULUM VITA

2010   Western Connecticut State University, Bachelors of Arts, Chemistry

2013   University of California, San Diego, Master of Science, Chemistry
         Chemistry

2017   University of California, San Diego, Doctor of Philosophy, Chemistry
         Advisor, Professor Joseph M. O'Connor
         Dissertation title: Conjugated Tri-Pi Systems: Investigations into Hexahapto
         Metal Complexes of Acyclic Conjugated Trienes and Thermal Reactions of
         Nitrogen Containing Enedyines

PUBLICATIONS

O'Connor, J. M.; Baldridge, K. K.; **Veccharelli, K. M**.; Cope, S.K.; Holland, R.L.; Qin, P., Rheingold, A. L.; "Hexahapto Metal Complexes of Acyclic Conjugated Trienes" 2017, *manuscript submitted*.

Qin, P.; O'Connor, J. M.; Baldridge, K. K.; Hitt, D. M.; Cope, S. K.; **Veccharelli, K. M**.; Holland, R. L.; Raub, A.; "Enediyne Cycloaromatization with Incorporation of Chlorine from Chloroform and Hydrogen from 1,4-Cyclohexadiene" **2017**, *manuscript submitted*.

Qin, P.; Cope, S. K.; Steger, H.; **Veccharelli, K. M**.; Holland, R. L.; Hitt, D. M,; Moore, C. E.; Baldride, K. K.; O'Connor, J. M.; "Photoactivated Transition-Metal Triggers for Ambient Temperature Enediyne and Dienyne Cyclization: Ruthenium-η^6 -Naphthalene Complexes" *Organometallics* **2017**, *36*, 3967-3973

Veccharelli, K. M.; Tong, V. K.; Young, J. L.; Yang, J. Gianneschi, N. C.; "Dual Responsive Polymeric Nanoparticles Prepared by Direct Functionalization of Polylactic Acid-based Polymers via Graft-from Ring Opening Metathesis Polymerization" *Chem. Commun*., **2016**, *52*, 567

ABSTRACT OF THE DISSERTATION

Conjugated Tri-Pi Systems: Investigations into Hexahapto Metal Complexes of Acyclic

Conjugated Trienes and Novel Cycloaromatization Reactions of Nitrogen-Containing Enediynes

by

Kate Marie Veccharelli

Doctor of Philosophy in Chemistry

University of California, San Diego, 2017

Professor Joseph M. O'Connor, Chair

The work contained within this thesis represents contributions to our understanding of ruthenium-mediated cycloaromatization reactions of trienes and novel cycloaromatization reactions of nitrogen-containing enediynes. Previous work done in the O'Connor lab demonstrated room temperature cyclizations of enediynes and dienynes via proposed hexahapto metal coordination. Preliminary calculations suggest that η^6-metal complexation to the π system lowers the activation energy for cyclization. The mechanistic hypothesis for this transformation involves η^6-metal complexation to the triene system, followed by a 6π electrocyclization.

The first η^6-acyclic conjugated triene ruthenium complex was successfully synthesized by the reaction of [CpRu(NCMe)$_3$]PF$_6$ with an (*E,E*) diphenyl-substituted 1,2-divinylcyclopentene

derivative. The presence of phenyl substituents is thought to inhibit the metal-mediated disrotatory ring closure of the triene due to steric congestion. This complex was further characterized by exploring electronic effects of para-substituted phenyl substituents on the overall geometry. More specifically, electronic effects were examined by hexahapto metal complexation to 1,2-bis((E)-4-(trifluoromethyl)styryl)cyclopentene and 1,2-bis((E)-4-methoxystyryl)cyclopentene. The more electron-deficient η^6-triene ruthenium complex adopted an *s-cis/s-cis* conformation, as determined by X-ray crystallographic analysis. The more electron-rich η^6-triene ruthenium complex adopted both *s-cis/s-cis* and s-*cis/s-trans* conformations in a 3:1 ratio. Additional analysis of this ratio by cold-probe variable temperature ^{1}H NMR spectroscopy confirms that the two isomers exists in equilibrium at room temperature. The relative stabilities of these diastereomeric complexes were examined by a time course migration study where the migration of ruthenium from (η^5-cyclopentadienyl)(η^6-1,2-bis((E)-4-(trifluoromethyl)styryl)cyclopentene) ruthenium(II) hexafluorophosphate to 2-bis((E)-4-methoxystyryl)cyclopentene was monitored by ^{1}H NMR spectroscopy. Based on the final ratio of isomers, it was estimated that the more electron-rich ruthenium complex is > -4.0 kcal/mol more stable than the electron-deficient η^6-triene ruthenium complex.

Finally, a recently discovered thermal cyclization of enediynes was extended to include pyridine-based enediynes. Thermolysis of 2-(1-pentynyl)-3-(1-propynyl)pyridine in CDX$_3$ (X = Br, I) and 1,4-cyclohexadiene led to the regioselective formation of 5-halo-6-methyl-7-propylquinoline derivatives. Halogen connectivity was established via HMBC and NOE NMR spectroscopic analysis. The cyclization is proposed to involve a key diene intermediate, (E)-3-(1-halo-1-propenyl)-2-(1-pentynyl)pyridine, which may form by one or both of the following mechanisms. The first mechanism involves addition of HX to the alkyne (X = Br, I). The hydrogen

halide is proposed to form *in situ* from the reaction of 1,4-cyclohexadiene with CDX_3 (X = Br, I) to form HX, $CDHX_2$, and benzene. In the second mechanism, the diene intermediate is proposed to form through free radical addition of a hydrogen atom from the cyclohexadienyl radical to an alkyne to give a dienyne radical, followed by abstraction of a halogen atom from CDX_3 to produce the halo-dienyne intermediate. This key dienyne intermediate is then proposed to undergo a Hopf-type cyclization to yield the halogenated aromatic product.

Chapter 1.

**Introduction and Overview of Tri-π-Systems: Facilitating Electrocyclization Reactions
Through Thermal and Metal-Mediated Pathways**

A. Introduction to Tri-π Systems

Cycloaromatization reactions allow for the construct of substituted arenes through thermal transformations of polyunsaturated systems. Herein we define the subset of polyunsaturated molecules that contain three conjugated multiple bonds within an acyclic framework as tri-π molecules. Widely encountered examples of tri-π molecules that undergo cycloaromatization reactions include: enediynes (**1**), dienynes (**2**) and trienes (**3**; Figure 1.1). Each of these substrates involve unique and fascinating mechanisms for the formation of arenes. However, one major limitation that has been observed with the tri-π cycloaromatization reactions is the high activation barrier required for these reactions to proceed; thus, these reactions are limited in their usefulness. The major goal of the work presented in this dissertation is: (A) to demonstrate the feasibility of accelerating 6π electrocyclizations via the intermediacy of late-metal η^6 tri-π complexes, and (B) investigations into novel thermal transformations of nitrogen-containing enediynes.

1   **2**   **3**
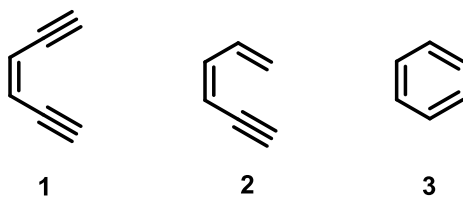
Figure 1.1. Representative tri-π systems.

B. Concerted Electrocyclization Reactions

Concerted electrocyclization reactions provided the foundation for Woodward and Hoffmann's principle of conservation of orbital symmetry which utilizes the concepts of molecular orbital theory to rationalize and predict stereochemical outcomes of concerted reactions.[1] Electrocyclization reactions are one of the most powerful synthetic tools in the chemist's toolbox.

These reactions exhibit predictable regioselectivity and stereoselectivity in the construction of many structurally complex natural products (Figure 1.2).[2]

Cinanthrenol A

Salvileucalin C

Thiaplidiaquinone A

Dictyodendrin F
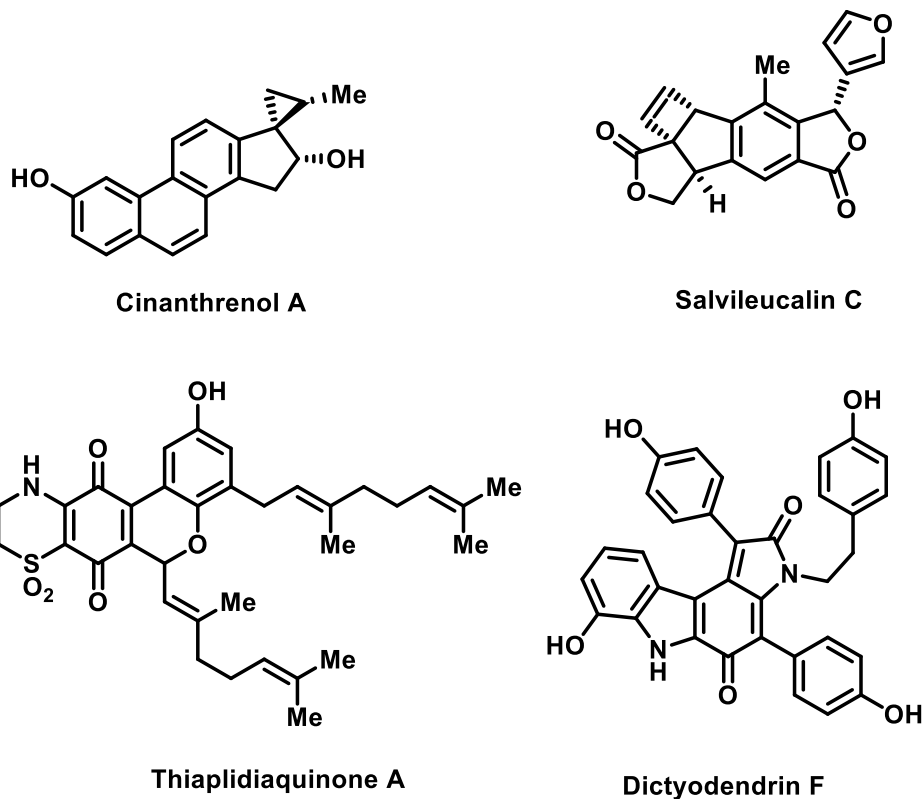
Figure 1.2. Selected examples of natural products synthesized via electrocyclization reactions.[2]

In a thermal system consisting of 4n π electrons, the orbital symmetry of the highest occupied molecular orbital (HOMO), is such that a bonding interaction between the termini will proceed through a conrotatory process so that the orbitals on opposite faces of the system will overlap constructively (Figure 1.3). Comparing the HOMO of the thermal system containing 4n + 2 π electrons, the orbitals on the same face of the system will have to interact. Thus, the termini must proceed through a disrotatory motion for constructive overlap. Lastly, in photochemical reactions, an electron from the HOMO is promoted to the lowest unoccupied molecular orbital

(LUMO), which leads to a reversal of terminal symmetry relationships and a reversal of stereospecificity of pericyclic reactions (Figure 1.4 and Scheme 1.1).[1]

HOMO   LUMO

4n π systems

conrotatory   disrotatory

4n +2 π systems

disrotatory   conrotatory
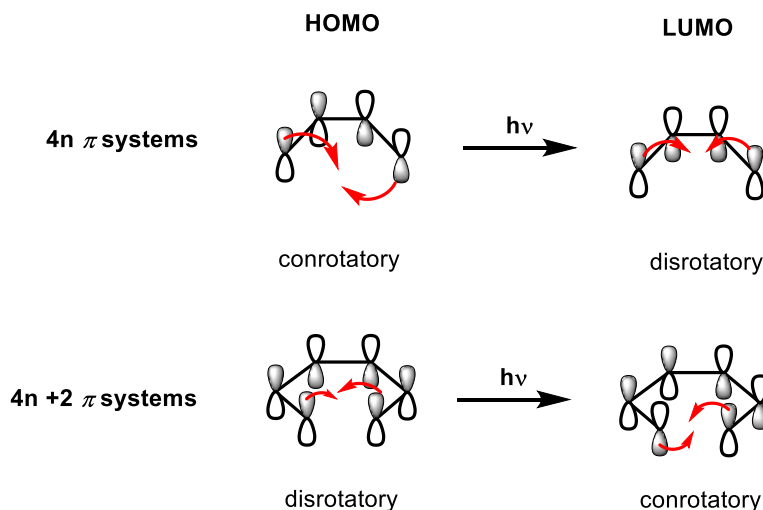
Figure 1.3. Woodward-Hoffman rules under thermal (left) and photochemical (right) conditions.
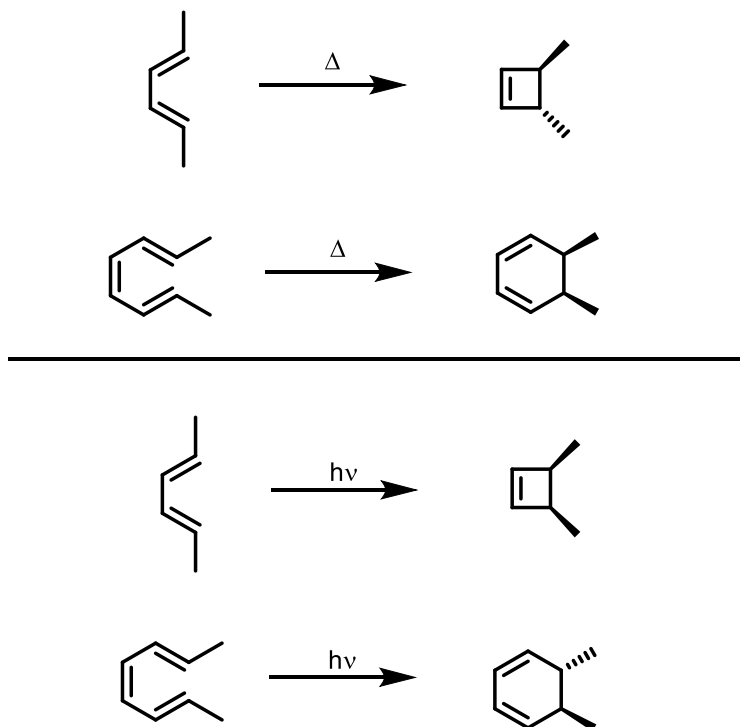
Scheme 1.1. Stereochemical electrocyclization outcomes under thermal (top) and photochemical (bottom) conditions as predicted by orbital symmetry conservation.

Interest in catalytic triene electrocyclizations began in the late 1960s, [3–5] however, it took over 40 years for Bergman and Trauner to report the first catalytic 6π electrocyclization of conjugated trienes with Lewis acids.[6] Utilizing density functional theory (DFT) calculations they were able to predict reaction conditions for successful catalysis and confirmed their predictions via experimental analysis.

Electron withdrawing groups located in the 2-postiton of a hexatriene system had been observed previously to lower electrocyclization barriers by 10 kcal/mol.[7] Thus, Bergman and Trauner reasoned that they could exploit this effect to catalyze 6π electrocyclization reactions by coordination of a Lewis acid catalyst to a Lewis basic electron-withdrawing group located on the 2-position of a hexatriene system. They hypothesized that the coordination of the Lewis acid should increase the electron-withdrawing effect of the substituent and thereby decrease the activation energy barrier to cyclized products.

They began their studies by calculating the reaction energies of hexatriene systems with a methyl ester substituent located at all possible positions and orientations. They chose a proton to serve as the simplest Lewis acid to bind to the carbonyl oxygen. As predicted, the system with the protonated ester in the 2-position had the lowest activation barrier of only 14 kcal/mol, which is 10 kcal/mol less than the unprotonated version.
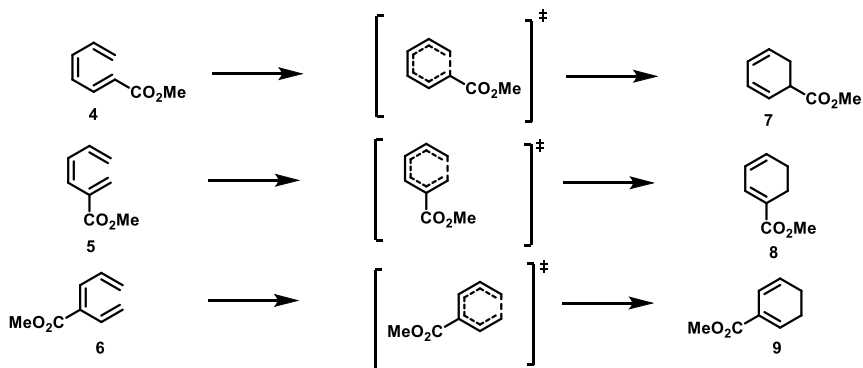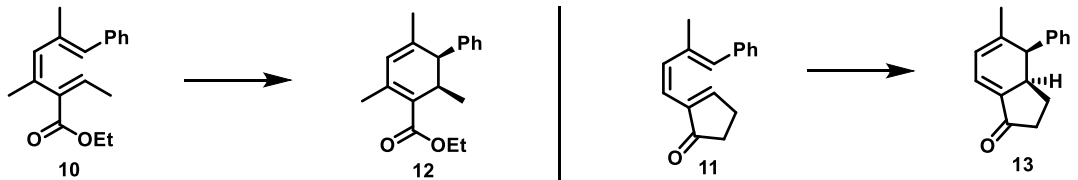
Scheme 1.2. Trienes studied computationally by Bergman and Trauner at the B3LYP/6-31G** level of theory.[6]

Table 1.1. Relative energies of the thermal electrocyclization (protonated carbonyl energies)*

Compound	EA (kcal/mol)	Product	$\Delta\Delta E^{\ddagger}$
4	31 (35)	-6 (9)	4
5	24 (14)	-20 (-29)	-10
6	26 (24)	-5 (-17)	-2

* In kcal mol calculated at the B3LYP/6-31G** level of theory.

After computational analysis, Bergman and Trauner synthesized trienes **10** and **11** and found that the rates of cyclization to products **12** and **13** were increased in the presence of the Lewis acid, Me$_2$AlCl. They observed that the reaction is catalytic and first order in both the Lewis acid and substrate. They also reported the Gibbs free energy of activation is 1.7 kcal/mol lower than the thermal pathway of **10** and 2.4 kcal/mol lower than the thermal pathway of **11** (Table 1.2.).

Table 1.2. Activation Parameters of the thermal and catalyzed electrocylizations.

Compound	ΔG thermal (kcal/mol)	ΔG catalyzed (kcal/mol)
10	25.2(5)	23.5(2)
11	24.0(5)	21.6(1)

C. Forbidden to Allowed Pericyclic Reactions by Complexation of Transition Metals

After Woodward and Hoffman published their rules of conservation of orbital symmetry, there have been reports in the literature reporting the reverse stereoselectivity of pericyclic reactions when the substrates are coordinated to transition metals.[3] In 1975, Mango published a set of selection rules on when the forbidden-to-allowed transformations could occur. In order to

catalyze the forbidden-to-allowed reaction path process, ideally the bonds of the substrate are fully coordinated to the metal and retain full coordination throughout the entire pericyclic process.[3]

One of the most studied metal-mediated electrocyclization reaction is the ring-opening of cyclobutene coordinated to $Fe(CO)_3$.[8–12] In the absence of metal coordination, this reaction proceeds in a symmetry-allowed, conrotatory fashion. However, the observed mode of ring opening for strained cyclobutenes upon $Fe(CO)_3$ coordination is through a disrotatory process. For the strained ring systems (Scheme 1.3.) the reaction is proposed to proceed first by metal coordination to cyclobutene **14**. Then for the reaction to proceed, $Fe(CO)_4$ must lose a ligand of CO to generate the coordinately unsaturated 16-electron intermediate **15**, followed by ring opening to give diene **16**. For this system a conrotatory ring opening is not possible due to the geometry constraints of the second cyclobutene ring.[8]
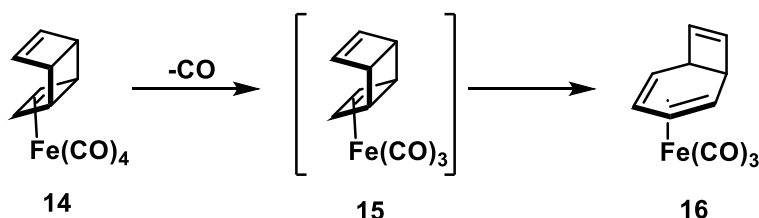
Scheme 1.3. $Fe(CO)_3$- mediated ring opening of a cyclobutene.[8]

While the unsubstituted cyclobutene system has been difficult to study experimentally,[13] Tantillo and Hoffmann performed calculations utilizing the HF-DFT-B3LYP method on the unsubstituted system (Scheme 1.4).[9,10] This system allows for the direct comparison of energies for the ring opening pathways without geometric constraints. They were able to identify two possible pathways for the transformation of **17** to **18**. The first pathway (path A) consists of loss of one CO ligand followed by ring opening, while the second pathway (path B) consist of ring opening, followed by CO ligand loss.

In path A, the loss of CO has an activation barrier of 31.1 kcal/mol for formation of the 16-electron complex **19**. Intermediate **19** undergoes a disrotatory ring opening with an activation barrier of 30.6 kcal/mol to form **18**. For path B, which is a non-pericyclic pathway, the first step of the reaction is oxidative addition of $Fe(CO)_4$ to the sp^3-sp^3 cyclobutene sigma bond, forming 18-electron complex **20**, which has a barrier of activation of 46.8 kcal/mol. Next, complex **20** loses a CO ligand, and the barrier to CO loss is 28.0 kcal/mol, which forms a 16-electron complex. Lastly, reductive elimination forms complex **18** with a 10 kcal/mol activation barrier.
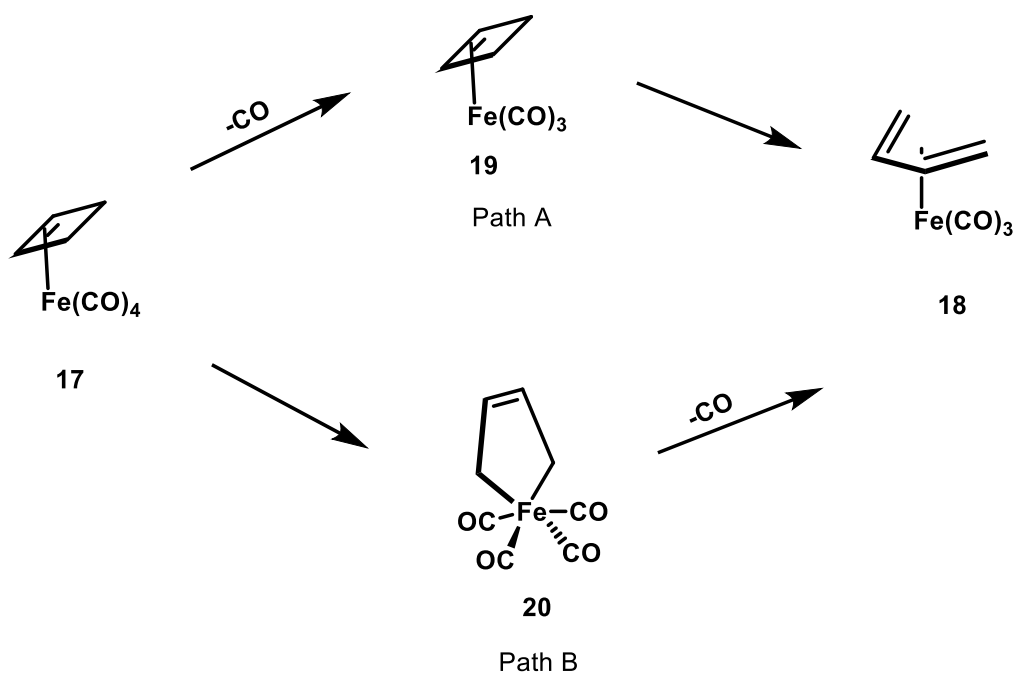
Scheme 1.4. Proposed ring opening pathways of **17** to **18**. [9,10]

From the above studies, the oxidative addition pathway is the lower energy pathway. In actual experimental systems the $Fe(CO)_3$ complexed cyclobutene ring is fused to another four-membered ring. Thus, rearrangement through pathway A would be more favorable for fused systems, since the pericyclic ring opening step would induce strain relief. For pathway B, complex **20** would be rather sterically congested, thus progression down this pathway is unfavorable.

Lastly, Tantillo and Hoffman stated that even for systems without geometric constraints, it is possible for the reaction to proceed in a pericyclic fashion, under the condition that CO ligand loss is irreversible. If CO loss is irreversible, then energetic barriers that are encountered after CO loss are negated. Dissociation of the CO ligand along path A is 15.3 kcal/mol lower in energy than in path B; thus, the electrocyclic ring-opening pathway may dominate over the oxidative addition pathway under certain conditions.

D. Selected Examples of Transition Metals Coordinated to Trienes

Metal-coordination to carbon-carbon double bonds has had an important impact on the chemical sciences. Metal-coordination to alkenes often accelerates rates of reactions, or induces reactivity that would not be possible without metal coordination.[14] One of the key findings of the 19th century, was the discovery of Zeise's salt **21** in 1831.[15] This is the first example of a transition metal alkene complex, albeit the solid-state structure was not determined until 1969.[16]

The historical progression from the first metal η^2-alkene to η^4-diene to η^6-triene complexes required over 100 years of experimental research. In 1930 Reihlen reported the first metal diene complex **22** and in 1958 Wilkinson reported the first η^6-triene complex **23**.[17,18] Since then, there have been numerous examples of η^6-triene complexes including: η^6-fulvene **24**,[19] η^6-cyclododecatriene **25**,[20] η^6-(methylene-heptadiene) complex **26**,[21] η^6-(5-methylene-1,3-diene) **27**,[22] and η^6-cyclohexatriene **28**.[23] Most notably absent from the world of η^6-triene complexes are examples of alicyclic conjugated trienes, where the three double bonds are not confined within a single ring.

21 **22** **23**

24 **25** **26**

27 **28**
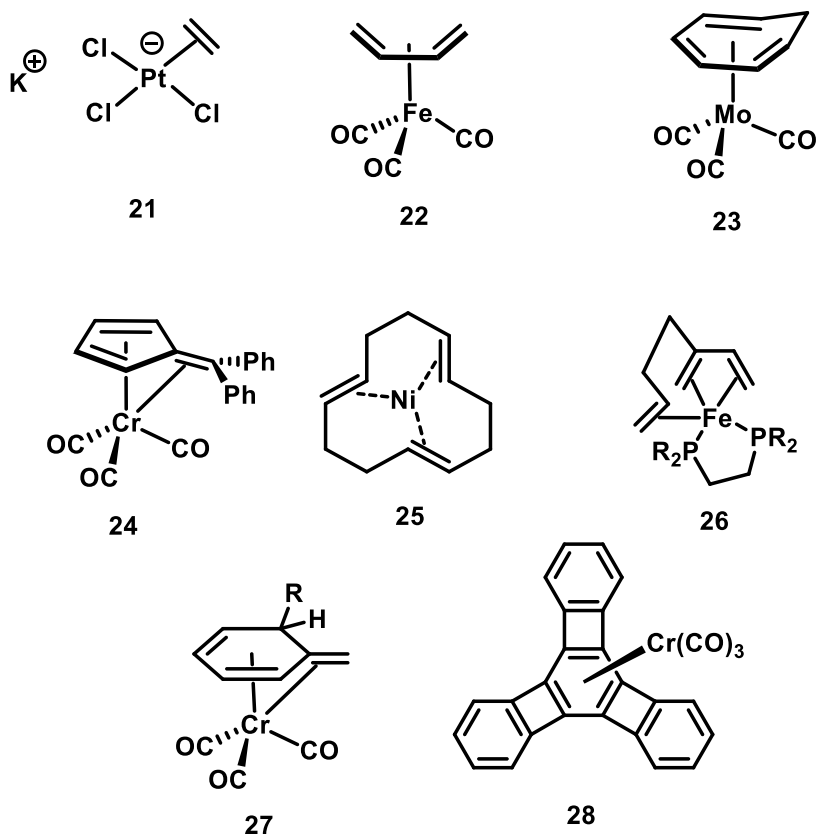
Figure 1.4. Historically significant metal-alkene complexes.

E. Room Temperature Metal-Mediated Cycloaromatizations of Tri-π Systems

Previously, the O'Connor group demonstrated that $[Cp^*Ru(NCMe)_3]^+$ triggers the room temperature cyclization of conjugated enediyne **29** and dienyne **32**.[24,25] The mechanistic hypothesis for both of these transformations involves the formation of hexahapto tri-π complexes: η^6-enediyne **30** and η^6-dieneyne **33** which cyclize to give ruthenium-arenes **31** and **34**, respectively. (Scheme 1.5).

10
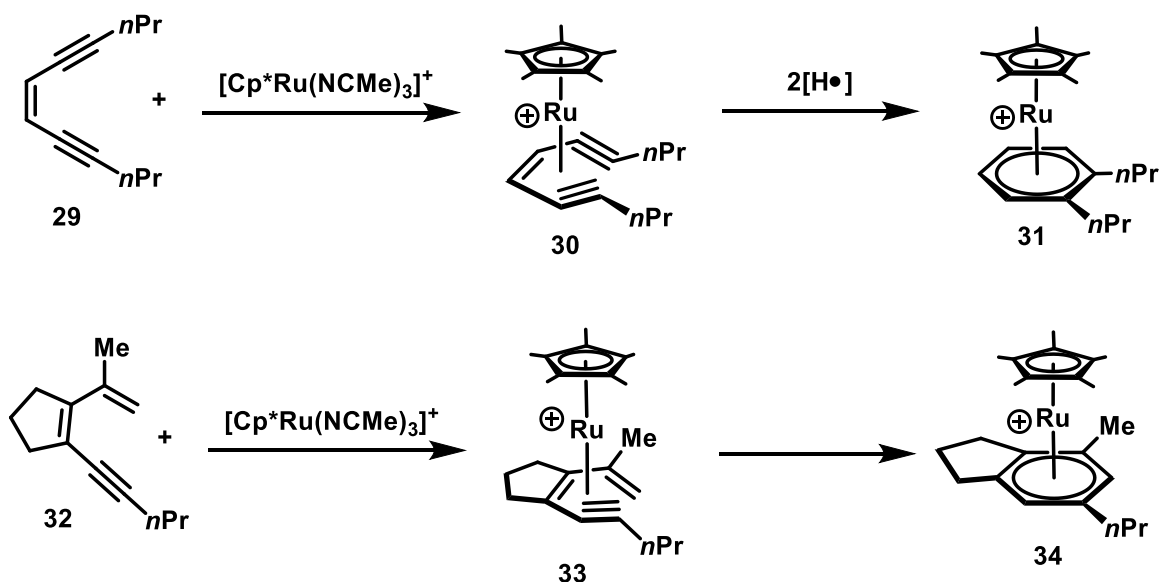
Scheme 1.5. [Cp*Ru]$^+$ triggers the room temperature cyclization of enediynes and dienynes. [24,25]

Through a series of computational and experimental studies,[26] the reaction mechanism for conversion of **29** to **31** is suggested to proceed as shown in Scheme 1.6. First, one ligand of MeCN is lost from [CpRu(NCMe)$_3$]$^+$ and coordination to one alkyne of enediyne **1** forms complex **35**. Calculations show η^2 alkyne binding is 13.5 kcal/mol more stable than η^2 alkene binding. Loss of a second MeCN and coordination of the remaining alkyne then forms intermediate **36**. Calculations illustrate that η^4 binding to both alkynes is 16.6 kcal/mol more stable than if the metal was bound η^4 to the alkene and one alkyne. Finally, the loss of the last MeCN ligand leads to η^6-coordination complex **37**. Complex **37** is proposed to undergo a spontaneous cycloaromatization reaction to *p*-benzyne diradical **38**, followed by hydrogen atom abstraction from a donor source to give arene complex **39**. The calculated η^6-enediyne structure, illustrates that the non-bonded distance between

C2 and C7 is 2.98 Å and the C5-C6-C7 and the C2-C3-C4 bond angles are 152° (Figure 1.5). Both

these factors are proposed to lower the activation energy for ring formation .
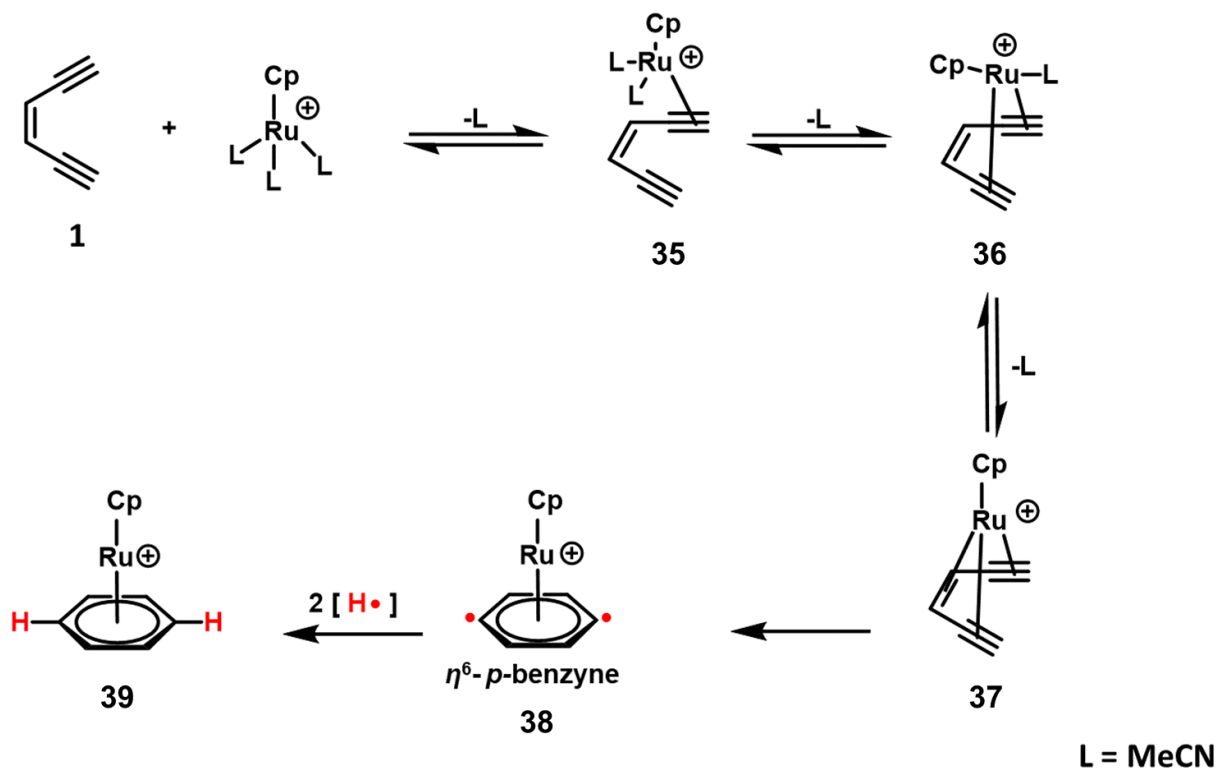
Scheme 1.6. Proposed mechanism for ruthenium-mediated enediyne cycloaromatization.[26]
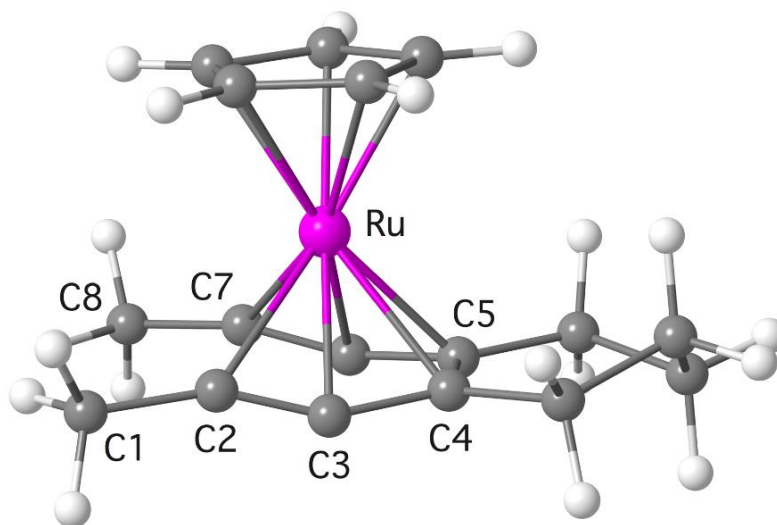
Figure 1.5. Calculated structure of CpRu(η^6-enediyne).[26]

In a much similar manner, Kündig and coworkers reported [Cr(CO)$_3$(η^6-naphthalene)] (**41**) readily cyclizes acyclic enediyne **40** in THF to give chromium-arene **42** in 72% yield (Scheme 1.7).[27] While substitution of the *n*-propyl groups for TMS groups on the alkyne carbons prevented enediyne **43** from cycling in the presence of **41** in THF-d_8, the authors were able to detect a potential intermediate via ^{13}C NMR spectroscopic analysis. They observed a large upfield shift for the alkene carbons at δ 83.8 ppm ($\Delta = 38$ ppm) upon addition of **41** and they assigned this intermediate as a THF stabilized chromium alkene complex **44**. They also calculated that the activation barrier of the η^6-enediyne binding to the *p*-benzyne diradical is only 16.7 kcal/mol.
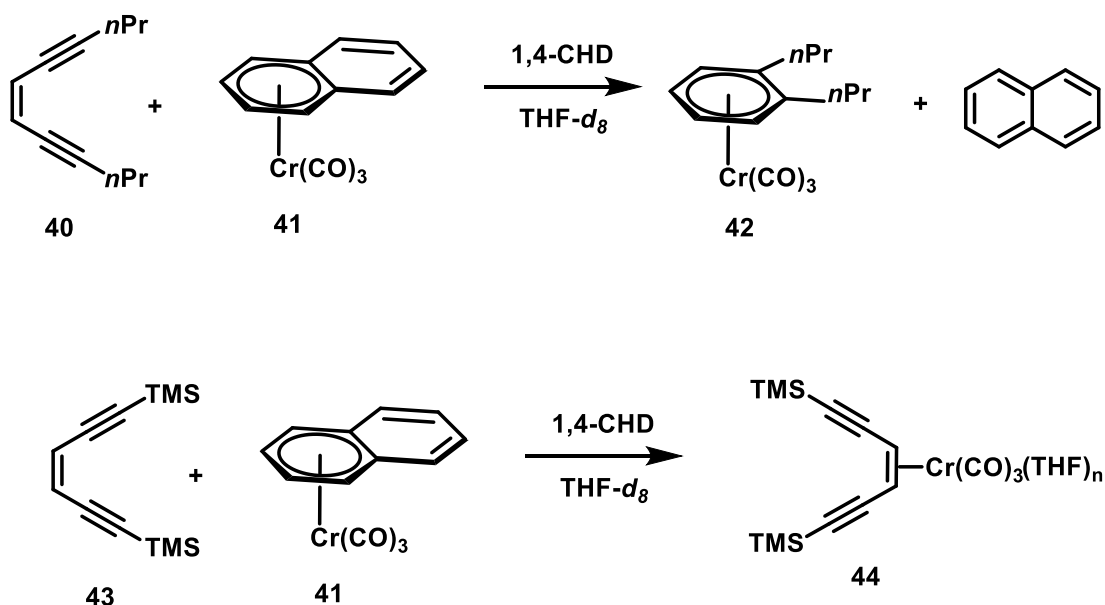
Scheme 1.7. Chromium-mediated cycloaromatization of enediyne **40** and possible intermediate **43**.[27]

For the transformation of dienyne **32** to arene **34**, the proposed intermediate is **33**. Through low temperature ^{1}H NMR experiments conducted at -60 °C, with **32** and [Cp*Ru(NCMe)$_3$]$^+$, new

resonances appeared which suggested the possible π-bound intermediate **33**. Complex **33** exhibited diagnostic ^{1}H NMR signals a δ 1.75 (s, 15H, Cp*), 3.27 (s, 1H, =CH$_{syn}$) and 0.11 (s, 1H, =CH$_{anti}$) The *anti*-hydrogen of **33** resonates significantly upfield compared to the anti-hydrogen of **32** (δ 4.90) and is similar to the chemical shifts of other Cp*Ru(η^5-pentadienyl) complexes. Additionally, a crystal of **33** was obtained by layering diethyl ether on a -78 °C cooled solution of CDCl$_3$ containing [Cp*Ru(NCMe)$_3$]$^+$ and **32**. This biphasic mixture was kept at -60 °C for five days until a single crystal formed. The crystal was kept cold during handling and the crystal was subjected to X-ray crystallographic analysis, which confirmed η^6-coordination of ruthenium to the π-bonds of the dienyne.[24]

Lastly, deuterium migration studies were conducted with **45**-*E* and **47**-*Z* (Scheme1.8).[28] When **45**-*E* was reacted with [Cp*Ru(NCMe)$_3$]$^+$, and monitored by ^{1}H NMR spectroscopy, the product exhibited a pair of doublets at δ 5.80 and 5.53 and a broad singlet at 5.65, with much lower intensity. This result is consistent with deuterium migration from the *E*-position, forming complex **46**. When **47**-*Z* was reacted with [Cp*Ru(NCMe)$_3$]$^+$, and the reaction progress monitored by ^{1}H NMR spectroscopy, the product exhibited a pair of singlets at δ 5.80 and 5.65 and a barely visible doublet at 5.53. This result is consistent with protium migration from the *E*-position of the alkene, forming complex **48**. With these results in hand, the proposed mechanism is shown in Scheme 1.9. The reaction begins with the formation of a ruthenium η^6-dieneyne complex **50**. Complex **50** undergoes a disrotatory 6π electrocylization with torquoselectivity for the *E*-position to come towards the metal, forming *iso*-benzene intermediate **51**. A metal mediated [1,2]-hydride shift forms complex **52**. Next, another metal-mediated [1,2]-hydride shift yields arene product **53**.
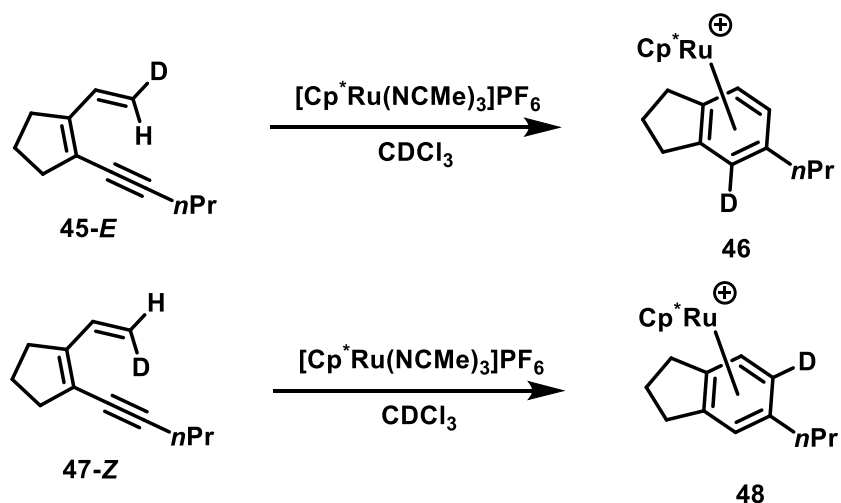
Scheme 1.8. Deuterium migration studies.[28]
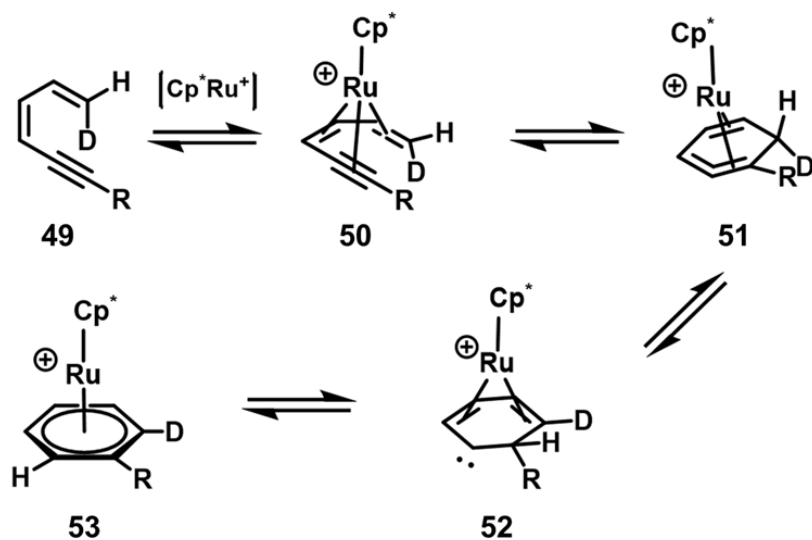
Scheme 1.9. Proposed mechanism with a hydrogen present in the *E*-position of the distal alkene.[28]

Lastly, Chaudret and co-workers demonstrated that (*E*)-1,3,5-hexatriene (**53**) undergoes a reaction with [Cp*Ru(OMe)]$_2$ and CF$_3$SO$_3$H to form the benzene derivative [Cp*Ru(η^6-C$_6$H$_6$)] (CF$_3$SO$_3$) (**54**) (Scheme 1.10).[29]
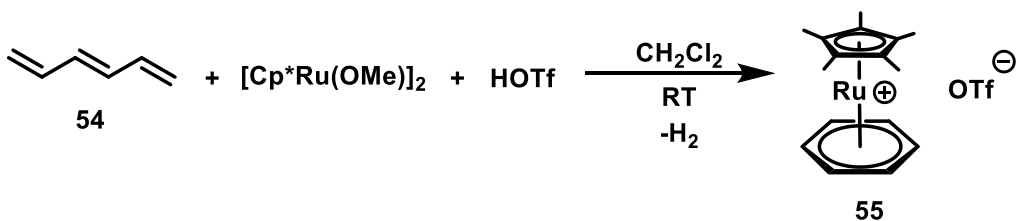
Scheme 1.10. Treatment of **54** with [Cp*Ru]⁺ yields arene product **55**.

While a mechanism was not discussed for this remarkable transformation, based on work presented by Older and Styker,[30] we propose that **54** cycloaromatizes via η^6-intermediate **56** and cyclohexadiene intermediate **57**. Conversion from **56** to **57** is proposed to involve a concerted 6π electrocyclization. Conversion of analogs of **57** to aromatic product **55** has been demonstrated by Stryker to proceed through a ruthenium-assisted protolytic C-H bond cleavage (Scheme 1.11).
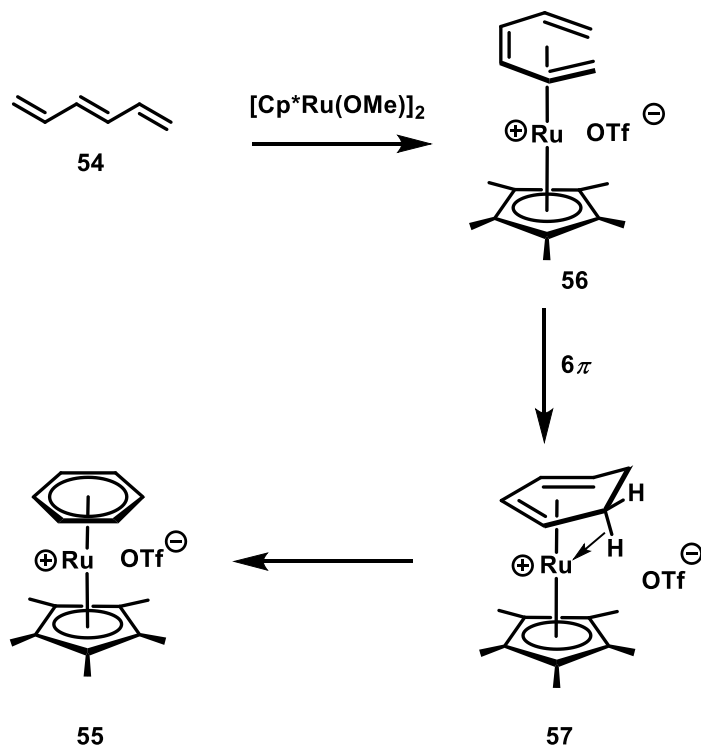
Scheme 1.11. Proposed transformation of **1** to **2** with [Cp*Ru]⁺.

Therefore, we propose that [CpRu]$^+$ could trigger the cyclization of trienes at room temperature via η^6 coordination of ruthenium to an acyclic triene. In chapter 2, we explore the feasibility of accelerating 6π electrocyclizations with late-metal η^6 complexes via computational analysis and investigate electronic effects of hexahapto ruthenium coordination to conjugated triene systems.

F. Chemistry of Enediynes: The Bergman Cyclization

In 1972, Bergman and Jones reported that when deuterium enriched *cis*-1,5-hexadiyn-3-ene (**58**) was heated in the gas phase at 200 °C, it rapidly equilibrated with the *cis*-enediyne isomer **59,** without evidence for formation of isomers that contained deuterium enrichment at both the vinyl and terminal acetylenic positions, **61** and **62**.[31] When **58** was heated in atom-donor solvents such as toluene, 1,4-cyclohexadiene (1,4-CHD), or CCl$_4$, arynes **63**, **64** and **65** were formed (Scheme 1.12). This evidence led Bergman to propose a symmetric *para*-benzyne diradical (**60**) as an intermediate for the interconversion of **58** and **59**.

While the Bergman cyclization is fascinating from a mechanistic standpoint, the high cycloaromatization activation barrier of 25 kcal/mol and low yields of this reaction limited it to an academic curiosity and was largely forgotten. Interest in enediynes was renewed in 1987 when the enediyne antitumor antibiotic Calicheamicin-$\gamma_1{}^I$ (Figure 1.6) was discovered.[32,33] Calicheamicin-$\gamma_1{}^I$ possesses a (*Z*)-hex-3-ene-1,5-diyne moiety which is highly reactive towards the minor groove of DNA. Once the enediyne interacts with the minor groove of DNA, a chemical transformation takes place which positions the enediyne under high strain conditions. This conformational change promotes the enediyne to cycloaromatize to the highly reactive *p*-benzyne diradical. The diradical then abstracts one proton from each strand of DNA, causing double-stranded DNA cleavage leading ultimately to cell death.[34]
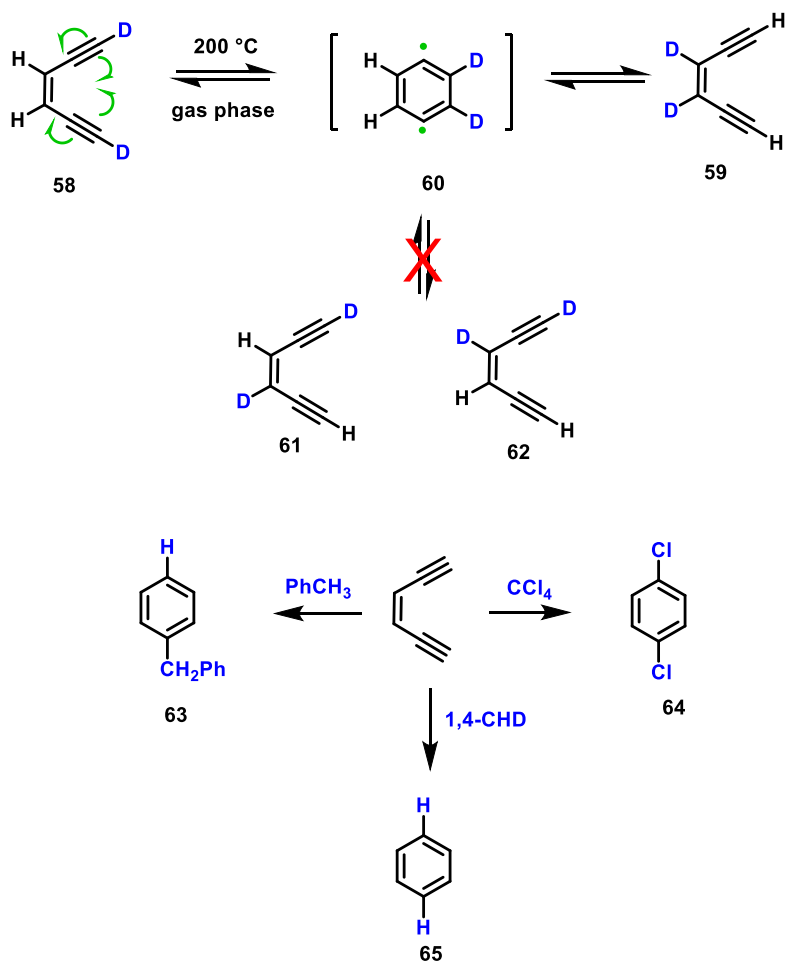
Scheme 1.12. Bergman's initial observations of cycloaromatization of enediyne **1**. [31]
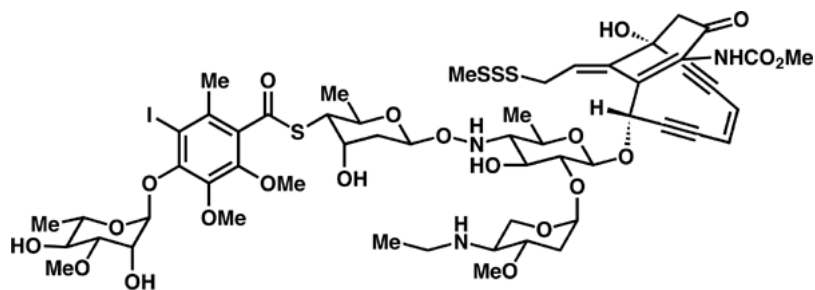
Figure 1.6. The enediyne natural product Calicheamicin-γ_1^I.

18

After Calicheamicin was discovered, there have been many efforts to understand and explore the energetic requirements for cyclization. In 1988, Nicolaou first proposed the enediyne "distance theory" through the use of molecular mechanics calculations on **66** and **67**. Specifically, he reported that the distance between carbons *c* and *d* of **65** to be 3.35 Å, while the activated 10-membered ring **66** distance was 3.16 Å (Figure 1.7).

cd = 3.35 Å
66

cd = 3.16 Å
67
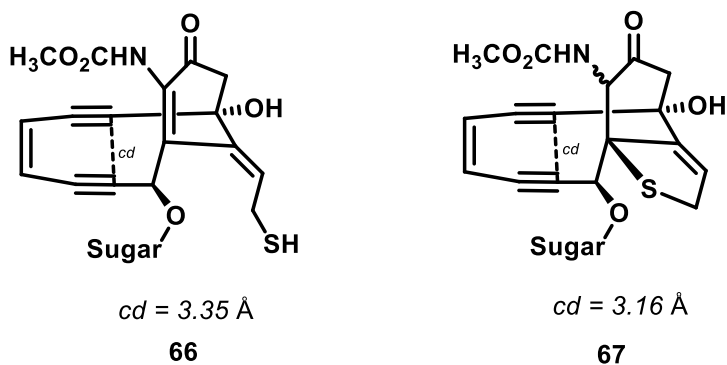
Figure 1.7. Shorter *cd* distances increase the chance of spontaneous cyclization by lowering the activation barrier.

Nicolaou also synthesized a series of strained ring enediynes (Figure 1.8) and the distance between the distal acetylenic carbons were measured computationally.[35] These measurements were correlated to the temperature required for cyclization. From these experiments, Nicolaou proposed a "critical distance" for spontaneous cyclization at room temperature to be within the range of 3.0-3.31 Å. Later Schreiner and co-workers suggested that the range could be expanded to 2.9-3.4 Å.[36,37]

cd = 3.25 Å

Cyclizes at 25 °C

cd = 3.61 Å

Cyclizes at 130 °C

cd = 4.12 Å

Cyclizes at 200 °C
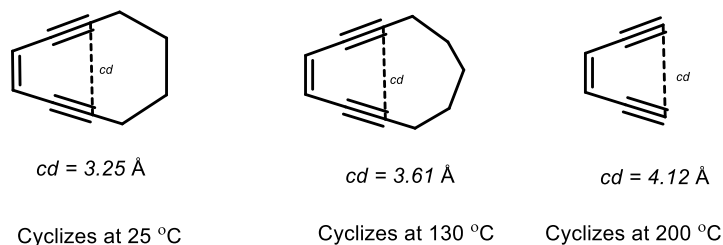
Figure 1.8. Modeled enediynes by Nicolaou.[35]

While reducing the *cd* distance does correlate to increased probability for cycloaromatizations to occur, more recent computational analysis has determined that the tendency for enediynes to cyclize at room temperature is more closely related to the distortion of ground state energies. Strain effects raise the ground state energy of the enediyne relative to the transition state, therefore the barrier to cycloaromatization is lower relative to acyclic enediyne systems.[37,36]

Compared to the use of steric strain, there have not been as many reports in the literature examining electronic contributions to cyclization. Schmittel and Kiau have demonstrated that electron-withdrawing groups attached to the alkyne termini lowers the activation enthalpy of the reaction, presumably by reducing the electron density and steric repulsion of the alkyne π-orbitals. Also, Maier and Greiner postulated that an electron-donating arene attached to the double bond of the enediyne inhibited cyclization by stabilizing the ground state of the starting material more than destabilizing the transition state.[39] Furthermore, there are very few examples of cycloaromatization reactions involving nitrogen-containing enediynes.[40–42]

Therefore, in chapter three, we investigate thermal cyclization reactions of nitrogen-containing enediynes, which may provide insight into how aromaticity and electronic factors influence cycloaromatization reactions. If successful, these investigations would expand the scope of these reactions. Lastly, the thermolysis of nitrogen-containing enediynes in haloforms were investigated and we report unexpected thermal conversions of enediynes to halogenated arenes and explore possible mechanisms of the *in situ* generation of HX from haloform and 1,4-cyclohexadiene.

G. References

(1) Woodward, R. B.; Hoffmann, R. *Angew. Chemie Int. Ed. Engl.* **1969**, *8*, 781-853.

(2) Bian, M.; Li, L.; Ding, H. *Synthesis* **2017**, *49*, 4383-4413.

(3) Mango, F. D. *Coord. Chem. Rev.* **1975**, *15*, 109-205.

(4) Brookhart, M.; Davis, E. R.; Harris, D. L. *J. Am. Chem. Soc.* **1972**, *94*, 7853-7858.

(5) Reardon, E. J.; Brookhart, M. *J. Am. Chem. Soc.* **1973**, *95*, 4311-4316.

(6) Bishop, L. M.; Barbarow, J. E.; Bergman, R. G.; Trauner, D. *Angew. Chemie Int. Ed.* **2008**, *47*, 8100-8103.

(7) Guner, V. A.; Houk, K. N.; . Davies, I. W. *J. Org. Chem.* **2004**, *69*, 8024-8028.

(8) Knölker, H. J. *Chem. Rev.* **2000**, No. 100, 2941-2961.

(9) Tantillo, D. J.; Hoffmann, R. *J. Am. Chem. Soc.* **2001**, *123*, 9855-9859.

(10) Tantillo, D. J.; Hoffmann, R. *Helv. Chim. Acta* **2001**, *84*, 1396-1404.

(11) Barlow, S.; Henling, L. M.; Day, M. W.; Schaefer, W. P.; Green, J. C.; Hascall, T.; Marder, S. R. *J. Am. Chem. Soc.* **2002**, *124*, 62856296.

(12) Slegeir, W.; Case, R.; McKennis, J. S.; Pettit, R. *J. Am. Chem. Soc.* **1974**, *96* (1), 287-288.

(13) Pinhas, A. R., Ph.D. Thesis, Cornell University, **1980**.

(14) Astruc, D. *Organometallic Chemistry and Catalysis*; Springer: New York, **2007**.

(15) Zeise, W. C. *Ann. Phys. Chem.* **1831**, *97*, 497-541.

(16) Black, M.; Mais, R. H. B.; Owston, P. G. *Acta Crystallogr. Sect. B* **1969**, 1753-1759.

(17) Reihlen, H.; Gruhl, A.; v. Heßling, G.; Pfrengle, O. *Justus Liebig's Ann. der Chemie* **1930**, *482*, 161-182.

(18) Abel, E. W.; Bennett, M. A.; Burton, R.; Wilkinson, G. *J. Chem. Soc.* **1958,** 4559-4563.

(19) Cooper, R. L; Fischer, E. O.; Semmlinger, W. *J. Organomet. Chem.* **1967**, *9*, 333-338.

(20) Wilke, G.; Bogdanovič, B.; Borner, P.; Breil, H.; Hardt, P.; Heimbach, P.; Herrmann, G.; Kaminsky, H.-J.; Keim, W.; Kröner, M.; Müller, H.; Müller, E. W.; Oberkirch, W.;

Schneider, J.; Stedefeder, J.; Tanaka, K.; Weyer, K.; Wilke, G. *Angew. Chemie Int. Ed. Engl.* **1963**, *2*, 105-115.

(21) Jolly, P. W.; Kopiske, C.; Krueger, C.; Limberg, A. *Organometallics* **1995**, *14*, 1885-1892.

(22) Blagg, J.; Davies, S. G.; Goodfellow, C. L.; Sutton, K. H. *J. Chem. Soc., Chem. Commun.* **1986**, 1283-1285.

(23) Nambu, M.; Mohler, D. L.; Hardcastle, K.; Baldridge, K. K.; Siegel, J. S. *J. Am. Chem. Soc.* **1993**, *115*, 6138-6141.

(24) O'Connor, J. M.; Friese, S. J.; Tichenor, M. *J. Am. Chem. Soc.* **2002**, *124*, 3506-3507.

(25) O'Connor, J. M.; Friese, S. J.; Rodgers, B. L. *J. Am. Chem. Soc.* **2005**, *127*, 16342-1643.

(26) Calculations performed by Kim Baldridge using BP86 density functional, Def2-TZVPP basis set, GAMESS Program.

(27) Ylijoki, K. E. O.; Lavy, S.; Fretzen, A.; Kündig, E. P.; Berclaz, T.; Bernardinelli, G.; Besnard, C. *Organometallics* **2012**, *31*, 5396-5404.

(28) Cope, S. K. Ph.D. Thesis, University California, San Diego, **2015**.

(29) Carreno, R.; Chaudret, B.; Labroue, D.; Sabo-Etienne, S. *Organometallics* **1993**, *12* (1), 13-14.

(30) Older, C. M.; Stryker, J. M. *J. Am. Chem. Soc.* **2000**, No. 122, 2784-2797.

(31) Jones, R. R.; Bergman, R. G. *J. Am. Chem. Soc.* **1972**, *94*, 660-661.

(32) Lee, M. D.; Dunne, T. S.; Siegel, M. M.; Chang, C. C.; Morton, G. O.; Borders, D. B. *J. Am. Chem. Soc.* **1987**, *109*, 3464-3466.

(33) Lee, M. D.; Dunne, T. S.; Chang, C. C.; Ellestad, G. A.; Siegel, M. M.; Morton, G. O.; McGahren, W. J.; Borders, D. B. *J. Am. Chem. Soc.* **1987**, *109*, 3466-3468.

(34) Nicolaou, K. C.; Smith, A. L.; Yue, E. W. *Proc. Natl. Acad. Sci. U. S. A.* **1993**, *90*, 5881-5888.

(35) Nicolaou, K. C.; Ogawa, Y.; Zuccarello, G.; Schweiger, E. J.; Kumazawa, T. *J. Am. Chem. Soc.* **1988**, *110* (14), 4866-4868.

(36) Schreiner, P. R. *J. Am. Chem. Soc.* **1998**, *120*, 4184-4190.

(37) Schreiner, P. R. *Chem. Commun.* **1998**, 483-484.

(38) Schmittel, M.; Kiau, S. *Chem. Lett.* **1995**, *24*, 953-954.

(39) Maier, M. E.; Greiner, B. *Liebigs Ann. der Chemie* **1992**, *1992*, 855.

(40) Sathyajith Kumarasinghe, E.; Peterson, M. A.; Robins, M. J. Tetrahedron Lett. **2000**, *41*, 8741-8745.

(41) Choy, N.; Russell, K. C.; Och, N. *Heterocycles* **1999**, *51*, 13-16.

(42) Kim, C.; Diez, C.; Russell, K. C. *Chem. - A Eur. J.* **2000**, *6* (9), 1555-1558.

Chapter 2.

Hexahapto Metal Complexes of Acyclic Conjugated Trienes

A. Introduction

Concerted 6π electrocyclizations of trienes laid the foundation for Woodward and Hoffmann formulating the principle of conservation of orbital symmetry,[1] and these reactions have found great practical importance in the world of synthetic chemistry.[2] Interest in catalytic triene electrocyclizations started in the 1960s,[3–5] but it was not until 2008 that the first catalytic 6π electrocyclizations of conjugated trienes were reported by Bergman and Trauner.[6,7] In the late 1990s, Chaudret and co-workers further demonstrated that (E)-1,3,5-hexatriene (**1**) undergoes a reaction with $[Cp^*Ru(OMe)]_2$ and CF_3SO_3H to form the benzene derivative $[Cp^*Ru(\eta^6\text{-}C_6H_6)][CF_3SO_3]$ (**2**) (Scheme 2.1).[8]
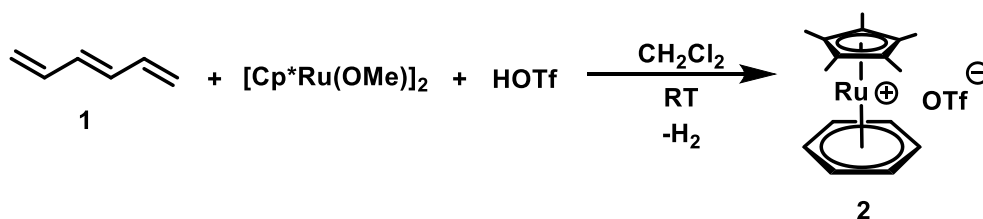
Scheme 2.1. Treatment of **1** with $[Cp^*Ru]^+$ yields arene product **2**.

At the time, a mechanistic rational was not discussed for this remarkable transformation; however, based on work presented by Older and Styker,[9] we propose that **1** cycloaromatizes via an η^6-intermediate **3** and cyclohexadiene intermediate **4**. Conversion of **3** to **4** is proposed to involve a concerted 6π electrocyclization. Conversion of an analogue of **4** to aromatic product **2** has been demonstrated by Stryker to proceed through a ruthenium-assisted protolytic C-H bond cleavage (Scheme 2.2).
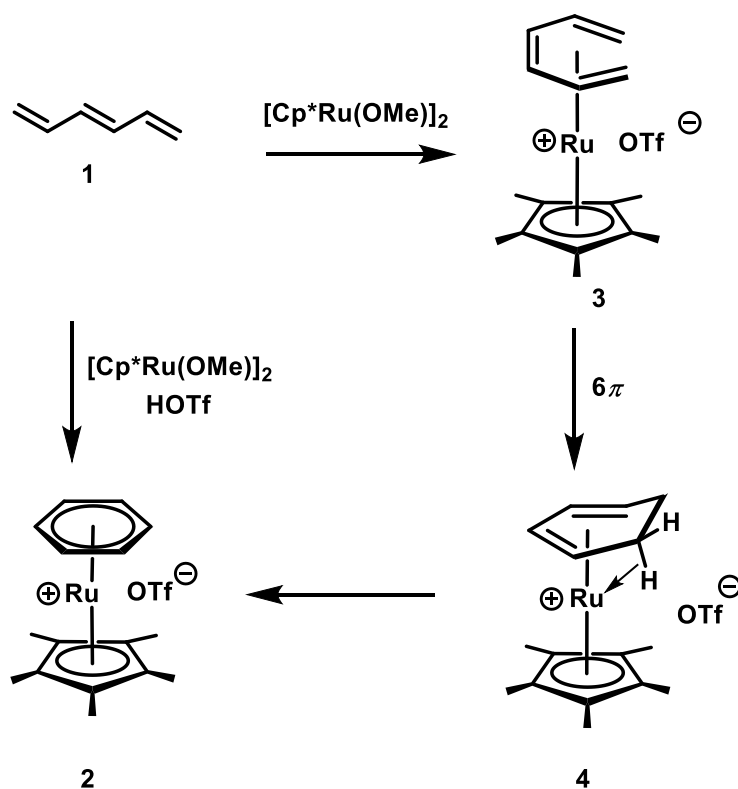
Scheme 2.2. Proposed transformation of **1** to **2** upon reaction with [Cp*Ru]⁺.

Previously, the O'Connor lab demonstrated that [Cp*Ru(NCMe)₃]⁺ triggers the room temperature cyclization of conjugated enediynes (**5**) and dienynes (**6**).[10,11] The mechanistic hypothesis for both of these transformations involves the formation of hexahapto tri-π complexes: η^6-enediyne **7** and η^6-dieneyne **8** which cyclize to arene products **9** and **10**, respectively (Scheme 2.3). In the former, the enediynes are proposed to cycloaromatize to an η^6-arene diradical, which is rapidly quenched via hydrogen atom abstraction from a hydrogen atom source, yielding arene product **9**. The latter is proposed to undergo a 6π electrocyclization, to form a ruthenium η^4-bound *iso*-benzene, followed by an intermolecular rearrangement to give arene **10**. Support for this proposed mechanism was provided by the isolation of intermediate **8**, which was obtained at low temperature, and characterized by X-ray crystallography.

26
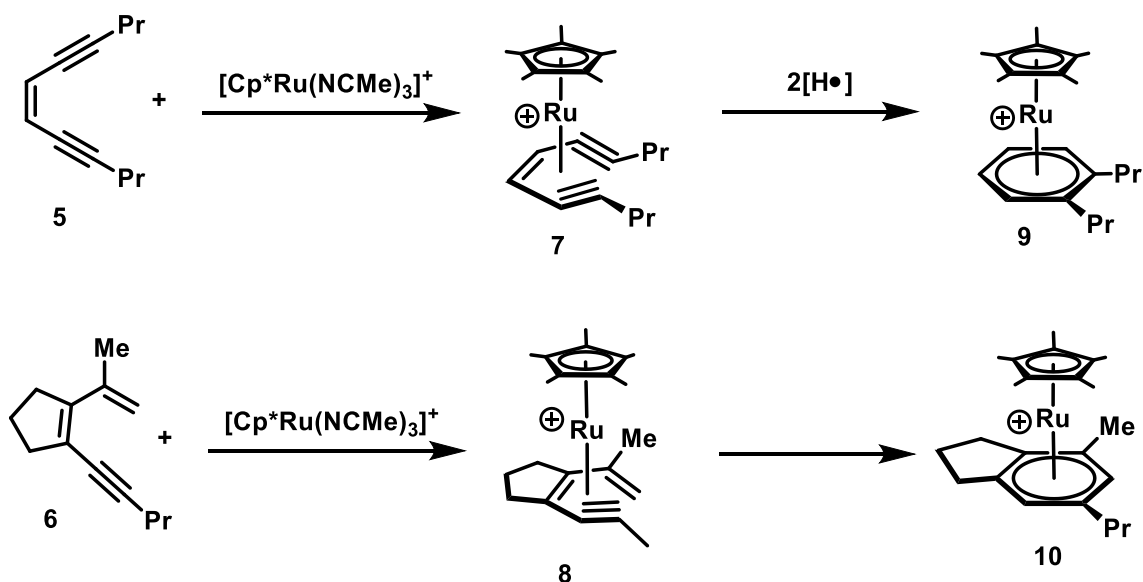
Scheme 2.3. [Cp*Ru]+ triggers the room temperature cyclization of enediynes and dienynes.

Drawing inspiration from both our previous work with dienynes and enediynes, and work by Chaudret, we postulated that [CpRu]$^+$ could facilitate the cyclization of trienes at room temperature via an η^6 coordination of ruthenium to the triene. Herein, we report the first examples of η^6 coordination to acyclic conjugated trienes, complimented by computational results that demonstrate the feasibility of accelerating 6π electrocyclizations via the intermediacy of late-metal η^6 complexes.

B. Results and Discussion.

1. Computational Analysis of Hexahapto Triene Cyclization

In order to establish the feasibility of a disrotatory 6π electrocyclization for the conversion of **11**-Cp^* to **13**-Cp^*, PB86/Def2-TZVPP(THF) calculations were performed by Kim Baldridge at Tianjin University on model compound **11**-Cp^* and intermediate **12**-Cp^* (Scheme 2.4). The minimum energy triene conformation for **11**-Cp^* was found to be the *s-cis/s-cis* conformer and the activation energy for the transformation of **11**-Cp^* to **12**-Cp^* was calculated to be 17.7 kcal/mol.

Conversion of **11-**Cp^* to **12-**Cp^* was calculated to be exothermic by 5.9 kcal/mol. For comparison, the non-metal mediated conversion of *Z*-1,3,5-hexatriene to cyclohexadiene was calculated at the same level of theory and the activation energy for this thermal transformation was calculated to be 10 kcal/mol higher in energy than the metal-mediated case at 27.7 kcal/mol.[12] A similar lowering of the 6π electrocyclization activation barrier was observed by Schleyer and co-workers using a RMP2(fc)/6-31G* basis set on the lithium complexation to 1,3-*cis*-hexatriene facilitating the transformation to 1,3-cyclohexadiene.[13] Taken together, these computational results support our working hypothesis that η^6 metal coordination accelerates 6π electrocyclizations.
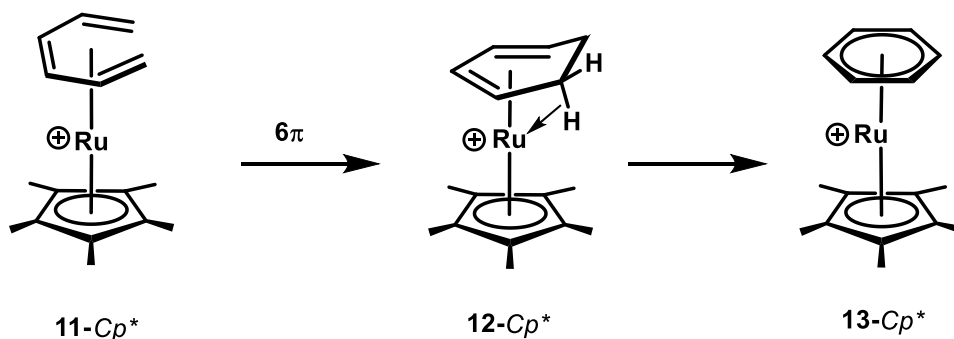
Scheme 2.4. Calculated η^6 complex **11-**Cp^* to agostic interaction **12-**Cp^* utilizing the PB86/Def2-TZVPP(THF) basis set.[14]

Taking a closer look at the calculations (Figure 2.1), the C1--C6 non-bonded distance for the transition state structure **11/12**^{TS} is significantly shorter than in precursor **11-**Cp^* (2.101 Å and 2.759 Å respectively, $\Delta = 0.658$ Å), indicating that the reaction is proceeding towards cyclization (structure **12-**Cp^*). Additionally, the *syn* hydrogens (H1^s and H6^s, Figure 2.1) in transition state structure **11/12**^{TS} are 0.09 Å closer to ruthenium than in **11-**Cp^*, which is indicative of progression towards a disrotatory ring closure.
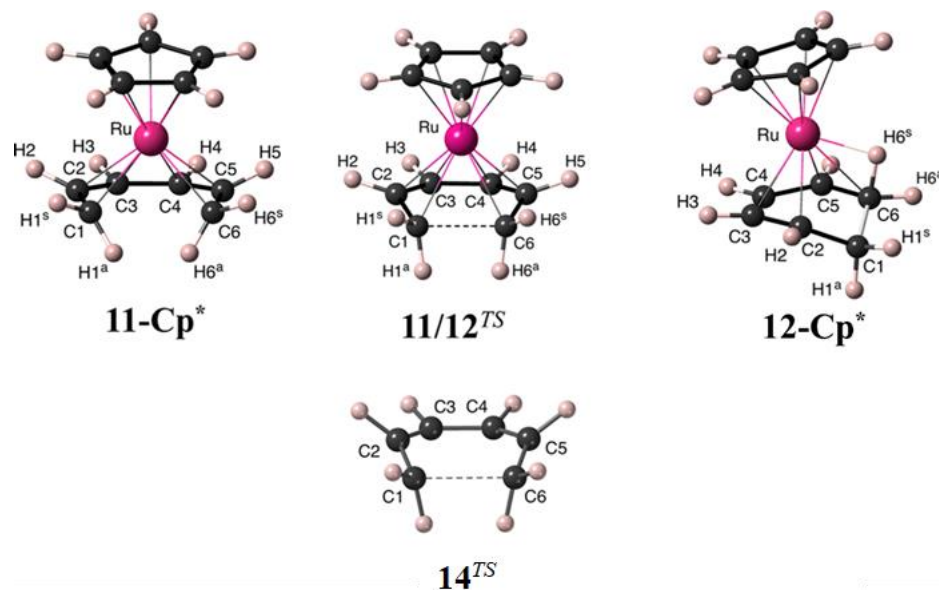
Figure 2.1. Calculated structures of **11-**Cp^*, **11/12**^{TS}, **13-**Cp^* and free triene **14**^{TS}.[14]

The effects of metal complexation can be further highlighted by comparison of transition state structure **11/12**^{TS} to the transition state structure in the metal-free triene electrocyclization, **14**^{TS}. Metal complexation shortens the C1--C6 non-bonded distance by 0.169 Å (2.101 Å for **11/12**^{TS} and 2.278 Å for **14**^{TS}), which may assist with cyclization by bringing the cyclizing termini closer together. Furthermore, an analysis of the transition state fold angles involving the C1-C2-C3 and C1-C3-C4-C6 mean planes for **11/12**^{TS} and **14**^{TS} shows that the fold angle for **11/12**^{TS} is 19.2° while the fold angle of **14**^{TS} is 27.0°. Thus, the boat conformer for **11/12**^{TS} is flattened compared to the free triene transition state structure, presumably as a means to optimize metal-triene orbital overlap.

Table 2.1. Selected fold angles and distances of $11/12^{TS}$, 11-Cp^* and 14^{TS}.

Compound	C1--C6 distance (Å)	Fold angle (°)*	*syn*-hydrogen distance (Å)**
$11/12^{TS}$	2.101	19.2	2.811
11-Cp^*	2.259	12.2	2.897
14^{TS}	2.278	27.0	N/A

* Fold angle between C1-C2-C3 and C1-C3-C4-C6 mean plane. **distance from H1^s and H6^s from the ruthenium metal (Figure 2.1).

The C1--C6 distances (Figure 2.2, black line) were then analyzed by scanning along the reaction coordinate as the reaction proceeds from η^6-coordination (11-Cp^*) to η^4-diene/agostic interaction (12-Cp^*) in a disrotatory fashion. The Ru--H1^s (blue line) and Ru--H6^s (red line)
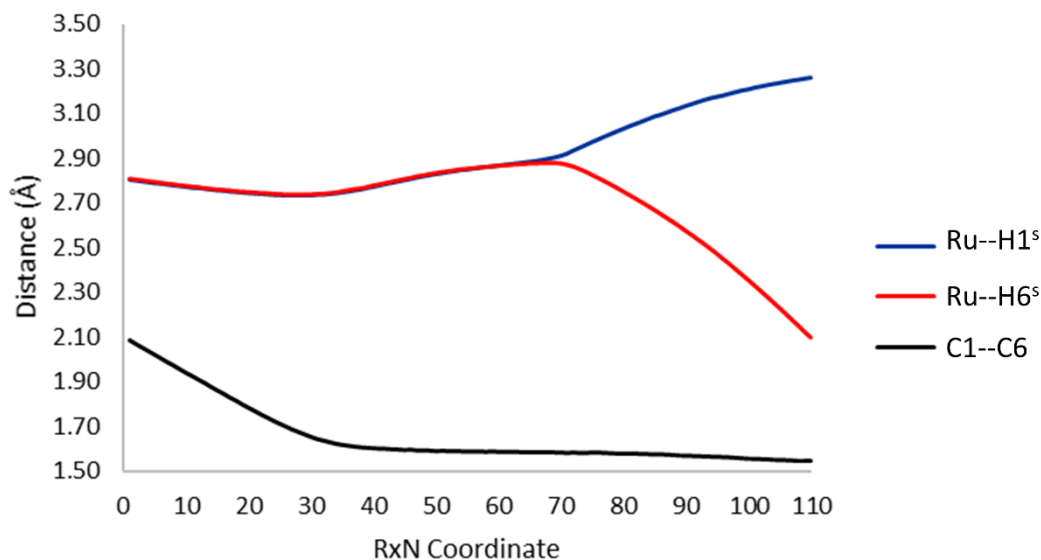
Figure 2.2. Reaction coordinate plotting Ru--H1^S Ru--H6^S and C1--C6 distances over time. Point 0 is complex 11-Cp^* and point 110 is 12-Cp^*.

distances were also examined as the reaction proceeded towards 12-Cp^*. Along the first one-third of the reaction coordinate (time points 0-35) the C1--C6 distance decreases significantly, and over the first two-thirds of the reaction coordinate (time points 1-75) the Ru--H6^S and the Ru--H1^S

distances remain fairly constant at 2.75 - 2.90 Å. During the last third of the reaction (time points 80-110) the Ru--H6^S distance decreases to 2.101 Å as the Ru--H1^S distance increases to 3.262 Å).

Agostic interactions are characterized by relativity short metal-hydrogen distances, typically within the range of 1.8-2.3 Å and with relatively small metal-hydrogen-carbon bond angles between 90-140°.[15] At the start of the reaction coordinate diagram, the Ru -- H1^S (2.806 Å) and Ru -- H6^S (2.806 Å) distances are too long to be considered classical agostic interactions. As the 6-membered ring begins to pucker, the H6^S hydrogen becomes close enough to participate in an agostic interaction, with a hydrogen-carbon bond angle of 90° and a Ru--H6S distance of 2.101 Å. Therefore, the computational data suggests that only agostic interactions prevail along the last third of the reaction coordinate.

Furthermore, previous work on metal complexes has demonstrated that 18-electron metal centers are able to electrostatically bond to hydrogen, creating what is called an anagostic interaction.[15] Anagostic interactions are characterized by relatively long metal-hydrogen distances, typically within the range of 2.3-2.9 Å, and the metal-hydrogen-carbon bond angles are typically within the range of 110-170°. Based on computational analysis by Oldfield and co-workers, anagostic interactions can vary from purely electrostatic to electrostatic with partial covalence.[16] Ru(II) has been previously observed to form anagostic complexes, such as Ru(I^{i}Pr$_2$Me$_2$)(P^{i}Pr$_3$)$_2$HCl (**15**), which has a Ru--H8 (methine) distance of 2.542(1) Å and a Ru-H8-C8 angle of 131°(Figure 2.3).[17] Unfortunately, while our Ru--H1^S and the Ru--H6^S distances are within the range of typical anagostic interactions in the beginning of the reaction coordinate (Figure 2.2), the metal-hydrogen-carbon bond angles are too small (between 55-60°) to be considered classical anagostic interactions.
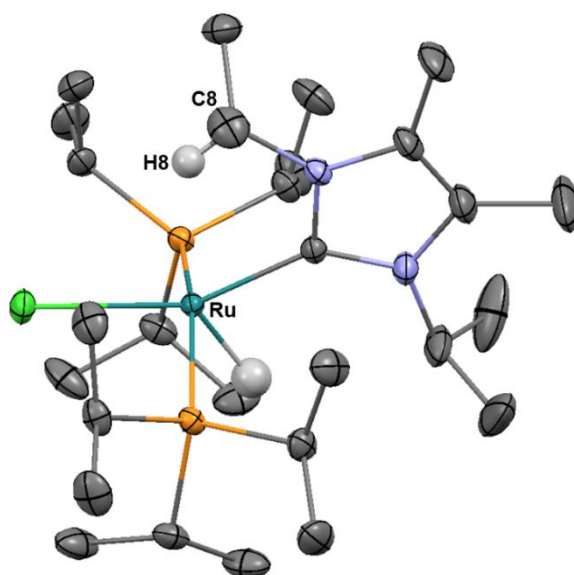
Figure 2.3. ORTEP drawing of **15**. An anagostic interaction has been proposed for the Ru—H8 interaction. Most hydrogen atoms have been omitted for clarity.

Finally, plotting the total energy along the reaction coordinate reveals no local energy minima (Figure 2.4). Therefore, the conversion of **11**-*Cp** to **12**-*Cp** occurs without the formation of a coordinatively unsaturated η^4-diene intermediate.[18] Therefore the computation data supports our working hypothesis of metal complexation facilitating 6π electrocylization reactions.
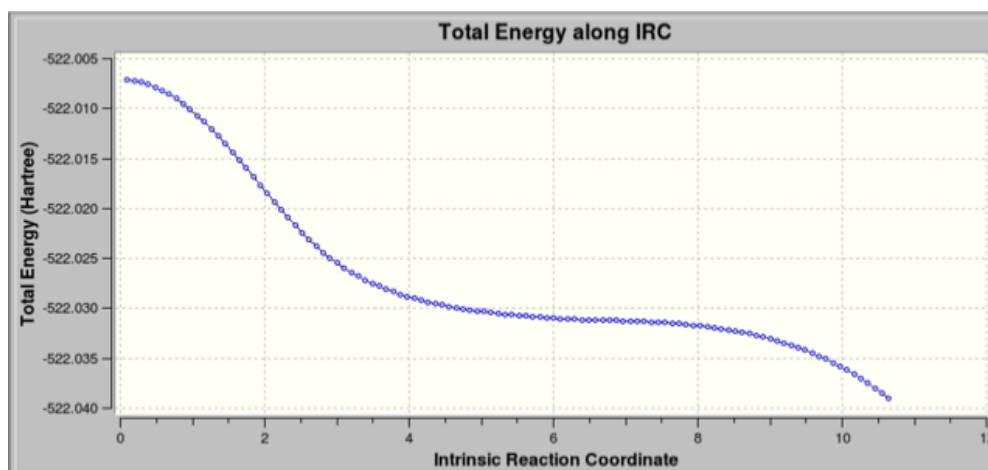
Figure 2.4. Total calculated energy of **11**-*Cp** to arene product **13**-*Cp** via agostic interaction **12**-*Cp** reveals no energy minimum.[14]

2. Synthesis of Acyclic Triene 18-*H*.

After analyzing the computational data, it was hypothesized that the reaction of trienes with bulky substituents located on the *E* positions of the vinyl carbons with [CpRu(NCMe)$_3$]PF$_6$ would permit the formation and isolation of an η^6-triene complex by hindering full disrotatory ring closure. As such, triene **18** was synthesized for initial studies to test our hypothesis. Starting with commercially available cyclopentanone (**16**), 1,2-dibromocyclopentene (**17**) was prepared in 35% yield via a three-step, one-pot procedure with PCl$_5$, Br$_2$ and potassium *t*-butoxide.[19] A double Heck reaction with styrene in DMF at 100 °C afforded **18-*H*** in 40% yield (Scheme 2.5).
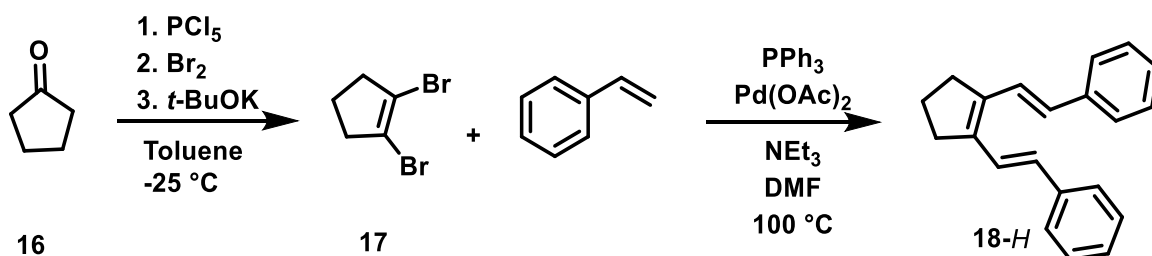
Scheme 2.5. Synthesis of **18-*H*.**

3. Complexation of 18-*H* with Ruthenium and Comparison of 19-*H* to the Calculated Structure 19-*H*-calc.

Reaction of **18-*H*** with [CpRu(NCMe)$_3$]PF$_6$ in chloroform-*d* was monitored via ^{1}H NMR spectroscopy and afforded η^6-triene complex **19-*H*.**[20] The solution exhibited a color change from pale yellow to bright orange and the ^{1}H NMR spectrum of the crude reaction mixture revealed new ^{1}H NMR resonances at δ 5.0 (s, 5H, Cp), 6.92 (d, J_{HH} = 10.3 Hz, 2H, =CHAr) and 4.10 (d, J_{HH} = 10.3 Hz, 2H, C*H*=CHAr). For comparison, vinyl hydrogens of free **18-*H*** resonate at δ 7.40 and 6.54. The upfield shift of the vinyl hydrogens to δ 4.10 indicates that both of the *E*-alkenes are bound to ruthenium. Also, in the ^{13}C NMR spectrum of **19-*H***, the internal alkene sp^2-carbon resonance is observed at δ 119, significantly upfield of the corresponding resonance of the free

triene **18-H** (δ 139.8). Therefore, the spectroscopic data is consistent with ruthenium coordination to all three of the double bonds.
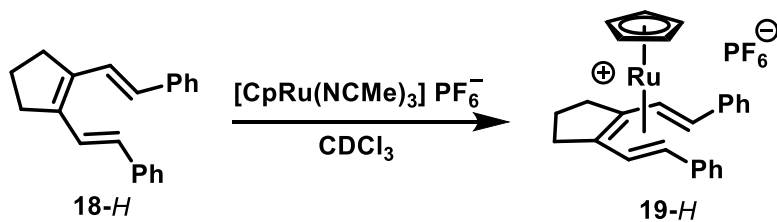
Scheme 2.6. Formation of η^6-triene complex **19-H**.

4. Analysis of X-ray Structure of 19-*H* and Comparison to the Calculated Structure, 19-*H*-calc

The NMR tube containing the reaction mixture of **18-H** and [CpRu(NCMe)$_3$]PF$_6$ was left to stand overnight at room temperature, during which time compound **19-H** precipitated as an orange block crystal. A single-crystal X-ray crystallographic analysis confirmed the formation of η^6-triene complex **19-H** (Figure 2.5).[20]
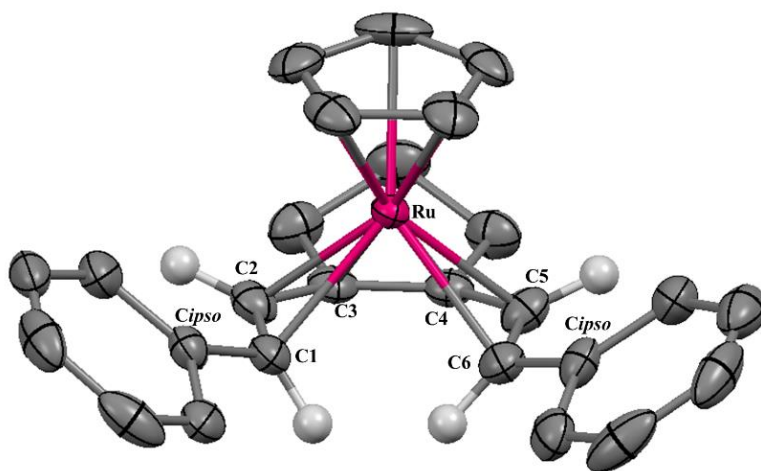
Figure 2.5. ORTEP drawing of **19-H**. Some hydrogens and the counter-ion have been omitted for clarity.[20]

The structure of **19**-*H* was also examined by computation, utilizing a PB86/Def2-TZVPP(THF) basis set.[14] Hexahapto **19-H** adopts a shallow boat conformation with a fold angle of 12.6(9)° (calcd 14.6°), which is similar to the fold angle in the calculated structure of the unsubstituted triene analogue, **11-***Cp*** (12.2°). Significant delocalization exists in the **19**-*H* triene π-system as evidenced by similar bond lengths: 1.382(6), 1.421(6), 1.412(6), 1.422(6) and 1.389(7) for bonds C1-C2, C2-C3, C3-C4, C4-C5 and C5-C6, respectively. For comparison the free calculated triene has bond distances of C1-C2 1.364 Å, C2-C3 1.436 Å, C3-C4 1.386 Å, C4-C5 1.436 Å and C5-C6 1.364 Å.

The bond lengths of **19**-*H* are very similar to the bond lengths observed previously in the O'Connor lab for the X-ray structure of $Cp^*Ru(\eta^6$-dienyne) **20** (Figure 2.6).[11] Compound **20** bond lengths for the diene are: 1.399(5) Å, 1.431(4) Å, 1.431(4) Å and 1.416(4) Å. Interestingly, the non-bonded C1--C6 distance of 2.7975(5) Å for **20** and the non-bonded C1--C6 of 2.821(5) Å for **19**-*H* are remarkably similar. The C1--C6 non-bonded distance of both triene **19**-*H* and dienyne **20** are very similar to the distal acetylenic distance (2.9-3.4 Å) that is typical for enediynes that undergo spontaneous enediyne cyclization at room temperature.[21] Computational analysis of strained ring enediynes has determined that the tendency for enediynes to cyclize at room temperature is closely related to the distortion of ground state energies. Strain effects raise the ground state energy of enediynes relative to the transition state, and thus the relative barrier to cycloaromatization decreases.[22,23] This concept can be applied to our transition metal complexes, η^6 metal coordination may distort the ground state energies of **19**-*H* and **20**, and thereby the barrier to cycloaromatization is lower relative to the free triene and free dienyne.

Table 2.2. Selected Bond Distances (Å) for **19-*H*** and **19-*H-calc***

Bond (A-B)	Length (Å)*	Bond (A-B)	Length (Å)*
Ru-C1	2.296(4) [2.348]	C1-C2	1.382(6) [1.414]
Ru-C2	2.190(4) [2.204]	C2-C3	1.421(6) [1.432],
Ru-C3	2.234(4) [2.267]	C3-C4	1.412(6) [1.443]
Ru-C4	2.238(4) [2.265]	C4-C5	1.422(6) [1.430]
Ru-C5	2.204(4) [2.202]	C5-C6	1.389(7) [1.413]
Ru-C6	2.314(4) [2.354]	C1--C6	2.821(5) [2.929]

*__19-*H-calc*__ was calculated with PB86/Def2-TZVPP(THF) - calculated values are in brackets

Table 2.3 Selected Angles and Torsion Angles (°) for **19-*H*** and **19**-*H-calc**

Angle	Degrees (°)	Angle	Degrees (°)
C1-Ru-C6	75.5(2) [77.0]	C*ipso*-C1-C2-C3	166.2(5) [171.9]
C1-C2-C3	127.6(5) [129.3]	C*ipso*-C6-C5-C4	167.1(5) [172.9]
C4-C5-C6	126.9(5) [127.7]	Fold angle**	12.6(9) [14.6]

*__19-*H-calc*__ was calculated with PB86/Def2-TZVPP(THF) - calculated values are in brackets. **
Fold angle between C1-C2-C3 and C1-C3-C4-C6 mean plane.
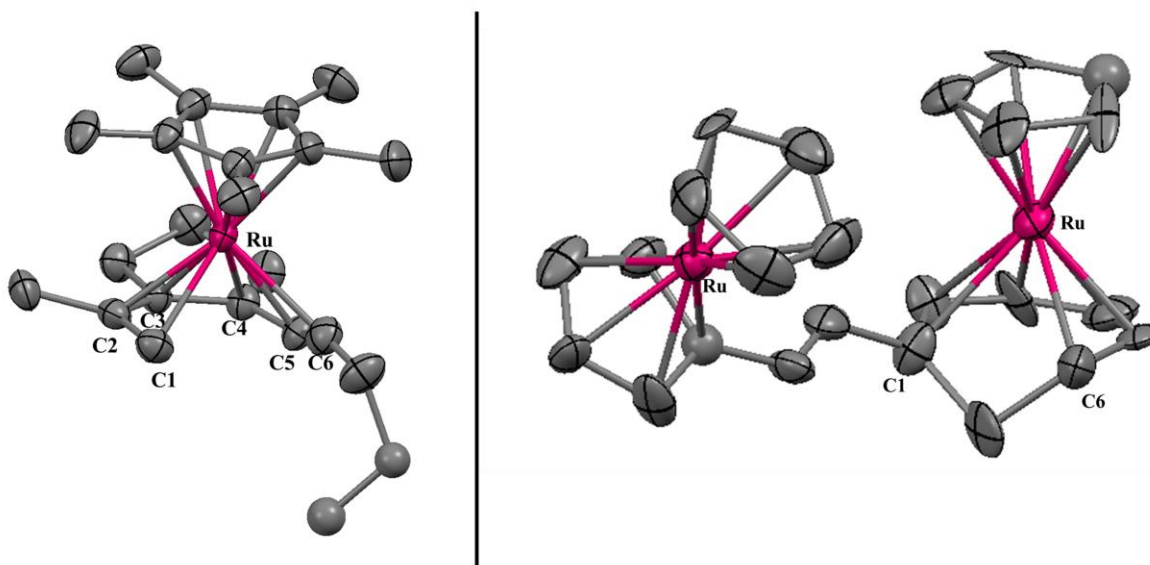
Figure 2.6. ORTEP drawing of **20** (right) and η^6-cycloheptatriene complex **21** (left). The hydrogens and the counter-ion have been omitted for clarity.

The C1-Ru-C2 bond angle of 75.5(2)° and the C1--C6 non-bonded distance of 2.8211(5) Å for **19-***H* can be compared to those for η^6-cycloheptatriene complex **21** (Figure 2.6).[24] Complex **21** has a C1-Ru-C2 angle of 61.7(7)° and C1--C6 distance of 2.42(3) Å. Lastly the ruthenium-carbon distances are similar in both complexes. The ruthenium-carbon bond distances in **19-***H* are 2.296(4), 2.190(4), 2.234(4), 2.238(4), 2.204(4) and 2.314(4) Å for bonds Ru-C1, Ru-C2, Ru-C3 Ru-C4, Ru-C5 and Ru-C6, respectively, while the ruthenium-carbon bond distances of **21** are 2.355(2), 2.243(2), 2.293(2), 2.286(2), 2.238 (2) and 2.315(2) Å for Ru-C1, Ru-C2, Ru-C3 Ru-C4, Ru-C5 and Ru-C6, respectively. Cycloheptatrienes undergo 6π electrocyclizations under thermal conditions,[25] however, to the best of our knowledge, there are no known examples of metal-cycloheptatriene complexes undergoing 6π electrocyclizations.

The structural analysis of **19-***H* and **19-***H-calc*, suggests that hexahapto metal complexation to the triene moves the triene along the reaction coordinate toward the cyclized product. The ruthenium positions the alkene termini in close proximity to one another, and facilitates the disrotatory 6π electrocyclization by shifting π-electron density in the direction of the diene product. However, as **19-***H* cyclizes, the bulky phenyl groups move toward [CpRu]$^+$, creating steric congestion. This steric congestion prevents formation of the cyclized product, allowing the isolation of hexahapto complex **19-***H*.

5. Preliminary Investigations into the Electronic Effects of Triene Substituents on η^6 Coordination

After the initial results with **19-***H*, a preliminary investigation of triene electronic effects on η^6 metal coordination was implemented. Therefore, electronic deficient **18-***CF$_3$* and electron rich **18-***OMe* were synthesized in the same manner as **18-***H*. A double Heck reaction in DMF at 100 °C of **17** with (trifluoromethyl)styrene or 4-methoxystyrene afforded **18-***CF$_3$* and **18-***OMe* in

40% and 45% yield, respectively. Next, **18-*CF₃*** and **18-*OMe*** were treated with [CpRu(NCMe)₃]PF₆, which led to the formation of **19-*CF₃*** as yellow needles and **19-*OMe*** as red block crystals (Scheme 2.7). Both compounds were characterized by X-ray crystallography (Figure 2.7 and Figure 2.8) and the structures of **19**-*CF₃* and **19**-*OMe* were also examined by computational analysis using a PB86/Def2-TZVPP(THF) basis set.[14]
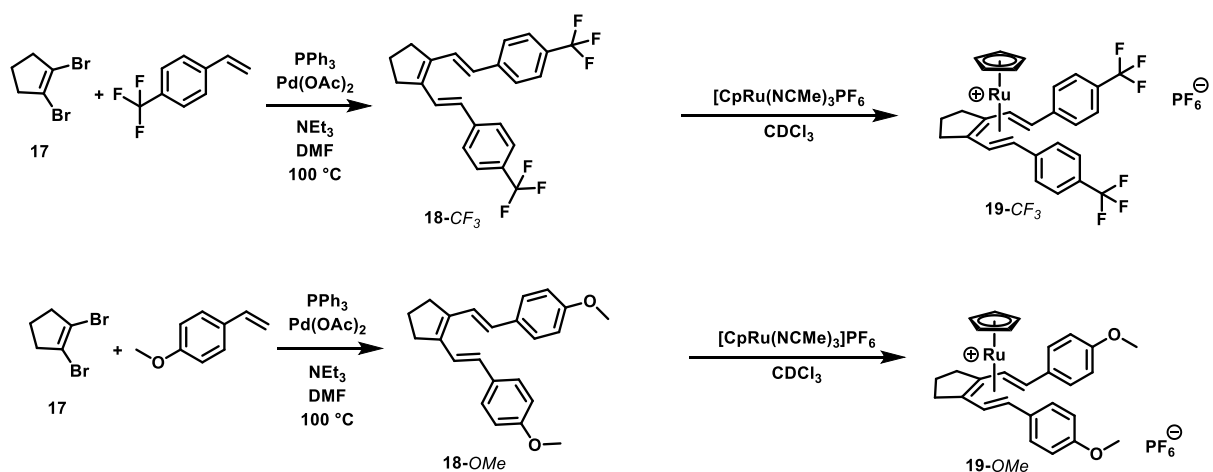
Scheme 2.7. Synthesis of η^6-triene complexes **19-*CF₃*** and **19-*OMe***.

The ¹H NMR spectrum (DC₂Cl₂) of **19-*CF₃*** exhibited diagnostic resonances at δ 4.87 (s, 5H, Cp), 6.65 (d, J = 10.2 Hz, 2H, =CHAr) and 3.54 (d, J = 10.2 Hz, 2H, CH=C*H*Ar). These resonances may be compared with the corresponding vinyl hydrogen resonance of the free triene **18-*CF₃***, which are observed at δ 7.46 (d, J = 15.7 Hz, 2H) and 6.59 (d, J = 15.7 Hz, 2H). Also, comparison of the ¹³C NMR chemical shift of the internal sp² alkene carbons reveals that the carbon resonance is shifted upfield to δ 119.3 relative to the free triene **18-*CF₃*** at 135.7. Thus, the NMR data support an η^6-triene structure for **19-*CF₃***.
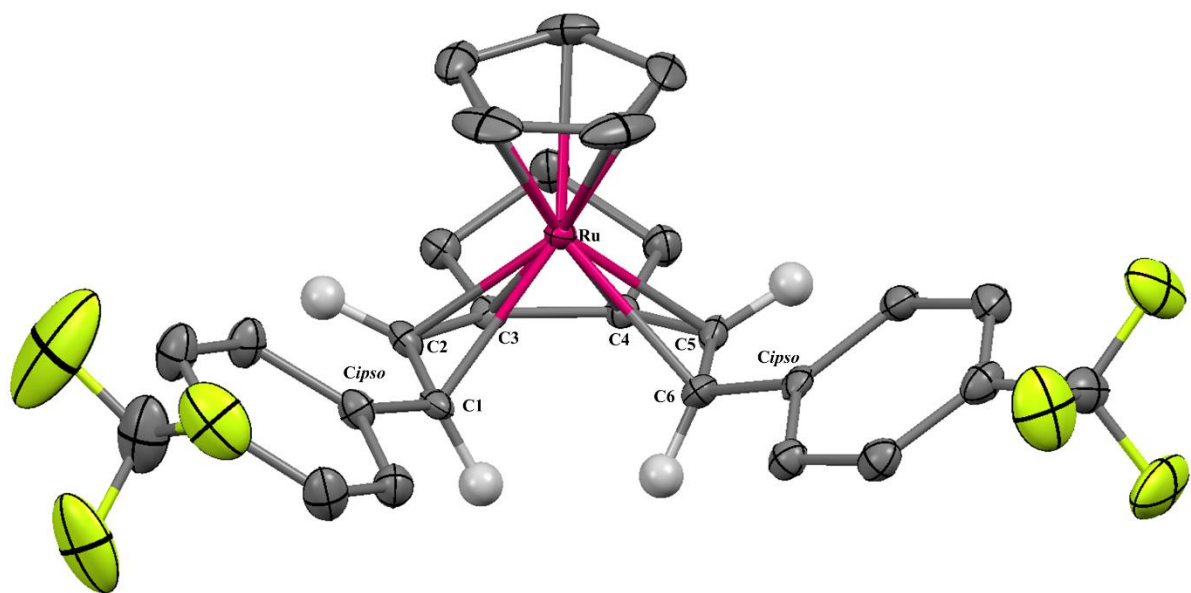
Figure 2.7. ORTEP drawing of **19-***CF₃*. Most of the hydrogens and the counter-ion have been omitted for clarity.

As observed for **19-***H*, **19-***CF₃* adopts a shallow boat conformation, with a fold angle of 17.0(7)° (calcd 15.1°). Also, all the bond lengths of the triene system are significantly delocalized as evidenced by similar bond lengths: 1.408(8), 1.423(7), 1.441(7), 1.428(6) and 1.412(6) for bonds C1-C2, C2-C3, C3-C4, C4-C5 and C5-C6, respectively. All the bond angles, bond distances and torsions are indistinguishable at the 3σ level of statistical analysis from those of **19-***H*. Thus, the electron deficient triene **19-***CF₃* does not significantly change the bond metrics related to hexahapto binding of ruthenium.

Table 2.4. Selected Bond Distances (Å) for **19-***CF₃* and **19-***CF₃-calc**

Bond (A-B)	Length (Å)*	Bond (A-B)	Length (Å)*
Ru-C1	2.290(5) [2.335]	C1-C2	1.408(8) [1.415]
Ru-C2	2.193(5) [2.202]	C2-C3	1.423(7) [1.431]
Ru-C3	2.243(4) [2.273]	C3-C4	1.441(7) [1.442]
Ru-C4	2.239(4) [2.270]	C4-C5	1.428(6) [1.430]
Ru-C5	2.190(4) [2.201]	C5-C6	1.412(6) [1.414]
Ru-C6	2.290(4) [2.340]	C1--C6	2.838(7) [2.915]

*19-*CF₃-calc* was calculated with PB86/Def2-TZVPP(THF) - calculated values are in brackets

Table 2.5 Selected Angles and Torsion Angles (°) for **19-***CF₃* and **19**-*CF₃-calc**

Angle	Degrees (°)	Angle	Degrees (°)
C1-Ru-C6	76.6(2) [77.2]	C*ipso*-C1-C2-C3	167.8(5) [171.9]
C1-C2-C3	125.1(5) [128.9]	C*ipso*-C6-C5-C4	166.7(4) [172.9]
C4-C5-C6	129.3(4) [127.4]	Fold angle**	17.0(7) [15.1]

*19-*CF₃-calc* was calculated with PB86/Def2-TZVPP(THF) - calculated values are in brackets.
** Fold angle between C1-C2-C3 and C1-C3-C4-C6 mean plane.

Next analysis of **19**-*OMe* was conducted by NMR spectroscopy. Interestingly, the reaction of **19**-*OMe* with [CpRu(NCMe)₃]PF₆ gave rise to a 3:1 diastereomeric ratio of η^6-triene complexes **19**-*OMe-meso* (major) and **19**-*OMe-rac* (minor). For **19**-*OMe-meso* a new Cp resonance was observed at δ 4.76 (s, 5H) and vinyl hydrogens resonances were observed at δ 6.46 (d, *J* = 10.3 Hz, 2H) and 3.71 (d, *J* = 10.3 Hz, 2H). For **19**-*OMe-rac* the Cp resonance was observed at δ 4.72 (s, 5H) and vinyl hydrogen resonances were observed at 7.09 (d, *J* = 13.7 Hz, 1 H), 6.19 (d, *J* = 10.3 Hz, 1H), 4.88 (d, *J* = 10.3 Hz, 1H) and 3.63 (d, *J* = 13.5 Hz, 1H). Hence, the NMR data supports *s-cis* and *s-trans* conformers of **19**-*OMe*.

X-ray crystallographic analysis of **19**-*OMe* fortuitously led to a disordered structure, consisting of 50% occupancy of each isomer (Figure 2.8). The crystal structure supports the NMR data in which one of the alkenes adopts an *s-cis* conformation (**19**-*OMe-meso*) with respect to the internal alkene, whereas the other alkene adopts an *s-trans* conformation (**19**-*OMe-rac*).

Isomer **19**-*OMe-meso*, like the previous hexahapto complexes, adopts a shallow boat conformation with a fold angle of 13.7(9)° (calcd 17.1°). The bond lengths of the **19**-*OMe-meso* isomer are significantly delocalized, as evidenced by similar bond lengths of 1.411(4), 1.431(4), 1.415(4), 1.436(7) and 1.411(9) Å for bonds C1-C2, C2-C3, C3-C4, C4-C5 and C5-C6, respectively. Lastly the C1--C6 nonbonded distance is 2.881(7) Å and the C1-Ru-C6 bond angle is 76.7(2)°.
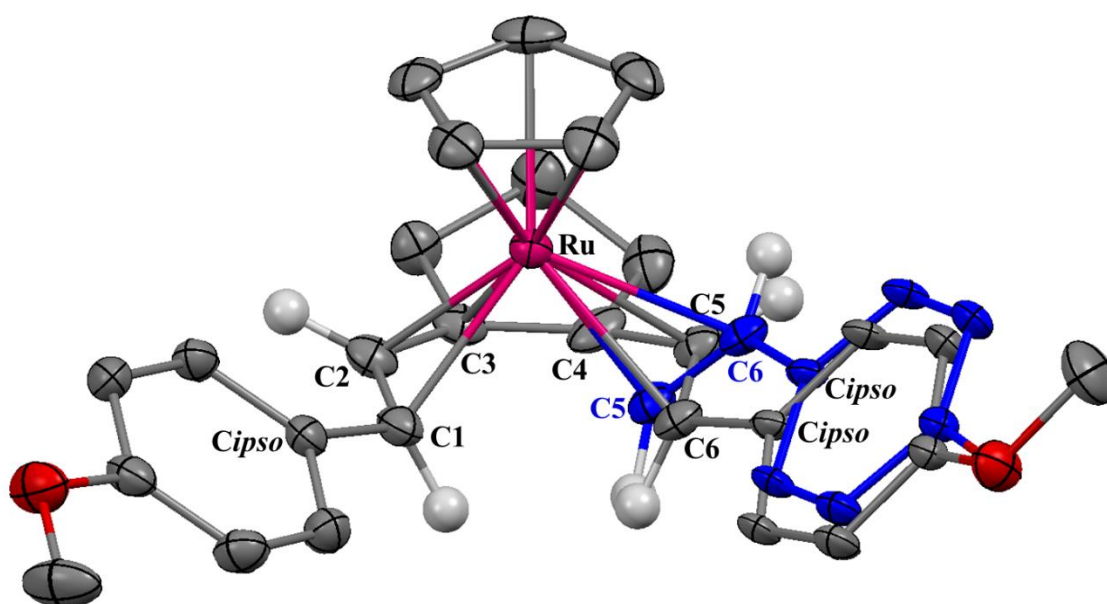
Figure 2.8. ORTEP drawing of **19-**OMe. Most of the hydrogens and the counter-ion have been omitted for clarity. **19-**OMe-rac (*s-trans)* conformer is labeled in blue.

Table 2.6. Selected Bond Distances (Å) for **19-***OMe* and **19-***OMe-calc**

Bond (A-B)	Length (Å)*	Bond (A-B)	Length (Å)*
Ru-C1	2.300(3) [2.383]	C1-C2	1.411(4) [1.413]
Ru-C2	2.189(3) [2.207]	C2-C3	1.431(4) [1.431]
Ru-C3	2.233(3) [2.258]	C3-C4	1.415(4) [1.442]
Ru-C4	2.221(3) [2.259]	C4-C5[a]	1.436(7) [1.432]
Ru-C5[a]	2.230(7) [2.207]	C5-C6[a]	1.411(9) [1.413]
Ru-C6[a]	2.344(6) [2.384]	C1--C6[a]	2.881(7) [2.951]
Ru-C5[b]	2.167(7) [2.244]	C4-C5[b]	1.516(7) [1.454]
Ru-C6 [b]	2.379(6) [2.587]	C5-C6[b]	1.360(1) [1.396]
		C1--C6[b]	3.697(7) [3.771]

*19-*OMe-calc* was calculated with PB86/Def2-TZVPP(THF) - calculated values are in brackets.
[a]**19-***OMe-meso*,[b]**19-***OMe-rac*.

Table 2.7 Selected Angles and Torsion Angles (°) for **19-***OMe* and **19-***OMe-calc**

Angle	Degrees (°)	Angle	Degrees (°)
C1-Ru-C6[a]	76.7(2) [76.5]	C*ipso*-C1-C2-C3	170.4(3) [172.7]
C1-C2-C3[a]	126.7(3) [128.7]	C*ipso*-C6-C5-C4[a]	-170.1(6) [-172.7]
C4-C5-C6[a]	121.2(6) [128.9]	Fold angle[a]**	13.7(9) [17.1]
C1-Ru-C6[b]	104.4(2)]100.4]	C*ipso*-C6-C5-C4[b]	173.8(6) [178.8]
C4-C5-C6[b]	113.4(5) [121.2]	Fold angle[b]**	25.9(7) [21.7]

*19-*OMe-calc* was calculated with PB86/Def2-TZVPP(THF) - calculated values are in brackets.
** Fold angle between C1-C2-C3 and C1-C3-C4-C6 mean plane. [a]**19-***OMe-meso* [b]**19-***OMe-rac*.

Comparing **19**-*OMe-rac* to **19**-*OMe-meso*, the **19**-*OMe-rac* isomer has a longer C4-C5 bond length of 1.516(7) Å and a shorter C5-C6 bond length of 1.360(1) Å. Also, the Ru-C6 bond of the **19**-*OMe-rac* isomer is longer by 0.034(7) Å with a length of 2.379(6) Å (calcd 2.587 Å). Lastly, the non-bonded C1--C6 distance for **19**-*OMe-rac* is 0.816(7) Å longer than the **19**-*OMe-meso* isomer with a non-bonded C1--C6 distance of 3.697(7) Å. The calculated Ru-C6 bond length is unusually long (calcd 2.587 Å). There are two examples in the literature of bond lengths that are similar: ruthenocene-stabilized carbocation **22** and half-sandwich ruthenium complex **23** (Figure 2.9).[26,27] Ruthenocene-stabilized carbocation **22** has a Ru1-C11 bond length of 2.604(8) Å and the carbocation is stabilized by resonance within the [(η^6-fulvene)(η^5-cyclopentadienyl)ruthenium]

cation. Ruthenium complex **23** has a Ru-C4 bond length of 2.608(5) Å, which corresponds to the

preference of the azapentadienyl ligand to engage in lone pair coordination by the nitrogen atom,

in tandem with η^3-allyl coordination.
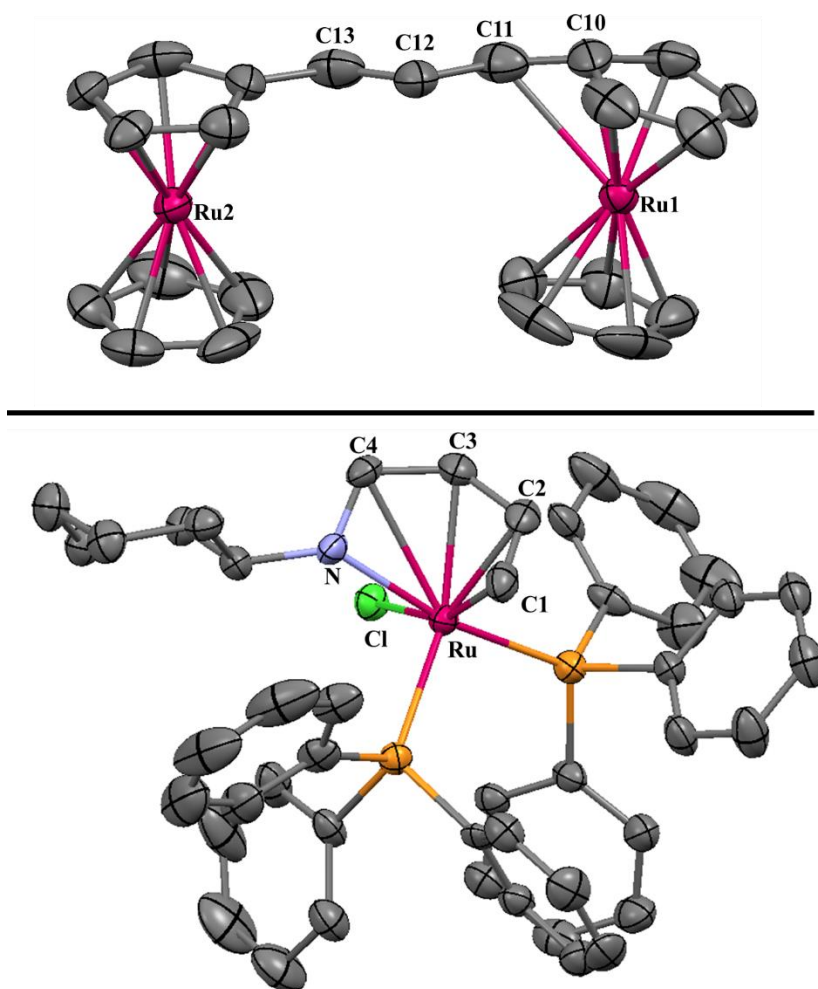
Figure 2.9. ORTEP drawing of **22** (top) and **23** (bottom). Counter-ion for **22** is omitted and all hydrogens have been omitted for clarity.[26,27]

Interestingly in the literature, CpRu(II) fragments coordinated in η^4-*s-trans* fashions to 1,3-

dienes are rare. To the best of our knowledge, there is only one example of a CpRu(II) fragment

coordinated to a conjugated diene in an *s-trans* fashion.[28] Green and co-workers synthesized *s-*

trans diene complexes **26** and **27** via protonation of **24** and **25** (Scheme 2.8). However, **26** and **27**

were not isolated, but instead were characterized *in situ* by comparison of their ^{1}H NMR chemical shifts and *J* values of with known *s-cis* isomers **28** and **29**. Identification was based on two spectroscopic features associated with the *s-cis* geometry: a higher *J* value for *J* (H^b-H^c) across the central double bond and a downfield shift of the signals arising from the exposed protons H^a and H^e (Table 2.8).
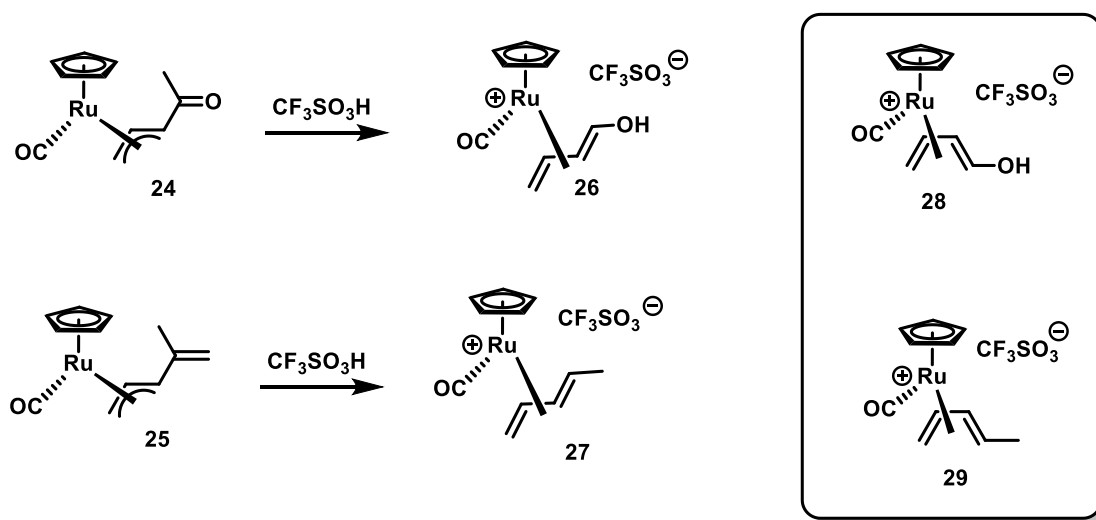
Scheme 2.8. Synthesis of *s-trans* diene complexes **26** and **27**.

Table 2.8. ^{1}H NMR spectroscopic data for the diene complexes **26**, **27**, **28** and **29**.

R = Me, OH
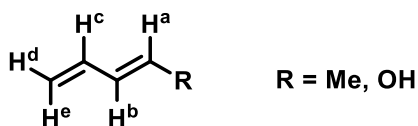
Complex	δ H^a (ppm)	δ H^e (ppm)	*J* (Hb-HC) Hz
26	8.05	3.65	8.1
27	4.84	4.31	7.7
28	5.48	1.64	6.3
29	2.65	1.65	5.8

The η^4-*s-trans*-diene coordination mode had originally only been identified in early-metal complexes.[29,30] Nevertheless, Ernst, Meléndez and Mashima have reported preferential *s-trans*

diene coordination in ruthenium(II) acetylacetonate ($Ru(acac)_2$) compounds **30**, **31** and **32** (Figure 2.10).[31–33] These compounds were all isolated and characterized by X-ray crystallography. Meléndez and Ernst suggested that *trans*-diene coordination occurs when the ligand to metal bond interaction (ligand sigma donation) is more important than the metal to ligand (π-back-bonding) interaction, as better ligand to metal donation makes the metal center more electron rich. In our case for the **19**-*OMe-rac* isomer, this rational could be invoked since the **19**-*OMe* complex is more electron donating than **19**-*CF₃* and **19**-*H*. Therefore, evidence suggests that the barrier for *s-cis* to *s-trans* conformational change is lower in **19**-*OMe* than its electron deficient counterparts, **19**-*CF₃* and **19**-*H*.
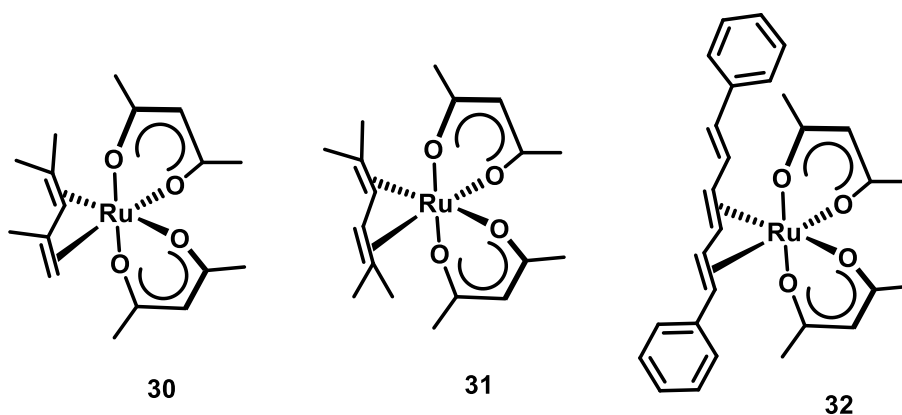
Figure 2.10. Known $Ru(\eta^4\text{-}trans\text{-diene})$ complexes.

6. Equilibrium Experiments

Given that the **19**-*OMe* crystallographic analysis led to a disordered structure, consisting of 50% occupancy of each isomer, and the ^{1}H NMR data revealed a 3:1 ratio of **19**-*OMe-meso* to **19**-*Ome-rac*, it was proposed that the isomers exist in equilibrium. Therefore, a variable temperature ^{1}H NMR experiment was conducted on **19**-*OMe*. 2.0 mg (0.0031 mmol) of **19-**-*OMe* and 1,3,5-tri-*tert*-butylbenzene (internal standard) were added to a J. Young tube. The tube was placed under vacuum on a high vacuum line and the tube was cooled to -78 °C in a dry ice acetone bath. Dry, degassed CD_2Cl_2 (1 mL) was distilled into the tube and the tube was kept at -78 °C until the NMR spectrometer probe was cooled to -60 °C. The J. Young tube was then quickly placed into the NMR spectrometer. Temperature points were taken at -60 °C, -50 °C, -40 °C, -30 °C, -20 °C, -10 °C, 0 °C, 10 °C and 20 °C. Ratio of the diastereomers were determined via integration of the vinyl hydrogens at δ 6.34 (**19**-*OMe-meso*) and 6.12 (**19**-*OMe-rac*) with respect to the internal standard. At each temperature point, the sample was allowed to equilibrate for 15 min to ensure a uniform temperature of the reaction mixture. At -60 °C, the ration of **19**-*OMe-meso* to **19**-*OMe-rac* was 0.90:1.00, which is consistent with X-ray analysis. Upon warming to 20 °C, the equilibrium ratio was reestablished, therefore the diastereomers exist in equilibrium with each other (Figure 2.11 and Table 2.7).
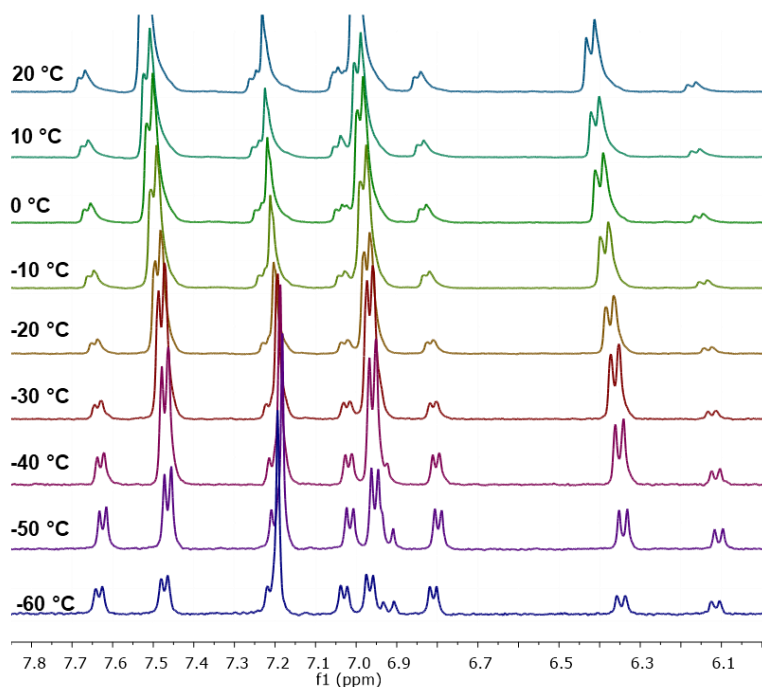
Figure 2.11. Variable temperature ^{1}H NMR of **19**-*OMe*, CD_2Cl_2, 500 MHz.

Table 2.9. Ratios of **19**-*OMe-meso* to **19**-*OMe-rac* at variable temperature.

Temperature (°C)	19-*OMe meso;rac* ratio
-60	0.90:1.00
-50	1.00:1.00
-40	2.00:1.00
-30	2.90:1.00
-20	3.30:1.00
-10	3.30:1.00
0	3.30:1.00
10	3.30:1.00
20	3.30:1.00

Computational analysis was conducted to determine the energy difference between **19**-*OMe-meso* and **19**-*OMe-rac* using a bp86Def2TZVPP(DCM) basis set and it was calculated that **19**-*OMe-meso* is -0.39 kcal/mol more stable in energy.[14] Thus, based on computational analysis one would predict a 2:1 ratio of *meso* to *rac* isomers at room temperature. The calculations are in

47

line with the room temperature experimental ratio of 3.3:1 *meso* to *rac* isomers. Thus, experimentally the **19**-*OMe-meso* isomer is -0.71 kcal/mol more stable in energy. Next, computational analysis was conducted utilizing a bp86Def2TZVPP(DCM) basis set on the equilibrium between **19**-*CF₃* and **18**-*OMe* yielding **18**-CF₃ and **19**-*OMe* (Scheme 2.9).[14] Calculations revealed that ΔG° = -3.64 kcal/mol, thus the equilibrium lies to the right of the reaction equation.
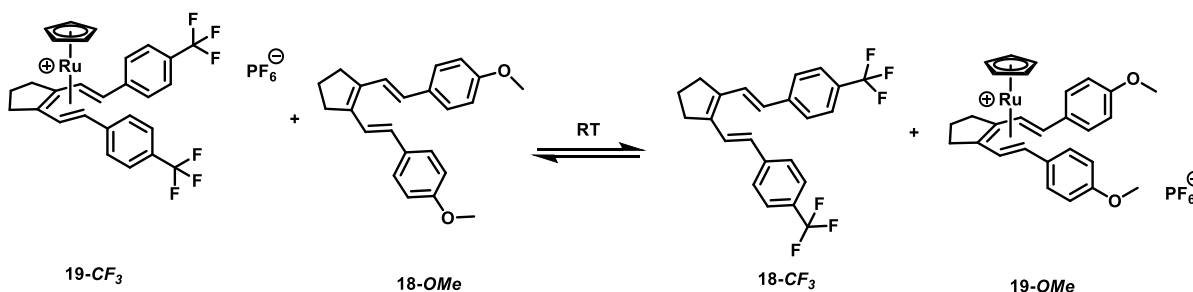
Scheme 2.9. Equilibrium experiment with **19**-*CF3* and **18**-*OMe.*

Following computational analysis, the experimental ratio was calculated via a ¹H NMR equilibrium experiment utilizing the equation: ΔG° = – RT ln K$_{eq}$. 3.0 mg (0.0052 mmol) of **19**-*CF₃* and 1.7 mg (0.0052 mmol) of **18**-*OMe* with 1,2,5-tri-*tert*-butylbenzene (internal standard) were added to a J. Young NMR tube and placed under vacuum on a high vacuum line. Then, dry, degassed CD₂Cl₂ was distilled to the tube. The tube was then taken immediately to the NMR spectrometer so a spectrum could be obtained on the reaction mixture. Time points were taken at 5 min, 7 h and 24 h (Figure 2.12). Ratios of the ruthenium complexes were determined via integration of the vinyl hydrogen resonances at *δ* 3.53 (**19**-*CF₃*) and 3.66 (**19**-*OMe-meso*) with respect to the internal standard (Table 2.8). At t = 5 minutes the ratio of **19**-*CF₃* to **19**-*OMe* was 1.0:0.0. After 24 h, the ratio of **19**-*CF₃* to **19**-*OMe* was 0.0:1.0 (3:1 ratio of **19**-*OMe-meso*:**19**-

OMe-rac) by ^{1}H NMR analysis. The ^{1}H NMR instrument sensitivity would allow one to see approximately a 96:4 ratio of two compounds at equilibrium, thus a 96:4 ratio of **19**-*OMe*: **19**-*CF₃* would lead to energy difference of 1.9 kcal/mol. Therefore, we can conclude that $\Delta G°$ must be greater than -1.9 kcal/mol. From this experiment we can conclude that the **19**-*OMe* complex must be -4.1 kcal/mol more stable in energy than the **19**-*CF₃* complex because a 4.1 kcal/mol energy difference leads to a 99.9:0.1 ratio of two species at equilibrium.
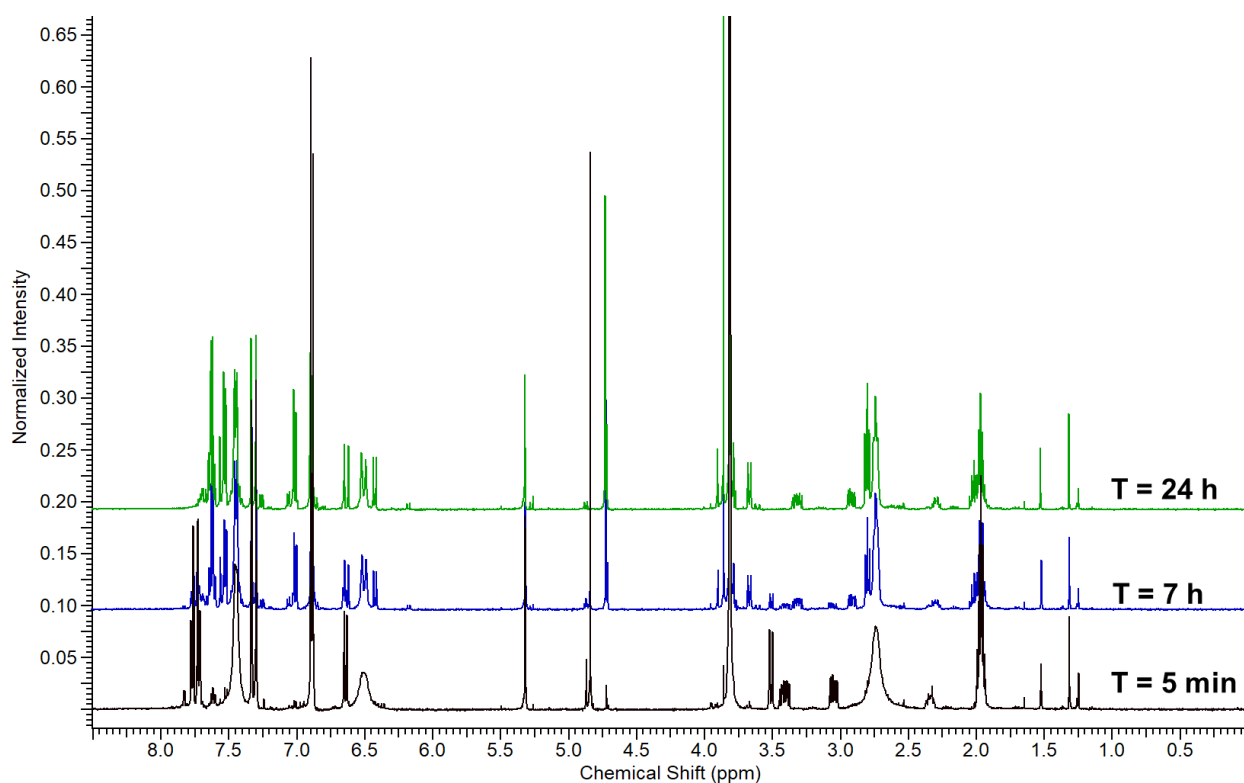
Figure 2.12. Equilibrium experiment with **19**-*CF₃* and **18**-*OMe*. Time pointes were taken at 5 min, 7 h and 24 h. Ratios were calculated via the integration of the vinyl (^{1}H NMR DC₂Cl₂, 500 MHz).

Table 2.10. Ratios of **19**-*CF₃* to **19**-*OMe-meso* at time points 5 min, 7 h and 24 h.

Time	18-*CF₃*: 18-*OMe-rac*
5 min	1.0:0.0
7 h	1.0:2.3
24 h	0.0:1.0

C. Conclusions and Future Directions

In conclusion, we have demonstrated, by computational analysis, that hexahapto transition metal coordination to 1,3,5-hexatrienes accelerates 6π electrocyclizations by lowering the activation energy barrier from 27.7 kcal/mol to 17.7 kcal/ mol. Also, comparing transition state structures for the ruthenium mediated process, **11/12**^{TS}, and the free hexatriene, **14**^{TS}, demonstrates a decrease in the non-bonded C1--C6 distance from 2.278 Å to 2.101 Å. Complexation also flattens the boat conformation from 27.0° to 19.2°, most likely in order to optimize metal d-orbital overlap with the triene p orbitals.

The first examples of η^6-acyclic triene complexes (**19**-*H*, **19**-*CF₃*, **19**-*OMe-meso* and **19**-*OMe-rac)* were prepared by reaction of [CpRu(NCMe)₃]PF₆ with 1,2-divinylcyclopent-1-ene derivatives, **18**-*H*, **18**-*CF₃* and **18**-*OMe*. The four triene complexes were characterized in solution by NMR spectroscopy and in the solid state by X-ray crystallography. The structures and energetics were further analyzed by computation. The more electron rich triene, **19**-*OMe,* exhibited *s-cis* and *s-trans* isomers in a 3.3:1 ratio. The *s-trans* isomer, **19**-*OMe-rac* exhibited a very long calculated Ru-C6 bond of 2.587 Å. Variable temperature ^{1}H NMR experiments were conducted on **18**-*OMe*, which established that the *meso* and *rac* isomers exist in equilibrium with each other at room temperature. Lastly, equilibrium experiments were conducted on **19**-*CF₃* and **18**-*OMe,* establishing that the ruthenium complex **19**-*OMe* is -4.1 kcal/mol more stable than the **19**-*CF₃* ruthenium complex.

Future work for this project will explore the potential role that hexahapto triene complexes may play in metal-accelerated 6π electrocyclization reactions. For example, a more electron rich triene such as 4,4'-((1E,1'E)-cyclopent-1-ene-1,2-diylbis(ethene-2,1-diyl))bis(N,N-dimethylaniline) (**24**) should be synthesized to further examine the electronic effects of the *s-cis*

to *s-trans* conformational change upon η^6 metal coordination. Lastly, 1,2-divinylcyclopent-1-ene (**25**) should be synthesized (Figure 2.13). Compound **25** can then be treated with [CpRu(NCMe)$_3$]PF$_6$ at low temperature to observe an agostic interaction via ^{1}H NMR spectroscopy or X-ray crystallography. If an agostic interaction is observable this intermediate could provide insight into our proposed mechanism: η^6-triene coordination followed by a concerted 6π electrocyclization and ruthenium-assisted protolytic C-H bond cleavage to form arene products.
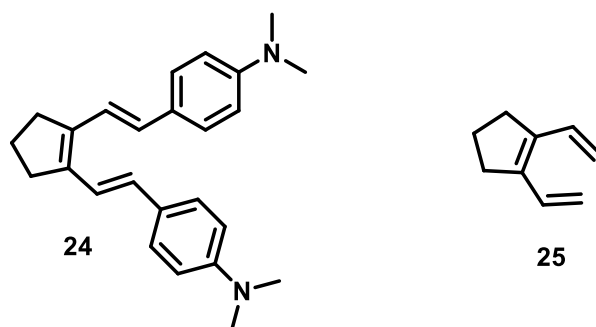
Figure 2.13. Future substrates of interest.

D. Experimental

1. General Methods:

Reagents were obtained from Aldrich, Fisher Scientific, Alfa Aesar, or Fluka, and were used without further purification unless stated otherwise. All solvents were obtained from Fisher scientific and dried on Alumina columns prior to use. Chromatography solvents were ACS technical grade and used without further purification. All reactions were performed using standard Schlenk techniques or in nitrogen filled Vacuum Atmospheres or MBraun glovebox, unless otherwise stated. ^{1}H and ^{13}C NMR spectra were recorded on a Bruker AVA 300 MHz, Varian Mercury Plus 400 MHz, Varian VX 500 MHz or JOEL ECA 500 MHz instruments. Chemical shifts are reported as δ in units of parts per million (ppm) referenced to residue solvent peak. Coupling constants are reported as a J value in Hertz (Hz). Mass spec analysis was performed by the UCSD Chemistry and Biochemistry Molecular Mass Spectrometry Facility on a ThermoFinnigan LCQdeca mass spectrometer with an atmospheric pressure electrospray ionization (APCI) source or an electrospray ionization (ESI) source. Infrared spectra were obtained on a Nicolet iS10 FT-IR. All solvents were dried by refluxing over calcium hydride for 24 h and then subsequently distilled under static vacuum into oven dried Schlenk storage tubes. Deuterated solvents were degassed using a Freeze-Pump-Thaw procedure, typically 5 cycles.

2. Synthesis of Compounds:

Synthesis of 1,2-Dibromocyclopentene (17): To a flame-dried three-neck 500 mL flask, equipped with a stir bar and rubber septum, phosphorus pentachloride (55.0 g, 0.264 mol) and toluene (120 mL) were added. Under a nitrogen atmosphere, cyclopentanone (20.2 g, 0.240 mmol, 21.2 mL) was slowly added over a period of 30 min. The reaction mixture was cooled to -20 °C and bromine (31.3 g, 0.196 mol, 10.0 mL) was added dropwise over the course of 30 min via an addition funnel.

The reaction mixture was allowed to stir for an additional 20 min and then the solvent was removed by concentrating *in vacuo*. The residue was dissolved in hexane (40 mL) and cooled to -25 °C. A solution of potassium *t*-butoxide (27.8 g, 0.248 mol) in THF (120 mL) was slowly added over a period of 30 min after which the mixture was allowed to warm to room temperature. Water (120 mL) and hexanes (80 mL) were added to the suspension and the suspension was filtered through a plug of Celite. The mixture was extracted with hexanes (3 x 300 mL) and the combined organic layers were washed once with brine (200 mL) and dried over $MgSO_4$. The organic layers were filtered and concentrated *in vacuo*. The crude material was purified by high vacuum distillation (65 °C at 1.2 mmHg) to give known compound **17** as a colorless viscous liquid (19.1 g, 35%). ^{1}H NMR (300 MHz, CDCl$_3$) δ 2.63 (d, J_{HH} = 7.5 Hz, 4H, CH$_2$), 2.12-2.01 (m, 2H, CH$_2$)**.**
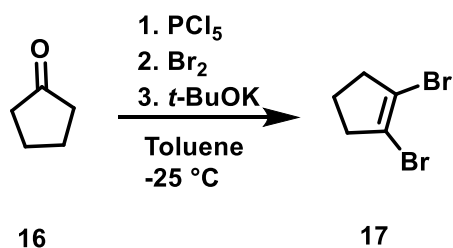
Synthesis of 1,2-di((E)-styryl)cyclopent-1-ene (18-*H*): To an oven dried 100 mL high pressure tube equipped with a stirbar and rubber septum, commercially available 1,2-dibromocyclopent-1-ene (500 mg, 2.21 mmol), DMF (10 mL) and NEt$_3$ (10 mL) were added, and the reaction mixture was purged by bubbling N$_2$ though the solution for 15 min. Under a steady stream of N$_2$, PPh$_3$ (232 mg, 0.885 mmol) and Pd(OAc)$_2$ (39 mg, 0.18 mmol) were added to the stirred solution. The mixture was allowed to stir for 10 min under N$_2$ before styrene (1.15 g, 11.07 mmol, 1.28 mL) was added via syringe. The needle-valve was sealed and the reaction mixture was allowed to stir at room temperature for 15 min and at 100 °C for 12 h. After cooling the reaction vessel to room temperature, the reaction mixture was diluted with ether (100 mL) and washed with water (3 x 100

mL). The organic layers were washed once with brine (100 mL) and dried over MgSO$_4$ and the solvent was concentrated *in vacuo* and the residue was purified by silica gel column chromatography in hexanes. The product was recrystallized from ethanol to give known **18-*H*** as thin yellow needles (240 mg, 40% yield). ^{1}H NMR (400 MHz, CDCl$_3$) δ 7.50 (d, J_{HH} = 7.1 Hz, 3H, aryl), 7.42 (d, J_{HH} = 15.8 Hz, 2H, HC=C), 7.35 (t, J_{HH} = 7.6 Hz, 3H, aryl), 7.29 – 7.20 (m, 4H, aryl), 6.56 (d, J_{HH} = 15.7 Hz, 2H, HC=C), 2.77 (t, J_{HH} = 7.6 Hz, 4H, CH$_2$), 2.05 (quint, J_{HH}=7.33 Hz, 2H, CH$_2$).

18-*H*
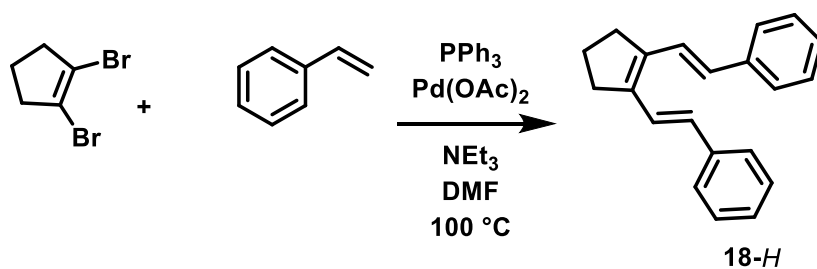
Synthesis of 1,2-di((E)-styryl)cyclopent-1-ene (18-*CF$_3$*): To an oven dried 100 mL high pressure tube equipped with a stirbar and rubber septum, commercially available 1,2-dibromocyclopent-1-ene (480 mg, 2.13 mmol), DMF (10 mL) and NEt$_3$ (10 mL) were added to the flask and the flask was purged by bubbling N$_2$ though the solution for 15 min. Under a steady stream of N$_2$, PPh$_3$ (223 mg, 0.852 mmol) and Pd(OAc)$_2$ (48 mg, 0.21 mmol) were added. The reaction mixture was allowed to stir for 10 min before commercially available 1-(trifluoromethyl)-4-vinylbenzene (1.10 g, 6.4 mmol, 0.94 mL) was added via syringe. The needle valve was sealed and the reaction mixture was allowed to stir at room temperature for 15 min and at 100 °C for 12 h. The solution was diluted with ether (100 mL) and washed with water (3 x 100 mL). The organic layers were washed once with brine (100 mL) and was dried over MgSO$_4$. The solvent was concentrated *in vacuo* and the residue purified by silica gel column chromatography in hexanes. The product was recrystallized from ether to give **18-*CF$_3$*** as yellow block crystals (348 mg, 40% yield). ^{1}H NMR (400 MHz,

CDCl$_3$) δ 7.70 – 7.51 (m, 8H, aryl) 7.46 (d, J_{HH} = 15.8 Hz, 2H, HC=C), 6.59 (d, J_{HH} = 15.7 Hz, 2H, HC=C), 2.79 (t, J_{HH} = 7.5 Hz, 4H, CH$_2$), 2.10 – 1.88 (quint, J_{HH} = 7.33 Hz, 2H, CH$_2$). ^{13}C\{^{1}H\} NMR (100 MHz, CDCl$_3$) δ 140.85 (aryl), 140.50 (C=C), 136.40 (C=C), 131.89 (aryl), 128.51 (aryl), 126.26 (C=C), 125.34 (aryl), 123.89 (CF$_3$), 33.50 (CH$_2$), 21.25 (CH$_2$). IR (NaCl, thin film): 2967, 2925, 2848, 1612 cm^{-1}. GC-MS (EI) m/z calcd for [C$_{23}$H$_{18}$F$_6$]$^+$ 408.13; found 408.1. Elemental analysis: calcd: C: 67.64, H 4.44 Found: C: 67.26, H: 4.64.

18-*CF$_3$*
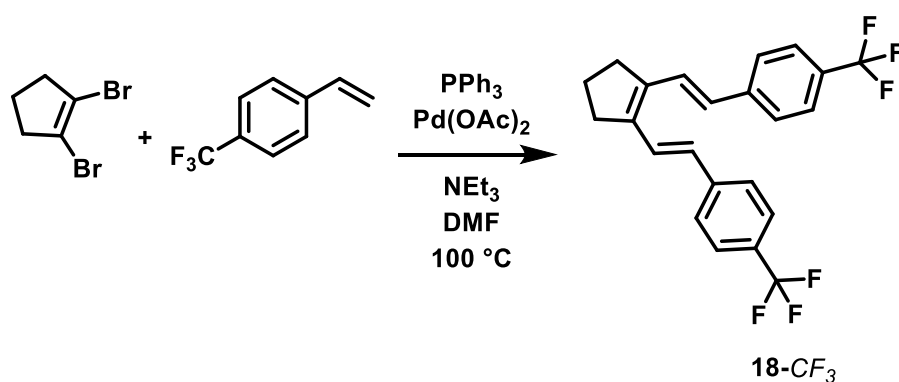
Synthesis of 1,2-di((E)-styryl)cyclopent-1-ene (18-*OMe*): To an oven dried 100 mL high pressure tube equipped with a stir bar and rubber septum, commercially available 1,2-dibromocyclopent-1-ene (500 mg, 2.21 mmol), DMF (10 mL) and NEt$_3$ (10 mL) were added to the flask and the reaction mixture was purged by bubbling N$_2$ though the solution for 15 min. Under a steady stream of N$_2$, PPh$_3$ (231 mg, 0.884 mmol) and Pd(OAc)$_2$ (50 mg, 0.22 mmol) were added. The reaction mixture was allowed to stir for 10 min and commercially available 1-methoxy-4-vinylbenzene (1.78 g, 13.27 mmol, 1.77 mL was added via syringe. The needle valve was sealed and the reaction was allowed to stir at room temperature for 15 min and at 100 °C for 12 h. The solution was diluted with ether (100 mL) and washed with water (3 x 100 mL). The organic layers were washed once with brine (100 mL) and dried over MgSO$_4$. The solvent was concentrated *in vacuo* and the residue was purified by silica gel column chromatography (1:9 EtOAc:hexanes).

The product was recrystallized from ether to give **18-***OMe* as yellow block crystals (330 mg, 45% yield). ^{1}H NMR (400 MHz, CDCl$_3$) δ 7.43 (d, J_{HH} = 8.5 Hz, 4H, aryl), 7.28 (d, J_{HH} = 15.6 Hz, 2H, HC=C), 6.89 (d, J_{HH} = 8.8 Hz, 4H, aryl), 6.49 (d, J_{HH} = 15.8 Hz, 2H, HC=C), 3.83 (s, 6H, O-CH$_3$), 2.74 (t, J_{HH} = 7.5 Hz, 4H, CH$_2$), 1.97 (quint, J_{HH} = 7.33, 2H, CH$_2$). ^{13}C{^{1}H} NMR (100 MHz, CDCl$_3$) δ 158.80 (aryl), 138.48 (C=C), 130.58 (C=C), 128.51 (aryl), 127.28 (aryl), 120.35 (C=C), 113.86 (aryl), 55.12 (O-CH$_3$), 33.54 (CH$_2$), 21.32 (CH$_2$). IR (NaCl, thin film) 3022, 3002, 2949, 2932, 2832, 1602 cm^{-1}. ESI-TOFMS (*m/z*) calcd for [C$_{23}$H$_{25}$O$_2$]$^+$ 333.1849; found 333.1851.
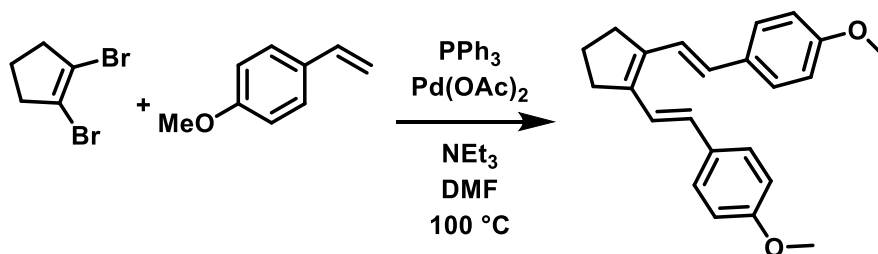
18-*OMe*

Synthesis of (η^5-cyclopentadienyl)(η^6-1,2-di((*E*)-styryl)cyclopent-1-ene)ruthenium(II) Hexafluorophosphate (19-*H*): To a J. Young tube **18-*H*** (18.0 mg, 0.066 mmol), and Tris(acetonitrile)cyclopentadienylruthenium(II) hexafluorophosphate (20.5 mg, 0.047 mmol) were added. The J. Young tube was sealed and evacuated on the Schlenk line. Dry, degassed CDCl$_3$ (1 mL) was then subsequently distilled into the J. Young tube on the Schleck line under static vacuum. The tube was kept at 0 °C and vortexed vigorously to dissolve all solids. The tube was left to stand for 1 hr at 0 °C which allowed the formation of orange block crystals. Filtration led to the isolation of **19-*H*** as an orange crystalline solid (22 mg, 83 % yield). ^{1}H NMR (300 MHz, CD$_2$Cl$_2$) δ 7.64 (d, J_{HH} = 7.70 Hz, 4 H, aryl), 7.54 (t, *J* = 7.70 Hz, 4 H, aryl), 7.48 (d, *J* = 6.79 Hz, 1 H, aryl) 7.36 - 7.41 (m, 1 H, aryl) 6.58 (d, *J* = 10.3 Hz, 2 H, HC=C), 4.80 (s, 5 H, Cp) 3.66 (d, *J* = 10.3 Hz, 2 H, HC=C), 3.46-3.33 (m, 2 H, CH$_2$), 3.02 (dd, *J* = 17.24, 8.44 Hz, 2 H, CH$_2$), 2.27 -

2.46 (m, 1 H, CH$_2$), 1.87 - 2.14 (m, 1 H, CH$_2$). ^{13}C{^{1}H} NMR (100 MHz, CD$_2$Cl$_2$) δ 138.86 (aryl), 129.93 (aryl), 129.25 (aryl), 126.46 (aryl), 118.18 (C=C), 88.76 (Cp), 81.23 (C=C), 77.96 (C=C), 39.50 (CH$_2$), 23.98 (CH$_2$). IR (NaCl, thin film): 3120, 2966, 2913 2844, 1617 cm^{-1}. ESI-MS (*m/z*) calcd for [C$_{26}$H$_{25}$Ru]$^+$ 439.1001; found 439.1002.
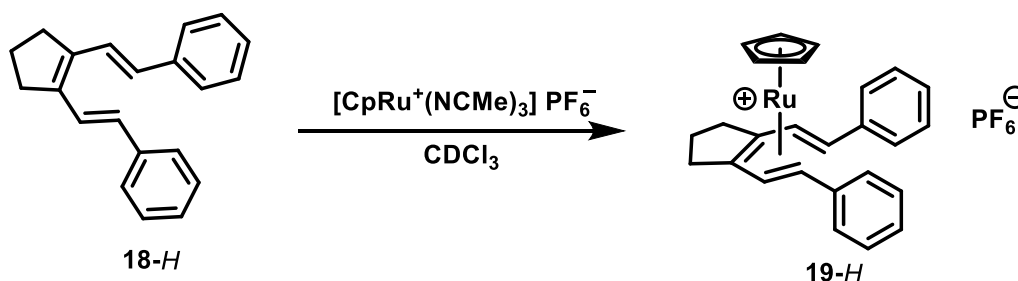
18-*H* [CpRu$^+$(NCMe)$_3$] PF$_6^-$, CDCl$_3$ → **19-*H***, PF$_6^\ominus$

Synthesis of (η^5-cyclopentadienyl)(η^6-1,2-bis((E)-4-(trifluoromethyl)styryl)cyclopent-1-ene) ruthenium(II) hexafluorophosphate (19-*CF$_3$*): To a J. Young tube compound **18-*CF$_3$*** (15.8 mg, 0.039 mmol), and Tris(acetonitrile)cyclopentadienylruthenium(II) hexafluorophosphate (12.6 mg, 0.029 mmol) were added. The J. Young tube was sealed and evacuated on the Schlenk line. Dry, degassed CDCl$_3$ (1 mL) was then subsequently distilled into the J. Young tube on the Schleck line under static vacuum. The tube was kept at 0 °C and vortexed vigorously to dissolve all solids. The tube was left to stand for 1 hr at 0 °C which allowed the formation of yellow needle crystals. Filtration led to the isolation of **19-*CF$_3$*** as a yellow crystalline solid (11.7 mg, 56% yield) ^{1}H NMR(400 MHz, CD$_2$Cl$_2$) δ 7.76 (dd, J_{HH} = 23.4, 8.3 Hz, 8H, aryl), 6.65 (d, J_{HH} = 10.2 Hz, 2H, HC=C), 4.87 (s, 5H, Cp), 3.54 (d, J_{HH} = 10.2 Hz, 2H, HC=C), 3.49 – 3.35 (m, 2H, CH$_2$), 3.06 (dd, J_{HH} = 15.8, 8.7 Hz, 2H, CH$_2$), 2.41-2.33 (m, 1H, CH$_2$), 2.02-1.93 (m, 1H, CH$_2$). ^{13}C{^{1}H} NMR (100 MHz, CD$_2$Cl$_2$) δ 150.71 (aryl), 142.75 (aryl), 126.85 (aryl), 126.83 (aryl), 126.68 (CF$_3$), 119.27 (C=C), 89.80 (Cp), 82.14 (C=C), 75.00 (C=C), 39.42 (CH$_2$), 23.90 (CH$_2$). IR (NaCl, thin

film) 2962, 2914, 2833, 1603 cm^{-1}. ESI-MS (*m/z*) calcd for for [C$_{28}$H$_{23}$F$_6$Ru]$^+$ 575.0747; found 575.0754.
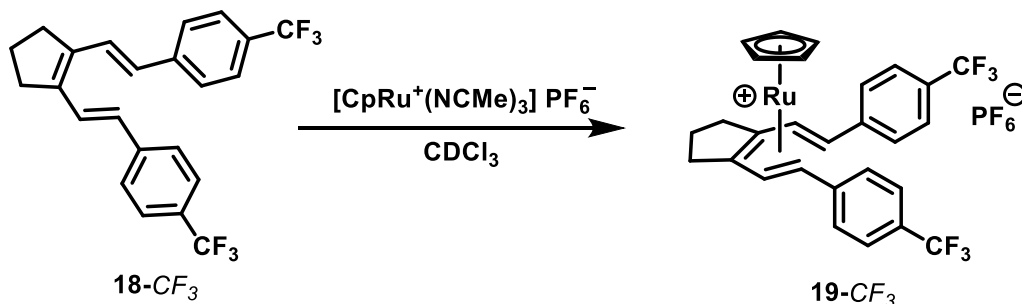
Synthesis of (η^5-cyclopentadienyl)(η^6-1,2-bis((E)-4-methoxystyryl)cyclopent-1-ene) ruthenium(II) hexafluorophosphate (19-*OMe*): To a J. Young tube compound **18-*OMe*** (20 mg, 0.060 mmol), and Tris(acetonitrile)cyclopentadienylruthenium(II) hexafluorophosphate (19.6 mg, 0.045 mmol) was added. The J. Young tube was sealed and evacuated on the Schlenk line. Dry, degassed CDCl$_3$ (1 mL) was then subsequently distilled into the J. Young tube on the Schleck line under static vacuum. The tube was kept at 0 °C and vortexed vigorously to dissolve all solids. The tube was left to stand for 1 hr at 0 °C which allowed the formation of red block crystals. Filtration led to the isolation of 18-*OMe* as a red crystalline solid. The product was formed as a mixture of diastereomers 3.0:1.0 (*meso:rac*). (13.5 mg, 60% yield). **19-*OMe-meso***: ^{1}H NMR (500 MHz, CD$_2$Cl$_2$) δ 7.56 (d, J_{HH} = 8.7 Hz, 4H, aryl), 7.04 (d, J_{HH} = 8.7 Hz, 4H, aryl), 6.46 (d, J_{HH} = 10.3 Hz, 2H, C=C), 4.76 (s, 5H, Cp), 3.89 (s, 6H, O-CH$_3$), 3.71 (d, J_{HH} = 10.3 Hz, 2H, C=C), 3.32 (ddd, J_{HH} = 16.1, 11.0, 7.8 Hz, 2H, CH$_2$), 2.93 (dd, J_{HH} = 16.0, 8.1, 2H, CH$_2$), 2.39 – 2.27 (m, 1H, CH$_2$), 2.02-1.92 (m, 1H, CH$_2$). **19-*OMe-rac***: ^{1}H NMR (500 MHz, CD$_2$Cl$_2$) δ 7.69 (d, J_{HH} = 8.7 Hz, 2H, aryl), 7.27 (d, J_{HH} = 8.7 Hz, 2H, aryl), 7.10 (d, J_{HH} = 8.7 Hz, 2H, aryl), 7.09 (d, J_{HH} = 13.7 Hz, 1 H, HC=C), 6.69 (d, J_{HH} = 8.7 Hz, 2H, aryl), 6.19 (d, J_{HH} = 10.3 Hz, 1H, HC=C), 4.88 (d, J_{HH} = 10.3 Hz, 1H, HC=C), 4.72 (s, 5H, Cp), 3.90 (s, 3H, O=CH$_3$), 3.79 (s, 3H, O-CH$_3$), 3.63 (d, J_{HH} =

13.5 Hz, 1H, HC=C), 3.14 (ddd J_{HH} =16, 11.0, 7.8 Hz, 1 H, CH$_2$), 2.69-2.62 (m 1H, CH$_2$), 2.57 (dd J_{HH} = 16.1, 8.5 Hz, 1H, CH$_2$), 2.17 (dd J_{HH} = 16.5, 8.3 Hz, 1H, CH$_2$), 1.81-1.65 (m, 2H, CH$_2$).

18-*OMe* ^{13}C{^{1}H} NMR (100 MHz, CD$_2$Cl$_2$) δ 130.78, 127.76, 116.90, 115.54, 115.21, 88.03, 87.67, 83.77, 80.25, 79.76, 55.51, 39.29, 23.88. ESI-MS (*m/z*) calcd for [C$_{28}$H$_{29}$O$_2$Ru]$^+$ 499.1213; found 499.1203. IR (NaCl thin film,) 3111, 2959, 2837, 1607 cm^{-1}.

18-*OMe*   **19**-*OMe*
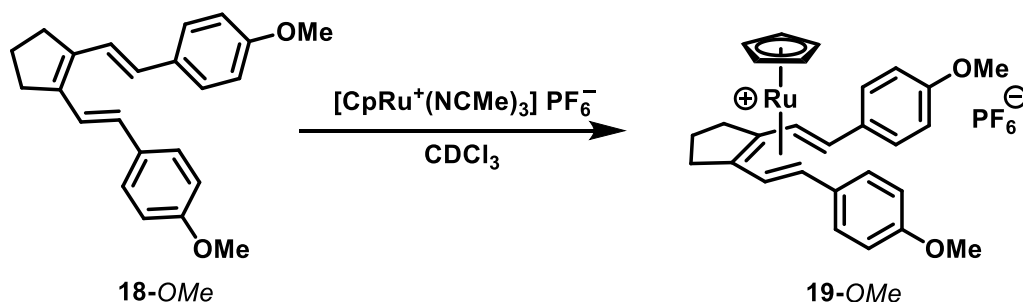
3. Equilibrium Experiments:

Cold-probe VT NMR experiments with 19-*OMe*: To a J. Young tube **19**-*OMe* (2.0 mg, 0.0031 mmol) and 1,3,5-tri-*tert*-butylbenzene (internal standard) were added. The J. Young tube was evacuated on a high vacuum line and was cooled to -78 °C and dry CD$_2$Cl$_2$ was distilled into the tube (1 mL). The tube was kept at -78 °C in the dry ice/acetone bath while the NMR probe was cooled down to -60 °C. After the NMR probe was cooled to -60 °C, the NMR tube was quickly inserted. NMR temperature points were taken at: -60 °C, -50 °C, -40 °C, -30 °C, -20 °C, -10 °C, 0 °C, 10 °C and 20 °C. Ratio of the diastereomers were determined via integration of the vinyl hydrogens at δ 6.34 (**19**-*OMe-meso*) and 6.12 (**19**-*OMe-rac*) with respect to the internal standard.

Equilibrium Experiment with 19-*CF3* and 18-*OMe:*

To a J. Young tube. 3.0 mg (0.0052 mmol) of **19**-*CF$_3$* and 1.7 mg (0.0052 mmol) of **18**-*OMe* with tri-tert-butylbenzene (internal standard) were added. The NMR tube was placed under vacuum on

a high vacuum line. Then, dry, degassed CD_2Cl_2 was distilled into to the tube. The tube was then taken immediately to the NMR so a spectrum could be obtained. Time points were taken at 5 min, 7 h and 24 h. Ratios of the ruthenium complexes were determined via integration of the vinyl hydrogens at δ 3.53 (**19**-*CF₃*) and δ 3.66 (**19**-*OMe-meso*) with respect to the internal standard.

E. Appendix
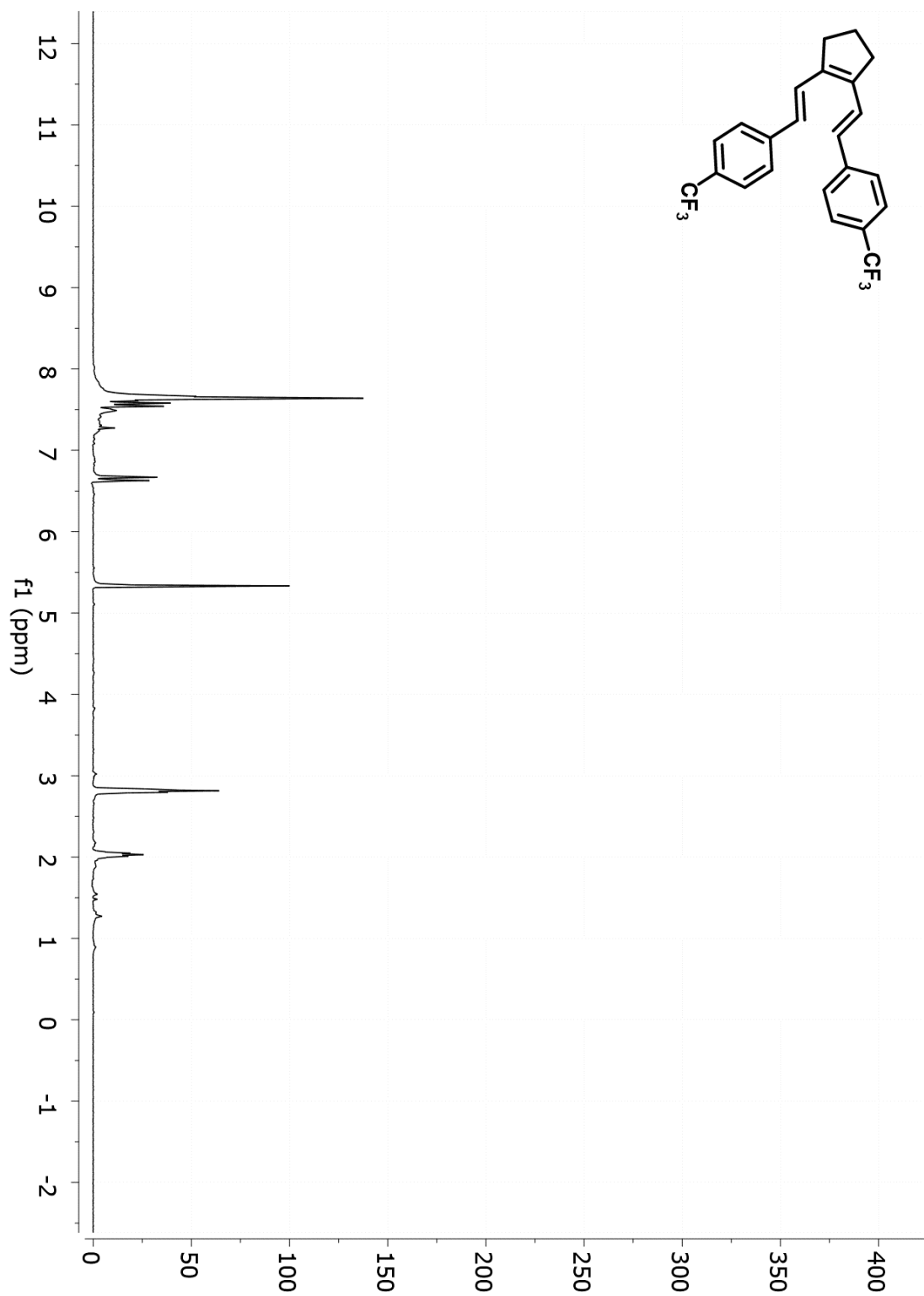
Figure 2.14. ^{1}H NMR spectrum of **18**-*CF₃* (CDCl₃, 400 MHz).
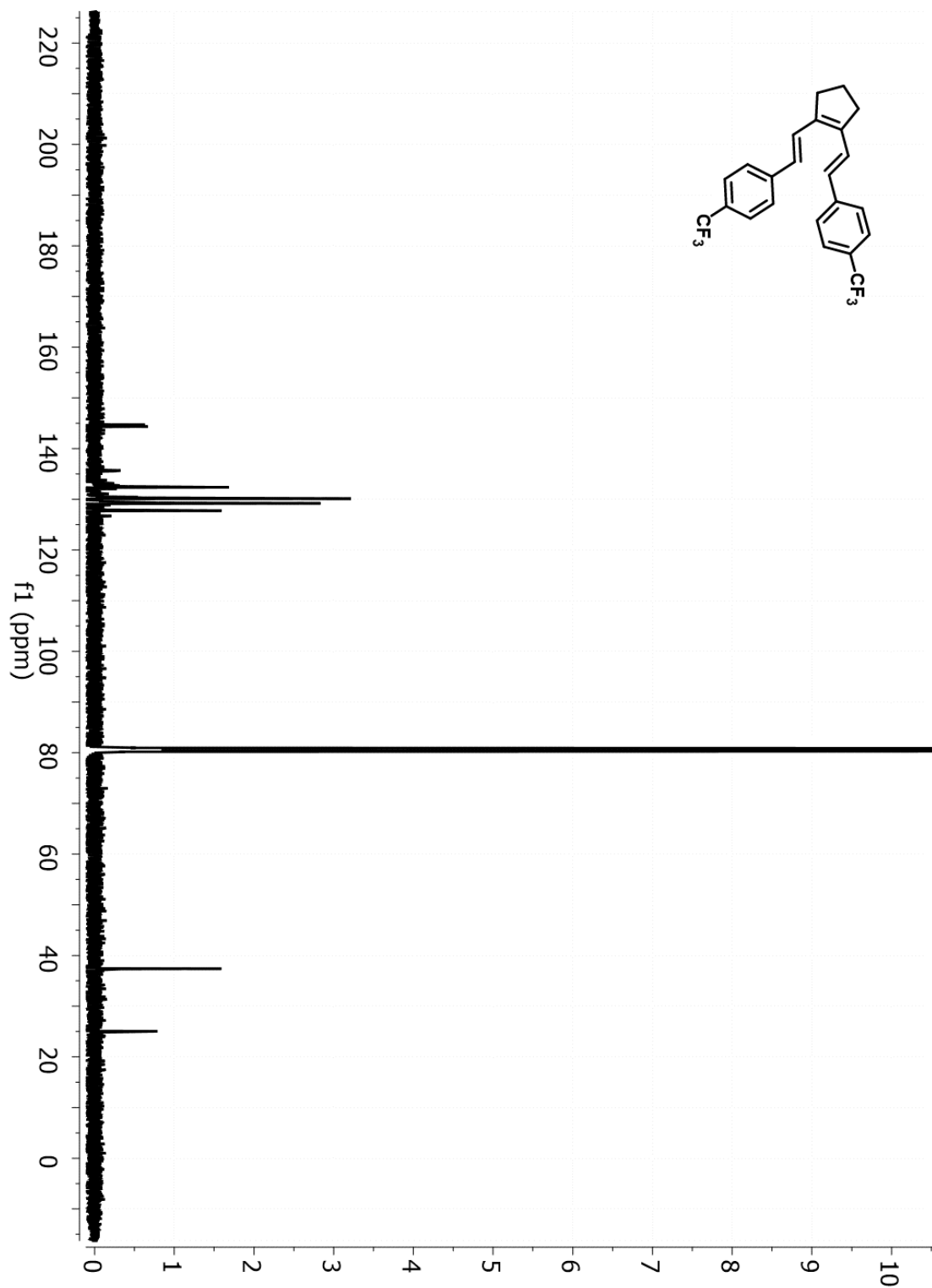
Figure 2.15. $^{13}C\{^1H\}$ NMR spectrum of **18**-*CF₃* (CDCl₃, 100 MHz).
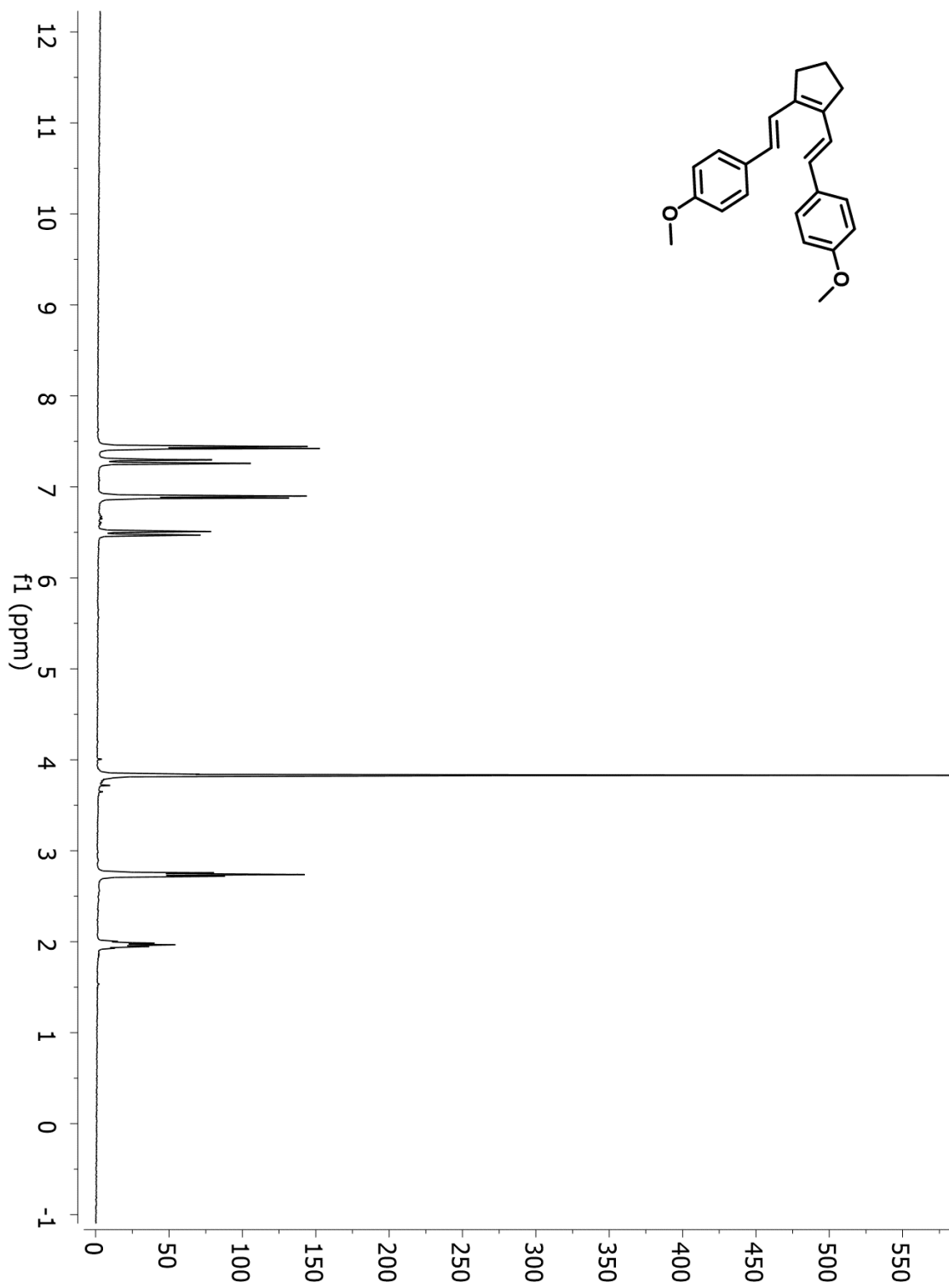
Figure 2.16. ^{1}H NMR spectrum of **18**-*OMe* (CDCl$_3$, 400 MHz).
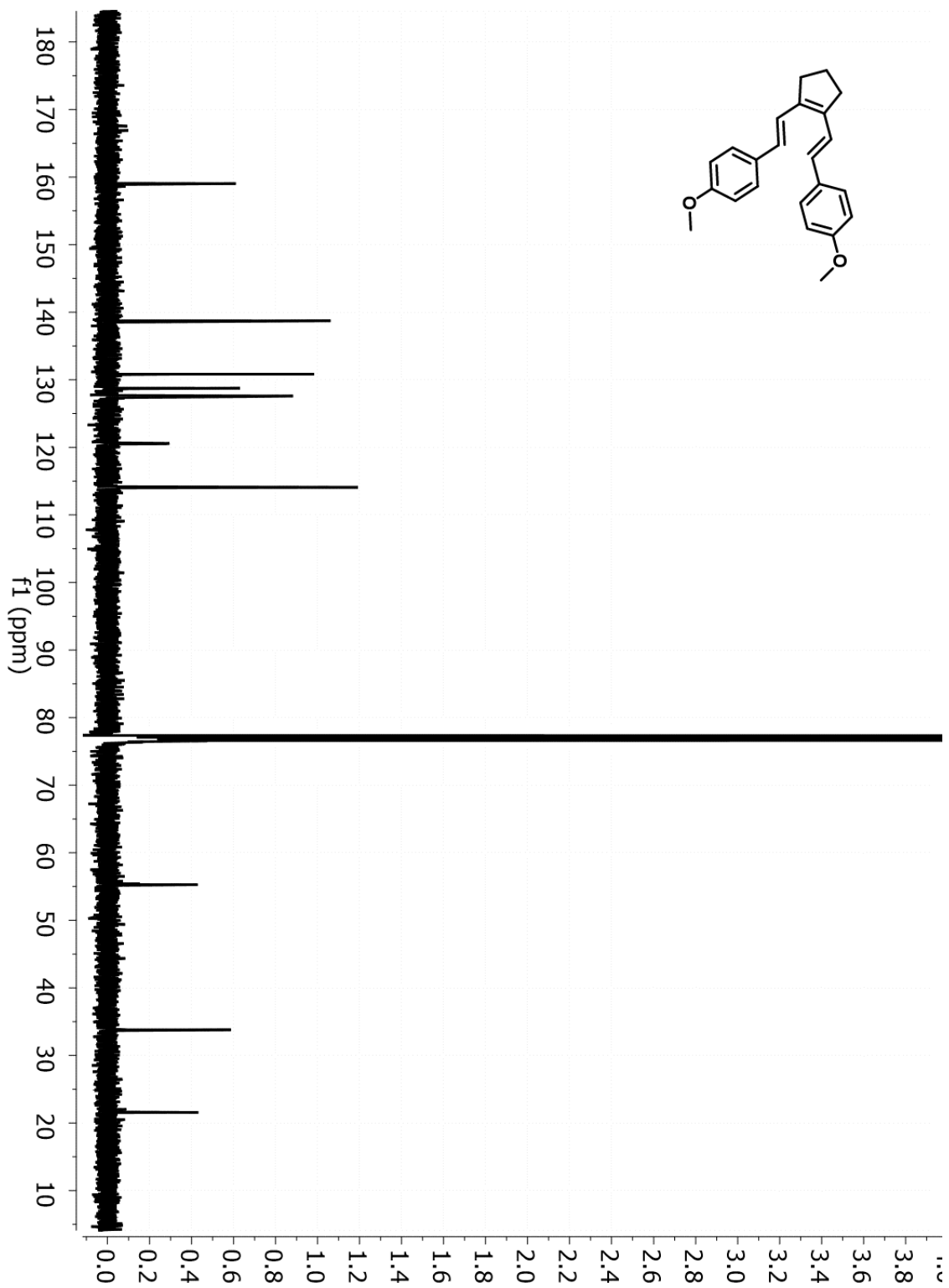
Figure 2.17. $^{13}C\{^{1}H\}$ NMR spectrum of **18**-*OMe* (CDCl$_3$, 100 MHz).
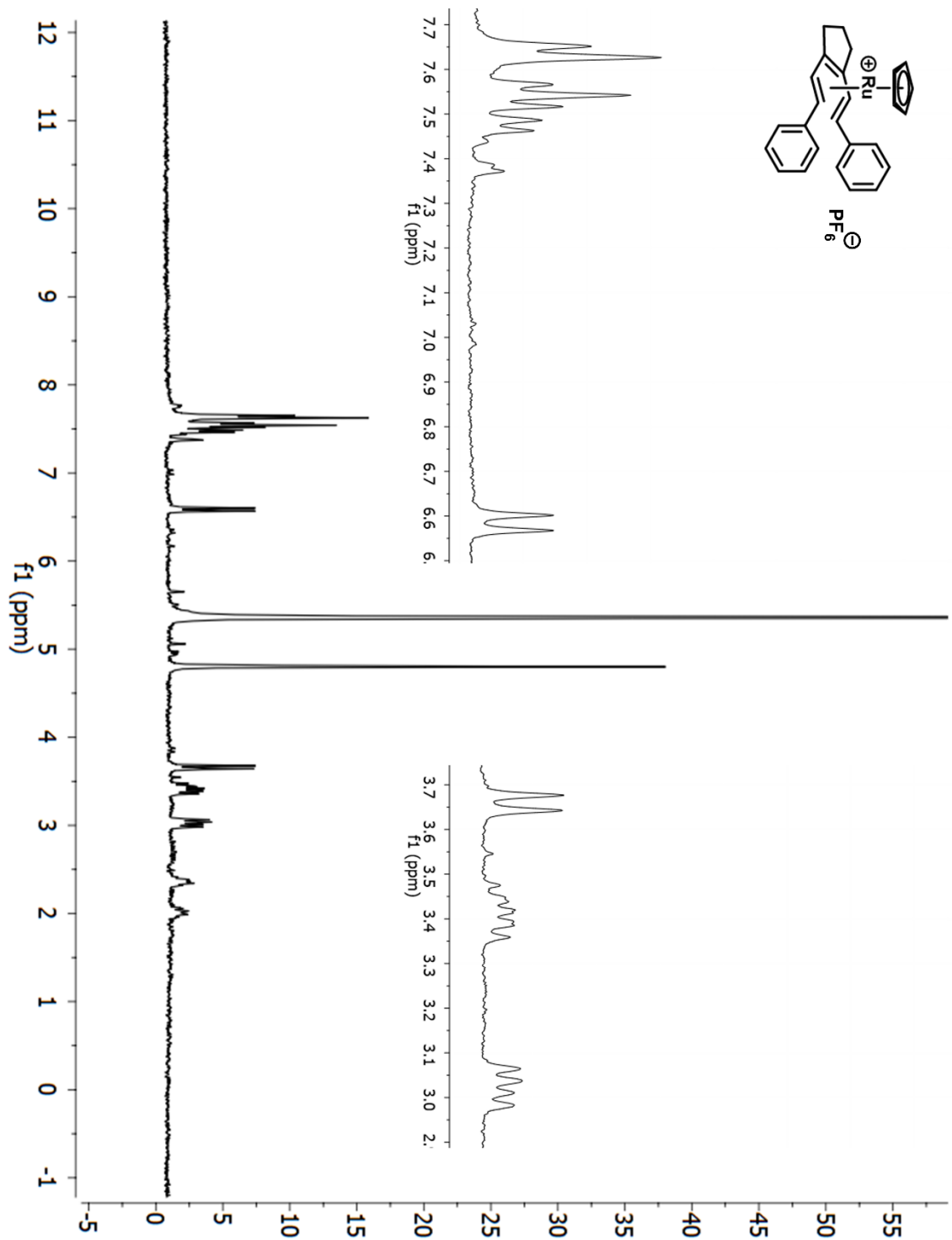
Figure 2.18. ^{1}H NMR spectrum of **19**-*H* (CD$_2$Cl$_2$, 300 MHz).
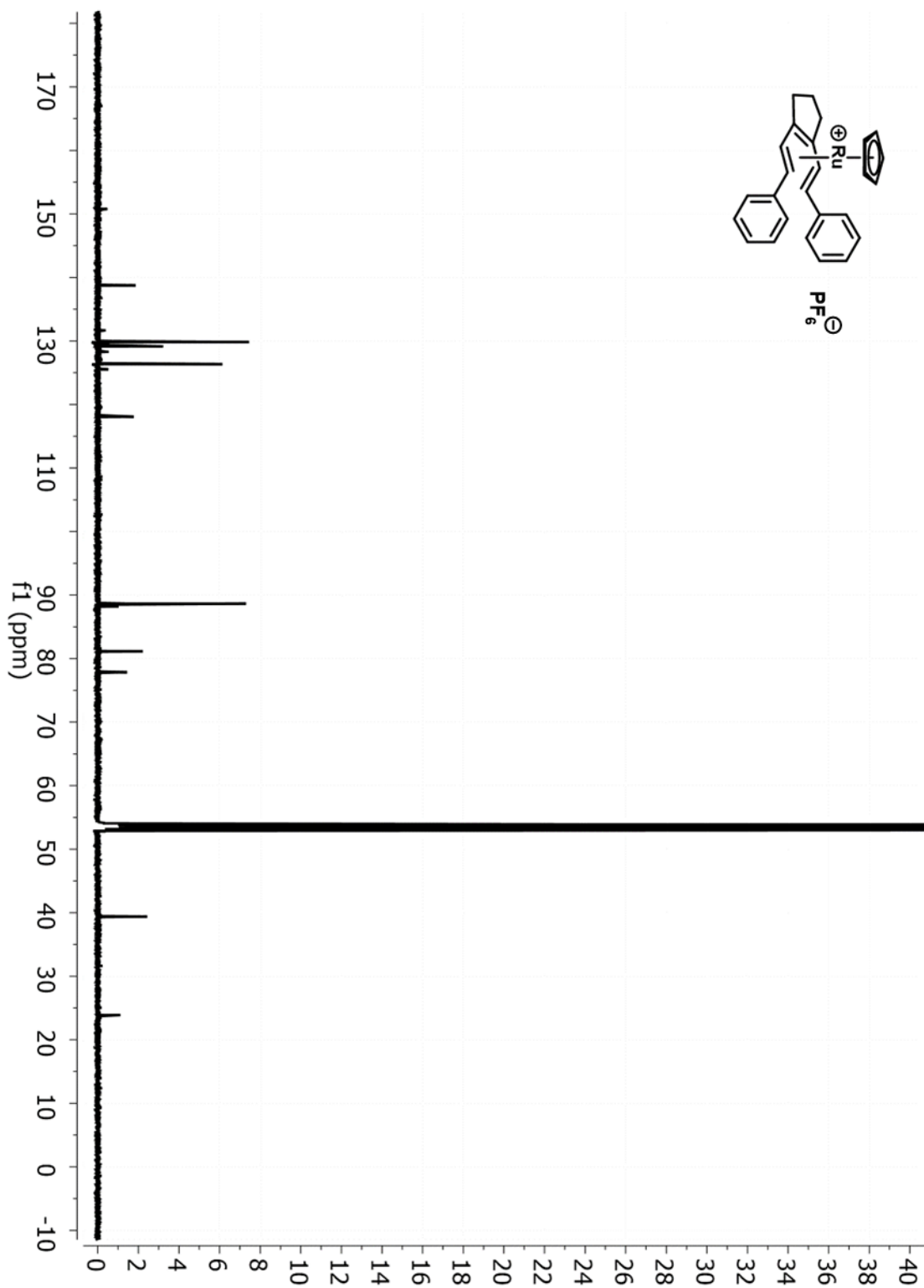
Figure 2.19. ^{13}C{^{1}H} NMR spectrum of **19**-*H* (CD$_2$Cl$_2$, 100 MHz).
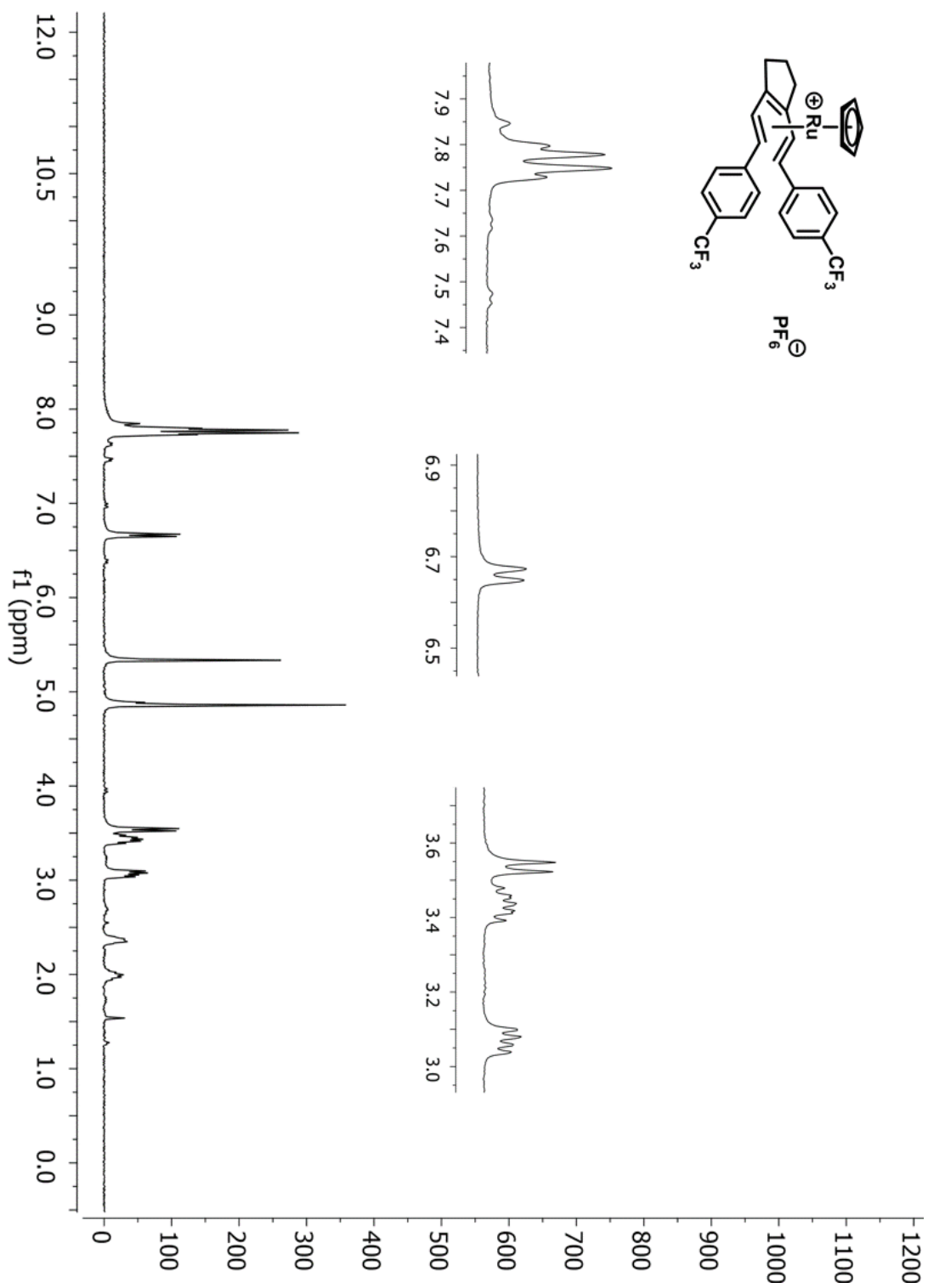
Figure 2.20. ^{1}H NMR spectrum of **19**-*CF$_3$* (CD$_2$Cl$_2$, 400 MHz).
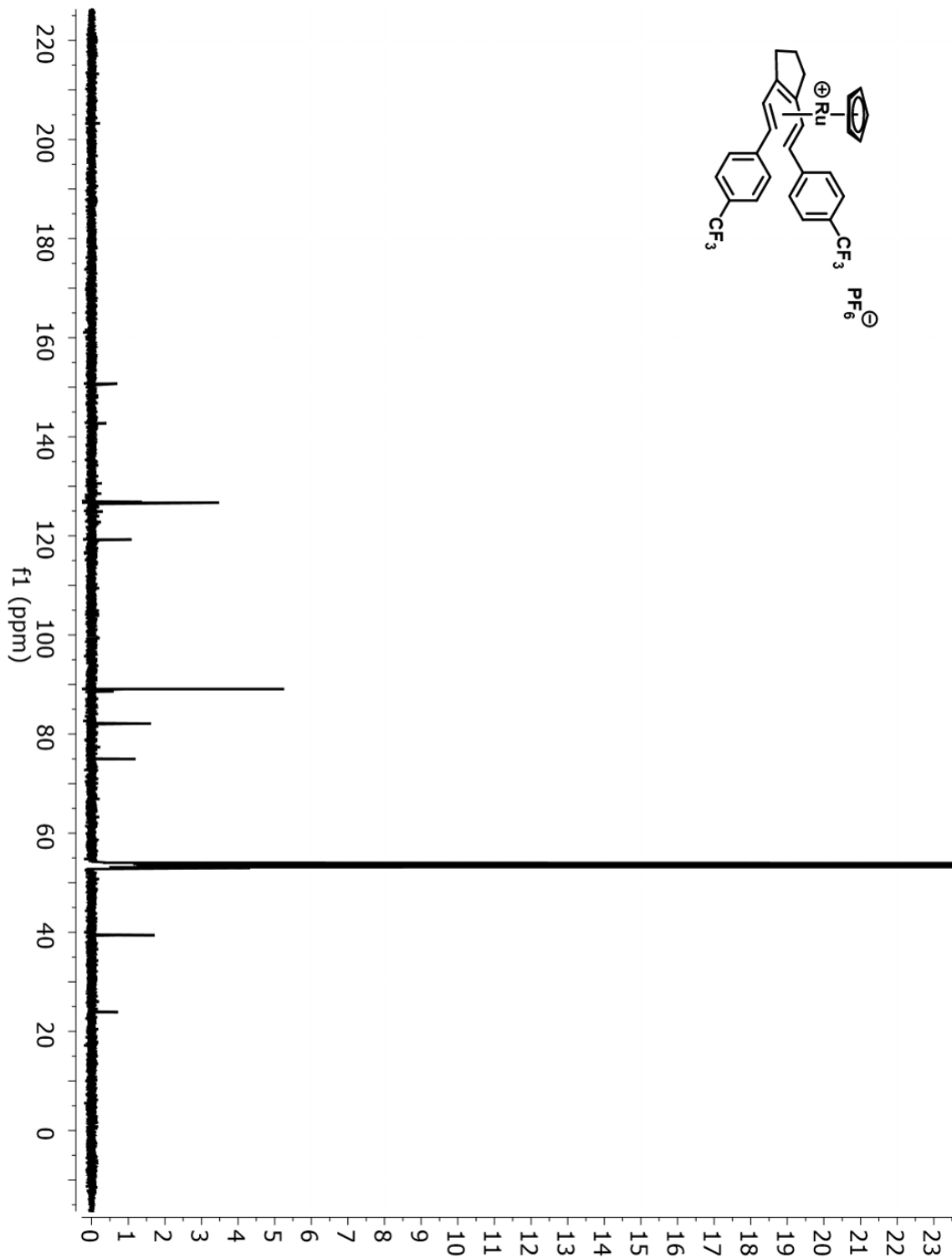
Figure 2.21. $^{13}C\{^1H\}$ NMR spectrum of **19**-*CF₃* (CD₂Cl₂, 100 MHz).
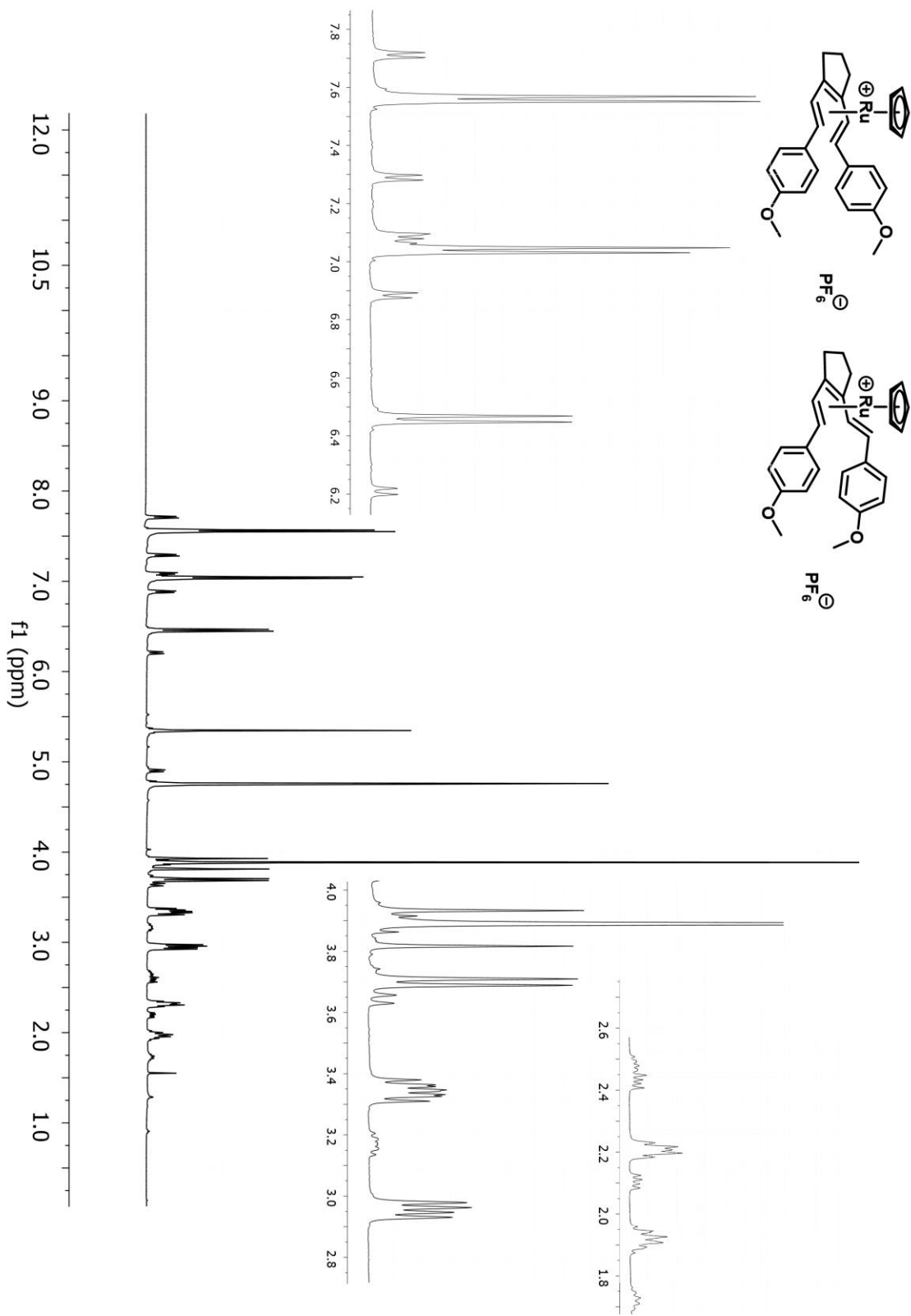
Figure 2.22. ^{1}H NMR spectrum of **19**-*OMe* (CD$_2$Cl$_2$, 500 MHz).
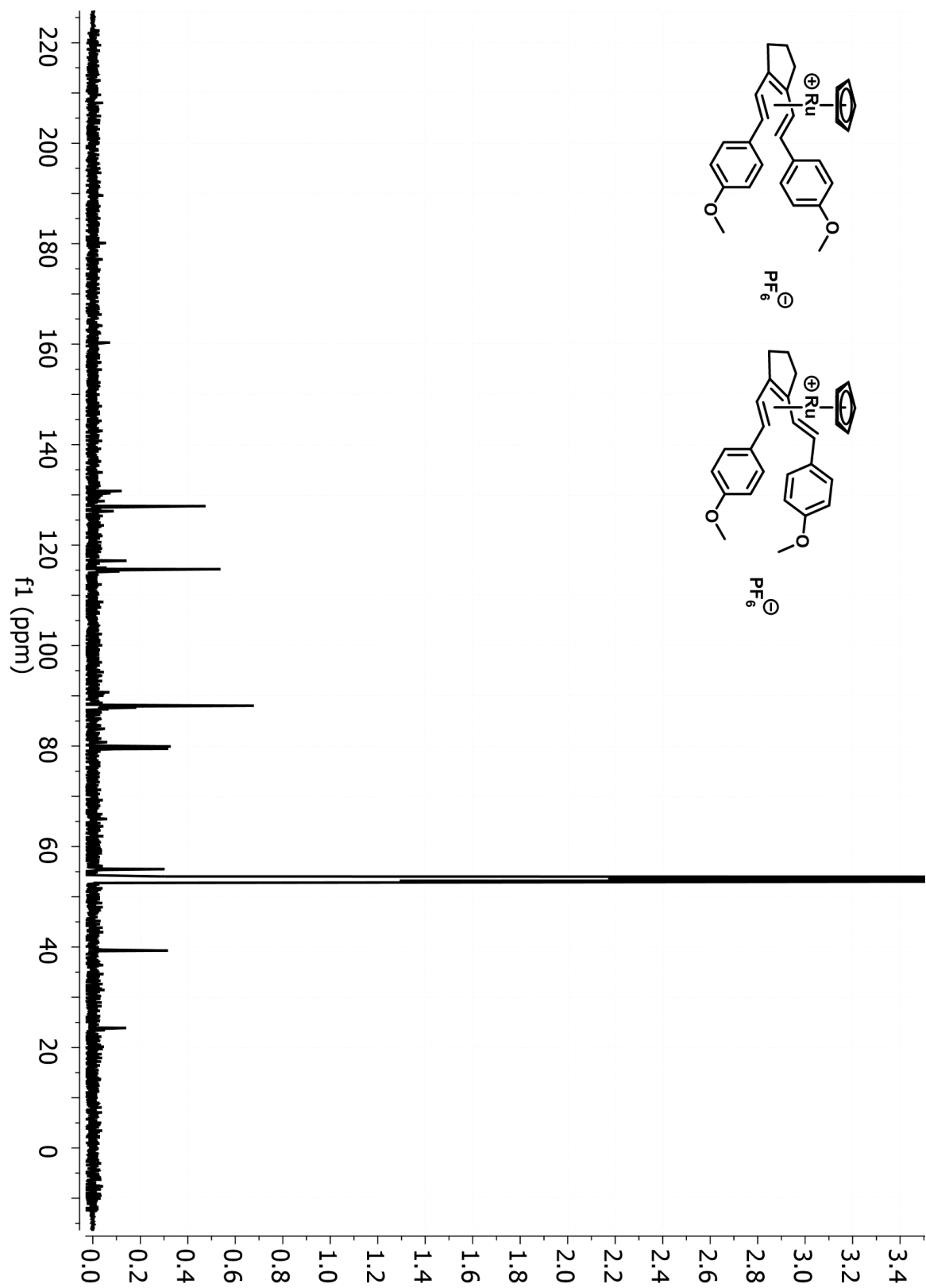
Figure 2.23. $^{13}C\{^1H\}$ NMR spectrum of **19**-*OMe* (CD$_2$Cl$_2$, 100 MHz).

Table 2.10. Crystal data and structure refinement for **18-***CF₃*.

Identification code	KMV2-134
Empirical formula	C28 H23 F12 P Ru
Formula weight	719.51
Temperature	100.0 K
Wavelength	0.71073 Å
Crystal system	Monoclinic
Space group	P2yb
Unit cell dimensions	a = 13.5614(5) Å $\alpha = 90°$.
	b = 13.4214(5) Å $\beta = 92.5550(10)$.
	c = 17.1969(6) Å $\gamma = 90°$.
Volume	3126.9(2)Å^3
Z	4
Density (calculated)	1.782 g/cm^3
Absorption coefficient	0.902 mm^{-1}
F(000)	1664
Crystal size	0.16 x 0.09 x 0.055 mm^3
Crystal color, habit	Orange Block
Theta range for data collection	1.185 to 26.777°.
Index ranges	-17<=h<=16, -16<=k<=16, -21<=l<=21
Reflections collected	38361
Independent reflections	13285 [R(int) = 0.0395]
Completeness to theta = 25.000°	100.0 %
Absorption correction	Semi-empirical from equivalents

Table 2.10 continued. Crystal data and structure refinement for **18-**_OMe_.

Max. and min. transmission	0.04910 and 0.04482
Refinement method	Full-matrix least-squares on F^2
Data / restraints / parameters	4824 / 114 / 370
Goodness-of-fit on F^2	1.040
Final R indices [I>2sigma(I)]	R1 = 0.0334, wR2 = 0.0765
R indices (all data)	R1 = 0.0452, wR2 = 0.0852
Extinction coefficient	n/a
Largest diff. peak and hole	0.362 and -0.436 e.Å^{-3}

Table 2.11. Crystal data and structure refinement for **18-**_OMe_.

Identification code	KMV2_153	
Empirical formula	C28 H29 F6 O2 P Ru	
Formula weight	643.55	
Temperature	100.0 K	
Wavelength	0.71073 Å	
Crystal system	Orthorhombic	
Space group	Pbca	
Unit cell dimensions	a = 18.2369(4) Å	α= 90°.
	b = 13.1440(3) Å	β= 90°.
	c = 21.9889(4) Å	γ = 90°.
Volume	5270.87(19) Å^3	
Z	8	
Density (calculated)	1.622 g/cm^3	

Table 2.11 continued. Crystal data and structure refinement for **18-*OMe***.

Absorption coefficient	0.723 mm^{-1}
F(000)	2608
Crystal size	0.187 x 0.176 x 0.092 mm^3
Crystal color, habit	Reddish Orange Block
Theta range for data collection	1.852 to $25.354°$.
Index ranges	$-21<=h<=17, -15<=k<=15, -26<=l<=26$
Reflections collected	47061
Independent reflections	4824 [R(int) = 0.0864]
Completeness to theta = $25.000°$	100.0 %
Absorption correction	Semi-empirical from equivalents
Max. and min. transmission	0.0852 and 0.0611
Refinement method	Full-matrix least-squares on F^2
Data / restraints / parameters	4824 / 114 / 370
Goodness-of-fit on F^2	1.040
Final R indices [I>2sigma(I)]	R1 = 0.0334, wR2 = 0.0765
R indices (all data)	R1 = 0.0452, wR2 = 0.0852
Extinction coefficient	n/a
Largest diff. peak and hole	0.362 and -0.436 e.Å^{-3}

F. Acknowledgements

Chapter 2, in part, is based on material which appears in "Hexahapto Metal Complexes of Acyclic Conjugated Trienes" O'Connor, J. M.; Baldridge, K. K.; Veccharelli, K. M.; Cope, S.K.; Holland, R.L.; Qin, P., Rheingold, A. L. *Submitted.* The dissertation author is a co-author on this paper.

G. References

(1)   Woodward, R. B.; Hoffmann, R. *Angew. Chemie Int. Ed. Engl.* **1969**, *8*, 781-853.

(2)   Bian, M.; Li, L.; Ding, H. *Synthesis.* **2017**, *49*, 4383-4413.

(3)   Mango, F. D. *Coord. Chem. Rev.* **1975**, *15*, 109-205.

(4)   Brookhart, M.; Davis, E. R.; Harris, D. L. *J. Am. Chem. Soc.* **1972**, *94*, 7853-7858.

(5)   Reardon, E. J.; Brookhart, M. *J. Am. Chem. Soc.* **1973**, *95*, 4311-4316.

(6)   Bishop, L. M.; Barbarow, J. E.; Bergman, R. G.; Trauner, D. *Angew. Chemie Int. Ed.* **2008**, *47*, 8100-8103.

(7)   Tantillo, D. J. *Angew. Chemie Int. Ed.* **2009**, *48*, 31-32.

(8)   Carreno, R.; Chaudret, B.; Labroue, D.; Sabo-Etienne, S. *Organometallics* **1993**, *12*, 13-14.

(9)   Older, C. M.; Stryker, J. M. *J. Am. Chem. Soc.* **2000**, *122*, 2784-2797.

(10)   O'Connor, J. M.; Friese, S. J.; Tichenor, M. *J. Am. Chem. Soc.* **2002**, *124* (14), 3506-3507.

(11)   O'Connor, J. M.; Friese, S. J.; Rodgers, B. L.; Rheingold, A. L.; Zakharov, L. *J. Am. Chem. Soc.* **2005**, *127*, 9346-9347.

(12)   Patel, A.; Barcan, G. A.; Kwon, O.; Houk, K. N. *J. Am. Chem. Soc.* **2013**, *135*, 4878-4883.

(13)   Jiao, H.; Schleyer, P. von R. *J. Am. Chem. Soc.* **1995**, *117*, 11529-11535.

(14)   Calculations performed by Kim Baldridge using BP86 density functional, Def2-TZVPP

basis set, GAMESS Program.

(15) Brookhart, M.; Green, M. L. H.; Parkin, G. *Proc. Natl. Acad. Sci. U. S. A.* **2007**, *104*, 6908-6914.

(16) Zhang, Y.; Lewis, J.C.; Bergman, R.G.; Ellman, J.A.; Oldfield, E. *Organometallics* **2006**, 25, 3515-3519.

(17) Burling, S.; Mas-Marz, E.; V Valpuesta, J. E.; Mahon, M. F.; Whittlesey, M. K. *Organometallics* **2009**, *28*, 66766686.

(18) Casey, C. P. *Science* **1993**, *259*, 1552-1558.

(19) Pijper, T. C.; Kudernac, T.; Browne, W. R.; Feringa, B. L. *J. Phys. Chem. C* **2013**, *117*

(20) Cope, S. K. Dissertation, University of California, San Diego, **2015**.

(21) Nicolaou, K. C.; Ogawa, Y.; Zuccarello, G.; Schweiger, E. J.; Kumazawa, T. *J. Am. Chem. Soc.* **1988**, *110*, 4866-4868.

(22) Schreiner, P. R. *J. Am. Chem. Soc.* **1998**, *120*, 4184-4190.

(23) Schreiner, P. R. *Chem. Commun.* **1998**, 483-484.

(24) Meyer-Friedrichsen, T.; Wong, H.; Prosenc, M. H.; Heck, J. *Eur. J. Inorg. Chem.* **2003**, *2003* (5), 936-946.

(25) Maier, G. *Angew. Chemie* **1967**, *79*, 402-414.

(26) Barlow, S.; Henling, L.M.; Day, M. W.; Schaefer, W.P.; Green, J. C.; Hascall, T.; Marder, S. R. *J. Am. Chem. Soc.* **2002**, *124*, 6285-6296.

(27) Reyna-Madrigal, A.; Moreno-Gurrola, A.; Perez-Camacho, O.; Navarro-Clemente, M. E.; Juárez-Saavedra, P.; Leyva-Ramirez, M. A.; Arif, A. M.; Ernst, R. D.; Paz-Sandoval, M. A. *Organometallics* **2012**, *31*, 7125-7145.

(28) Benyunes, S. A.; Day, J. P.; Green, M.; Al-Saadoon, A. W.; Waring, T. L. *Angew. Chemie Int. Ed. English* **1990**, *29*, 1416-1417.

(29) Okamoto, T.; Yasuda, H.; Nakamura, A.; Kai, Y.; Kanehisa, N.; Kasai, N. *J. Am. Chem. Soc.* **1988**, *110* (15), 5008.

(30) Erker, G.; Krüger, C.; Müller, G. *Adv. Organomet. Chem.* **1985**, 24, 1–39.

(31) Ernst, R. D.; Melendez, E.; Stahl, L.; Ziegler, M. L. *Organometallics* **1991**, *10*, 3635-3642.

(32)   Meléndez, Enrique; Ilarraaza, Raimundo; Yap, Glenn P.A.; Rheingold, A. L. *J. Organomet. Chem.* **1996**, *522*, 1-7.

(33)   Fukumoto, H.; Mashima, K. *Organometallics* **2005**, 24, 3932–3938.

Chapter 3.

Novel Cycloaromatization Reactions of Nitrogen-Containing Enediynes with Incorporation of Halide from Haloform and Hydrogen from 1,4-Cyclohexadiene

A. Introduction

In 1972, Bergman and Jones reported that when deuterium enriched *cis*-1,5-hexadiyn-3-ene (**1**) was heated in the gas phase at 200 °C, it rapidly equilibrated with the *cis*-enediyne isomer **2,** without evidence for formation of isomers that contained deuterium enrichment at both the vinyl and terminal acetylenic positions (**4** and **5**). When **1** was heated in atom-donor solvents such as toluene, 1,4-cyclohexadiene (1,4-CHD), or CCl₄, arynes **6**, **7** and **8** were formed (Figure 3.1). This evidence led Bergman to propose a symmetric *para*-benzyne diradical (**3**) as an intermediate for the interconversion of **1** and **2**.[1]
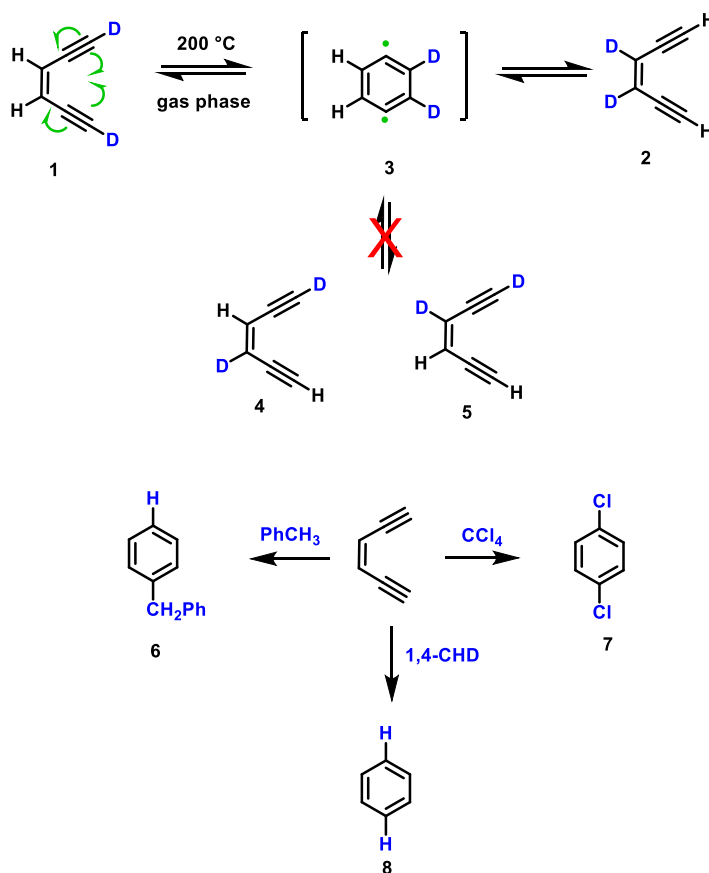
Figure 3.1. Bergman's initial observations of cycloaromatization of enediyne **1**.

Previously, in the O'Connor lab, it was demonstrated that Cp^*Ru^+ triggers cycloaromatization reactions of enediynes **9** and **10** in the presence of 1,4-CHD at room temperature, to yield arene products **11** and **12** in good to excellent yields.[2,3]

9 (n = 2)
10 (n = 1)

11 (n = 2)
12 (n = 1)
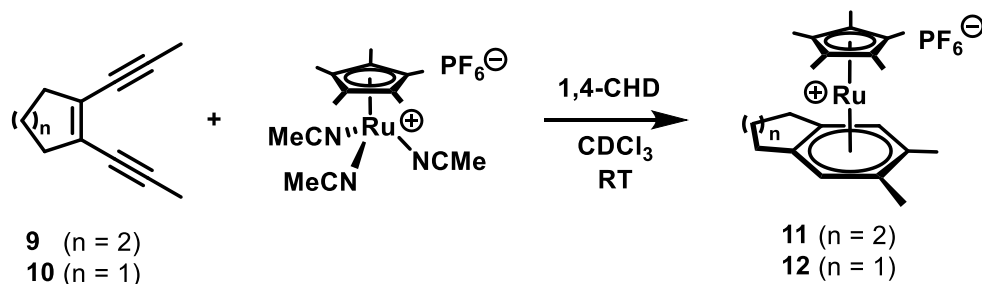
Scheme 3.1. Ruthenium-mediated cyclization of acyclic enediynes

As an extension to this work, the O'Connor group sought to compare the activation parameters for the metal-mediated and thermal reactions. Thus, compounds **9** and **10** were examined under thermolysis conditions in chloroform with 1,4-CHD as the hydrogen atom donor.[4,5] Unexpectedly, there was no spectroscopic evidence that **13** or **14** were formed. Instead, halogenated arene products **15** and **16** were formed as the major products in 85% and 76% yield respectively. Minor products **17** and **18** were also formed in 7.7% and 19% yield, respectively.

9 (n = 2)
10 (n = 1)

13 (n = 2)
14 (n = 1)

15 (n = 2)
16 (n = 1)

17 (n = 2)
18 (n = 1)
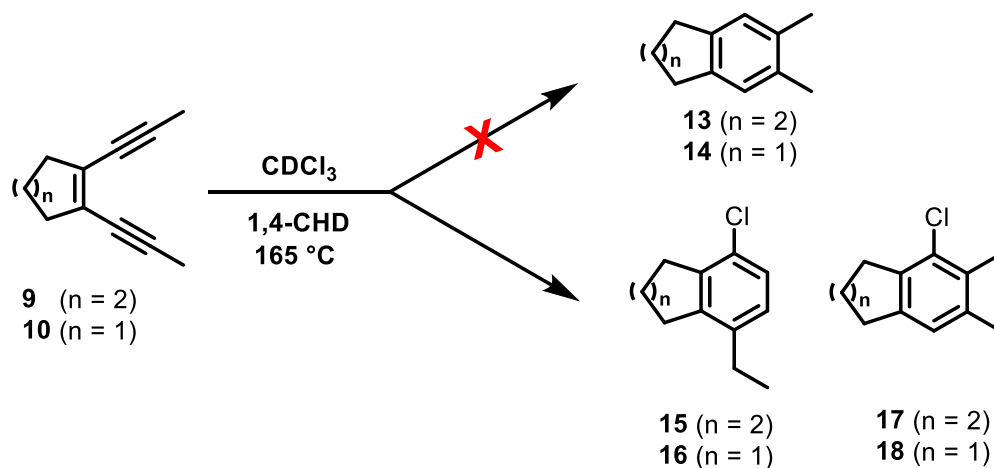
Scheme 3.2. Thermal conversion of enediynes **9** and **10** to halogenated arenes.

The connectivity for **15** was established by reaction with [Cp*Ru(NCMe)$_3$]PF$_6$ to yield the sandwich complex **19**, and X-ray crystallography characterization revealed that the chlorine and ethyl substituents are *para* to each other.
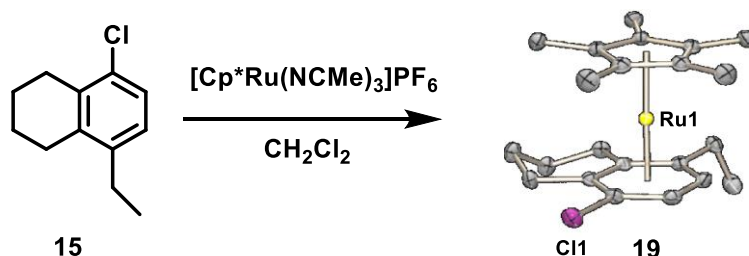
Scheme 3.3. Absolute structure determination of **15** through the formation of Cp*Ru complex **19**.[4]

A key observation that provided insight into the possible mechanism of formation of products **15-18** was the presence of a resonance at δ 5.29 (t, J_{HD} = 1.0 Hz) in the ^{1}H NMR spectra taken on the crude reaction mixtures. Additionally, there was a resonance observed at δ 53.35 (t, J_{CD} = 27.3 Hz) in the ^{13}C{^{1}H} NMR spectra taken on the crude reaction mixtures. These resonances are consistent with the formation of CDHCl$_2$.[6] Therefore, it was hypothesized that under thermolysis conditions the chloroform and 1,4-CHD are converted to benzene, CDHCl$_2$ and HCl (by mass balance). This observation led to a theory that HCl would promote the cyclizations of **9** and **10** without 1,4-CHD as the hydrogen atom source. When compound **9** and HCl were heated at 150 °C for 46 h, **15** was formed in 55% yield along with vinyl chloride **20-*E*** in 12% yield (Scheme 3.4).

Additionally, **20-*E*** was synthesized in 85% yield by reacting **9** with 2 M HCl in diethyl ether. Compound **20-*E*** was reacted at 165 °C for 42 h and yielded the cyclized product **15** in 96% yield. In a similar fashion, compound **10** was reacted with 2M HCl in diethyl ether to afford the

isolated vinyl chloride **21** (96:4 E/Z ratio). Thermolysis of **21** under the same reaction conditions as those employed for **20** afforded cyclized product **16** in 93% yield.[4,5]
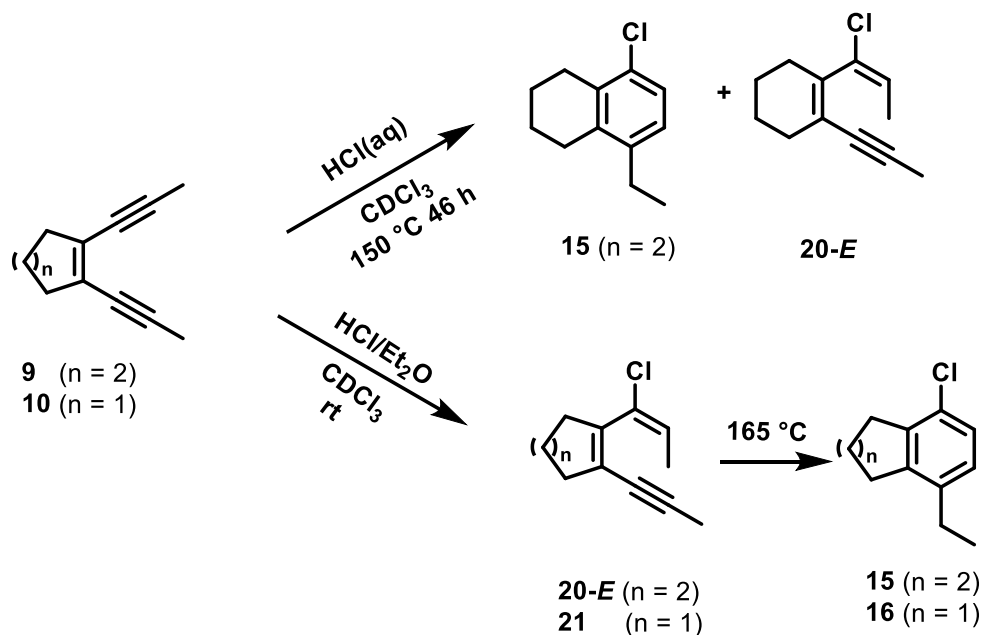
Scheme 3.4. Reactions of **9** and **10** with HCl.[4,5]

In a final experiment, **9** was prepared with ^{13}C-enrichment located in the propargylic methyl groups. ^{13}C-enriched **9** was heated at 140 °C in CDCl$_3$ in the presence of HCl for 3 days. Product **15** was observed with the ^{13}C-enrichment located at the C7 carbon position and at the methyl carbon of the ethyl group. With these results in hand, the mechanism for conversion of **9** to **15** was proposed to begin with *in situ* generation of HCl. The HCl then adds across one of the alkynes, forming vinyl chloride **20-E**. Compound **20-E** then undergoes a 1,7-H shift to form allene **22**, followed by 6π electrocyclization to form **23**. Lastly, a rearrangement affords aromatized product **15** (Scheme 3.5).[4]
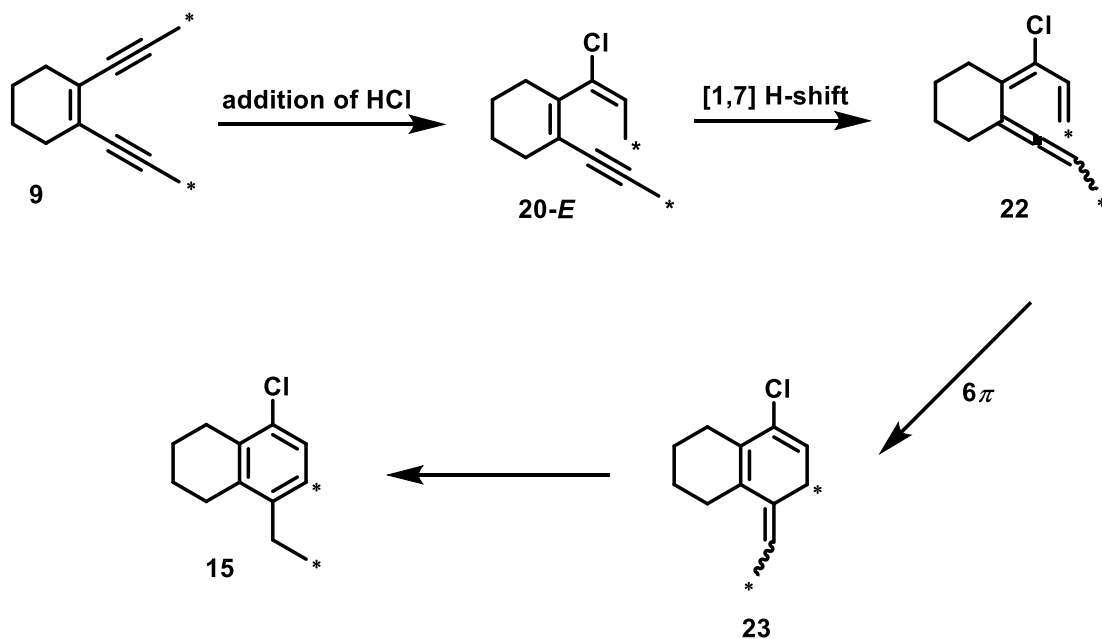
Scheme 3.5. Mechanistic hypothesis of the conversion of **9** to **15**.[4]

In the literature, there are few examples of cycloaromatization reactions involving nitrogen-containing enediynes.[7–10] Exploring thermal cyclizations with heteroatom-containing enediynes could provide insight into how aromaticity and electronic factors influence cycloaromatization reactions. Also, preparing nitrogen-containing enediynes could provide insight into functional group tolerance for the thermal conversion of enediynes to halogenated aromatics. Herein, this chapter further explores the mechanism of HCl generation from chloroform and the cycloaromatization reactions of nitrogen-containing enediynes.

B. Results and Discussion

1. Synthesis of 2-(1-pentynyl)-3-(1-propynyl)pyridine (26).

Pyridine enediyne **26** was synthesized from commercially available 2-bromo-3-pyridinecarboxaldehyde (**23**) in three steps in 62% overall yield. Sonogashira coupling of **23** with 1-pentyne afforded **24** in 90% yield. Installation of the second alkyne functional group was achieved via a homologation reaction with trimethylsilyldiazomethane and *n*-BuLi to afford **25** in 80% yield. Lastly, target compound **26** was synthesized by deprotonation of the terminal acetylene hydrogen by LiHMDS and subsequent methylation with methyl iodide.
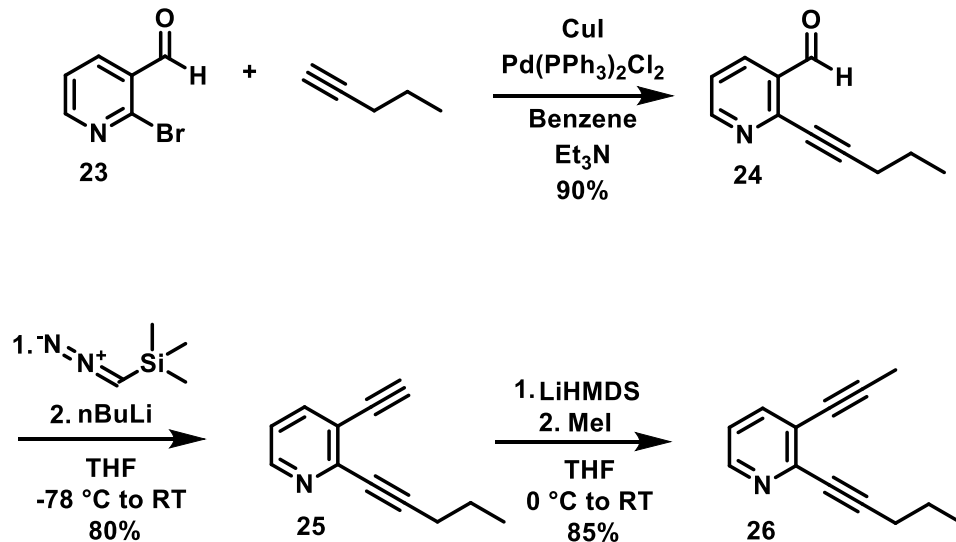
Scheme 3.6. Synthesis of enediyne **26**.

2. Cycloaromatization Reactions of Interest

After synthesizing compound **26** the thermal reactivity of this compound was examined under standard thermal Bergman conditions and in the presence of haloform (CHX_3). It was hypothesized that thermal Bergman conditions would afford compound **27**, and in the presence of haloform would produce 1,7-H shift product **28** (Figure 3.2).
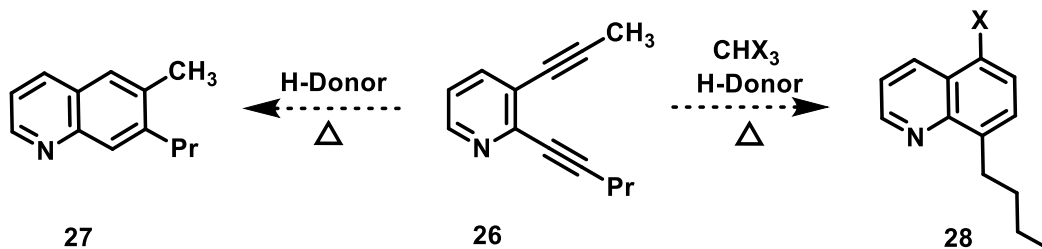
Figure 3.2. General cycloaromatization reactions of interest.

3. Cycloaromatization Products

Unexpectedly, when **26** (0.027 mmol) was heated for 24 h at 165 °C in a flame-sealed NMR tube with 10 equivalents of 1,4-CHD (0.27 mmol) in benzene-d_6 with 1,4-bis(trimethylsilyl)benzene (internal standard), no reaction was observed based on ^{1}H NMR spectroscopic analysis of the crude reaction mixture. The thermolysis of **26** (0.027 mmol) was then conducted under similar reaction conditions in neat THF-d_8 (1 mL), which also afforded no reaction. In a flame-sealed NMR tube **26** (0.027 mmol) was then heated for 24 h at 165 °C in CDCl$_3$ (1 mL) with added 1,4-CHD (0.27 mmol), leading to large amounts of dark intractable solids. The presence of the solids prevented us from obtaining a high resolution ^{1}H NMR spectrum of the crude reaction mixture. Consequently, the reaction was scaled up to 0.56 mmol of **26** (100 mg) and 5.5 mmol of 1,4-CHD (0.55 mL) in 15 mL of CDCl$_3$ and heated at 165 °C for 24 h. Preparative TLC was utilized in an attempt to purify any arene products. However, the purification was difficult due to large amounts of dark, insoluble materials that had formed in the reaction mixture. The intractable solids may be polyquinoline-type compounds. Also, ^{1}H NMR analysis was conducted on the isolated bands from the preparative TLC, however there were no ^{1}H NMR signals that corresponded to either arene products or starting material. There were broad resonances centered around δ 1.50, 1.25 and 0.86 which might be due to aliphatic oligomers. No

further experiments were conducted with $CDCl_3$ due to unproductive formation of unidentifiable side products.

Following the above results, other haloforms were examined and the next haloform chosen was bromoform. When a solution of **26** (100 mg, 0.56 mmol), $CHBr_3$ (0.050 mL, 0.56 mmol), and 1,4-CHD (0.50 mL, 5.6 mmol) in benzene (15 mL) was heated at 165 °C for 24 h in a pressure tube equipped with a Teflon needle-valve, the formation of compound **28** was not observed by NMR spectroscopic analysis of the crude reaction mixture. Instead, two unanticipated compounds were formed, **29**-*Br* and Bergman product **27** in 30% and 10% isolated yield, respectively (Scheme 3.7).

Compound **29**-*Br* was tentatively assigned based on its ^{1}H NMR spectrum. This compound exhibited four resonances in the aromatic region: δ 8.84 (d, J_{HH} = 2.7 Hz, 1H, aryl), 8.58 (d, J_{HH} = 8.5 Hz, 1H, aryl), 7.88 (s, 1H, aryl) and 7.44 (dd, J_{HH} = 8.6, 4.3 Hz, 1H, aryl). Compound **29**-*Br* also exhibited resonances that are indicative of a methyl group δ 2.64 (s, 3H, CH_3) and an *n*-propyl group [δ 2.85 (t, J_{HH} = 7.5 Hz 2H, CH_2), 1.74 (sex, J_{HH} = 7.7 Hz, 2H, CH_2) and 1.05 (t, J_{HH} = 7.3 Hz, 3H, CH_3)]. These observations led to the tentative identification of **29**-*Br*, however, the initial NMR data did not establish regiochemistry.

Compound **27** was also assigned based on its ^{1}H NMR spectrum. This compound exhibited five resonances in the aromatic region: δ 8.85 (d, J_{HH} = 2.8 Hz, 1H, aryl), 8.11 (d, J_{HH} = 8.0 Hz, 1H, aryl), 7.93 (s, 1H, aryl), 7.61 (s, 1H, aryl) and 7.36 (dd, J_{HH} = 8.1, 4.3 Hz, 1H, aryl). Compound **27** also exhibited resonances that are indicative of a methyl group δ 2.51 (s, 3H, CH_3) and an *n*-propyl group [δ 2.81 (t, J_{HH} = 7.7 Hz 2H, CH_2), 1.77 (sex, J_{HH} = 7.3 Hz, 2H, CH_2) and 1.07 (t, J_{HH} = 7.3 Hz, 3H, CH_3)].

The reaction was then repeated with iodoform in place of bromoform. A solution of **26** (100 mg, 0.56 mmol) CHI_3 (215 mg, 0.56 mmol) and 1,4-CHD (0.55 mL, 5.6 mmol) in benzene (15 mL) was reacted at 165 °C for 24 h in a pressure tube equipped with a Teflon needle-valve. Once again compound **28** was not formed, based upon ^{1}H NMR spectroscopic analysis. Instead, the Bergman cyclization product, **27**, was formed in 15% yield along with a second product, **29**-*I* in 30% yield, that was tentatively assigned as an iodo-quinoline (Scheme 3.6).

Compound **29**-*I* exhibited four resonances in the aromatic region: δ 8.79 (d, J_{HH} = 4.40 Hz, 1H, aryl), 8.49 (d, J_{HH} = 9.0 Hz, 1H, aryl), 7.86 (s, 1H, aryl) and 7.40 (dd, J_{HH} = 8.62, 4.22 Hz, 1H, aryl). Compound **29**-*I* also exhibited indicative resonances of a methyl group δ 2.74 (s, 3H, CH_3) and an *n*-propyl group [δ 2.92 (t, J_{HH} = 7.7 Hz 2H, CH_2) 1.79 (sex, J_{HH} = 7.3 Hz 2H, CH_2) 1.06 (t, J_{HH} = 7.33 Hz, 3H, CH_3)]. As with **29**-*Br*, these observations led to the tentative identification of **29**-*I*, however, the initial NMR data did not establish regiochemistry of the product. Lastly, **27** was identified via ^{1}H NMR spectroscopy and exhibited identical ^{1}H NMR resonances as previously stated above.

One equivalent of haloform was chosen for the above reactions in order to minimize possible unproductive decomposition pathways, as was previously observed for the thermolysis of **9** and **10** in the presence of bromoform and iodoform.[5] It should be noted that ^{1}H NMR yields for reactions of **28** in bromoform and iodoform were not obtained due to the formation of large amounts of intractable solids in the NMR tube which led to broadening of the NMR signals.
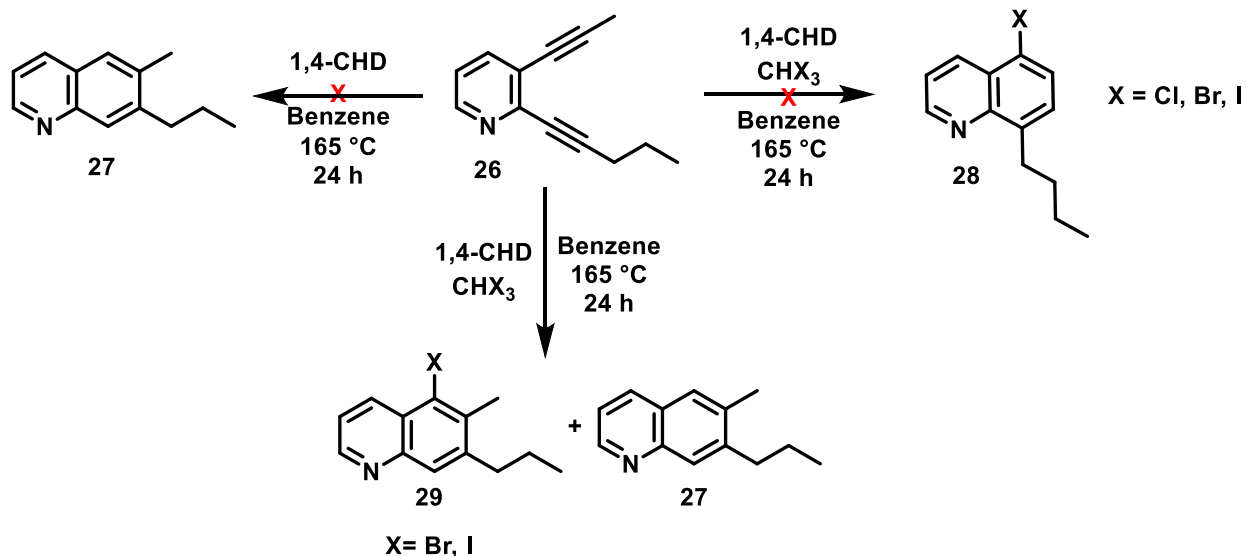
Scheme 3.7. The thermolysis of **26** afforded **27** and **29**.

4. Connectivity of Halogenated Quinoline Derivatives

From the above results, halogen connectivity needed to be verified for **29**-*Br* and **29**-*I* since the initial ¹H NMR experiments did not establish regiochemistry. The halogen needed to be verified if it was connected to the C5 or C8 position of **29**-*Br* and **29**-*I*. Therefore, heteronuclear multiple bond correlation (HMBC) NMR experiments were conducted on **29**-*Br* and **29**-*I*.

Compound **29**-*Br* exhibits a HMBC correlation (Figure 3.3) of the methyl hydrogen resonance at δ 2.64 with the ¹³C NMR resonance at 123.78 (carbon K). The aromatic hydrogen resonance on C8 (carbon E) at δ 7.85 (s) exhibits a HMBC correlation with the ¹³C resonance at 123.78 (carbon K). Lastly, the aromatic proton resonance on C3 (carbon I) at δ 8.58 (d, $J_{HH} = 8.5$ Hz) exhibits a HMBC correlation with the ¹³C resonance at 123.78 (carbon K). The assigned connectivity was also supported by nuclear Overhauser effect (NOE) spectroscopy (Figure 3.4).

87

Irritation at the aromatic hydrogen resonance at δ 7.85 for compound **29-Br** led to enhancement of the *n*-propyl group resonances at 2.83, 1.72 and 1.05.

Next, a HMBC experiment was conducted on **29-I.** This compound has a HMBC correlation (Figure 3.5) of the methyl hydrogen resonance at δ 2.74 (s) with the ^{13}C resonance at 106.23 (carbon K). The aromatic proton resonance on C8 (carbon E) at δ 7.86 (s) has a HMBC correlation with the ^{13}C resonance at 106.23 (carbon K). Lastly, the aromatic proton resonance on C3 (carbon I) at δ 8.49 (d, J_{HH} = 9.0 Hz) has a HMBC correlation with the ^{13}C resonance at 106.23(carbon K). Also, a NOE spectroscopy experiment was conducted to verify relative connectivity. Irradiation of the aromatic hydrogen resonance at δ 7.86 for compound **29-I** resulted in enhancement of the signals of the *n*-propyl group at 2.88, 1.72 and 1.04 (Figure 3.6). These results establish that the halogen functional group is connected to the C5 carbon of the quinoline derivatives for both **29-Br** and **29-I**.
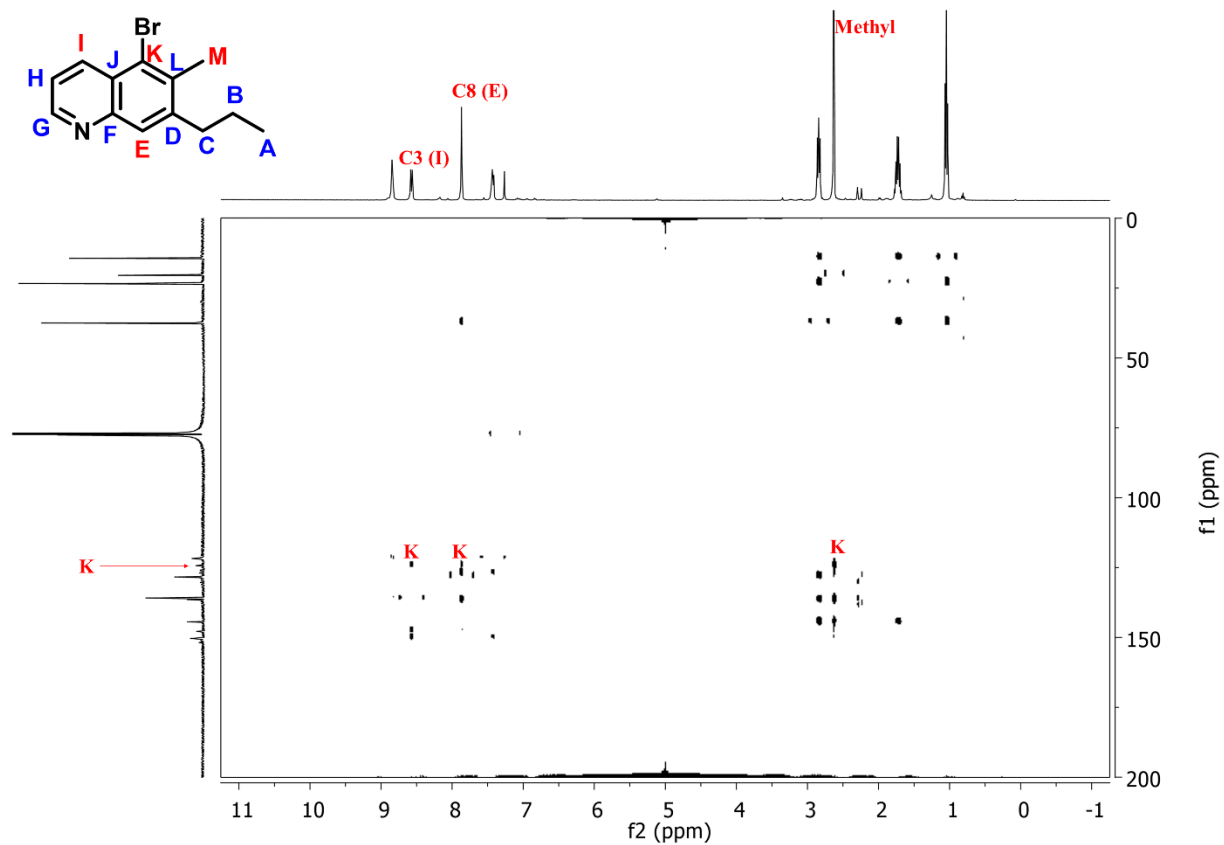
Figure 3.3. HMBC spectrum of **29-*Br*** (500 MHz, CDCl₃).
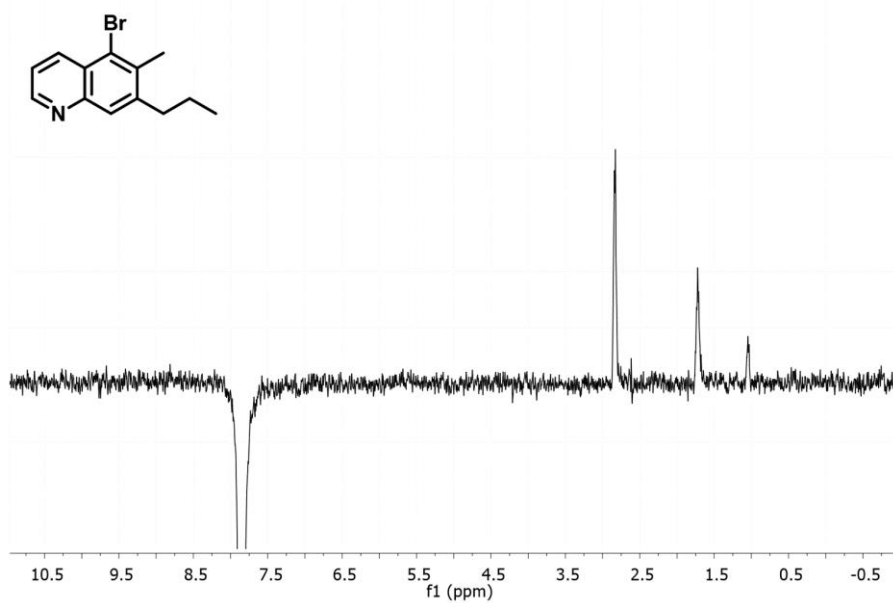
Figure 3.4 NOE spectrum of **29-*Br*** (500 MHz, CDCl₃).
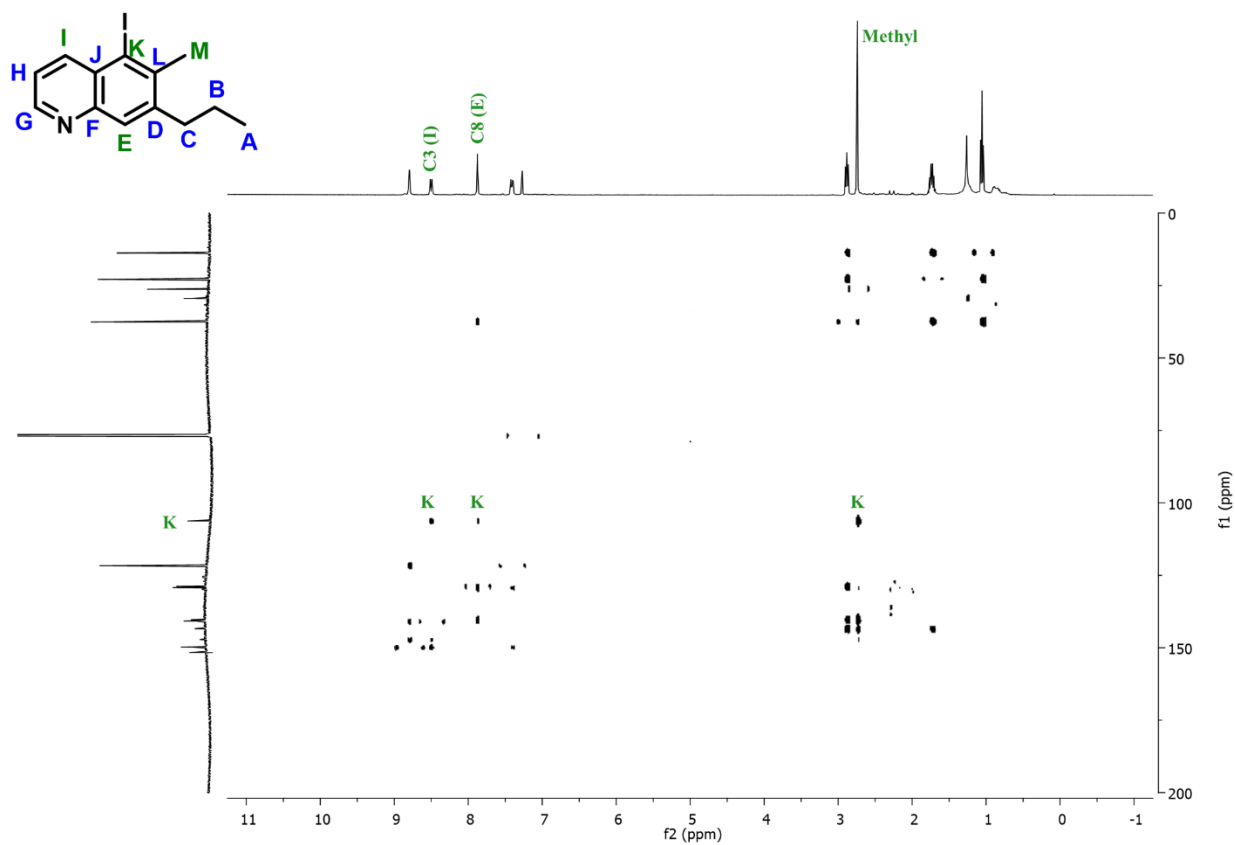
Figure 3.5. HMBC spectrum of **29-*I*** (500 MHz, CDCl₃).
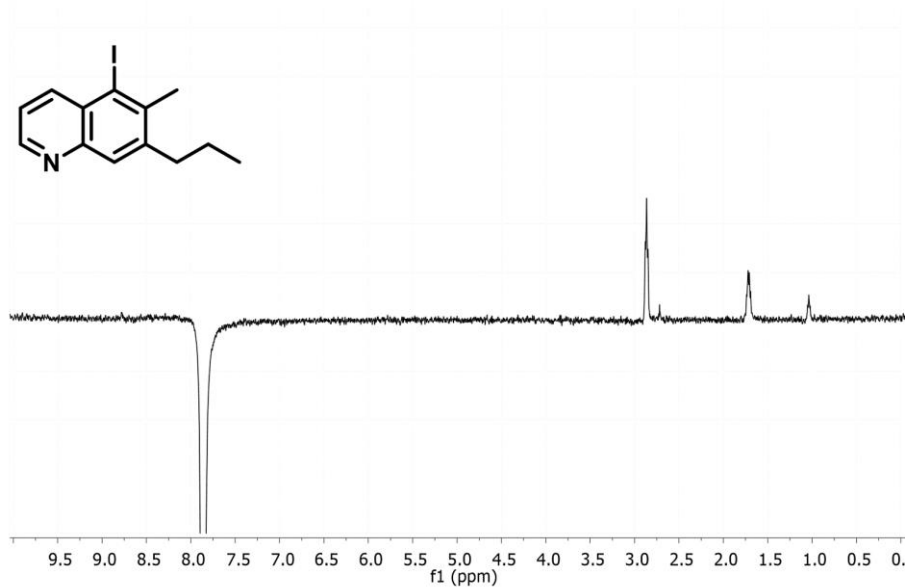
Figure 3.6 NOE spectrum of **29-*I*** (500 MHz, CDCl₃).

5. Proposed Mechanism of the Generation of HX via Haloform

From previous studies, it was hypothesized that HX was generated from the thermolysis of chloroform and 1,4-CHD at 165 °C based on the generation of $CHDCl_2$ which exhibited a signal at δ 5.27 (t, J = 1 Hz) in the ^{1}H NMR spectrum of the crude reaction mixture. Also, calculations on the thermolysis reaction indicate that the net reaction is exothermic by 42.2 kcal/mol (Scheme 3.8).[11]

$$\Delta G° = \text{-42.2 kcal/mol}$$
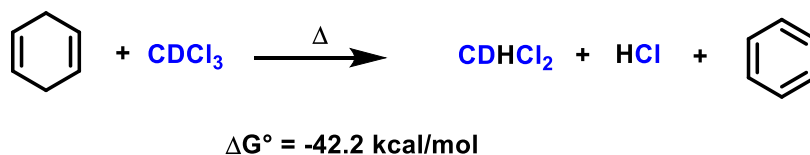
Scheme 3.8. Enthalpy calculation for the conversion of 1,4-CHD and chloroform to benzene, $CDHCl_2$ and HCl. Calculations performed by Kim Baldridge using BP86 density functional, Def2-TZVPP basis set, GAMESS Program.

A set of control experiments confirmed that HCl is generated under the reaction conditions. Heating a solution containing $CDCl_3$, 1,4-CHD and 1,3,5-tris(trifluoromethyl)benzene (internal standard) in a flame-sealed NMR tube at 165 °C for 24 h resulted in the formation of benzene (δ 7.36, s) in 70% yield and $CDHCl_2$ (δ 5.32, t, J_{HD} = 1.0 Hz) in 67% yield, based on consumed 1,4 CHD (53%). After the reaction was complete, the tube was opened and N,N,N',N'-tetramethyl-1,8-naphthalenediamine (proton sponge) was added, and a subsequent ^{1}H NMR spectrum was acquired. This spectrum exhibited a broad resonance at δ 18.96, which is indicative of the protonated diamine.[12] Notably, when the $CDCl_3$ solvent was dried over CaH_2 and distilled under a N_2 atmosphere in the dark, no reaction occurred between 1,4-CHD and the solvent at 165 °C. When the solution was subsequently photolyzed utilizing a broad-spectrum UV irradiation source (Oriel

1000 watt Universal Xenon ArcLamp model 8540) for 30 min, the formation of CDHCl$_2$ was observed by ^{1}H NMR spectroscopy.

The methylene carbon-hydrogen bond strength in 1,4-CHD is 76.9 kcal/mol while the carbon-chlorine bond strength for CHCl$_3$ is 76.6 kcal/mol. [13,14] As a result, the conversion of 1,4 CHD and CDCl$_3$ to benzene, CDHCl$_2$, and HCl, must be a radical chain reaction for it to occur efficiently at 165 °C. While it is difficult to determine the initiation step for radical chain mechanisms, chloroform often contains impurities such as Cl$_2$ and phosgene.[15] On the basis of the control reactions described above, a radical chain mechanism is proposed for the generation of HCl upon thermolysis of CDCl$_3$ and 1,4-CHD (Scheme 3.9). Light possibly triggers homolytic cleavage of the Cl-Cl bond to give radical initiators for the chain reactions (Scheme 3.9 and 2.12.) After initiation, radical propagation occurs via the CDCl$_2$ radical **30**. This radical then abstracts a hydrogen atom from 1,4-CHD, forming CHDCl$_2$ and cyclohexadienyl radical **31** (step 1, Scheme 3.9). Next, **31** abstracts a chlorine atom from CDCl$_3$, to generate benzene, HCl and a new CDCl$_2$ radical, **30** (step 2, Scheme 3.9), continuing the radical process.
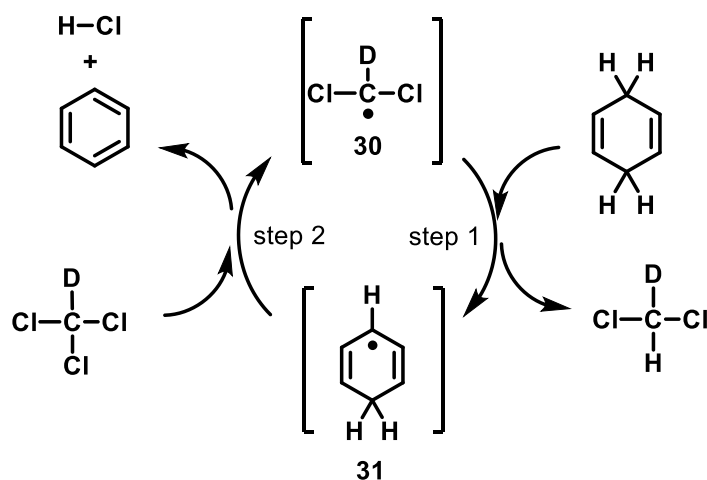
Scheme 3.9. Proposed radical chain mechanism for HCl generation.

There are three reports in the literature that support the proposed mechanism. Foremost, the bond dissociation energy for cyclohexadienyl radical **31** is approximately 22 kcal/mol.[16] It has been reported that **31** undergoes a homolytic hydrogen-carbon bond cleavage at 186 °C, to generate a hydrogen radical and benzene (Scheme 3.10).[17] Lastly, it has been demonstrated that hydrogen radicals generated by pulse radiolysis react quantitatively with benzyl chloride to form HCl and benzyl radicals (Scheme 3.11).[18]
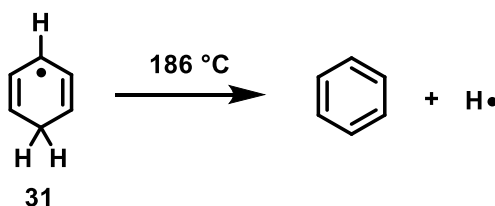
Scheme 3.10. Generation of a hydrogen radical from **31**.[17]
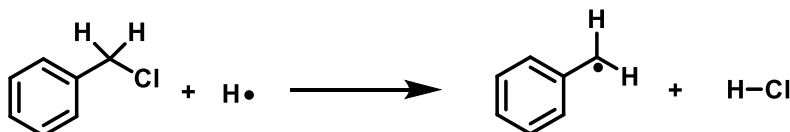
Scheme 3.11. HCl is formed via reaction of a hydrogen radical with benzyl chloride.[18]

6. An Alternative Radical Chain Mechanism for Incorporation of Hydrogen from 1,4-CHD and Halogen from Haloform

Another plausible mechanism for the incorporation of hydrogen from 1,4-CHD and halogen from haloform begins with the CDX_2 radical **30**-*X*. This radical then abstracts a hydrogen atom from 1,4-CHD, forming $CHDX_2$ and cyclohexadienyl radical **31** (step 1, Scheme 3.12) Next,

free radical addition of a hydrogen atom from **31**, forms radical **32** and benzene (step 2, Scheme 3.12). Lastly, radical **32** abstracts a halogen atom from CDX$_3$, to generate **33** and a new CDX$_2$ radical **30**-*X* (step 3, Scheme 2.12), continuing the radical process. One or both of the mechanisms proposed in sections 5 and 6 may be occurring during the course of the thermolysis reaction of **26**. Dienyne **33** is proposed to undergo a Hopf-type cycloaromatization mechanism to form **29**-*Br* and **29**-*I* (Section 7).
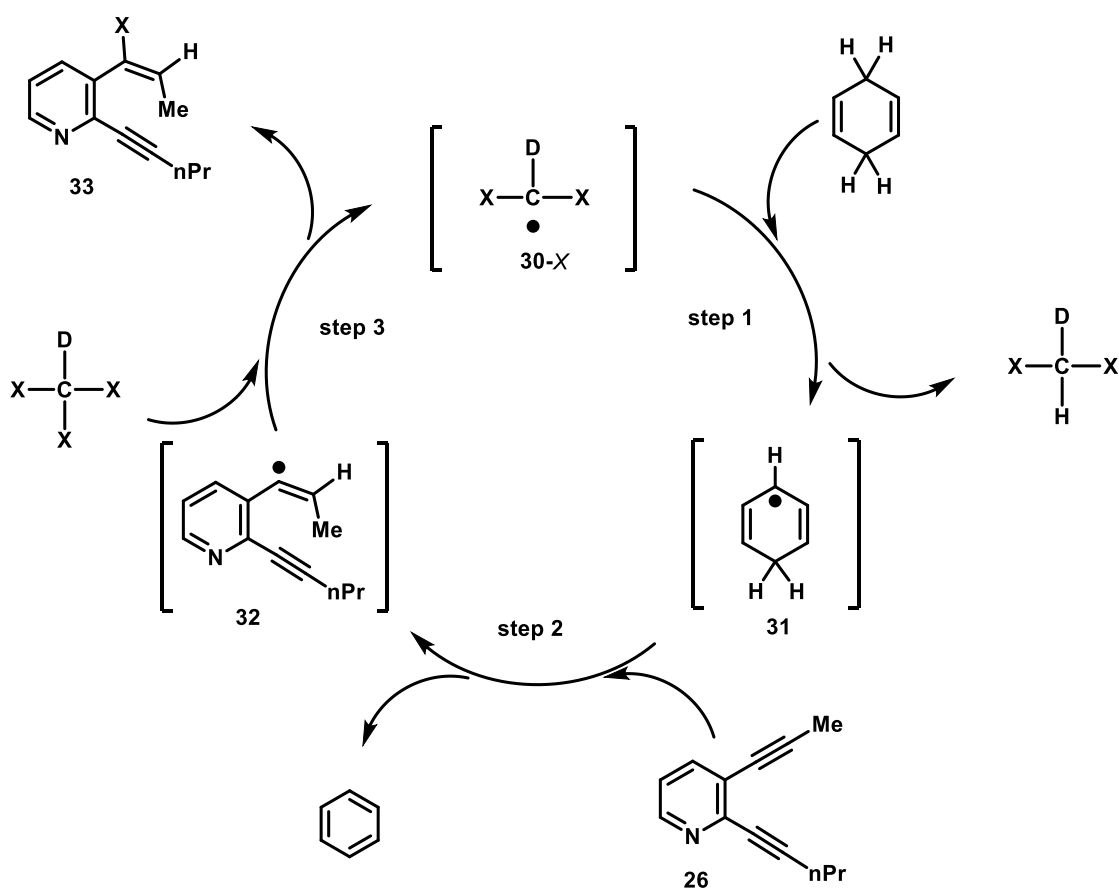
Scheme 3.12. An alternative radical chain mechanism to that shown in Scheme 3.9.

94

7. Proposed Mechanism of the Generation of 29-*Br* and 29-*I*

The observation that HX is formed from 1,4-CHD and CDX$_3$ suggested that HX would promote the cyclization of **26** in the absence of 1,4-CHD. Hence, **26** was protonated with aqueous mineral acids, HBr and HI, to form pyridinium compounds **32-*Br*** and **32-*I*** in quantitative yields. Thermolysis of **32-*Br*** and **32-*I*** in benzene at 165 °C for 24 h yielded **29-*Br*** and **29-*I*** in 50% and 64% isolated yields, respectively (Scheme 3.13).
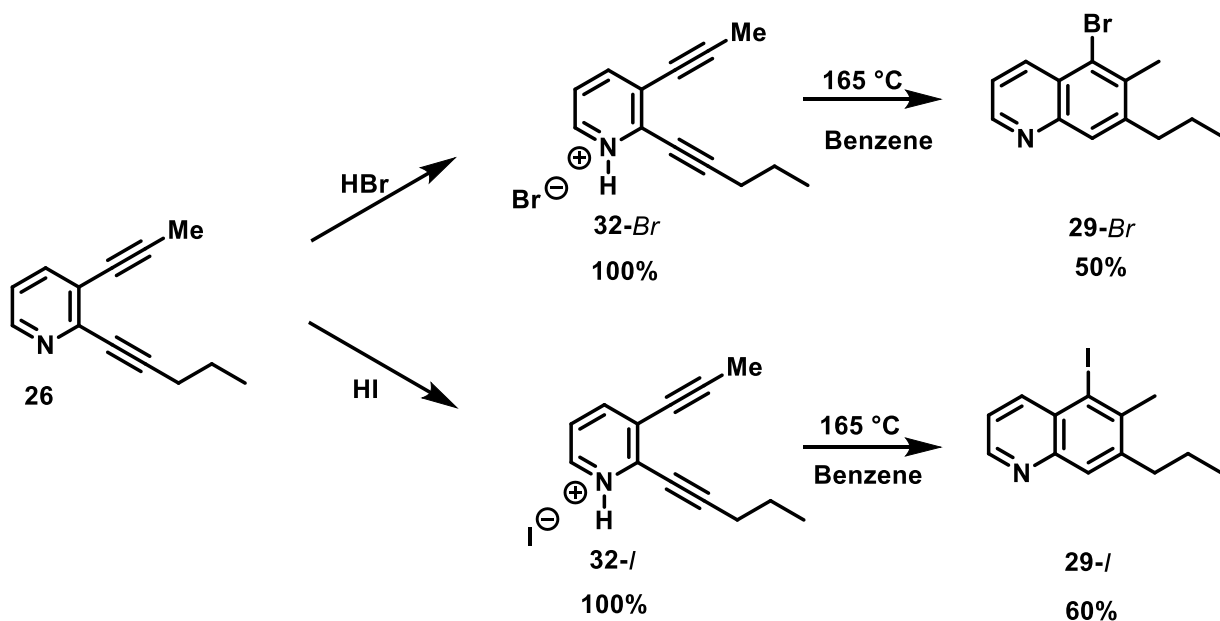
Scheme 3.13. Synthesis and thermolysis of pyridinium variants **32-*Br*** and **32-*I***.

Based upon the above results, a mechanism for the formation of **29-*Br*** and **29-*I*** can be proposed. Dienyne **33** is proposed to form from either (or both) the free radical addition of a hydrogen atom from a cyclohexadienyl radical and halogen abstraction from haloform and/or the *in situ* generation of HX which then adds across propynyl triple bond of **26**.

If HX is generated *in situ,* it would lead to reversible protonation of **26** at nitrogen to form pyridinium salt **26-*H***. Addition of mineral acid to alkynes has been suggested to favor a concerted *cis*-addition in non-polar solvents.[19] Consequently, at elevated temperatures, HX is proposed to add across the alkyne to form dienyne **33-*E***, which then undergoes a 6π electrocyclization to form

iso-benzene **34**. A [1,2]-H shift forms carbene biradical **35** and another [1,2]-H shift would form arene product **29** (Scheme 3.14).
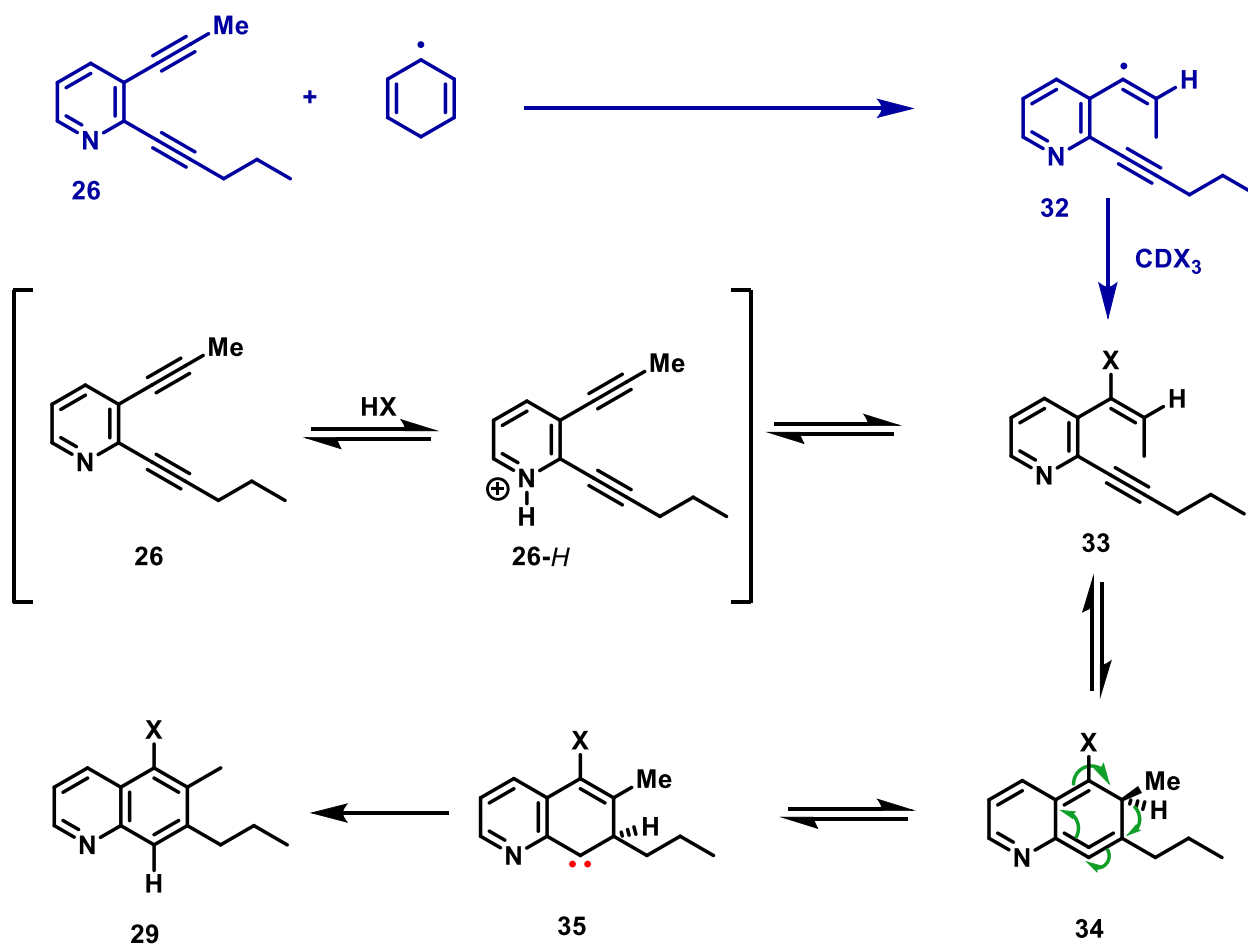
Scheme 3.14. Proposed mechanism of the formation of **29** from **26**. In blue: the free radical addition of a hydrogen atom from cyclohexadienyl radical and halide from haloform. In black: the *in situ* generation of HX.

The addition of HX to alkynes, promoting enediyne cyclization to arene products, is supported by reports by Liu and co-workers.[20] They proposed a double addition of aqueous HX (X = Cl, Br, and I) to 1,2-diethynylcyclohexene (**36**). Upon heating **36** and HI at 100 °C in 3-

pentanone, cyclized product **38** (X = I) was isolated in 46% yield along with **37** (X = I) in 33%

yield. Upon heating **36** with HCl or HBr, mono-halogenated aromatic products **38** (X =Cl, Br)

were formed in 54% and 51% yield respectively via the proposed loss of HX. They did not observe

the formation of **37** (X = Cl, Br) upon reaction of **36** with HX (X = Cl, Br) (Scheme 3.15).
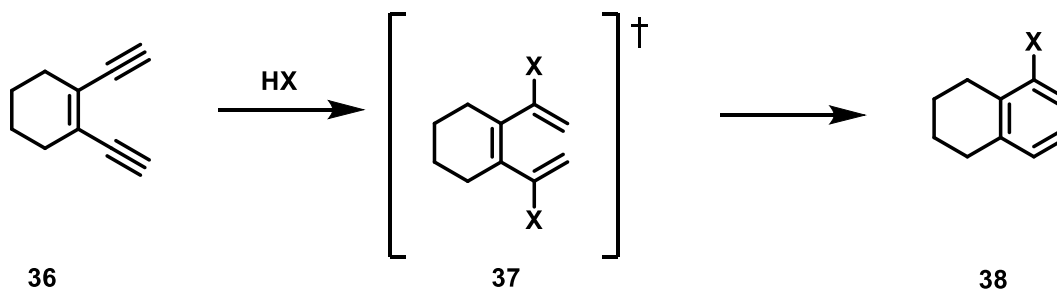
Scheme 3.15. Cyclization of enediynes **36** and **37** observed by Liu.[20]

Additionally, the mechanism that we propose is similar to Hopf's proposed mechanism

for conversion of dienyne **39** to benzene at 274 °C (Scheme 3.16).[21] Based on both experimental

and computational results, he proposed that dienyne **39** undergoes a 6π electrocyclization via a

disrotatory ring closure to form isobenzene intermediate **40**. Intermediate **40** then undergoes a

[1,2]-H shift, to give singlet or triplet carbene **41** and **42**. The singlet/triplet gap for **41** and **42** was

calculated to be 1 kcal/mol. Lastly, another [1,2]-H shift on intermediate **41** yields benzene.[22,23]
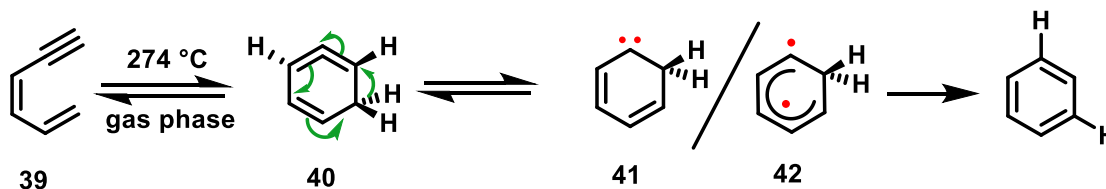
Scheme 3.16. Proposed Hopf cycloaromatization of dienynes to form aromatic products.[22,23]

8. Regioselectivity of Product **29-*Br*** and **29-*I***

One interesting observation concerning the thermolysis of **26** in haloform is the regioselective formation of quinoline derivatives **29-*Br*** and **29-*I***, with no evidence of quinoline isomers **43-*Br*** or **43-*I*** (Scheme 3.17).
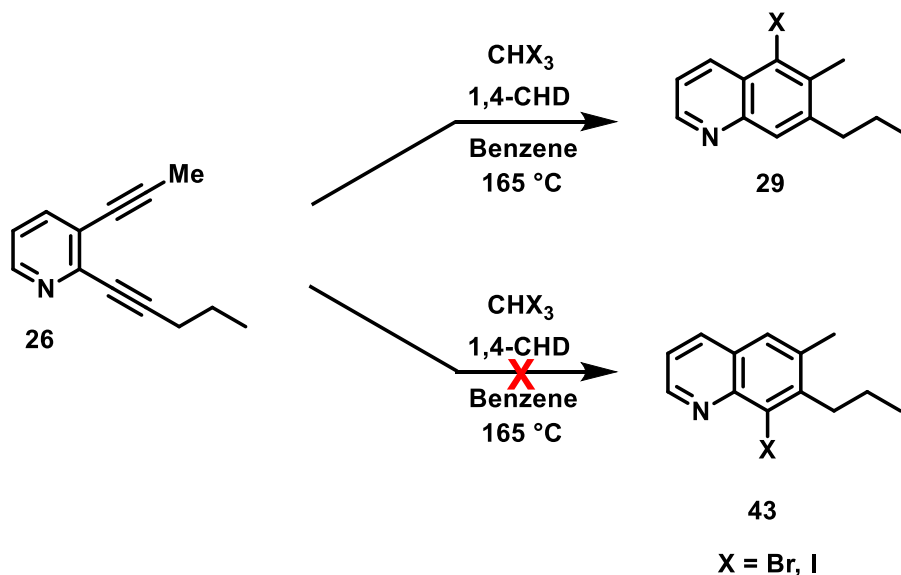
Scheme 3.17. Regioselectivity of the thermolysis of **26** in haloform.

If HX is added across the methyl alkyne in a *syn* fashion, there will be a buildup of positive charge on the C2, C4 and C5 positions of the pyridine ring and the vinyl carbon. However, if HX is added across the *n*-propyl alkyne, there will be positive charge buildup on the vinyl carbon, C3, C5, and nitrogen of the pyridine ring. Nitrogen is more electronegative (3.04) than carbon (2.55) based on the Pauling scale of electronegativity.[24] Therefore, one plausible explanation for the selectivity of formation of products **29-*Br*** and **29-*I*** is due to the positive charge buildup on the nitrogen atom, which is a relatively minor resonance contributor. Consequently, addition of HX is selective to the alkyne to give the regioisomer with the greatest resonance stabilization. (Scheme 3.18).
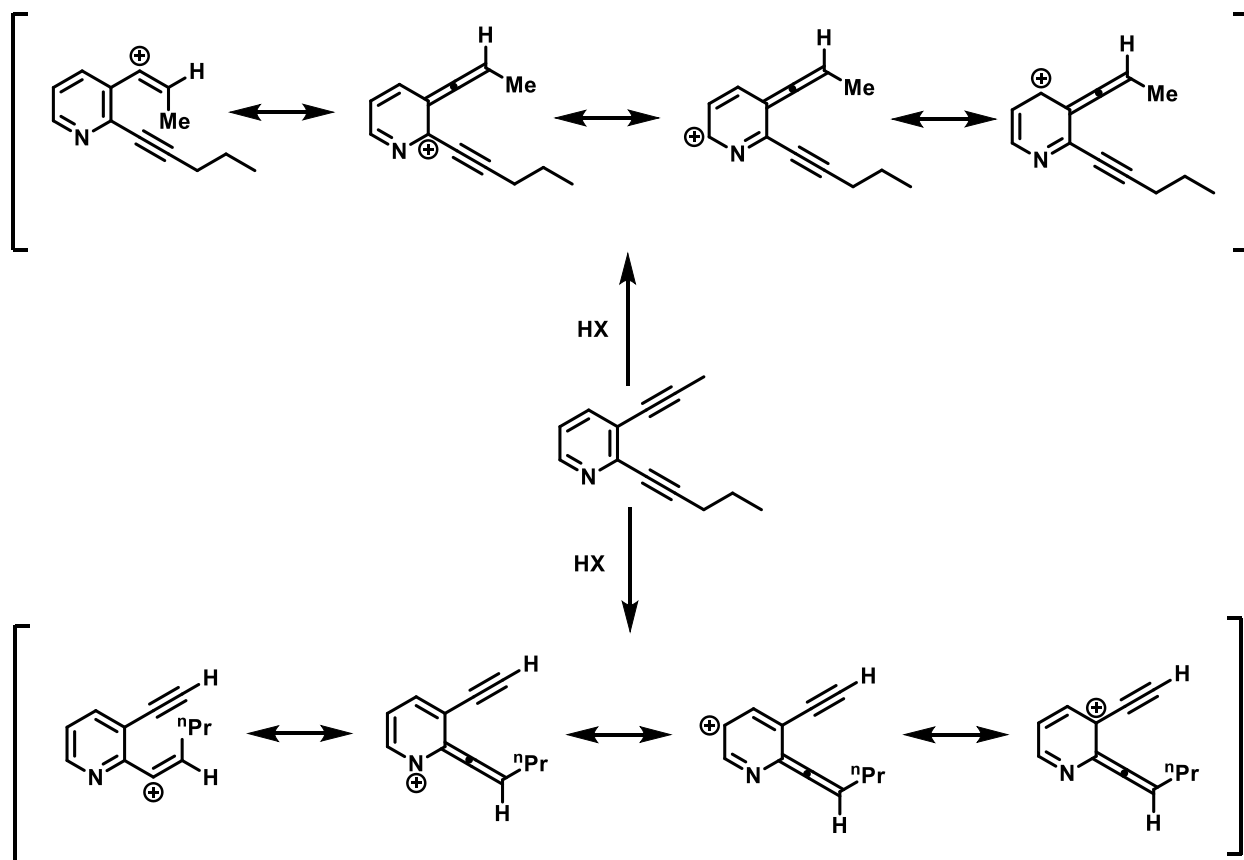
Scheme 3.18. Resonance forms for the intermediate formed upon protonation of **26**.

9. Formation of Bergman Product in the Presence of Haloform

Another curious result is that Bergman product **27** only formed in the presence of haloform, but not under standard Bergman cyclization conditions. This result is unexpected since it has been reported that electron withdrawing groups lower the activation energy for cycloaromatization.[25] Also, Russell and co-workers reported a similar enediyne **44** cyclizes to Bergman product **45**, upon thermolysis of **44** in CCl₄ at 120 °C for 20 h. Product **45** was detected by GC-MS analysis, and no yield was given (Scheme 3.19). Russell and co-workers determined that the activation energy of this reaction was 21.5 kcal/mol by plotting the rate of disappearance of **44** via analytical gas chromatography and calculated the activation energy from the slope of the Arrhenius plot.[9]
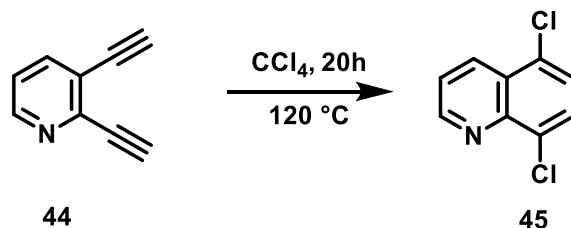
Scheme 3.19. Bergman cyclization reported by Russell.[9]

It is still unclear why **26** did not form **27**, however one theory consistent with the results and literature reports[25] is that the activation energy of **26** might be higher due to the presence of electron donating methyl and *n*-propyl groups on the terminal alkynes. It has been shown in the literature that electron donating alkyne substituents increase the activation energy for thermal cycloaromatization because the steric repulsion is increased between the in-plane π-orbitals.[25,26]

One hypothesis for the formation of **27** in haloform is that protonation of the ring nitrogen may increase the rate of the Bergman cyclization, since the pyridinium variants are more electron-withdrawing than the parent enediyne **27**. Russell and co-workers synthesized 4-substituted-1,2-diethynylbenzene derivatives **46**, **47** and **48** and determined that electron-deficient aromatic enediyne **46** ($t_{1/2}$ = 4.3 min) cyclized faster than electron-rich derivative **48** ($t_{1/2}$ = 15.6 min) (Scheme 3.20).[27]
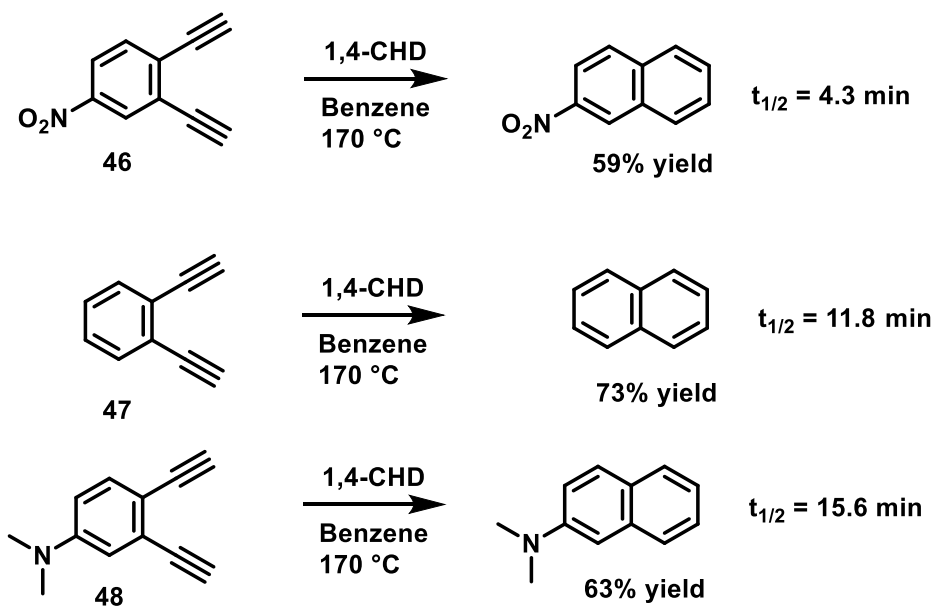
Scheme 3.20. Russell's observations that electronic deficient aromatic enediynes cyclize faster than electron-rich enediynes.

To test this hypothesis, pyridinium enediyne **50** was synthesized in quantitative yield beginning with refluxing **26** and methyl iodide in MeCN to form **49**. To increase the solubility of **49** in benzene, counter-ion exchange was performed by dissolving **49** in methanol and precipitating **50** upon addition of aqueous NH_4PF_6 (Scheme 3.21). Subsequently, upon thermolysis of **50** in benzene with 10 equivalents of added 1,4-CHD, **51** was formed in 10% yield (Scheme 3.22) This result suggests that the formation of **27** is facilitated by protonation of the enediyne. Protonation creates an electronic deficient enediyne, which in turn causes the rate of the reaction to increase.
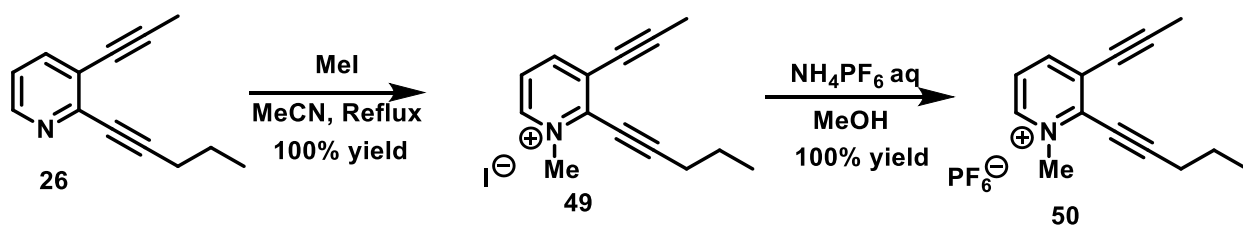
Scheme 3.21. Synthesis of enediyne **53**.
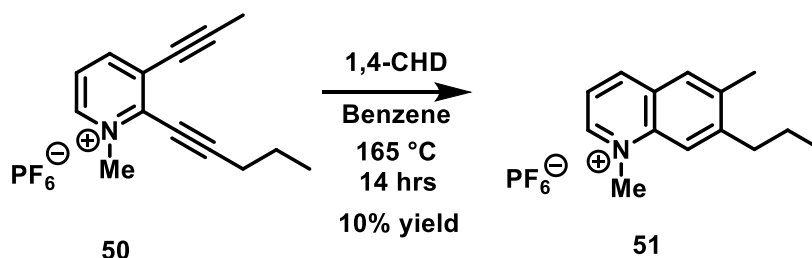
Scheme 3.22. Thermolysis of **54** in 1,4-CHD yields Bergman product **55**.

C. Conclusions and Future Directions.

In conclusion, the thermolysis of pyridine enediyne **26** in bromoform or iodoform, leads to the unprecedented regioselective formation of halogenated quinoline products **29-*Br*** and **29-*I***, along with Bergman product **27**. Halogen connectivity was established by HMBC and NOE NMR spectroscopic analysis. Also, a Hopf-type mechanism is proposed for the conversion of **26** to the halogenated aromatics **29-*Br*** and **29-*I***. The key dienyne intermediate **33**, is proposed to form by one (or both) of two mechanisms: a) via an unprecedented radical chain mechanism for the *in situ* generation of HX, CDHX$_2$, and benzene from 1,4-CHD and haloform; or b) free radical addition of a hydrogen atom from cyclohexadienyl radical **31,** followed by abstraction of halide from haloform. Electron-poor enediyne **49** was synthesized and observed to undergo Bergman cyclization in benzene and 1,4-CHD, whereas the parent enediyne **26** did not undergo cyclization

102

under similar conditions. The formation of cyclized product **50** was hypothesized to form due to the electronic-deficient nature of **49**.

Future directions for this project are centered around the synthesis of 2,3-di(prop-1-yn-1-yl)pyridine (**52**), 1,2-di(prop-1-yn-1-yl)benzene (**53**) and 1-(pent-1-yn-1-yl)-2-(prop-1-yn-1-yl)benzene (**54**) (Figure 3.7). Thermolysis of these enediynes in the presence of haloform or acid could give insights on the electronic and steric effects of halogen selectivity of compound **29**. Future outlooks on this project are also centered around computational analysis. Computational studies could produce valuable information on the selectivity of 6π electrocyclizations versus [1,7]-H shifts of the aromatic and alicyclic enediynes.
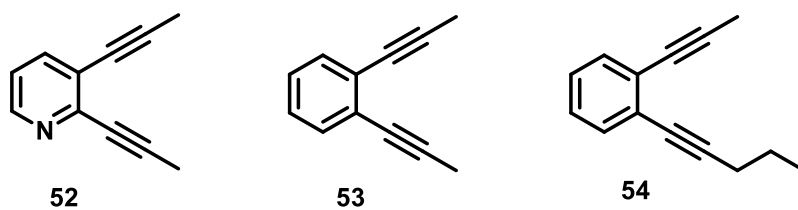
Figure 3.7. Enediyne molecules of future interest.

D. Experimental

1. General Methods

Reagents were obtained from Aldrich, Fisher Scientific, Alfa Aesar, or Fluka, and were used without further purification unless stated otherwise. All solvents were obtained from Fisher scientific and dried on Alumina columns prior to use. Chromatography solvents were ACS technical grade and used without further purification. ^{1}H NMR and ^{13}C NMR spectra of all compounds were recorded on a Bruker AVA 300 MHz, Varian Mercury Plus 400 MHz, Varian VX 500 MHz, or JOEL ECA 500 MHz instruments. Chemical shifts are reported as δ in units of parts per million (ppm) referenced to residue solvent peak. Coupling constants are reported as a *J* value

in Hertz (Hz). Mass spec analysis was performed by the UCSD Chemistry and Biochemistry Molecular Mass Spectrometry Facility on a ThermoFinnigan LCQdeca mass spectrometer with an atmospheric pressure electrospray ionization (APCI) source or an electrospray ionization (ESI) source. Infrared spectra were obtained on a Nicolet iS10 FT-IR. Deuterated NMR solvents, used for routine NMR analysis and NMR scale reactions, were dried over 3 Å activated molecular sieves and then distilled under static vacuum into oven-dried Schlenk storage tubes. Deuterated solvents were degassed using a Freeze-Pump-Thaw procedure, typically 5 cycles.

2. Synthesis of Enediynes:

Synthesis of 2-(pent-1-yn-1-yl)nicotinaldehyde (24): To a flame-dried 200 mL Schlenk flask, equipped with a stir bar and rubber septum, commercially available 2-bromonicotinaldehyde (2.00 g, 10.75 mmol), benzene (50 mL) and trimethylamine (50 mL) were added and the flask was purged by bubbling N_2 through the solution for 15 min. Under a steady stream of N_2, CuI (290 mg, 1.150 mmol) and Pd(PPh)$_3$Cl$_2$ (380 mg, 0.53 mmol) were added to the stirred solution. The mixture was allowed to react, under N_2, for 10 min before 1-pentyne (2.12 mL, 21.43 mmol) was added via syringe. After stirring for an additional 3 h, the reaction mixture was filtered through a plug of celite, which was subsequently washed with methylene chloride (100 mL). The combined washings were concentrated *in vacuo* and purified by silica gel column chromatography (1:9 EtOAc:hexanes) to give **24** as a yellow oil (1.70 g, 90%). ^{1}H NMR (400 MHz, CDCl$_3$) δ 10.54 (s, 1H, C(O)H), 8.74 (d, J_{HH} = 4.6 Hz, 1H, aryl), 8.15 (d, J_{HH} = 7.9 Hz, 1H, aryl), 7.34 (dd, J_{HH} = 7.5, 4.9 Hz, 1H, aryl), 2.51 (t, J_{HH} = 7.0 Hz, 2H, CH$_2$), 1.72 (sex, J_{HH} = 7.2 Hz, 2H, CH$_2$), 1.08 (t, J_{HH} = 7.3 Hz, 3H, CH$_3$). ^{13}C{^{1}H} NMR (100 MHz, CDCl$_3$) δ 191.59 (C(O)H), 154.61 (aryl), 146.92 (aryl), 134.83 (aryl), 131.94 (aryl), 123.01 (aryl), 98.74 (C≡C), 77.03 (C≡C) 21.93 (CH$_2$), 21.75

(CH$_2$), 13.94 (CH$_2$). IR (KBr, thin film): 2964, 2931, 2870, 2226, 1696 cm^{-1}. ESI-MS (*m/z*) calcd for [C$_{11}$H$_{11}$NO]$^+$ 174.0913; found 174.0916.
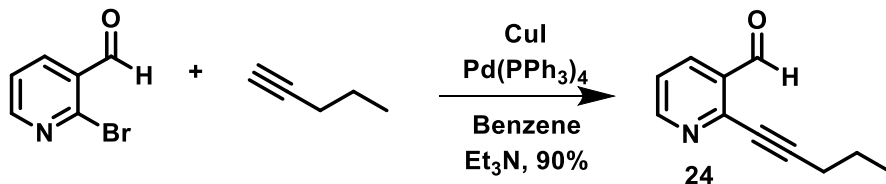
Synthesis of 3-ethynyl-2-(pent-1-yn-1-yl)pyridine (25): To a flame-dried 100 mL round-bottom flask, equipped with a stir bar and rubber septum, THF(30 mL) and trimethylsilyldiazomethane (1.73 mL, 2.00 M in ether, 3.46 mmol) were added and the flask was purged by bubbling N$_2$ through the solution for 5 min. The solution was cooled to -78 °C and *n*-BuLi (2.66 mL, 1.30 M in hexanes, 3.46 mmol) was added dropwise. The reaction mixture was allowed to react for 1 h. A degassed THF (5 mL) solution of **24** (1.50 g 8.65 mmol) was added dropwise via syringe over the course of 20 min. The reaction mixture was then allowed to react for 1 h at -78 °C, and then for 30 min at 0 °C. The reaction mixture was warmed to room temperature over the course of 1 h, quenched with a saturated aqueous NH$_4$Cl solution, and the mixture extracted with Et$_2$O (3 x 25 mL). The combined organic layers were washed once with brine (25 mL) and dried over MgSO$_4$. The organic layers were filtered and the volatiles were concentrated *in vacuo*. The crude material was purified by silica gel column chromatography (1:9 EtOAc:hexanes) to give **25** as a yellow oil (1.17 g, 80%). ^{1}H NMR (400 MHz, CDCl$_3$) δ 8.51 (d, J_{HH} = 4.6 Hz, 1H, aryl), 7.77 (d, J_{HH} = 7.9 Hz, 1H, aryl), 7.17 (dd, J_{HH} = 7.9, 4.9 Hz, 1H, aryl), 3.40 (s, 1H, -C≡CH), 2.50 (t, J_{HH} = 7.0 Hz, 2H, CH$_2$), 1.69 (sex, J_{HH} = 7.1 Hz, 2H, CH$_2$), 1.09 (t, J_{HH} = 7.3 Hz, 3H, CH$_3$). ^{13}C{^{1}H} NMR (100 MHz, CDCl$_3$) δ 149.30 (aryl), 146.23 (aryl), 139.91 (aryl), 121.68 (aryl), 121.51 (aryl) 95.76 (C≡C), 83.34 (C≡C), 80.39 (C≡C), 79.47 (C≡C), 22.00 (CH$_2$), 21.73 (CH$_2$), 13.81 (CH$_2$). IR (KBr,

thin film): 3284, 2958, 2930, 2229 cm^{-1}. ESI-MS (m/z) calcd for [C$_{12}$H$_{12}$N]$^+$ 170.0963; found 170.0964.
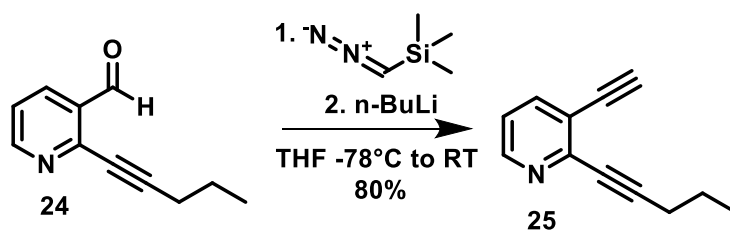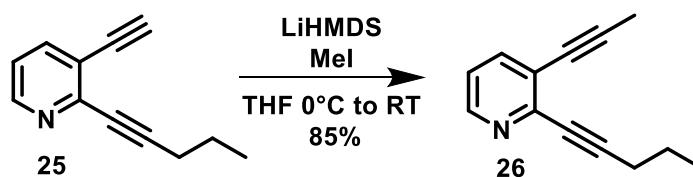

Synthesis of 2-(pent-1-yn-1-yl)-3-(prop-1-yn-1-yl)pyridine (26): To a flame-dried 200 mL round-bottom flask, equipped with a stir bar and rubber septum, THF (55 mL) and hexamethyldisilazane (1.84 mL, 8.85 mmol) were added and flask was purged by bubbling N$_2$ through the solution for 15 min. The flask was cooled to -78 °C and n-BuLi (6.36 mL, 1.30 M in hexanes, 8.26 mmol) was added dropwise. The reaction mixture was warmed to 0 °C and the mixture was allowed to react for an additional 30 min. A degassed THF (5 mL) solution of **25** (1.0 g, 5.91 mmol) was added dropwise via syringe. The reaction mixture was maintained at 0 °C for 3 h before quickly adding methyl iodide (11.00 mL, 177 mmol) via syringe. The mixture was stirred for 2 h before quenching with a saturated aqueous NH$_4$Cl solution. The reaction mixture was extracted with Et$_2$O (3 x 25 mL) and the combined organic layers were washed once with brine (25 mL) and dried over MgSO$_4$. The combined organic extracts were filtered, and the solution was concentrated *in vacuo*. The crude material was purified by silica gel column chromatography (1:9 EtOAc:hexanes) to give **26** as a dark yellow oil (920 mg, 85%). ^{1}H NMR (400 MHz, CDCl$_3$) δ 8.43 (d, J_{HH} = 3.6 Hz, 1H, aryl), 7.66 (dd, J_{HH} = 7.9, 1.7 Hz, 1H, aryl), 7.13 (d, J_{HH} = 4.8 Hz, 1H, aryl), 2.50 (t, J_{HH} = 6.9 Hz, 2H, CH$_2$), 2.12 (s, 3H, CH$_3$), 1.69 (sex, J_{HH} = 7.2 Hz, 2H, CH$_2$), 1.11 (t, J_{HH} = 7.4 Hz, 3H, CH$_3$). ^{13}C{^{1}H} NMR (100 MHz, CDCl$_3$) δ 147.49 (aryl), 144.96 (aryl), 138.83 (aryl), 122.92 (aryl), 121.25 (aryl), 94.65 (C≡C), 92.27 (C≡C), 79.29 (C≡C),

76.20 (C≡C), 21.53 (CH$_2$), 21.28 (CH$_2$), 13.18 (CH$_2$), 4.41(CH$_3$). IR (KBr, thin film): 2959, 2934, 2911, 2870 2223 cm^{-1}. ESI-MS (*m/z*) calcd for [C$_{13}$H$_{13}$N]$^+$ 184.1121; found 184.1120.

Synthesis of 2-(pent-1-yn-1-yl)-3-(prop-1-yn-1-yl)pyridinium bromide (32-*Br*): A DCM solution (1.5 mL) of **26** (48 mg, 0.26 mmol) was added to a 5 mL round-bottom flask equipped with a stir bar. Concentrated HBr (8.9 M, 0.03 mL, 0.029 mmol) was then added. The reaction mixture was allowed to react for 1 h at ambient temperature. The volatiles were concentrated *in vacuo*. The crude material was then taken up in a minimum of DCM (~0.5 mL) and the product was precipitated upon addition of cold diethyl ether. Filtration led to isolation of **32-*Br*** as an amorphous tan solid (65.5 mg, 100% yield). ^{1}H NMR (400 MHz, CDCl$_3$) δ 8.62 (d, J_{HH} = 5.50 Hz, 1H, aryl) 8.23 (d, J_{HH} = 6.97 Hz, 1H, aryl) 7.65 (dd, J_{HH} = 8.07, 5.87 Hz, 1H, aryl) 2.65 (t, J_{HH} = 6.97 Hz, 2H, CH$_2$) 2.19 (s, 3H, CH$_3$) 1.82 (sex, J_{HH} = 7.33 Hz, 2H, CH$_2$) 1.13 (t, J_{HH} = 7.33 Hz, 3H, CH$_3$) ^{13}C{^{1}H} NMR (100 MHz, CDCl$_3$) δ 151.76 (aryl), 146.77 (aryl), 139.55 (aryl), 127.16 (aryl), 123.63 (aryl), 111.47 (C≡C), 99.17 (C≡C), 73.22 (C≡C), 72.07 (C≡C), 22.02 (CH$_2$), 21.01 (CH$_2$), 13.34 (CH$_2$), 4.71 (CH$_3$). IR (KBr, thin film): 3059, 2964, 2939, 2886, 2234, 2215 cm^{-1}. ESI-MS (*m/z*) calcd for [C$_{13}$H$_{14}$N]$^+$ 184.1121; found 184.1122.
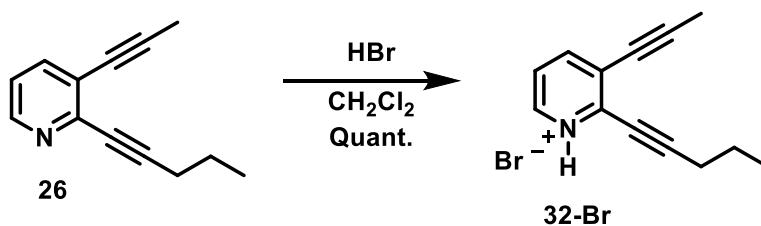
Synthesis of 2-(pent-1-yn-1-yl)-3-(prop-1-yn-1-yl)pyridinium iodide (32-*I*): A DCM solution (2.0 mL) of **26** (109 mg, 0.60 mmol) was added to a 5 mL round-bottom flask equipped with a stir bar. Concentrated HI (7.5 M, 0.2 mL, 0.1.19 mmol) was then added. The reaction mixture was allowed to react for 1 h at ambient temperature. The volatiles were concentrated *in vacuo*. The crude material was then taken up in a minimum of DCM (~0.5 mL) and the product was precipitated upon addition of cold diethyl ether. Filtration led to isolation of **32-*I*** as an amorphous yellow/brown solid (181 mg, 100% yield). ^{1}H NMR (400 MHz, CDCl$_3$) δ 8.68 (d, J_{HH} = 5.50 Hz, 1H, aryl) 8.27 (d, J_{HH} = 8.07 Hz, 1H, aryl) 7.73 (dd, J_{HH} = 7.88, 5.68 Hz, 1H, aryl) 2.66 (t, J_{HH} = 6.97 Hz, 2H, CH$_2$) 2.20 (s, 3H, CH$_3$) 1.86 (sex, J_{HH} = 7.33 Hz 2H, CH$_2$) 1.14 (t, J_{HH} = 7.52 Hz, 3H, CH$_3$). ^{13}C{^{1}H} NMR (100 MHz, CDCl$_3$) δ 146.93 (aryl), 139.46 (aryl), 136.87 (aryl), 127.05 (aryl), 123.66 (aryl), 111.68 (C≡C), 99.36 (C≡C), 72.92 (C≡C), 71.74 (C≡C), 21.86 (CH$_2$), 20.86 (CH$_2$), 13.27 (CH$_2$), 4.66 (CH$_3$). IR (KBr, thin film): 3052, 3016, 2958, 2922, 2871, 2851, 2221 cm^{-1}. ESI-MS (*m/z*) calcd for [C$_{13}$H$_{14}$N]$^+$ 184.1121; found 184.1119.

26   HI / CH$_2$Cl$_2$ / Quant.   **32-I**
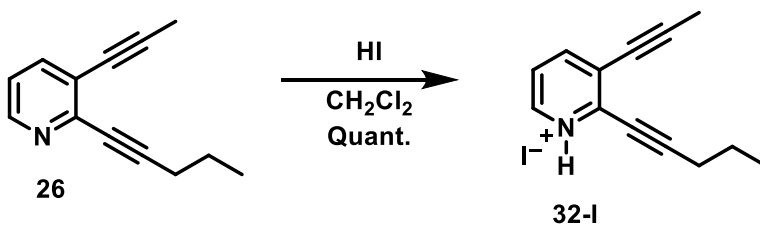
Synthesis of 1-methyl-2-(pent-1-yn-1-yl)-3-(prop-1-yn-1-yl)pyridinium iodide (49): An acetonitrile solution (20 mL) of **26** (306 mg, 1.66 mmol) and methyl iodide (0.21 mL, 474 mg, 3.34 mmol) were added to a 100 mL round-bottom flask equipped with a stir bar and reflux condenser. The reaction mixture was heated to reflux for 6 h. The volatiles were concentrated *in vacuo* to give **49** as an amorphous brown powder (540 mg, 100% yield). ^{1}H NMR (400 MHz, CDCl$_3$) δ 9.88 (d, J_{HH} = 6.23 Hz, 1H, aryl) 8.30 (d, J_{HH} = 8.07 Hz, 1H, aryl) 7.98 (dd, J_{HH} = 8.07,

6.23 Hz, 1H, aryl) 4.64 (s, 3H, -N-CH$_3$) 2.71 (t, J_{HH} = 6.97 Hz, 2H, CH$_2$) 2.18 (s, 3H, CH$_3$) 1.77

(sex, J_{HH} = 7.19 Hz, 2H, CH$_3$) 1.17 (t, J_{HH} = 7.33 Hz, 3H, CH$_3$). ^{13}C{^{1}H} NMR (100 MHz, CDCl$_3$)

δ 146.06 (aryl), 145.98 (aryl), 139.51 (aryl), 128.15 (aryl), 125.27 (aryl), 116.02 (C≡C), 99.51

(C≡C), 73.39 (C≡C), 72.00 (C≡C), 48.59 (N-CH$_3$), 22.08 (CH$_2$), 20.92 (CH$_2$), 13.15 (CH$_2$), 4.63

(CH$_3$). IR (KBr, thin film): 3016, 2958, 2922, 2871, 2221 cm^{-1}. ESI-MS (*m/z*) calcd for

[C$_{14}$H$_{16}$N]$^+$ 198.1277; found 198.1280.
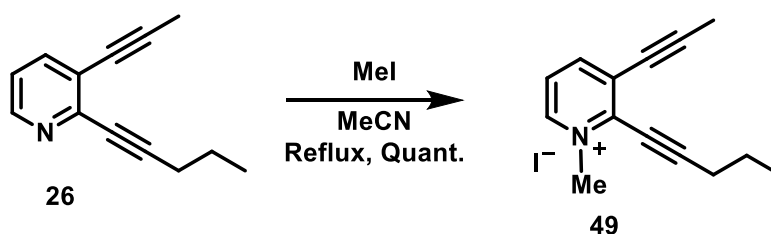
Synthesis of 1-methyl-2-(pent-1-yn-1-yl)-3-(prop-1-yn-1-yl)pyridinium hexafluoro-phosphate (50): A methanol solution (2 mL) of **49** (480 mg, 1.48 mmol) was added to a 25 mL

beaker equipped with a stir bar. NH$_4$PF$_6$ (aq) (2 mL), 1.20 g, 7.38 mmol) was added to the solution

and the product precipitated from solution. Filtration led to the isolation of **50** as a tan amorphous

solid (508 mg, 100% yield). ^{1}H NMR (300 MHz, CDCl$_3$) δ 8.75 (d, J_{HH} = 6.24 Hz, 1H, aryl) 8.29

(d, J_{HH} = 8.07 Hz, 1H, aryl) 7.83 (dd, J_{HH} = 8.16, 6.33 Hz, 1H, aryl) 4.44 (s, 3H, N-CH$_3$) 2.72 (t,

J_{HH} = 6.97 Hz, 2H, CH$_2$) 2.20 (s, 3H, CH$_3$) 1.79 (sex, J_{HH} = 7.15 Hz, 2H, CH$_2$) 1.16 (t, J_{HH} = 7.34

Hz, 3H, CH$_3$). ^{13}C{^{1}H} NMR (100 MHz, CDCl$_3$) δ 150.19 (aryl), 146.06 (aryl), 145.08 (aryl),

128.38 (aryl), 125.13 (aryl), 116.16 (C≡C), 99.39 (C≡C), 73.35 (C≡C), 71.95 (C≡C), 48.20 (N-

CH$_3$), 21.96 (CH$_2$), 20.89 (CH$_2$), 13.13 (CH$_2$), 4.58 (CH$_3$). ^{19}F NMR (376 MHz, CDCl$_3$) δ -72.49,

-74.38. IR (KBr, thin film): 3117, 2975, 2936, 2875, 2223 cm^{-1} ESI-MS (*m/z*) calcd for [C$_{14}$H$_{16}$N]$^+$

198.1277; found 198.1279.
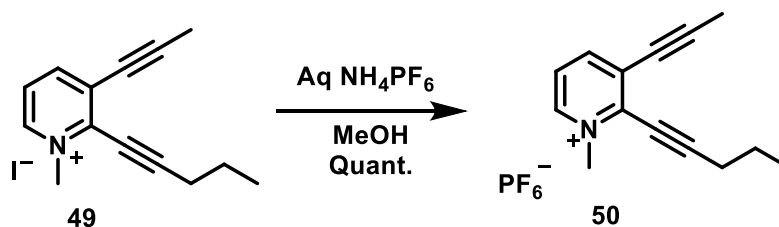
3. Thermolysis of Chloroform (Control Reactions):

Thermal Reaction of 1,4-CHD in CDCl₃ exposed to ambient light: 1,4-Cyclohexadiene (37.7 mg, 0.47 mmol), and 1,3,5-tris(trifluoromethyl)benzene (internal standard) were added to an oven dried medium-walled NMR tube. Chloroform-*d* (0.4 mL) was distilled into the tube and the solution was freeze/pump/thaw/degassed five times. The NMR tube was then flame-sealed under vacuum. An initial ^{1}H NMR spectrum was obtained prior to submerging the tube in a constant temperature oil bath maintained at 165 °C. After heating for 24 h at 165 °C, a ^{1}H NMR spectrum of the sample indicated 53% conversion of 1,4-CHD. Resonances at δ 7.38 and 5.29 (t, J_{HD} = 1.0 Hz) indicated the formation of benzene and CDHCl₂ in 70% and 67% yield, respectively, based on consumed 1,4-CHD. In addition, a new resonance was observed at δ 0.96 ppm (s, br). The NMR tube was opened and 1,8-bis(dimetylamino)naphthalene (proton sponge; 30.0 mg, 0.140 mmol) was added. A subsequent ^{1}H NMR spectrum exhibited resonances attributed to the HCl salt of proton sponge at δ 18.96 ppm (s, br, 1H), and δ 3.43 (s, 12H).
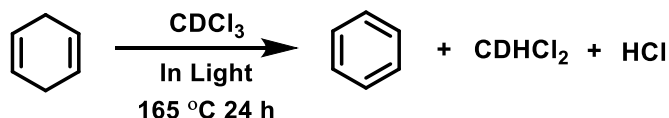
Thermal Reaction of 1,4-CHD in CDCl₃ in the dark: All manipulations were carried out in the dark, taking extra care that the chloroform was not exposed to ambient light, during the drying and distilling process. Also, the NMR tube was wrapped in aluminum foil during the experimental

procedure. 1,4-CHD (37.7 mg, 0.47 mmol), and 1,3,5-tris(trifluoromethyl)benzene (internal standard) were added to an oven dried medium-walled NMR tube. The NMR tube was placed under vacuum and $CDCl_3$ (0.4 mL) was distilled into the NMR tube. The resulting solution was subsequently degassed via 5 cycles of freeze/pump/thaw. The medium-walled NMR tube was then subsequently flame sealed under vacuum. An initial ^{1}H NMR spectrum was taken immediately. The tube was submerged in a constant temperature oil bath maintained at 165 °C for 24 h. The tube was removed from the oil bath and allowed to cool to room temperature and a ^{1}H NMR spectrum was collected, indicating no generation of $CDHCl_2$ or HCl had occurred.

Photolysis was then performed via broad spectrum UV irradiation from an Oriel 1000 watt Universal Xenon ArcLamp, model 8540 for 30 min. Another ^{1}H NMR spectrum was collected, indicating no generation of $CDHCl_2$ or HCl had occurred. The tube was then submerged again in the constant temperature oil bath maintained at 165 °C for another 24 h. The tube was then removed from the oil bath and allowed to cool to room temperature and a ^{1}H NMR spectrum was collected. The spectrum showed 7% conversion of the starting 1,4-CHD. The benzene signal at δ 7.38 ppm was formed in 28% yield. The benzene signal was normalized from the starting amount of benzene in the initial reaction by integration with the internal standard. An ^{1}H NMR resonance for $CDHCl_2$ was observed at δ 5.29 ppm (t, J = 1.0 Hz), which was formed in 27% yield. Additionally, a new ^{1}H NMR resonance was formed at δ 0.96 ppm (s, broad), which is formed in 26 % yield.
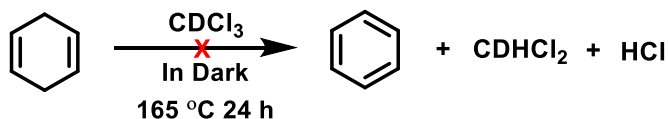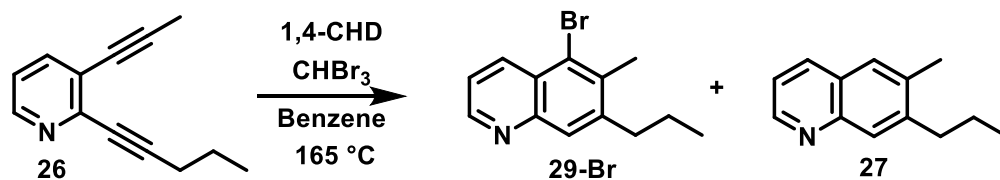

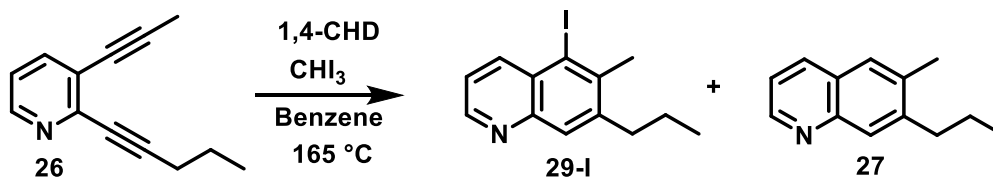## 4. Thermal Cycloaromatization Reactions:

Procedure for the Thermal Cycloaromatization with Bromoform: To a flame-dried 20 mL pressure tube compound equipped with a rubber septum, **26** (100 mg, 0.56 mmol), $CHBr_3$ (0.050 mL, 0.56 mmol), 1,4-CHD (0.55 mL, 5.6 mmol) and benzene (15 mL) were added. The pressure tube was purged by bubbling N_2 through the solution for 15 min. The pressure tube was subsequently sealed with a Teflon needle-valve and was placed in a 165 °C oil bath up to the solvent level of the pressure tube for 24 h. The tube was allowed to cool to room temperature and the solution was transferred to a 50 mL round-bottom flask and the volatiles were concentrated *in vacuo.* The crude material was purified via preparative TLC (1:99 acetone:toluene) to give **29-*Br*** (44.5 mg, 30%) and **27** (10.4 mg, 10%) as tan amorphous powders. Compound **29-*Br*:** ^{1}H NMR (300 MHz, $CDCl_3$) δ 8.84 (d, J_{HH} = 2.7 Hz, 1H, aryl), 8.58 (d, J_{HH} = 8.5 Hz, 1H, aryl), 7.88 (s, 1H, aryl), 7.44 (dd, J_{HH} = 8.6, 4.3 Hz, 1H, aryl), 2.85 (t, J_{HH} = 7.5 Hz 2H, CH_2), 2.64 (s, 3H, CH_3), 1.74 (sex, J_{HH} = 7.7 Hz, 2H, CH_2), 1.05 (t, J_{HH} = 7.3 Hz, 3H, CH_3). ^{13}C{^{1}H} NMR (100 MHz, $CDCl_3$) δ 151.32 (aryl), 149.79 (aryl), 147.25 (aryl), 143.83 (aryl), 135.90 (aryl), 135.31 (aryl), 127.79 (aryl), 123.78 (aryl), 121.24 (aryl), 36.92 (CH_2), 22.79 (CH_2), 19.88 (CH_3), 13.79 (CH_3). IR (KBr, thin film): 2964, 2926, 2871 cm^{-1}. ESI-MS (*m/z*) calcd for $[C_{13}H_{15}BrN]^+$ 264.0382; found 264.0378.

Compound **27**: ^{1}H NMR (400 MHz, $CDCl_3$) δ 8.85 (d, J_{HH} = 2.8 Hz, 1H, aryl), 8.11 (d, J_{HH} = 8.0 Hz, 1H, aryl), 7.93 (s, 1H, aryl), 7.61 (s, 1H, aryl), 7.36 (dd, J_{HH} = 8.1, 4.3 Hz, 1H, aryl), 2.81 (t, J_{HH} = 7.7 Hz 2H, CH_2), 2.51 (s, 3H, CH_3), 1.77 (sex, J_{HH} = 7.3 Hz, 2H, CH_2), 1.07 (t, J_{HH} = 7.3 Hz, 3H, CH_3). ^{13}C{^{1}H} NMR (100 MHz, $CDCl_3$) δ 151.68 (aryl), 149.11 (aryl), 143.72 (aryl), 135.82 (aryl), 134.82 (aryl), 127.51 (aryl), 127.18 (aryl), 126.53 (aryl), 120.07 (aryl), 35.33 (CH_2), 22.67 (CH_2), 19.14 (CH_3), 13.87 (CH_3). IR (KBr, thin film): 3039, 3010, 2958, 2922, 2871 cm^{-1}. ESI-MS (*m/z*) calcd for $[C_{13}H_{16}N]^+$ 186.1277; found, 186.1274.

Procedure for the Thermal Cycloaromatization with Iodoform: To a flame-dried 20 mL pressure tube equipped with a rubber septum, **3** (100 mg, 0.56 mmol), CHI_3 (215 mg, 0.56 mmol), 1,4-CHD (0.55 mL, 5.6 mmol) and benzene (15 mL) were added. The pressure tube was purged by bubbling N_2 through the solution for 15 min. The pressure tube was subsequently sealed with a Teflon needle-valve and was placed in a 165 °C oil bath up to the solvent level of the pressure tube for 24 h. The tube was allowed to cool to room temperature and the solution was transferred to a 50 mL round-bottom flask and the volatiles were concentrated *in vacuo.* The crude material was purified via preparative TLC (1:99 acetone:toluene) to give **29-I** (44.5 mg, 30%) and **27** (10.4 mg, 15%) as tan amorphous powders. Compound **29-I**: ^{1}H NMR (400 MHz, CDCl$_3$) δ 8.79 (d, J_{HH} = 4.40 Hz, 1H, aryl) 8.49 (d, J_{HH} = 9.0 Hz, 1H, aryl) 7.86 (s, 1H, aryl) 7.40 (dd, J_{HH} = 8.62, 4.22 Hz, 1H, aryl) 2.92 (t, J_{HH} = 7.7 Hz 2H, CH$_2$) 2.74 (s, 3H, CH$_3$) 1.79 (sex, J_{HH} = 7.3 Hz 2H, CH$_2$) 1.06 (t, J_{HH} = 7.33 Hz, 3H, CH$_3$). ^{13}C{^{1}H} NMR (100 MHz, CDCl$_3$) δ 151.66 (aryl), 149.79 (aryl), 143.43 (aryl), 140.78 (aryl), 140.3 (aryl), 129.25 (aryl), 128.80 (aryl), 121.67 (aryl), 106.23 (aryl), 37.56 (CH$_2$), 26.29 (CH$_2$), 22.85 (CH$_3$), 13.77 (CH$_3$). IR (KBr, thin film): 2961, 2919, 2871, 2845 cm^{-1}. ESI-MS (*m/z*) calcd for [C$_{13}$H$_{15}$IN]$^+$ 312.0244; found, 312.0244.

Thermal Cycloaromatization with 1-methyl-2-(pent-1-yn-1-yl)-3-(prop-1-yn-1-yl)pyridin-1-ium Hexafluorophosphate (54): synthesis of 1,6-dimethyl-7-propylquinolinium (55): To a flame-dried 20 mL pressure tube equipped with a rubber septum, **54** (220 mg, 0.64 mmol) and THF (20 mL) were added. The pressure tube was purged by bubbling N_2 through the solution for 15 min. The pressure tube was subsequently sealed with a Teflon needle-valve and was placed in a 165 °C oil bath up to the solvent level of the pressure tube for 24 h. The tube was cooled to room temperature and the solution was transferred to a 50 mL round bottom flask and the volatiles were concentrated *in vacuo*. The crude material was purified via preparatory HPLC utilizing a Jupiter Proteo90 Å phenomenex column (150 x 4.60 mm) with a gradient of 20%-40% ACN:H_2O over 40 min with a 4 mL flow rate to give **55** as a light yellow amorphous solid. Percent conversion (10%) was calculated via an ^{1}H NMR tube scale reaction with 1,4-bis(trimethylsilyl)benzene as an internal standard. ^{1}H NMR (500 MHz, CDCl$_3$) δ 10.30 (d, J_{HH} = 4.01 Hz, 1H, aryl) 8.73 (d, J_{HH} = 8.02 Hz, 1H, aryl) 7.97 - 8.00 (m, 1 H) 7.96 (s, 1H, aryl) 7.95 (s, 1H, aryl) 4.83 (s, 3H, -N-CH$_3$) 2.99 (t, J_{HH} = 8.02 Hz 2H, CH$_2$) 2.63 (s, 3H, CH$_3$) 1.79 (sex, J_{HH} = 8.02 Hz, 2H, CH$_2$) 1.12 (t, J_{HH} = 7.45 Hz, 3, CH$_3$) ^{13}C{^{1}H} NMR (100 MHz, CDCl$_3$) δ 152.26 (aryl), 151.57 (aryl), 144.71 (aryl), 140.59 (aryl), 137.34 (aryl), 129.72 (aryl), 127.81 (aryl), 121.27 (aryl), 116.09 (aryl), 44.78 (N-CH$_3$), 36.29 (CH$_2$), 22.83 (CH$_2$), 19.43 (CH$_3$), 13.82 (CH$_3$). IR (KBr, thin film): 3116, 2967, 2938, 2876 cm^{-1} ESI-MS (*m/z*) calcd for [C$_{14}$H$_{18}$N]$^+$ 200.1434 observed 200.1435.
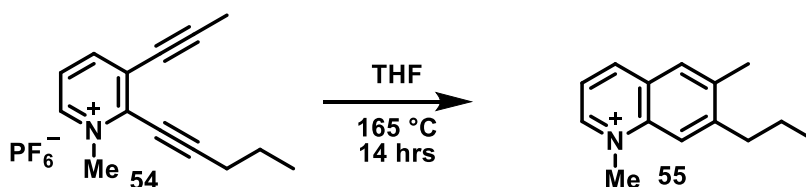
Synthesis of 5-bromo-6-methyl-7-propylquinoline (29-*Br*) via 32-*Br*: To a flame-dried pressure tube compound equipped with a rubber septum, **29-*Br*** (11 mg, 0.042 mmol) and benzene (5 mL) were added. The pressure tube was purged by bubbling N_2 through the solution for 15 min. The pressure tube was subsequently sealed with a Teflon needle-valve and was placed in a 165 °C oil bath up to the solvent level of the pressure tube for 24 h. The tube was cooled to room temperature and the solution was transferred to a 50 mL round bottom flask and the volatiles were concentrated *in vacuo.* The crude material was purified via preparative TLC (1:99 acetone:toluene) to give **29-*Br*** as a tan amorphous powder (5 mg, 50%).
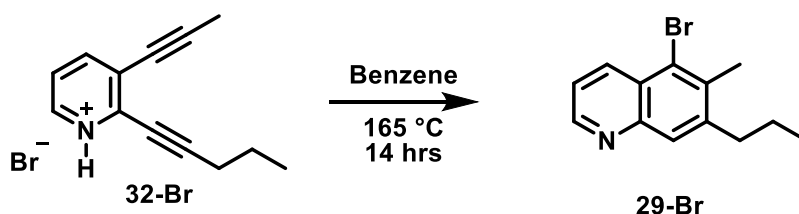
Synthesis of 5-iodo-6-methyl-7-propylquinoline (29-I) via 32-*I*: To a flame dried pressure tube equipped with a rubber septum, **32-I** (5 mg, 0.015 mmol) and benzene (5 mL) were added. The pressure tube was purged by bubbling N_2 through the solution for 15 min. The pressure tube was subsequently sealed with a Teflon needle-valve and was placed in a 165 °C oil bath up to the solvent level of the pressure tube for 24 h. The tube was cooled to room temperature and the solution was transferred to a 50 mL round bottom flask and the volatiles were concentrated *in vacuo.* The crude material was purified via preparative TLC (1:99 acetone:toluene) to give **29-*I*** as a tan amorphous powder (3 mg, 64%).
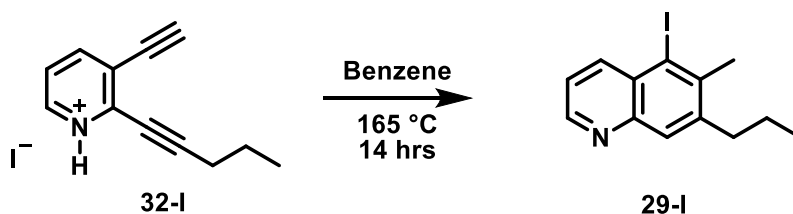
E. Appendix
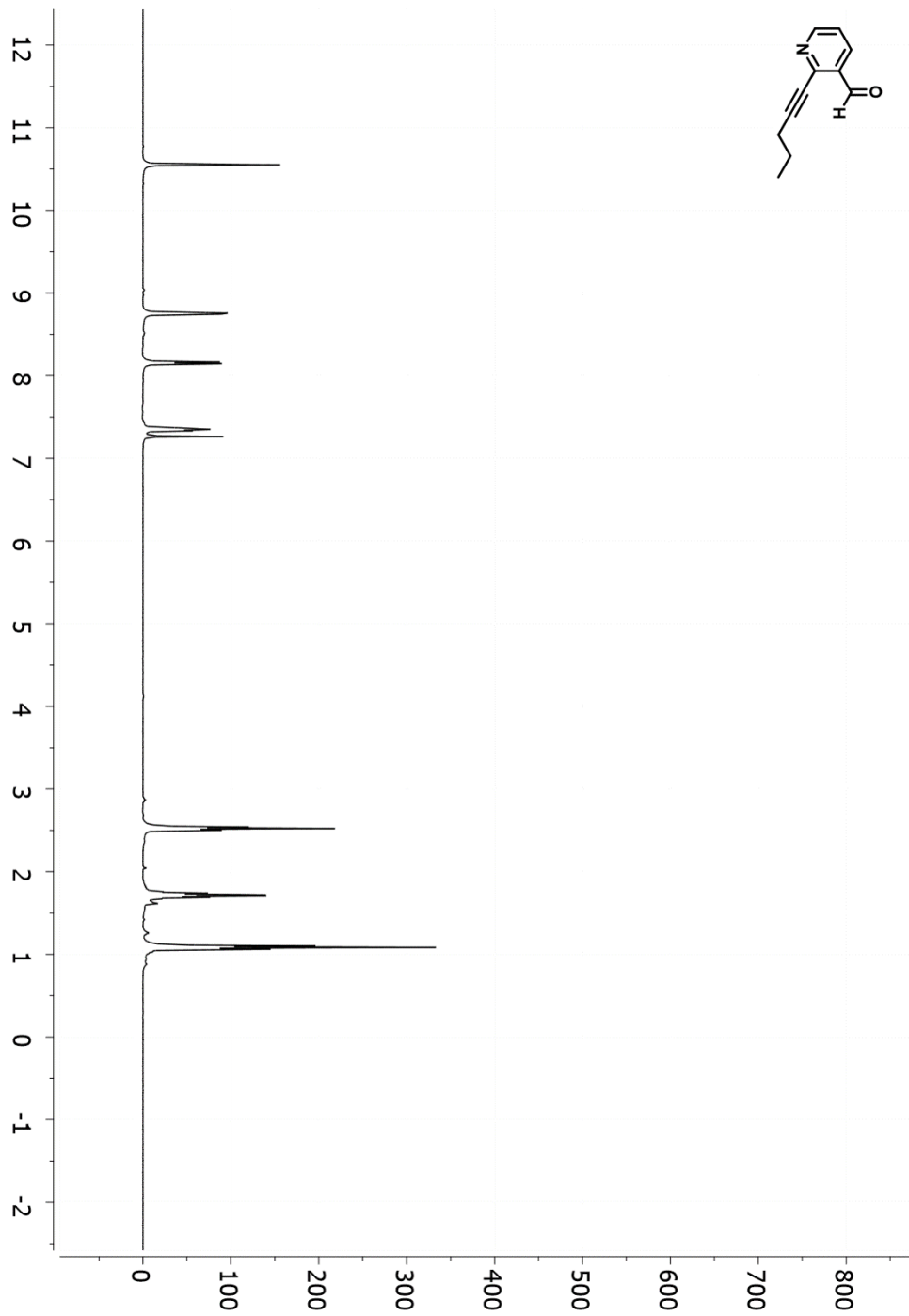
Figure 3.8. ^{1}H NMR spectrum of **24** (CDCl$_3$, 400 MHz).
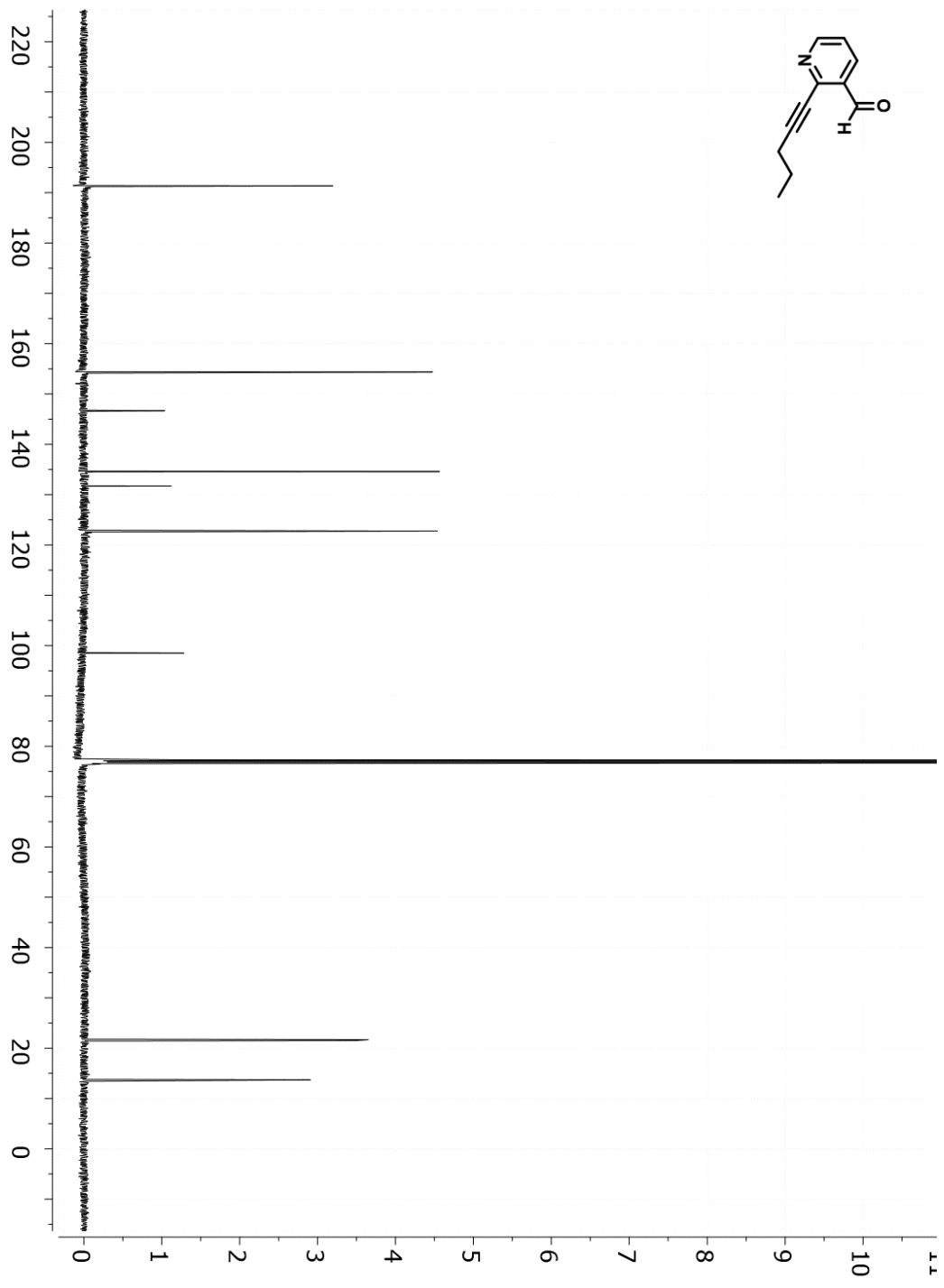
Figure 3.9. $^{13}C\{^1H\}$ NMR Spectrum of **24** (CDCl$_3$, 100 MHz).
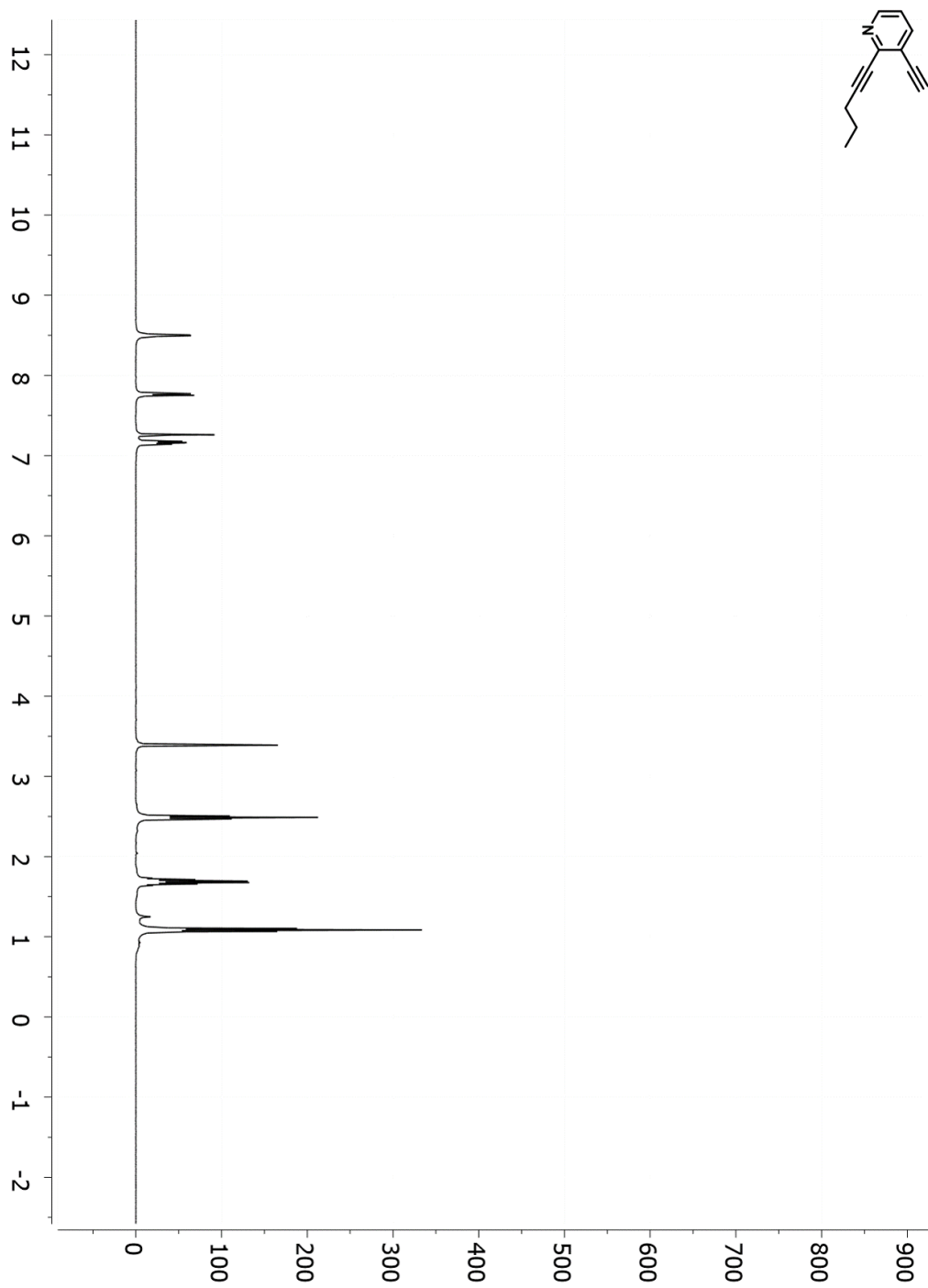
Figure 3.10. ^{1}H NMR spectrum of **25** (CDCl$_3$, 400 MHz).
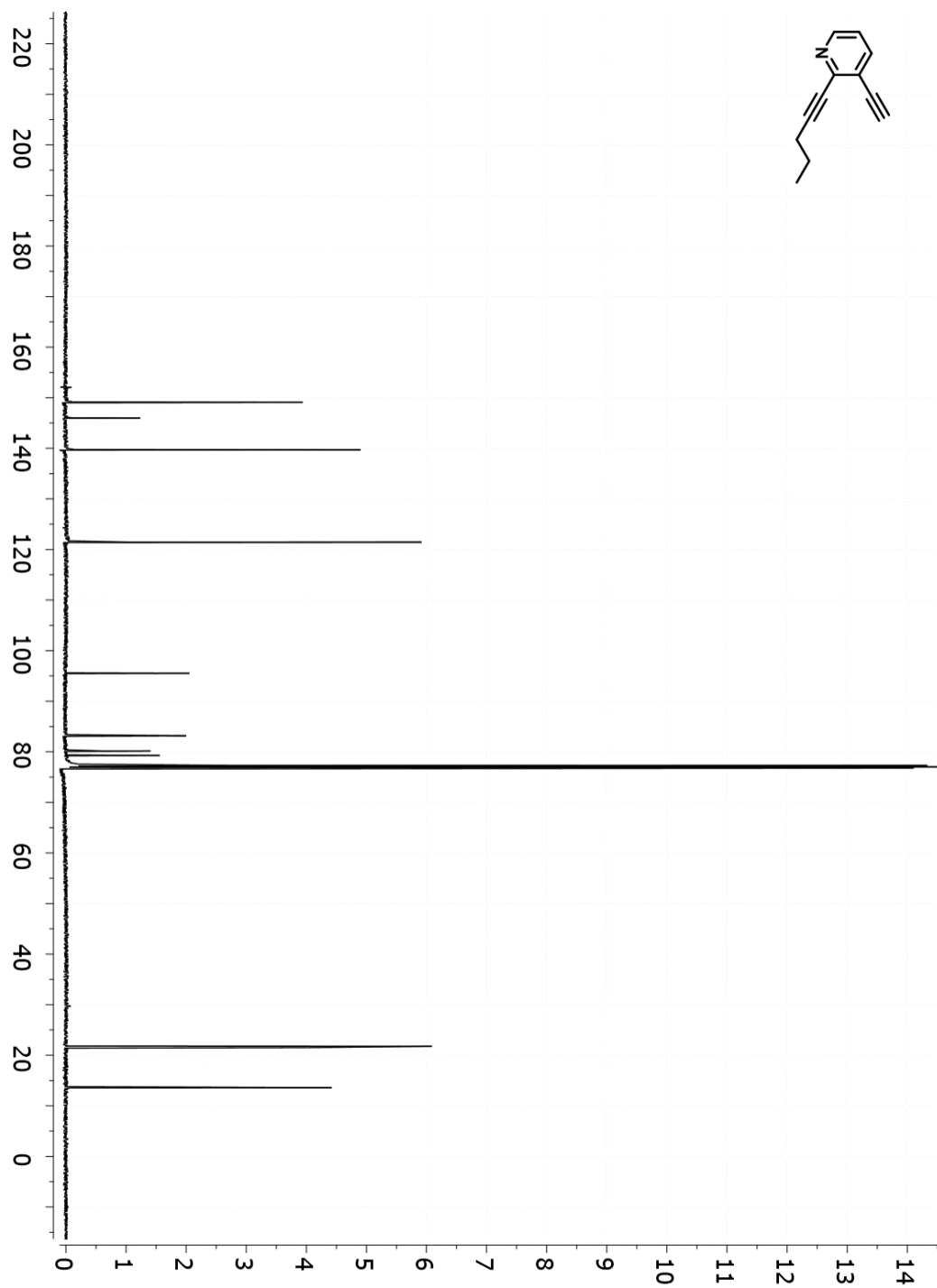
Figure 3.11. $^{13}C\{^1H\}$ NMR spectrum of **25** (CDCl$_3$, 100 MHz).
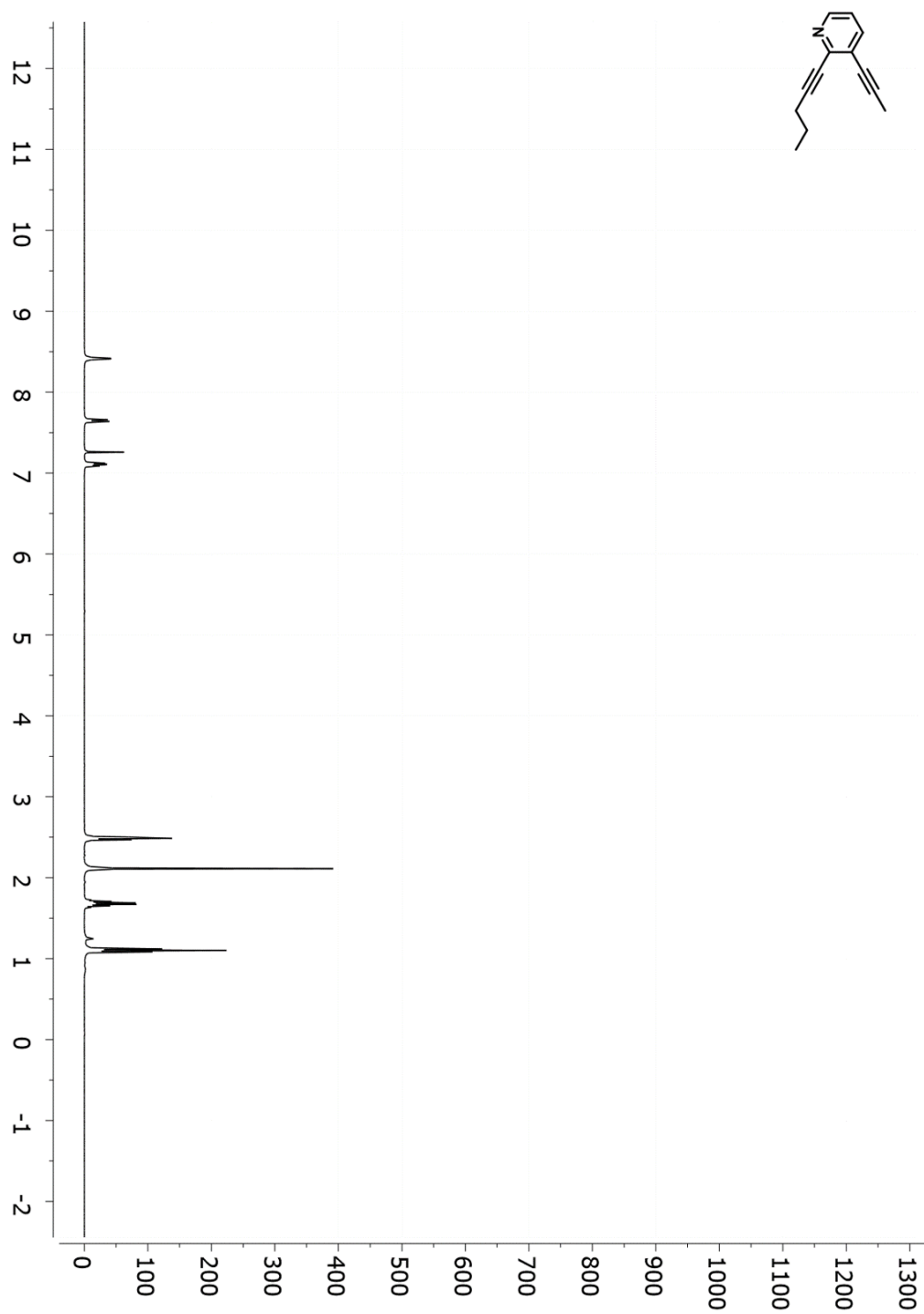
Figure 3.12. ^{1}H NMR spectrum of **26** (CDCl$_3$, 400 MHz).
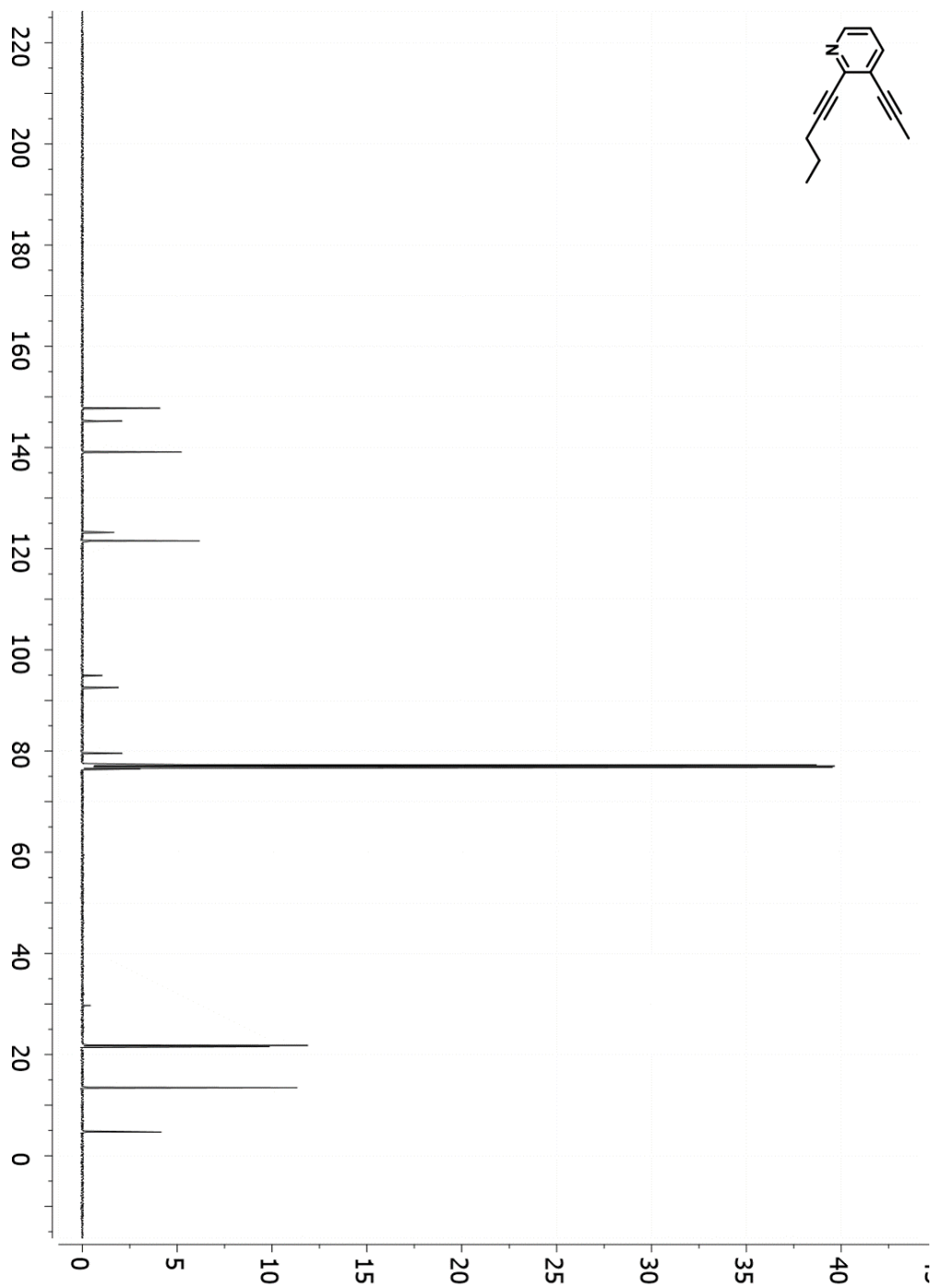
Figure 3.13. $^{13}C\{^1H\}$ NMR spectrum of **26** (CDCl$_3$, 100 MHz).
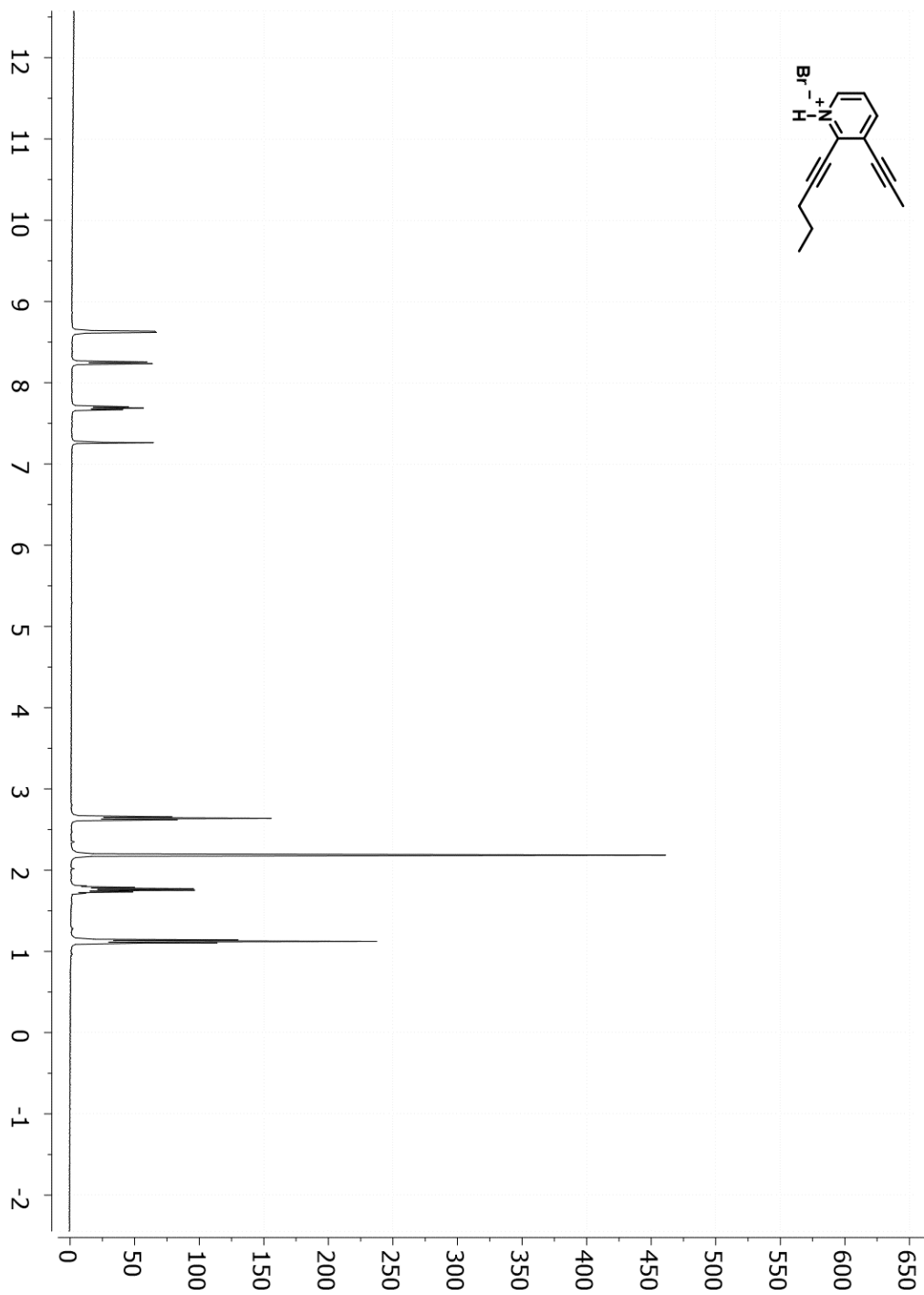
Figure 3.14. ^{1}H NMR spectrum of **32-*Br*** (CDCl$_3$, 400 MHz).
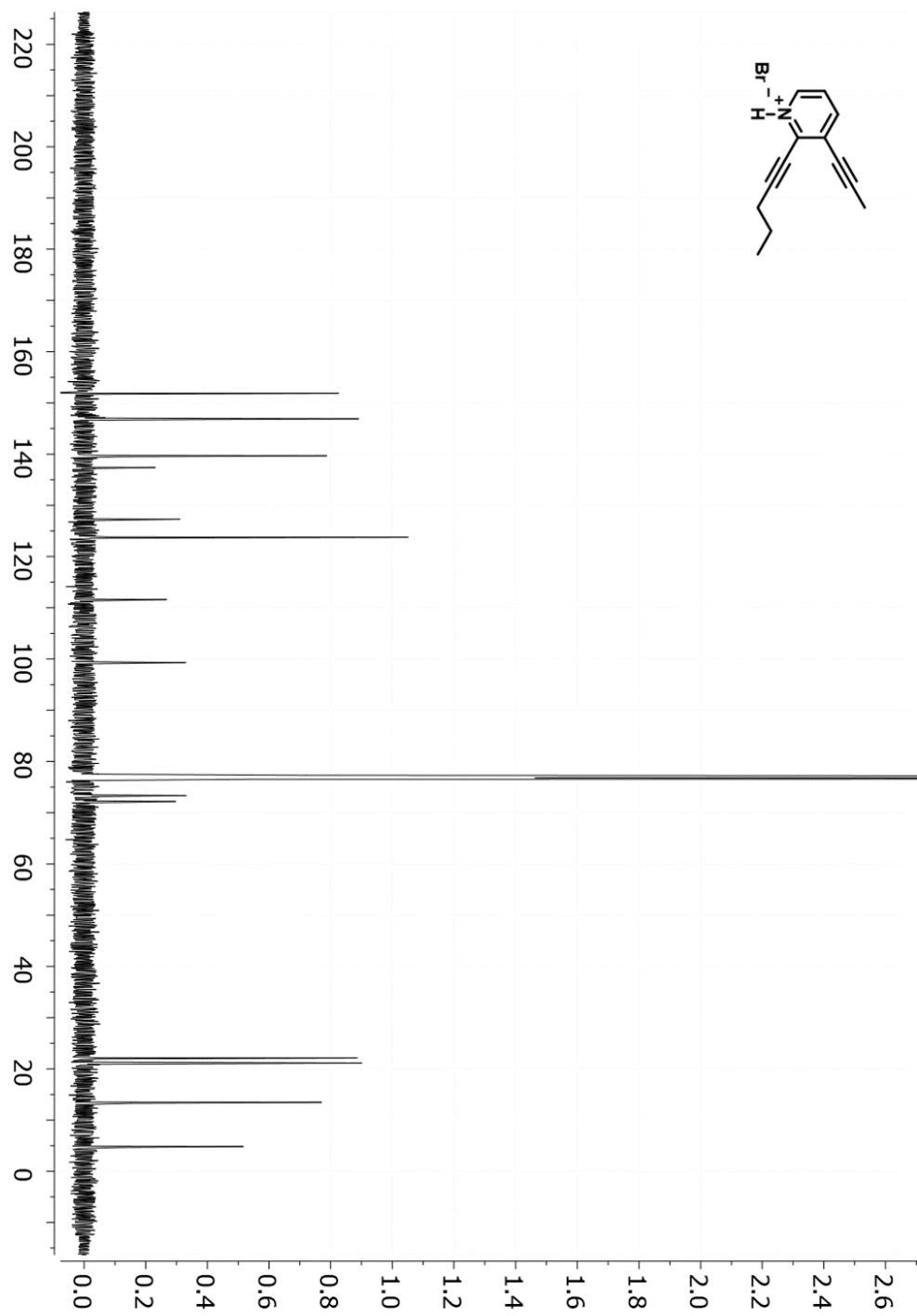
Figure 3.15. $^{13}C\{^1H\}$ NMR spectrum of **32-*Br*** (CDCl$_3$, 100 MHz).
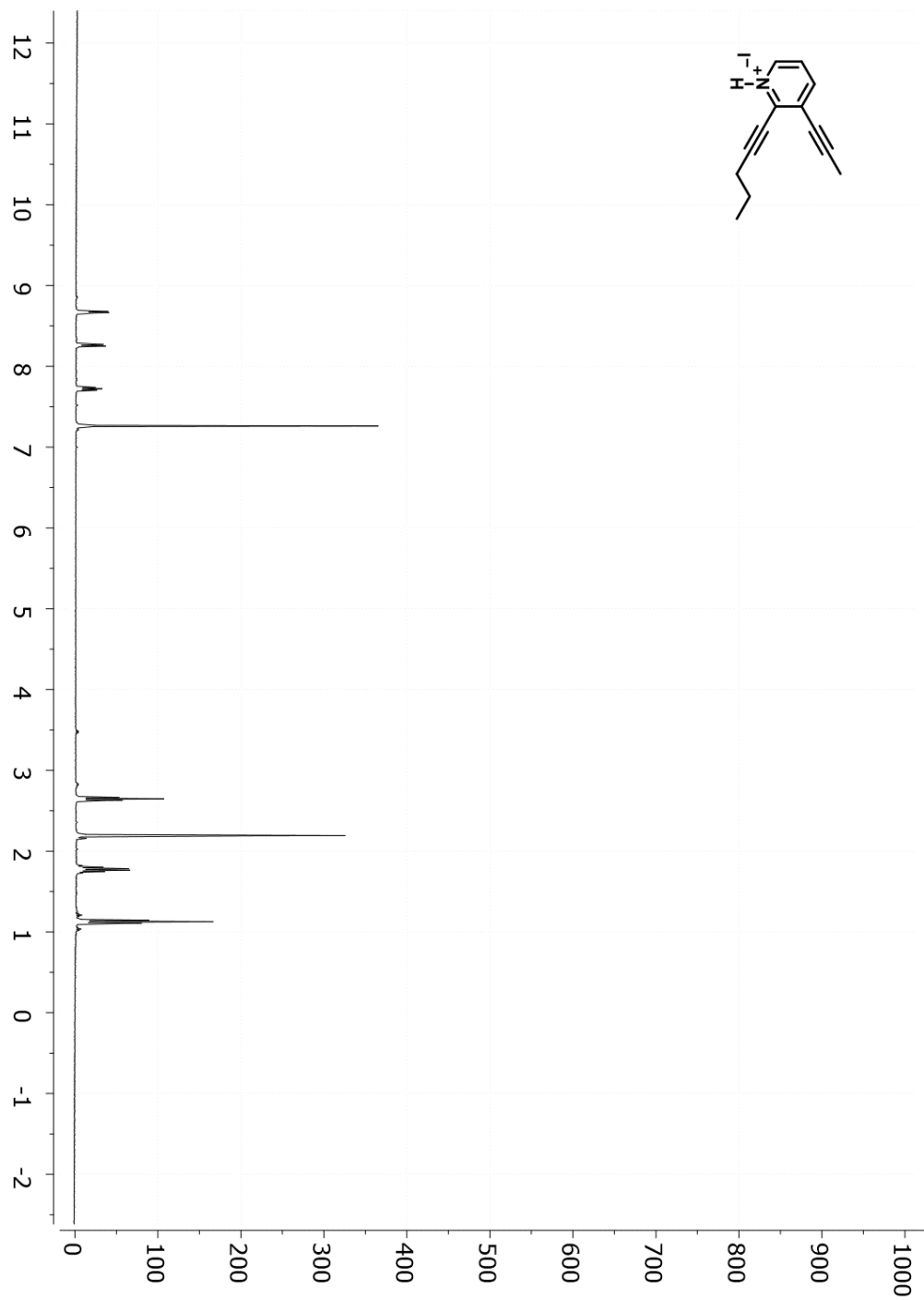
Figure 3.16. ^{1}H NMR spectrum of **32-*I*** (CDCl$_3$, 400 MHz).
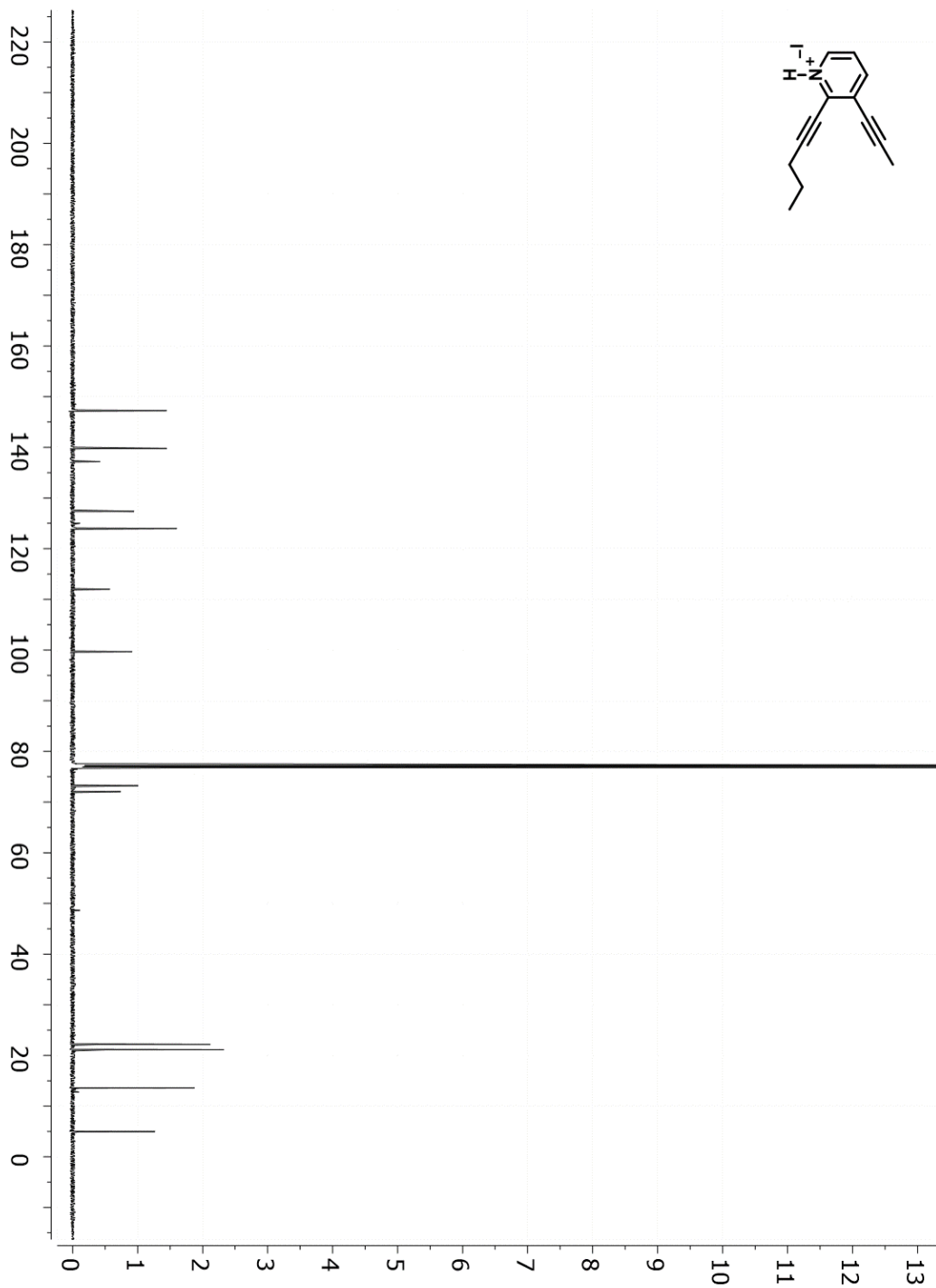
Figure 3.17. $^{13}C\{^1H\}$ NMR spectrum of **32-*I*** (CDCl$_3$, 100 MHz).
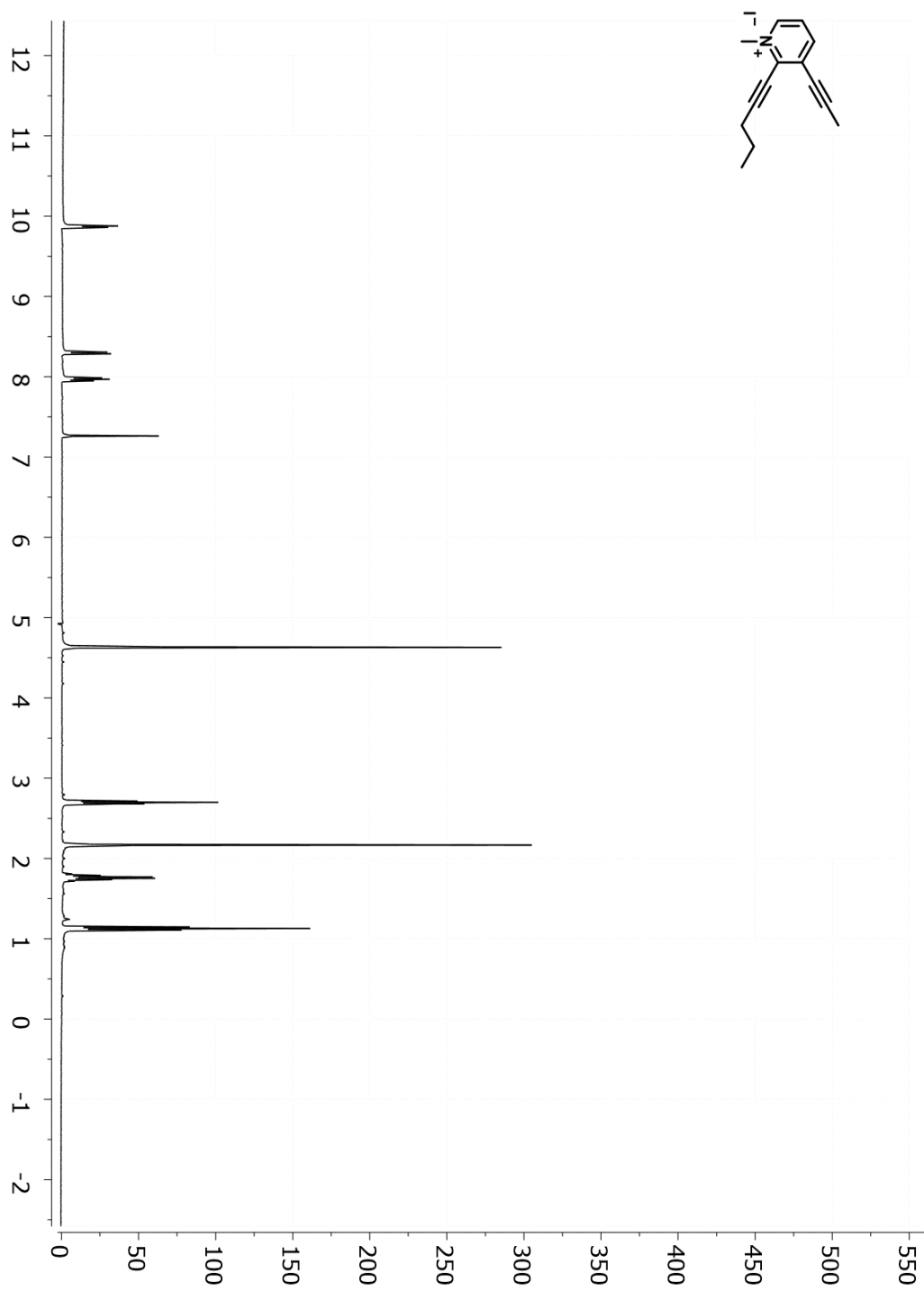
Figure 3.18. ^{1}H NMR spectrum of **52** (CDCl$_3$, 400 MHz).
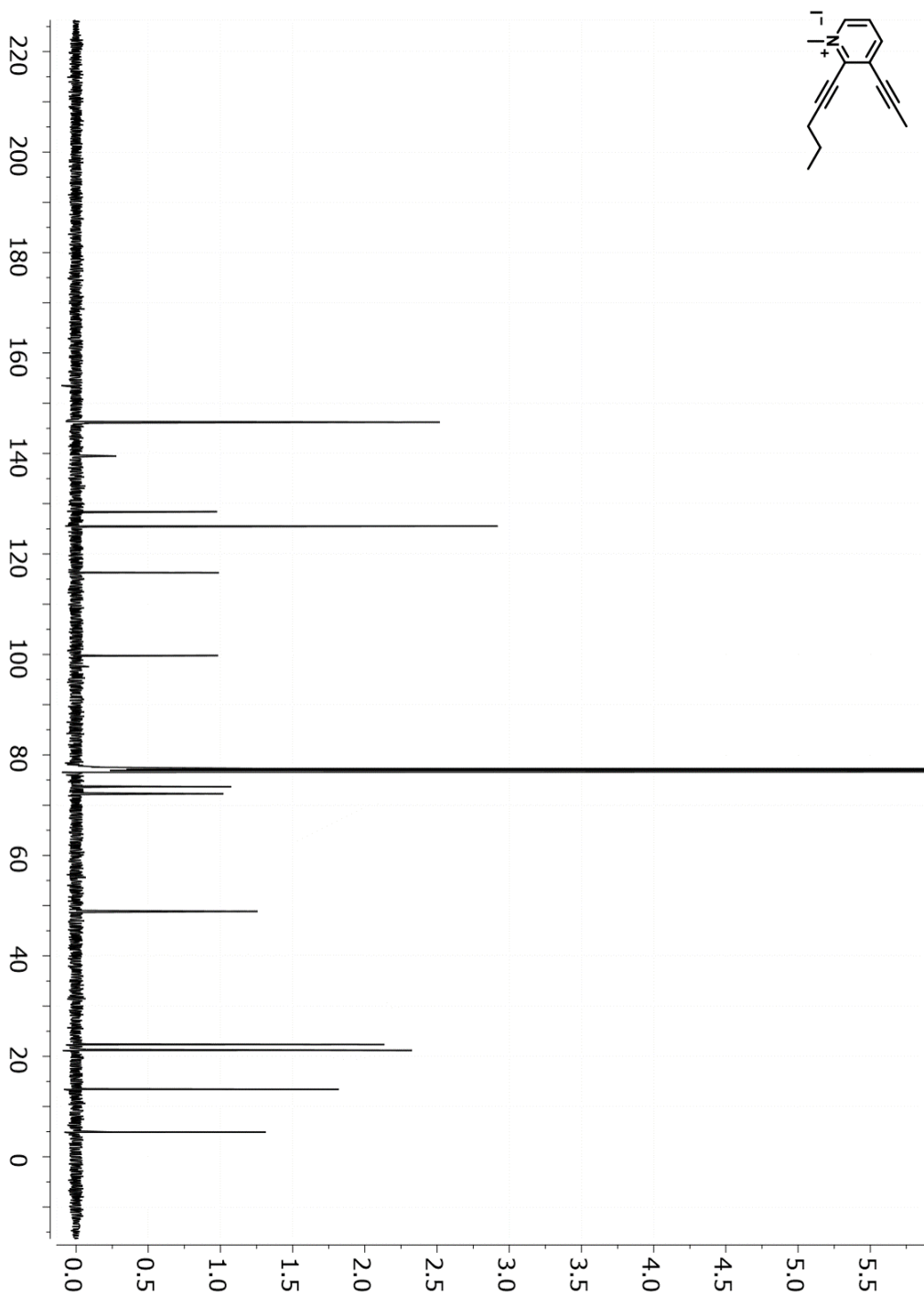
Figure 3.19. $^{13}C\{^1H\}$ NMR spectrum of **52** (CDCl$_3$, 100 MHz).
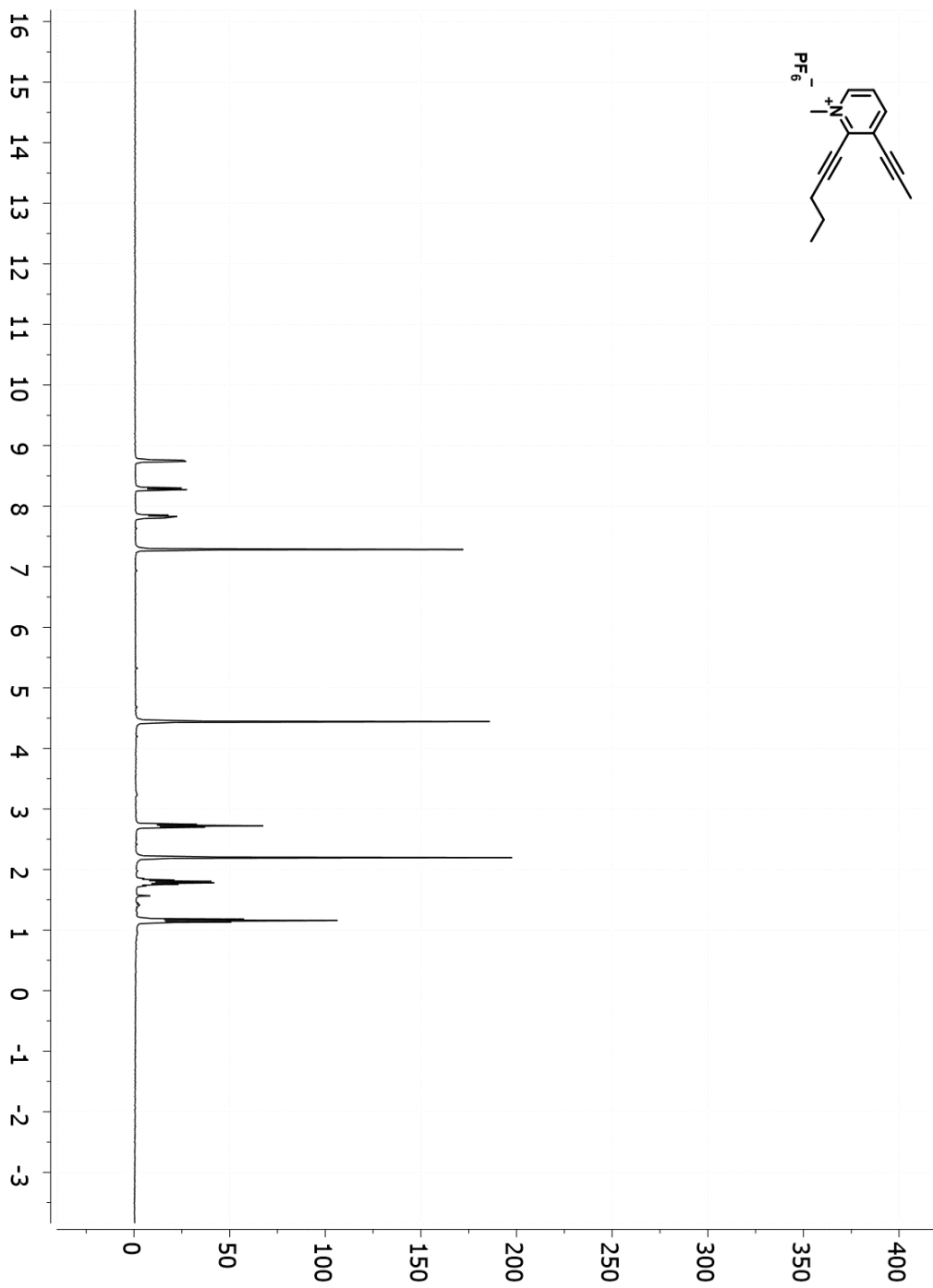
Figure 3.20. ^{1}H NMR spectrum of **53** (CDCl$_3$, 300 MHz).
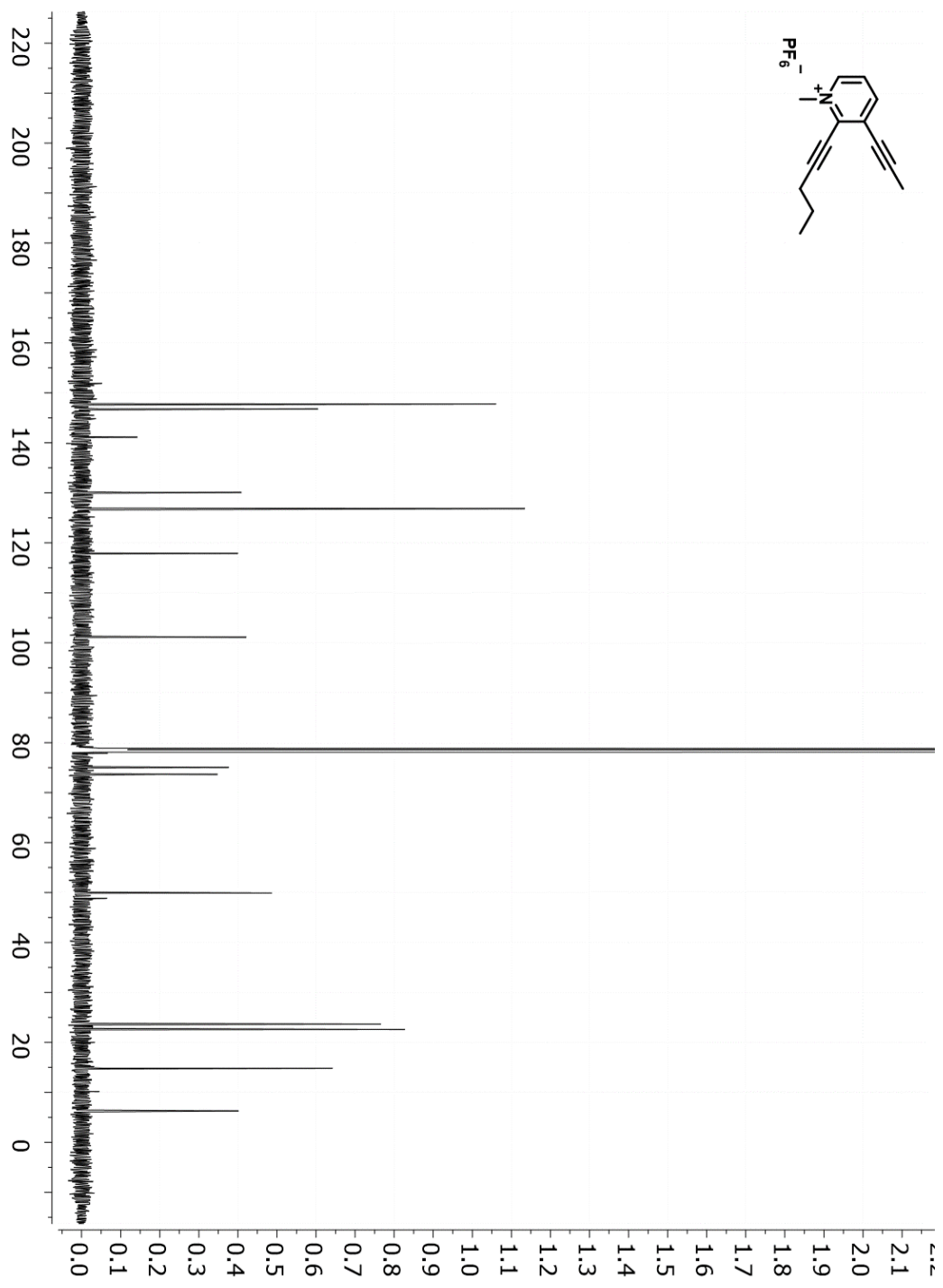
Figure 3.21. $^{13}C\{^1H\}$ NMR spectrum of **53** (CDCl$_3$, 100 MHz).
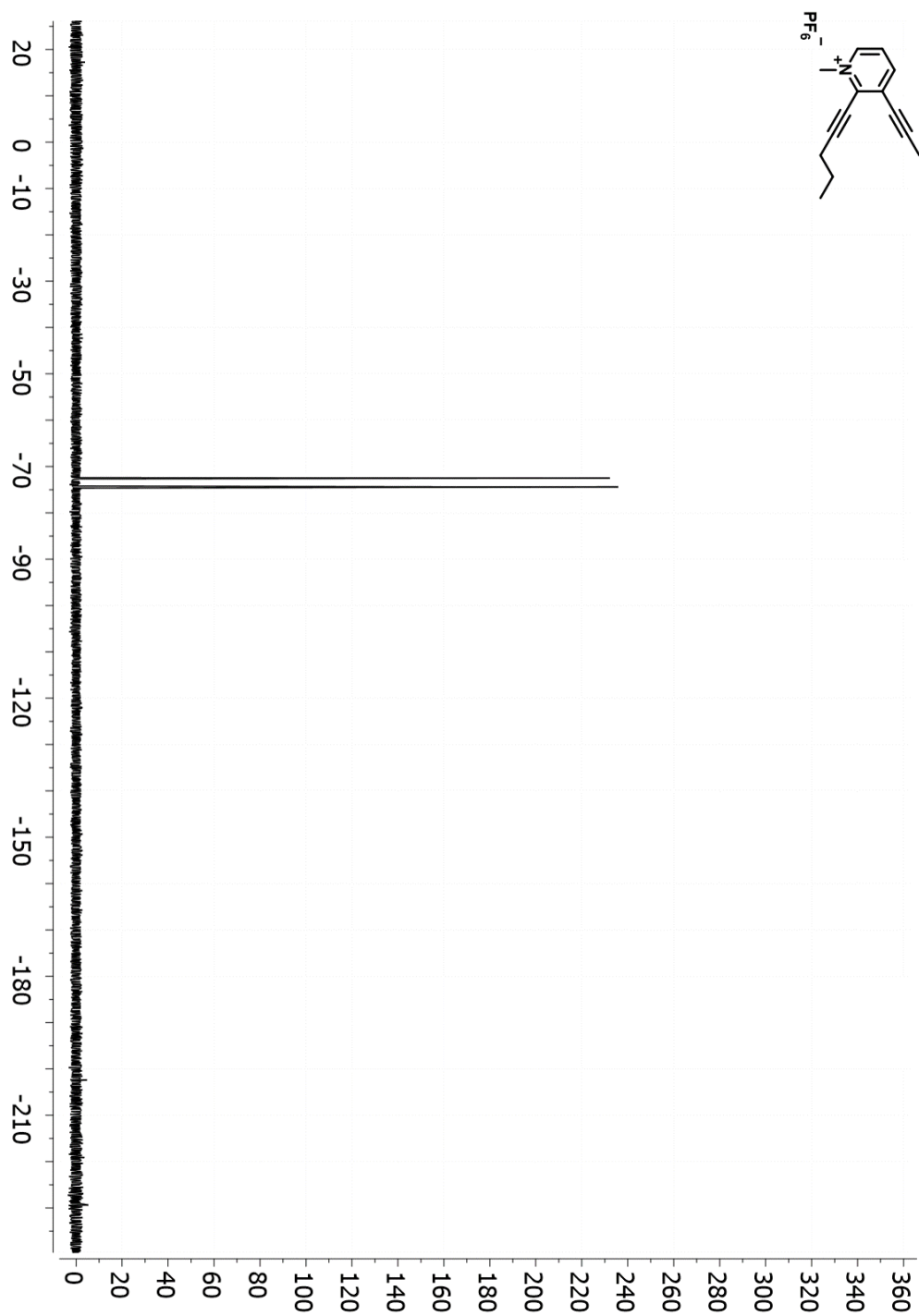
Figure 3.22. ^{19}F NMR spectrum of **53** (CDCl$_3$, 376 MHz).
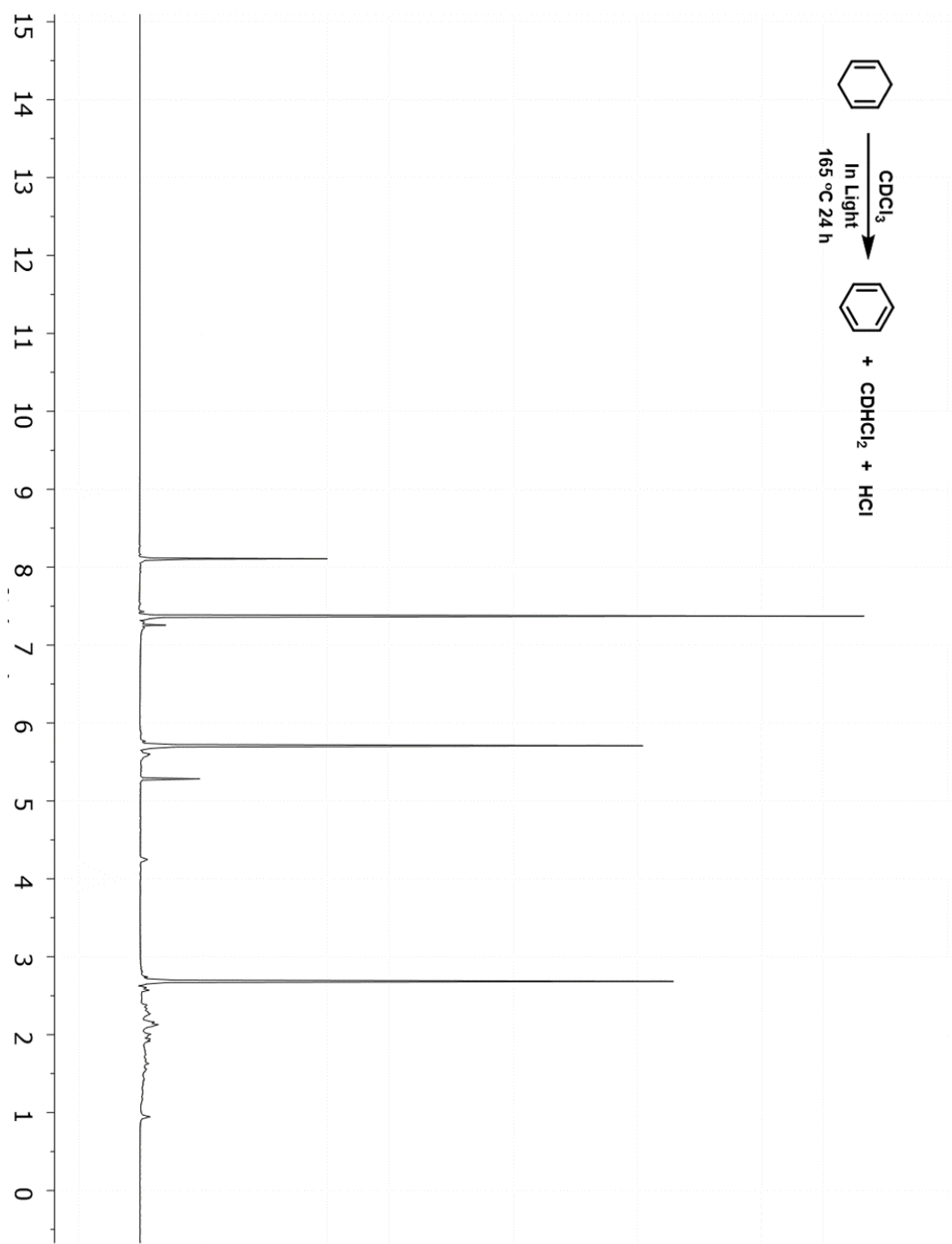
Figure 3.23. ^{1}H NMR spectrum of 1,4-CHD in CDCl$_3$, exposed to light after heating at 165 °C for 24 h (400 MHz).

131
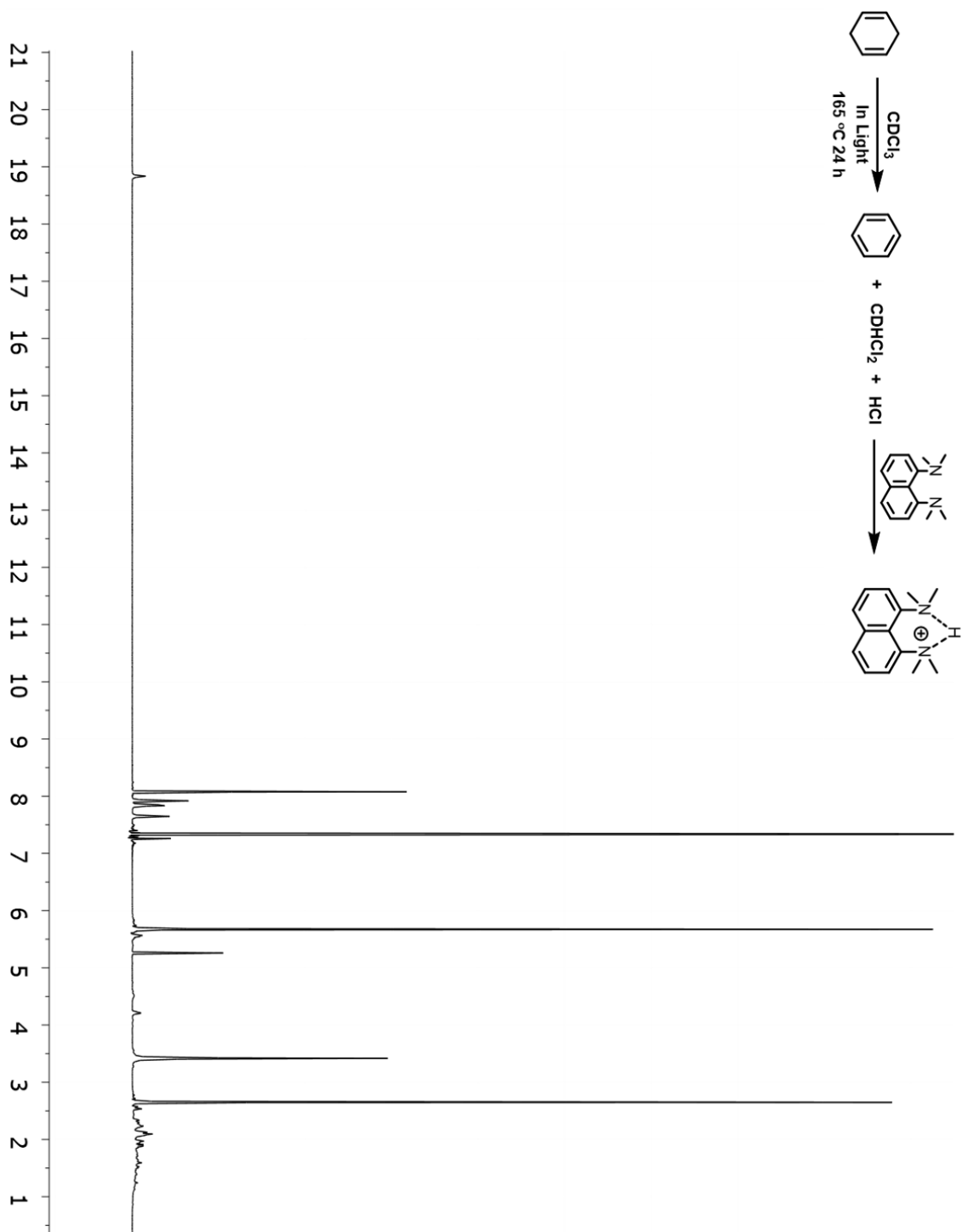
Figure 3.24. ^{1}H NMR spectrum of 1,4-CHD in CDCl$_3$, exposed to light after addition of proton sponge (400 MHz).
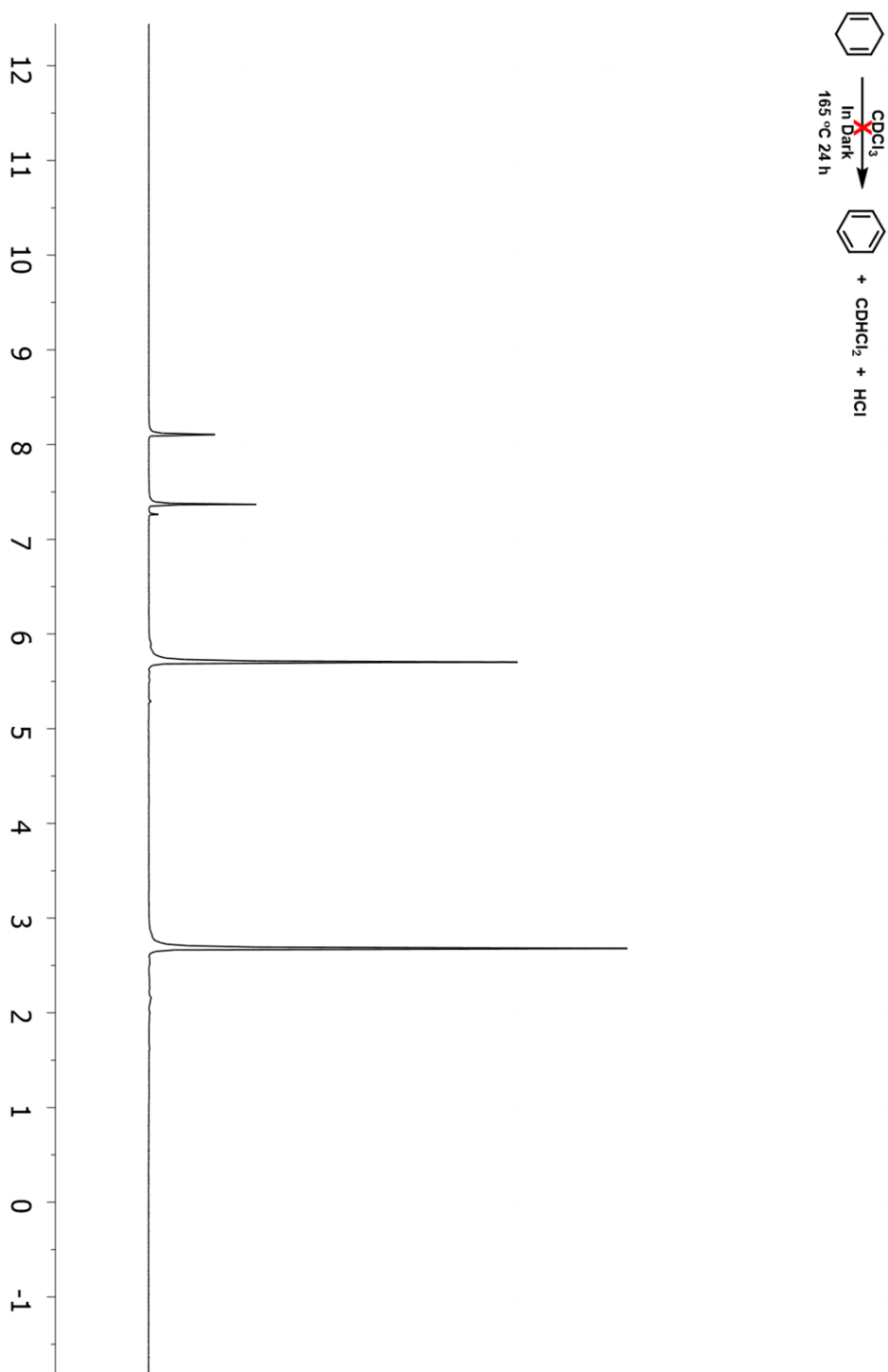
Figure 3.25. ^{1}H NMR spectrum of 1,4-CHD in CDCl$_3$, in the dark after heating at 165 °C for 24 h (400 MHz).
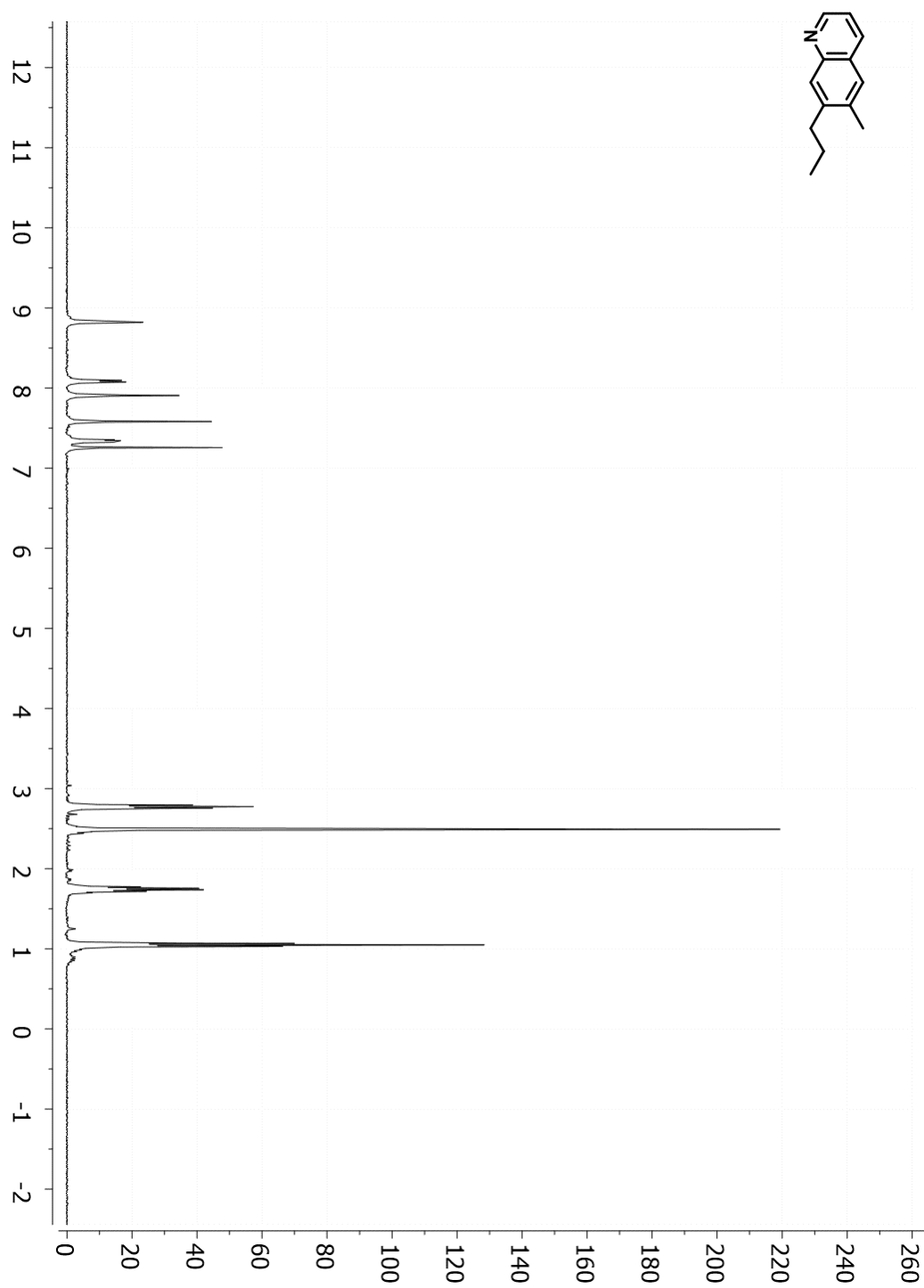
Figure 3.26. ^1H NMR spectrum of **27** (CDCl$_3$, 400 MHz).
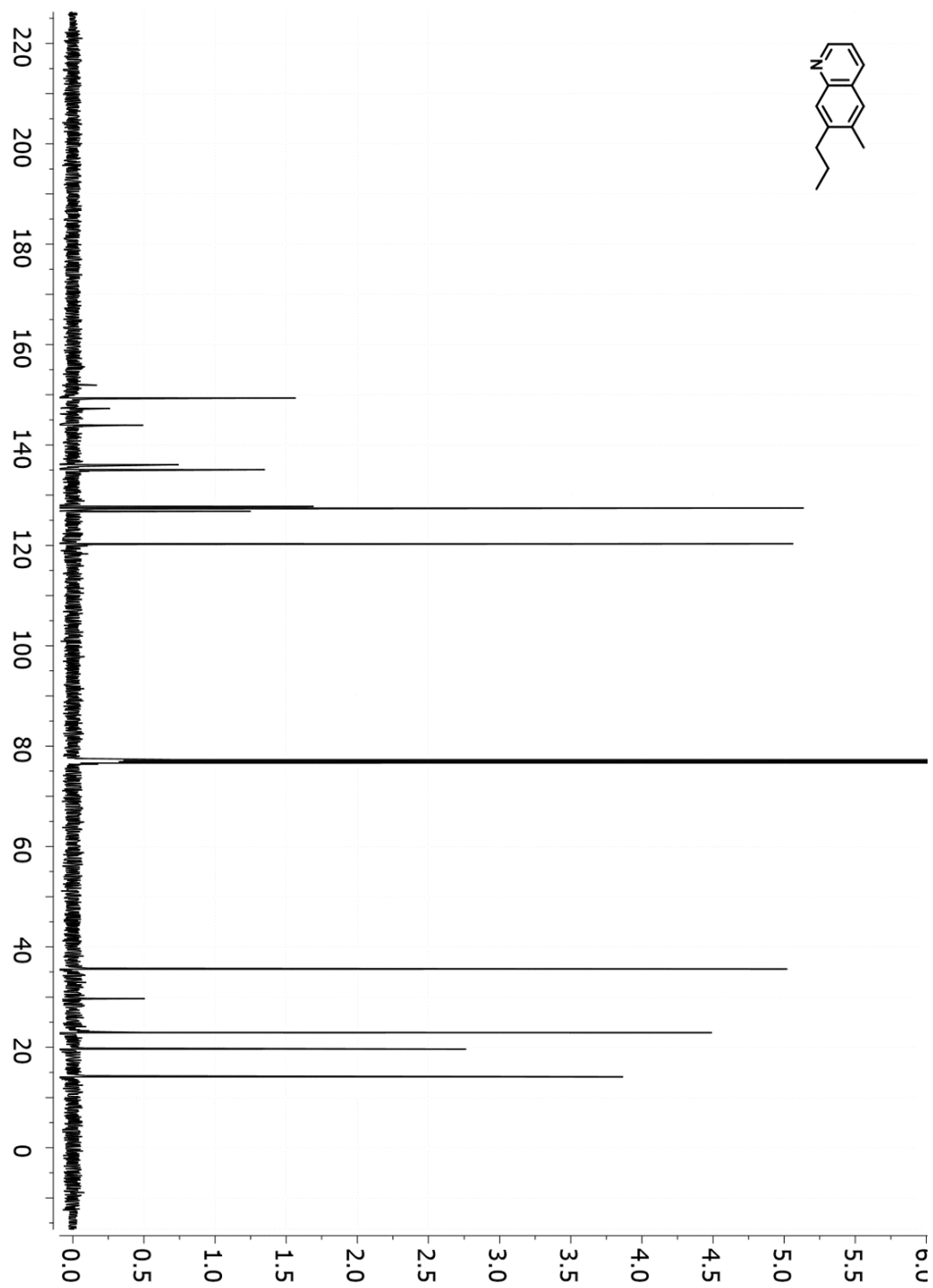
Figure 3.27. $^{13}C\{^1H\}$ NMR spectrum of **27** (CDCl$_3$, 100 MHz).

135
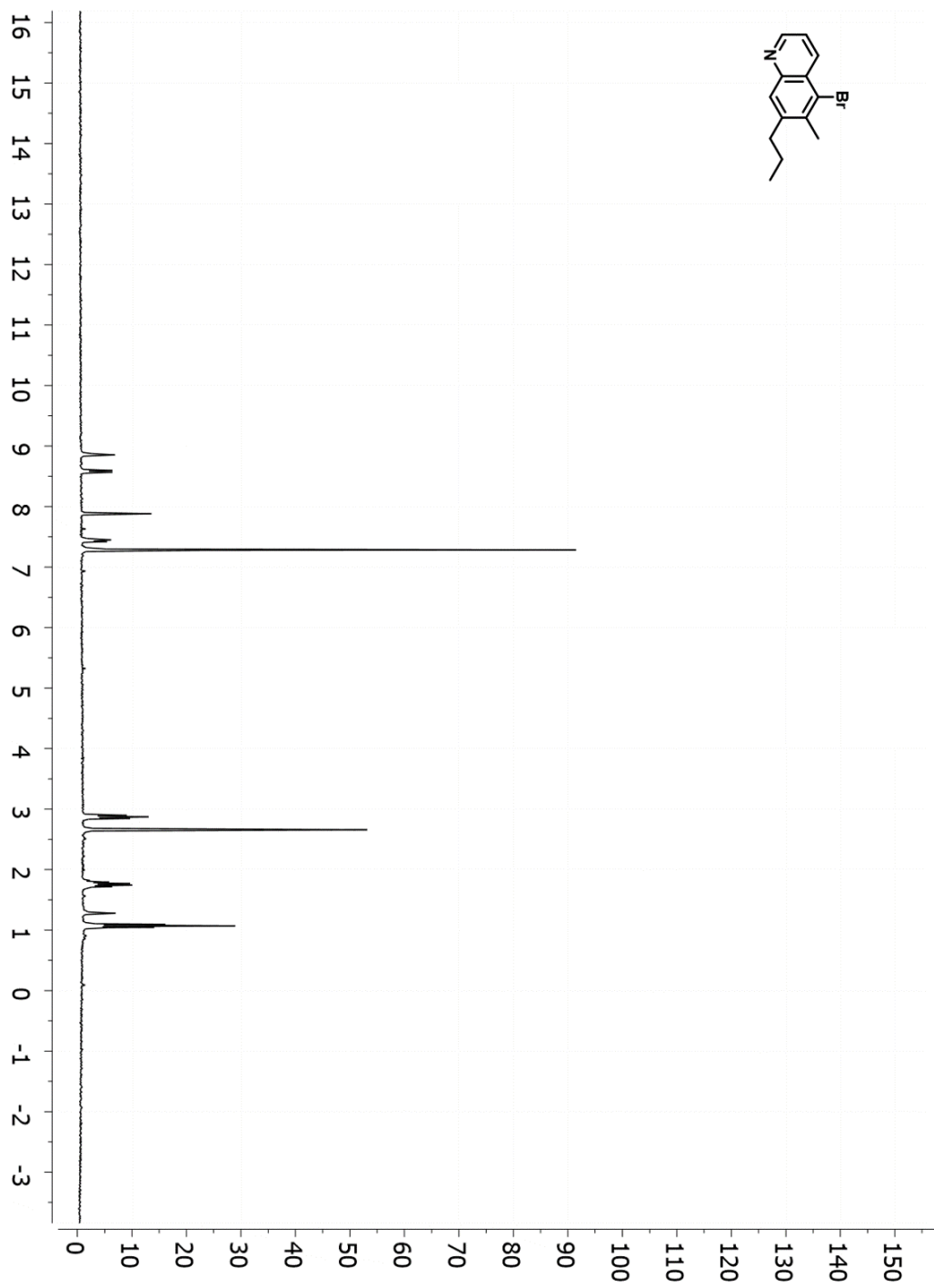
Figure 3.28. ^{1}H NMR spectrum of **29-*Br*** (CDCl₃, 300 MHz).
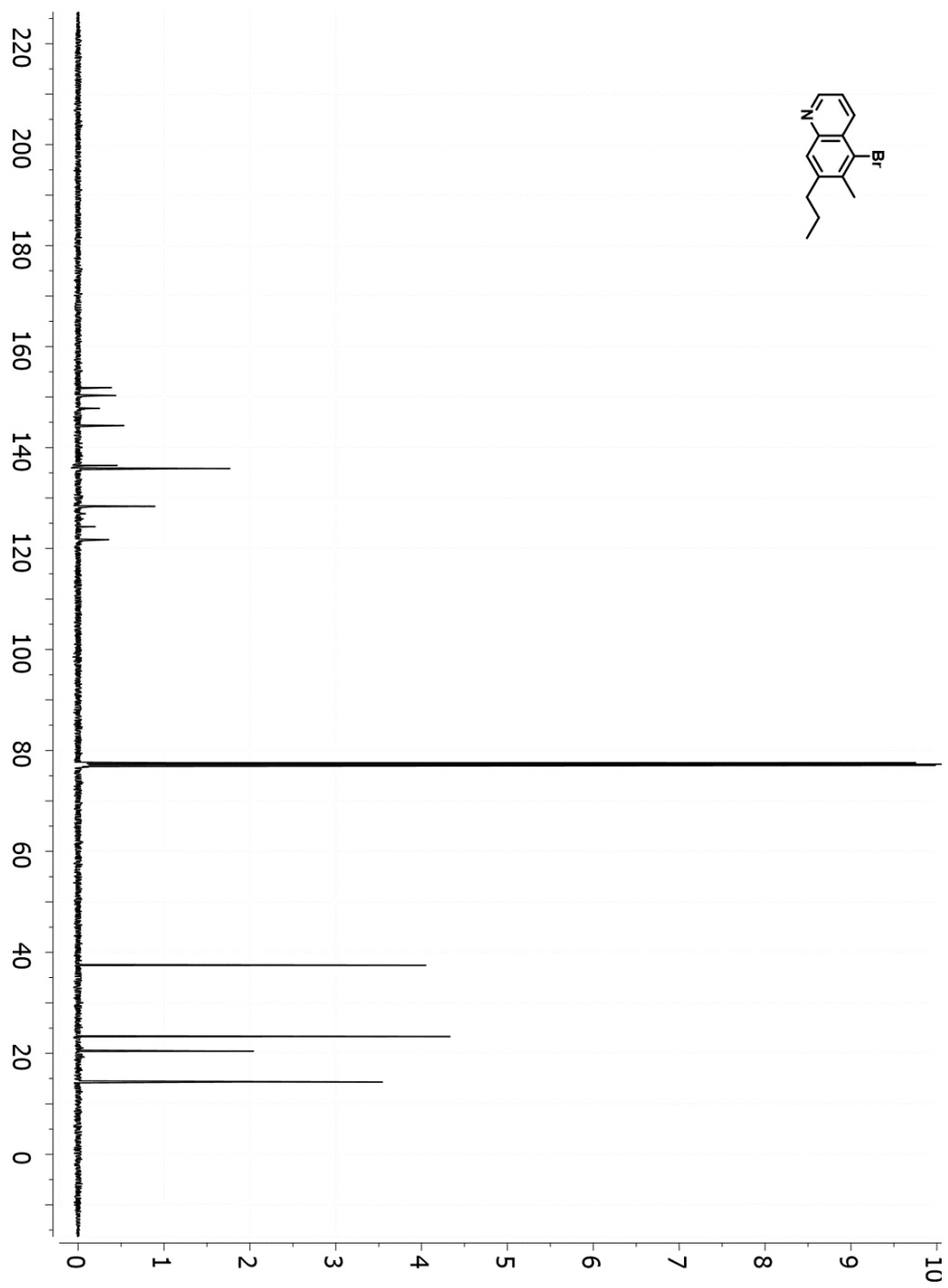
Figure 3.29. $^{13}C\{^{1}H\}$ NMR spectrum of **29-*Br*** (CDCl$_3$, 100 MHz).
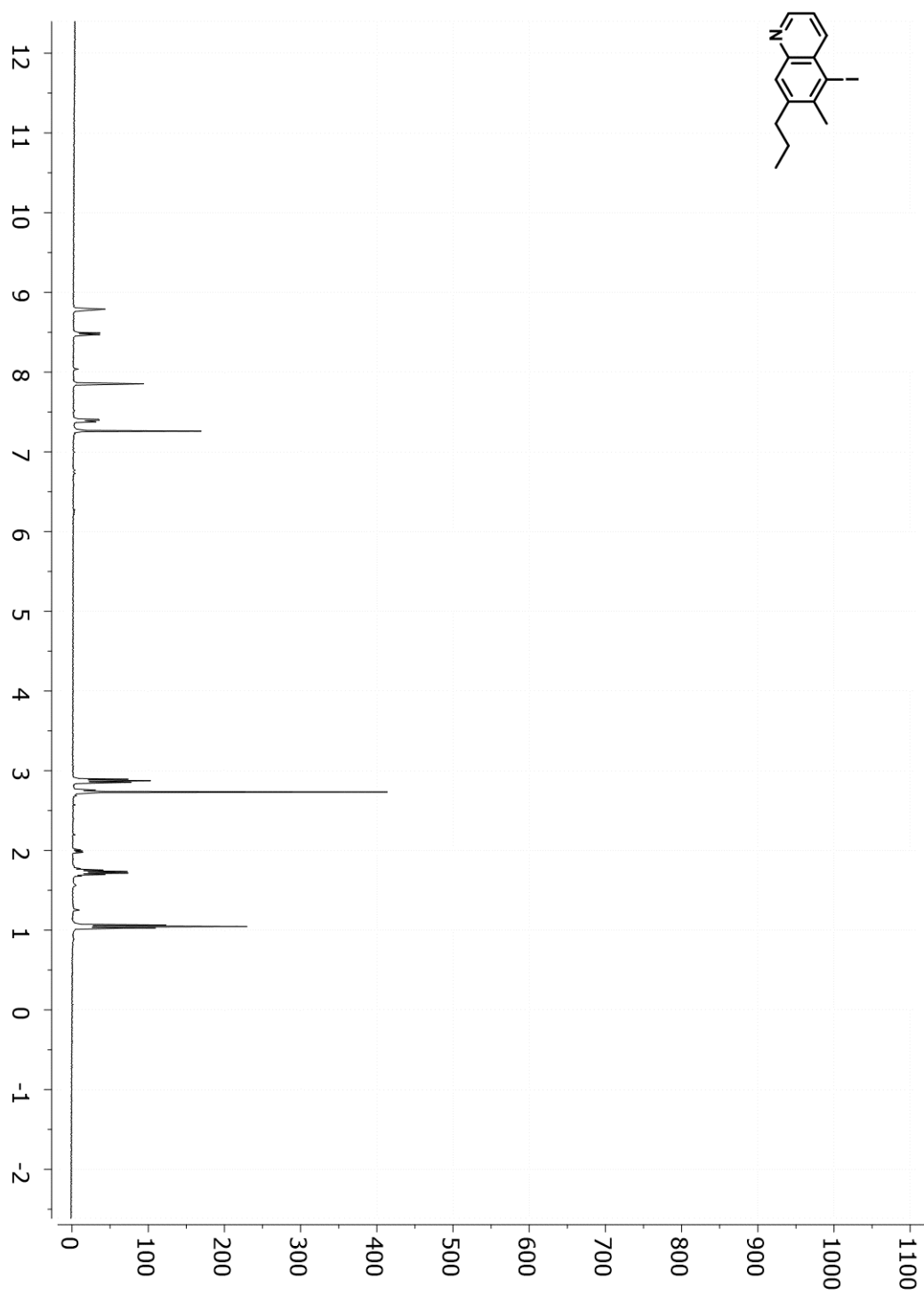
Figure 3.30. ^{1}H NMR spectrum of **29-*l*** (CDCl$_3$, 400 MHz).

Figure 2.31. $^{13}C\{^1H\}$ NMR spectrum of **29-*I*** (CDCl$_3$,100 MHz).
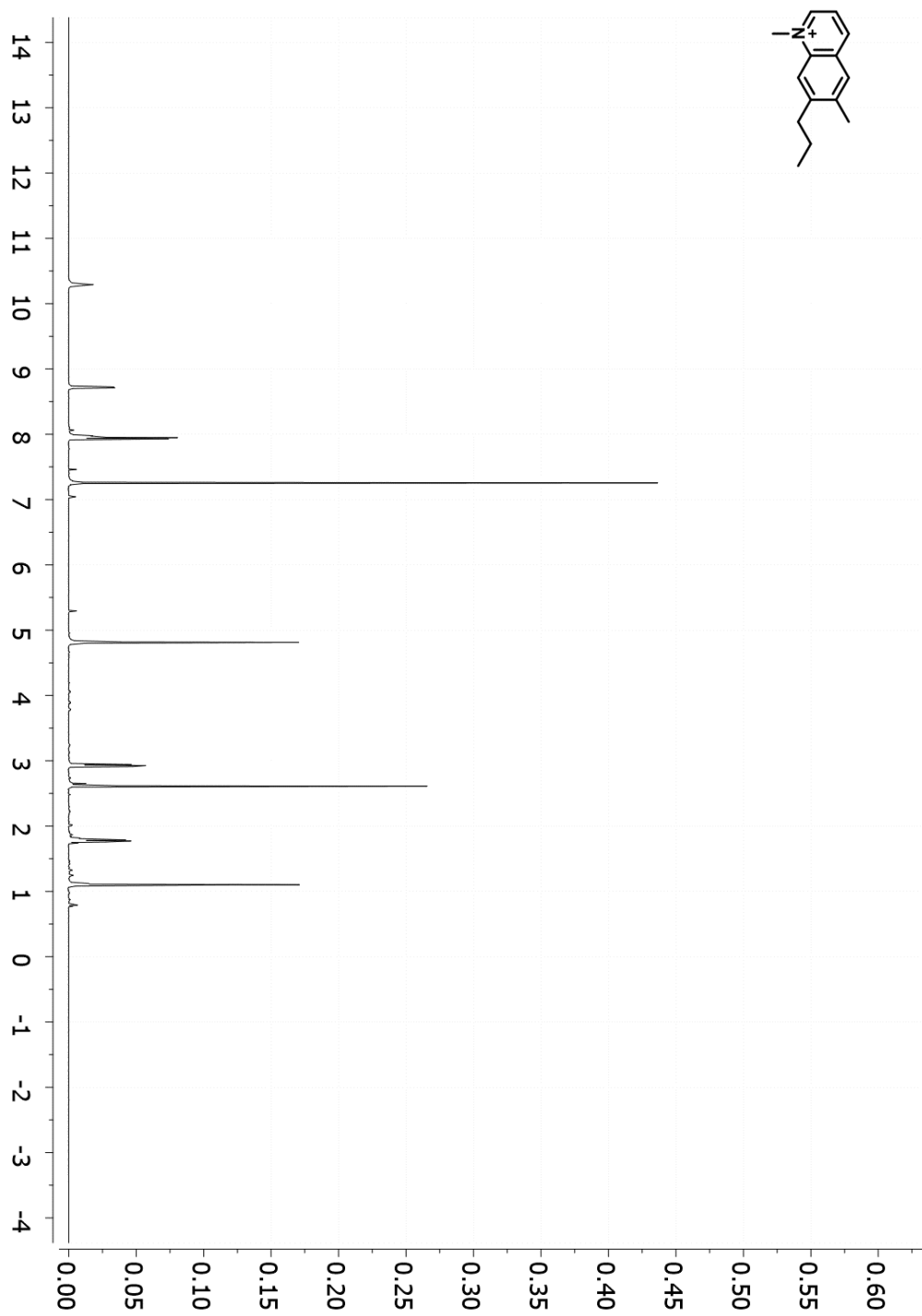
Figure 2.32. ^{1}H NMR spectrum of **55** (CDCl$_3$, 500 MHz).

140
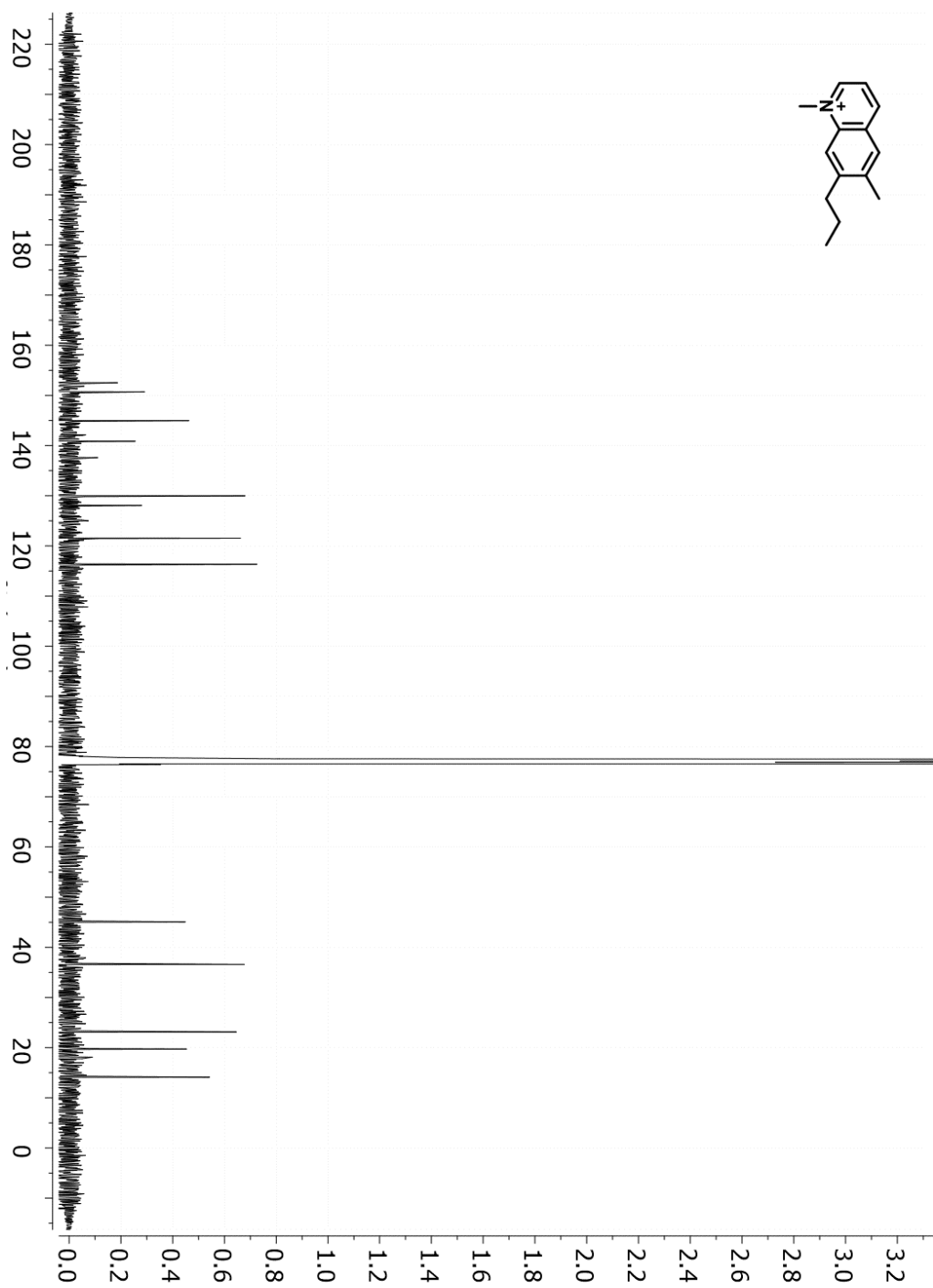
Figure 3.33. $^{13}C\{^1H\}$ NMR spectrum of **55** (CDCl$_3$, 100 MHz).

F. Acknowledgments

Chapter 3, contains material which appears in "Enediyne Cycloaromatization with Incorporation of Chlorine from Chloroform and Hydrogen from 1,4-Cyclohexadiene" Qin, P.; O'Connor, J. M.; Baldridge, K. K.; Hitt, D. M.; Cope, S. K.; Veccharelli, K. M.; Holland, R. L.; Raub, A. *Submitted to JACS*. The dissertation author is a co-author on this paper.

G. References

(1)   Jones, R. R.; Bergman, R. G. *J. Am. Chem. Soc.* **1972**, *94*, 660-661.

(2)   O 'Connor, J. M.; Friese, S. J.; Tichenor, M. *J. Am. Chem. Soc.* **2002**, *124*, 3506-3507.

(3)   O'Connor, J. M.; Friese, S. J.; A.; Rodgers, B. L. *J. Am. Chem. Soc.* **2005**, *127*, 16342-16343.

(4)   Hitt, D. M. Dissertation, University of California, San Diego, **2011**.

(5)   Cope, S. K. Dissertation, University of California, San Diego, **2015**.

(6)   Rodriguez, V.; Sabo-Etienne, S.; Chaudret, B.; Thoburn, J.; Ulrich, S.; Limbach, H.-H.; Eckert, J.; Barthelat, J.-C.; Hussein, K.; Marsden, C. J. *Inorg. Chem.* **1998**, *37*, 3475-3485.

(7)   Sathyajith Kumarasinghe, E.; Peterson, M. A.; Robins, M. J. *Tet. Lett.* **2000**, *41*, 8741-8745.

(8)   Choy, N.; Russell, K. C.; Och, N. *Heterocycles* **1999**, *51*, 13-16.

(9)   Kim, C.-S.; Russell, K. C. *J. Org. Chem.* **1998**, *63*, 8229-8234.

(10)   Kim, C.; Diez, C.; Russell, K. C. *Chem. Eur. J.* **2000**, *6*, 1555-1558.

(11)   Calculations performed by Kim Baldridge using BP86 density functional, Def2-TZVPP basis set, GAMESS Program.

(12)   Dega-Szafran, Z.; Nowak-Wydra, B.; Szafran, M. *Magn. Reson. Chem.* **1993**, *31*, 726-730.

(13)   Blanksby, S. J.; Ellison, G. B. *Acc. Chem. Res.*, **2003**, *36*, 255-263.

(14)   Jaworski, J. S.; Cembor, M.; Koliński, M. *J. Phys. Org. Chem.* **2006**, *19*, 276-280.

(15)   Armarego, W. L. F.; Chai, C. L. L. *Purification of Laboratory Chemicals*; 6th ed.; Elsevier Inc: Oxford, U.K., 2009

(16)   Gao, Y.; Deyonker, N. J.; Chauncey, E.; Iii, G.; Wilson, A. K.; Cundari, T. R.; Marshall, P. *J. Phys. Chem. A.* **2009**, *113*, 6955-6963

(17)   James, D. G. L.; Suart, R. D. *Trans. Faraday Soc.* **1968**, *64*, 2752-2769.

(18)   Lichtscheidl, J.; Getoff, N. *Monatsh. Chem.* **1979**, *110*, 1377-1386.

(19)   Fahey, R. C.; Lee, D. J. *J. Am. Chem. Soc.* **1966**, *88*, 5555- 5560.

(20)   Lo, C.-Y.; Kumar, M. P.; Chang, H.-K.; Lush, S.-F.; Liu, R.-S. *J. Org. Chem.* **2005**, *70*, 10482- 10487.

(21)   Höpf, H.; Musso, H. *Angew. Chemie Int. Ed. Engl.* **1969**, *8*, 680-680.

(22)   Prall, M.; Krüger, L. A.; Schreiner, P. R.; Höpf, H. *Chem. Eur. J.* **2001**, *7*, 4386-4394.

(23)   Litovitz, A.E.; Carpenter, B.K.; A.; Hopf, H. *Org. Lett.* **2005**, *7*, 507-510.

(24)   Allred, A. L. *Nucl. Chem* **1961**, *17*, 215-221.

(25)   Klein, M.; Walenzyk, T.; König, B. *Collect. Czechoslov. Chem. Commun.* **2004**, *69*, 945-965.

(26)   Koga, N.; Morokuma, K. *J. Am. Chem. Soc.* **1991**, *113*, 1907-1911.

(27)   Choy, N.; Kim, C.; Ballestero, C.; Artigas, L.; Diez, C.; Lichtenberger, F.; Shapiro, J.; Russell, K.C. *Tet. Lett.* **2000**, *41*, 6955-6958.

Chapter 4.

Dual Responsive Polymeric Nanoparticles Prepared by Direct Functionalization of Polylactic Acid-Based Polymers via Graft-From Ring Opening Metathesis Polymerization

A. Introduction

Polymers with hydrolyzable backbones such as polylactic acid (PLA) have opened new avenues for research and development with their enhanced biodegradability and resulting low toxicity for *in vivo* use.[1] PLA has been utilized heavily as a biodegradable polymer in numerous in vivo applications ranging from surgical sutures,[2] surgical implants[3] and drug delivery systems.[4,5] However, the utility of PLA is limited as the polymer backbone is difficult to chemically functionalize. As such, significant effort has been expended to increase functionalization of PLA polymers and to tune its mechanical properties.[6–9]

Current strategies for functionalizing PLA typically involve copolymerization of D,L-lactide with functionalized lactides in the presence of a catalyst and an initiator to generate functionalized PLA copolymers via ring opening polymerization (ROP).[10–15] While this technique has led to the development of a range of functionalized PLA polymers, it remains synthetically challenging to produce high molecular weight polymers with a large weight percentage of the added functionality. This is likely due to decreased rates of polymerization resulting from the steric bulk of functionalized lactides, leading to incomplete polymerization of the substituted monomer.[11,16] Therefore, ring substitution has a major impact on the polymerizability of functionalized lactide monomers.[11,16] To generate PLA polymers with a higher degree of functionality, post polymerization modification strategies via a graft-to approach have been demonstrated. For example "Click" chemistry allows functionality to be incorporated into the polymer relatively easily since the backbone and the side chains can be prepared separately prior to coupling.[12,15,17–20] However, efforts to increase graft densities are usually limited as a result of steric repulsion between the bulky side chains.[21–24] Another way to prepare functionalized PLA

145

materials is to utilize a graft-through polymerization method. In this scenario, a macromonomer is polymerized via polymerizable end groups to create a brush polymer. PLA polymers have been synthesized via this method by coupling the PLA polymer to a strained olefin and subsequently polymerizing the olefin, synthesizing bottle-brush PLA polymers.[25–28] Utilizing this grafting-through technique is attractive for polymer synthesis because it does not entail orthogonal chemistries for grafting various side chains. However, this polymerization technique can be challenging due to the increased steric hindrance of the propagating polymer chain. As a result, polymerizations can be slow and not proceed to complete conversion.[21–24]

An alternative technique utilizes a graft-from polymerization strategy to incorporate initiation groups into ROP monomers, such as cyclic esters and carbonates, prior to ROP. This novel technique has been demonstrated in the literature only a handful of times.[29–33] In this method, polymer chains are grown from the polymer as a macroinitiator, with multiple initiation sites located along its backbone. This technique should allow for greater graft densities along the polymer backbone since only small monomers are added to the growing polymer chain, mitigating steric repulsion.[21–24]
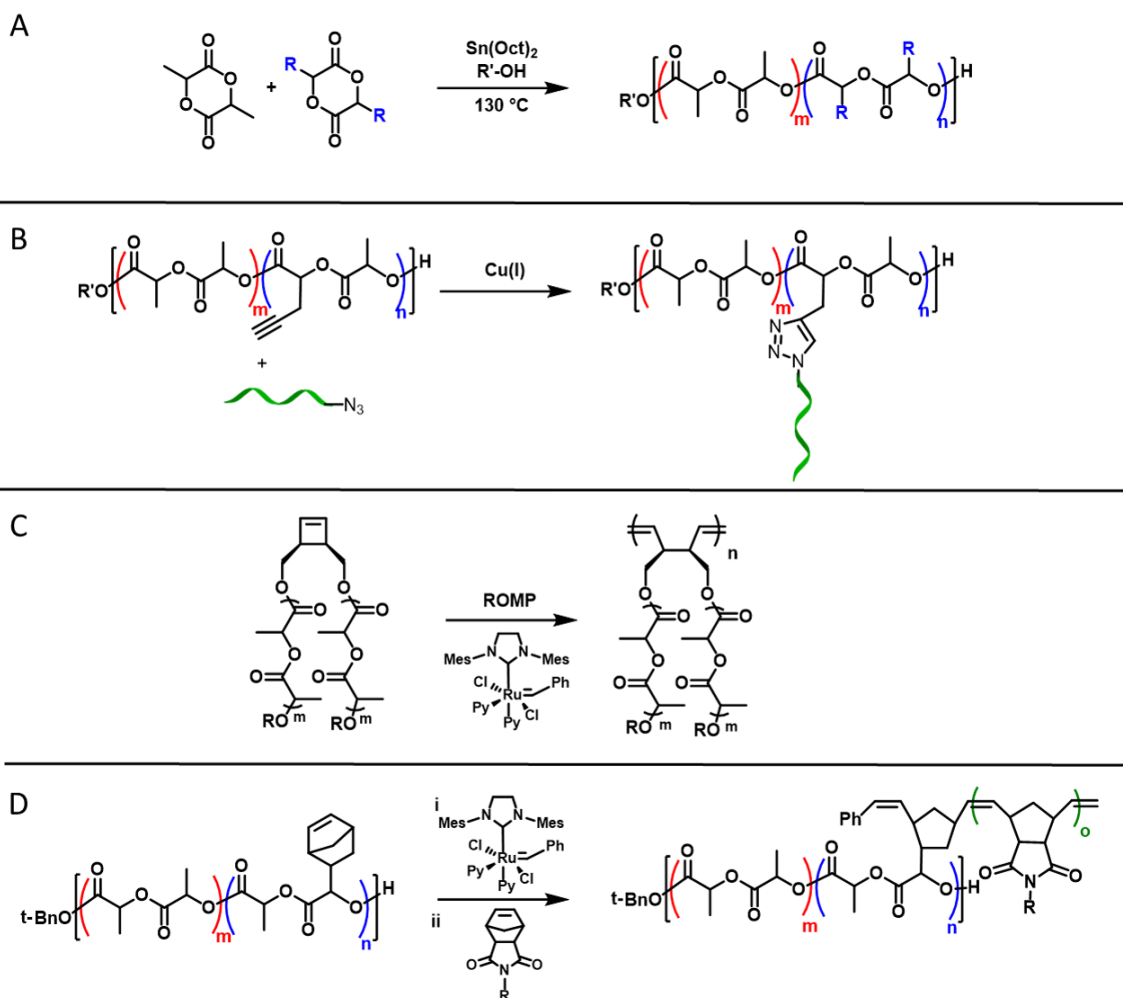
Figure 4.1. Strategies for the functionalization of PLA. (**A**) Copolymerizing R-functionalized lactide (**B**) graft-to polymerization. (**C**) graft-through polymerization. (**D**) graft-from polymerization (this work).

The purpose of this current research is to further expand upon the graft-from polymerization techniques by installing chemical functionality onto a PLA backbone via ring opening metathesis polymerization (ROMP). ROMP was chosen as the grafting technique because it can be initiated by catalysts with known tolerance to a range of functional groups and results in polymers with narrow dispersity.[34] In this method, PLA polymers containing ROMP-reactive

norbornene handles were first prepared. The norbornene units on this starting polymer were then used to prepare an initiator, which could be readily functionalized by reaction with substituted norbornene monomers. In addition, to demonstrate the utility of this strategy, nanoparticles that change morphology in response to both pH and UV light were prepared and evaluated.

B. Results and Discussion

1. Synthesis of Monomer 1 and Polymer 2

Preparation of a norbornene-functionalized PLA backbone began with the synthesis of the bifunctional lactide **1** which was prepared in five steps from commercially available exo-5-norbornenecarboxylic acid in 14% overall yield. Specifically, exo-5-norbornenecarboxylic acid was reduced to alcohol **1.1** utilizing LiAlH$_4$ in quantivative yeild. Compound **1.1** was subsequenly oxidized to the corrisponding aldyhde **1.2** utalizing Dess–Martin periodinane in 80% yield. A Passerini-Type condensation of **1.2** gave *N*-acylindole **1.3** in 41% yield. Hydrolysis of **1.3** under basic conditions gave alpha hydroxy acid **1.4** in 86% yield. Bifunctional lactide **1** was synthesized by reacting 1.4 with 2-bromopropionyl bromide and trimethylamine in 42% yeild. Norbornene-substituted PLA polymers were then synthesized by copolymerizing lactide with 15 mol % of monomer **1**, utilizing 0.7 mol % of stannous octoate as the catalyst and 4-tert-butylbenzyl alcohol as an initiator (Scheme 4.1).[11]
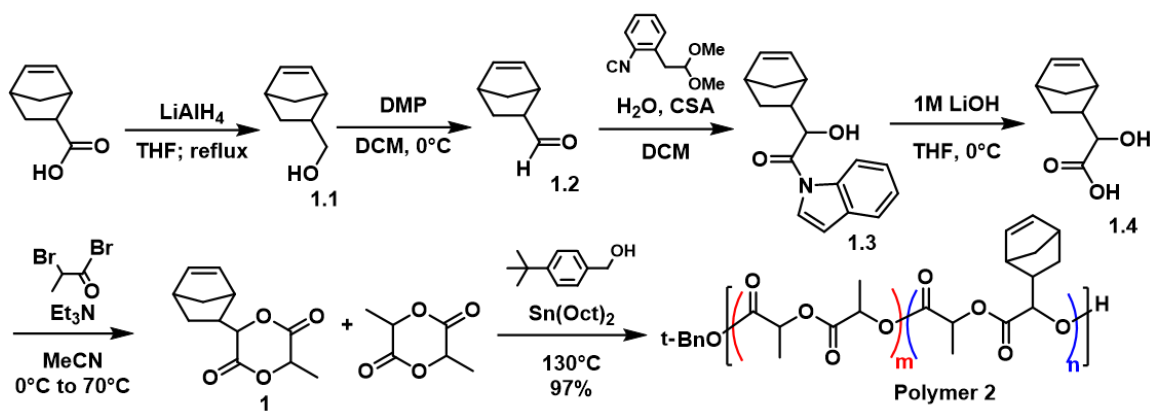
Scheme 4.1. Synthesis of polymer **2**.

The resulting polymers were then characterized by size exclusion chromatography coupled with multiangle light scattering (SEC-MALS) and ^{1}H-NMR to determine the percent conversion of lactides to polymer, the number-average molecular weight (M_n), and the dispersity (Đ or M_w/M_n) of the copolymers. ROP of the lactides afforded a 98% conversion of monomers to norbornene functionalized polymer **2**, with a M_n of 13 kg/mol, M_w of 15 kg/mol and a dispersity of 1.2 (Figure 4.2A).
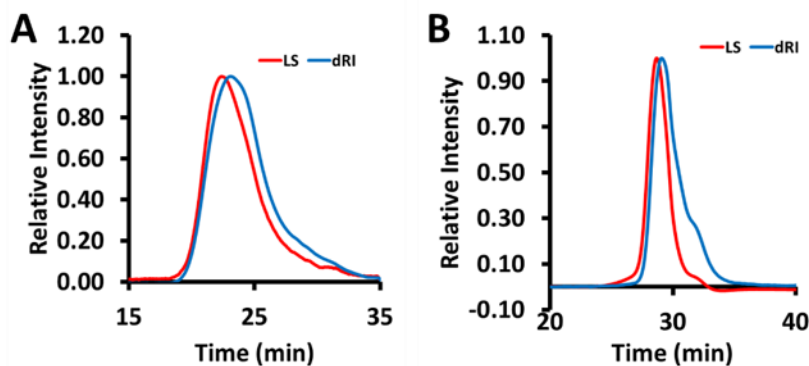
Figure 4.2. SEC-MALS traces of (A) polymer **2** in DMF as the eluent M_n= 32,260, Đ=1.4 and (B) polymer **3** in chloroform as the eluent M_n= 51,290, Đ=1.8

2. Synthesis and Nanoparticle Formation of Polymer 3

The norbornene units on polymer **2** were then prepared as initiation sites by addition of polymer **2** dropwise to a pyridine-modified variant of Grubbs' second generation catalyst, $(IMesH_2)(C_5H_5N)_2(Cl)_2RuCHPh$.[35] This catalyst was chosen due to its exceptional functional group tolerance and favorable rates of initiation and propagation to afford well-defined polymers with low dispersity. Polymer **2** was pre-loaded with 1.1 equivalents of Grubbs' catalyst with respect to the norbornene units for 10 min. The polymer was precipitated with methanol and excess/unreacted catalyst washed away to avoid competing polymerization events not originating from the PLA polymer-bound initiation sites. Following polymer resuspension in methylene chloride, phenyl-modified monomer **3** (5 equivalents with respect to norbornene units on the PLA backbone) was added to the catalyst-loaded polymer **2** and allowed to stir for 1 hour before quenching with ethyl vinyl ether, generating polymer **3** (Scheme 4.2).
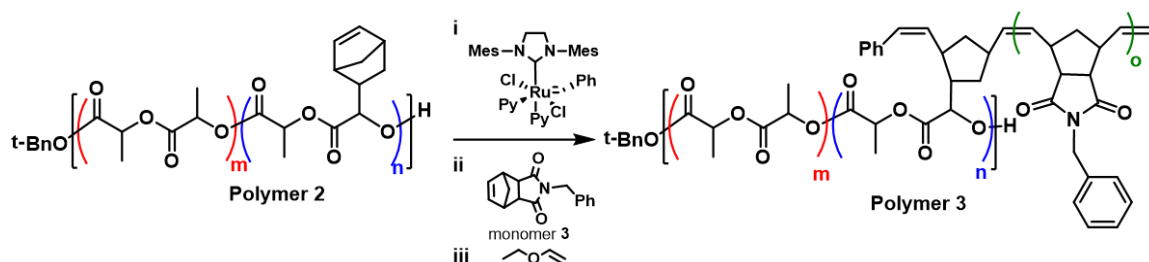
Scheme 4.2: Synthesis of polymer **3**.

This technique allowed for the generation of polymer **3** without generating any free ROMP polymer as verified by the presence of a monomodal distribution in the SEC-MALS chromatogram (Figure 4.2B). SEC-MALS also verified the success of the grafting technique by showing an increase in molecular weight of the PLA polymer **3** from M_n = 32,000 (Đ 1.4) to M_n = 51,000 (Đ 1.8) after the addition of the phenyl monomer (Figure 4.2A,B). As a negative control, unfunctionalized PLA polymers were exposed to the same solution conditions and reagents

including the Ru-initiator that were used for the preparation of polymer **3**. This treatment yielded

unfunctionalized PLA and no free homopolymer of monomer **3**, based on ^{1}H-NMR and SEC-

MALS, demonstrating the reliability of the precipitation step to eliminate any free, unreacted

initiator from solution (Figure 4.3).
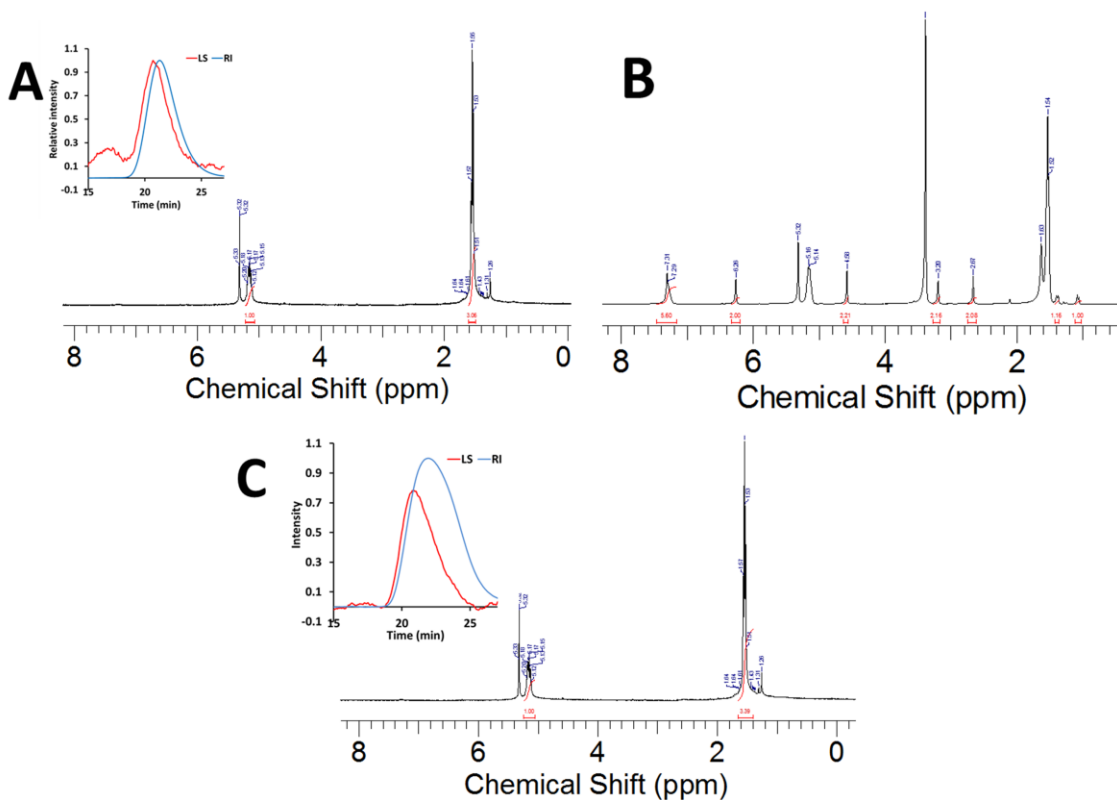
Figure 4.3. (A) Before reaction SEC-MALS in DMF as the eluent (Mn= 12,000 and Đ 1.2) and ^{1}H NMR. Unfunctionalized PLA polymer was added to a solution of 2nd generation Grubb's catalyst followed by precipitate with cold degassed methanol (B) Add 5 equivalents of phenyl monomer ^{1}H NMR t = 30 min. None of the phenyl peaks in the NMR are broadened and olefin peak δ = 6.26 ppm is still present which indicates no polymerization. (C) After the reaction: SEC-MALS in DMF as the eluent (Mn= 13,000 and Đ 1.3) and ^{1}H NMR. The product was precipitated with cold MeOH which yielded unfunctionalized PLA.

In order to demonstrate that no undesired cross linking of the PLA polymers were taking place, another control reaction was performed. Polymer **2** was resynthesized and this polymer was added to the Grubbs' catalyst. The solution was let to stir for 1 hour and then a large excess of ethyl vinyl ether (30 equivalents with respect to norbornene backbone units) was added to the reaction to produce a cross metathesis product and to terminate the opened olefin. Polymer **2** was analyzed by SEC-MALS before the reaction (M_n= 44,000 Đ= 1.1) and after the reaction (M_n=46,000 and Đ= 1.1). The M_n did not increase a substantial amount, confirming no crosslinked product. (Figure 4.4).
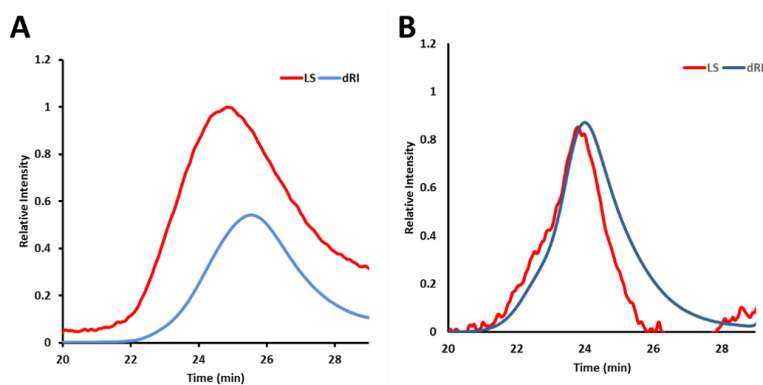
Figure 4.4. SEC-MALS traces of cross-linking control reaction. (A) SEC-MALS traces of polymer **2** in DMF as the eluent M_n= 44,000 Đ=1.1 and (B) after loading 2nd generation Grubb's and utilizing ethyl vinyl ether as a cross metathesis reactant. DMF as the eluent M_n= 46,000 Đ=1.1 There is no evidence of crosslinked polymers based on SEC-MALS.

To demonstrate graft-from polymers could be prepared as higher molecular weight assemblies, the polymers were allowed to assemble by dissolution in THF followed by slow addition to water and concentration *in vacuo* to form polymeric nanoparticles. Transmission electron microscopy (TEM) was then used to verify the formation of these nanoscale assemblies. Samples for TEM were prepared on carbon TEM grids by drop deposition followed by staining with 1% uranyl acetate solutions. Comparison of these TEM images (Figure 4.5) and dynamic

light scattering (DLS) data (Figure 4.6) of unfunctionalized PLA, polymer **2** and polymer **3,** indicated that each material had very similar morphology, consisting of spherical nanoparticles with diameters of 100 - 200 nm.
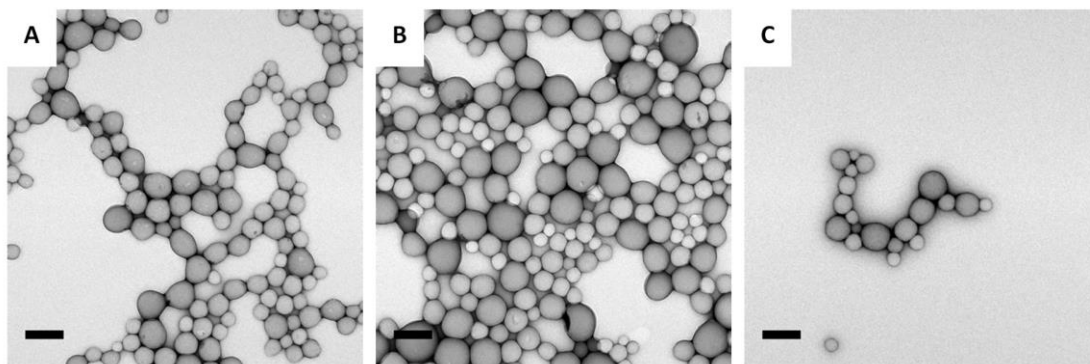
Figure 4.5. TEM images of nanoparticles comprised of (A) unfunctionalized PLA, (B) polymer **2**, and (C) polymer **3** with phenyl functionality. Stained with 1% uranyl acetate. Scale bars = 200 nm. These nanospheres were prepared by the solvent evaporation method by dissolving each polymer in THF and adding DI water dropwise. The polymers formed nanospheres after concentrating the solutions *in vacuo*.
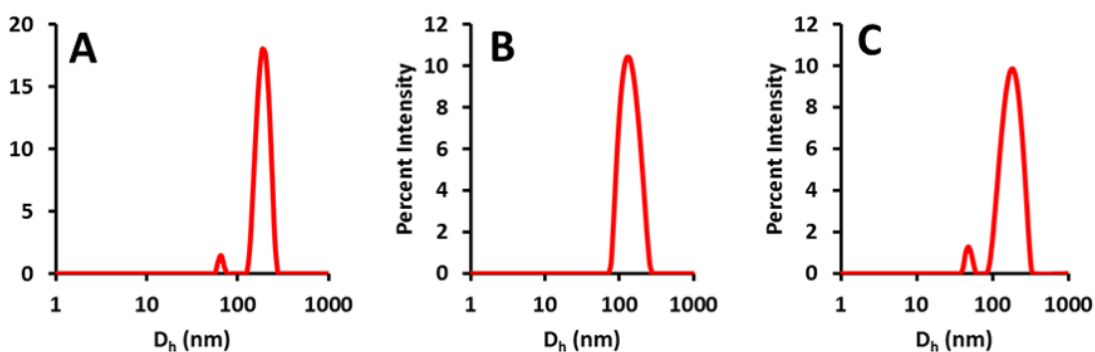
Figure 4.6. DLS of (A) unfunctionalized PLA (B) polymer **2** and (C) polymer **3**. All DLS traces are in DI water.

3. Synthesis of Polymer 4 and Polymer 4b

To exhibit one potential application of this graft-from polymerization technique, graft polymers featuring a stimuli-responsive functional moiety were synthesized. In this example, a grafted PLA polymer was synthesized by incorporating a norbornene monomer functionalized with a 5-dimethoxy-2-nitrobenzyl caged imidazole moiety. This moiety was chosen due to its potential to change its physical properties in response to two separate stimuli; UV light (via cleavage of the 2-nitrobenzyl cage) and pH (by way of protonation of the imidazole unit). Moreover, imidazole, in particular, was of interest since its protonation (pK_a of the immidazolium ion is ~7) is within a biologically relevant range (pH 5.0-7.4) and would demonstrate the possibility of triggering a morphology change in this material upon exposure to mild changes in pH environments.

The caged imidazole-containing norbornenyl monomer **4** readily polymerized, yet the resulting polymer **4** (Scheme 4.3 (A)) formed only amorphous aggregates rather than well dispersed spherical particles. As such, this monomer was copolymerized with tetra(ethylene glycol) norbornene monomer **5** to increase the water solubility of the resulting polymer **4b** (Scheme 4.3 (B)). The polymers were characterized by ^{1}H-NMR to determine the degree of polymerization (DP=59 kg/mol) (Figure 4.7). Note: a detailed characterization of the polymer's molecular weight was not possible by SEC-MALS due to aggregation on the SEC column.
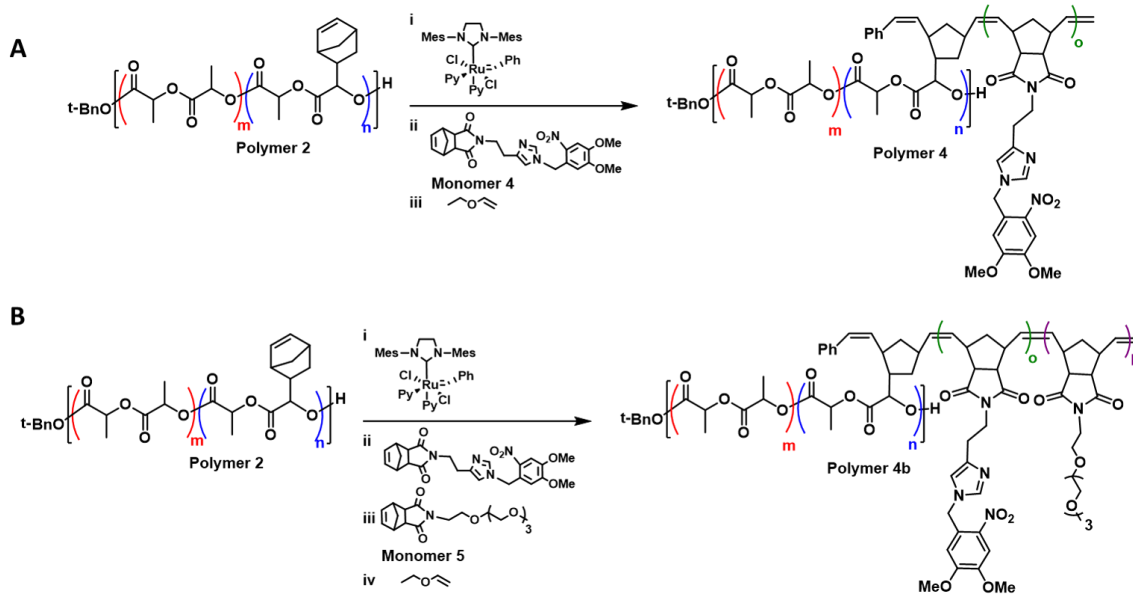
Scheme 4.3: Synthesis of (A) polymer **4** and (B) polymer **4b**.
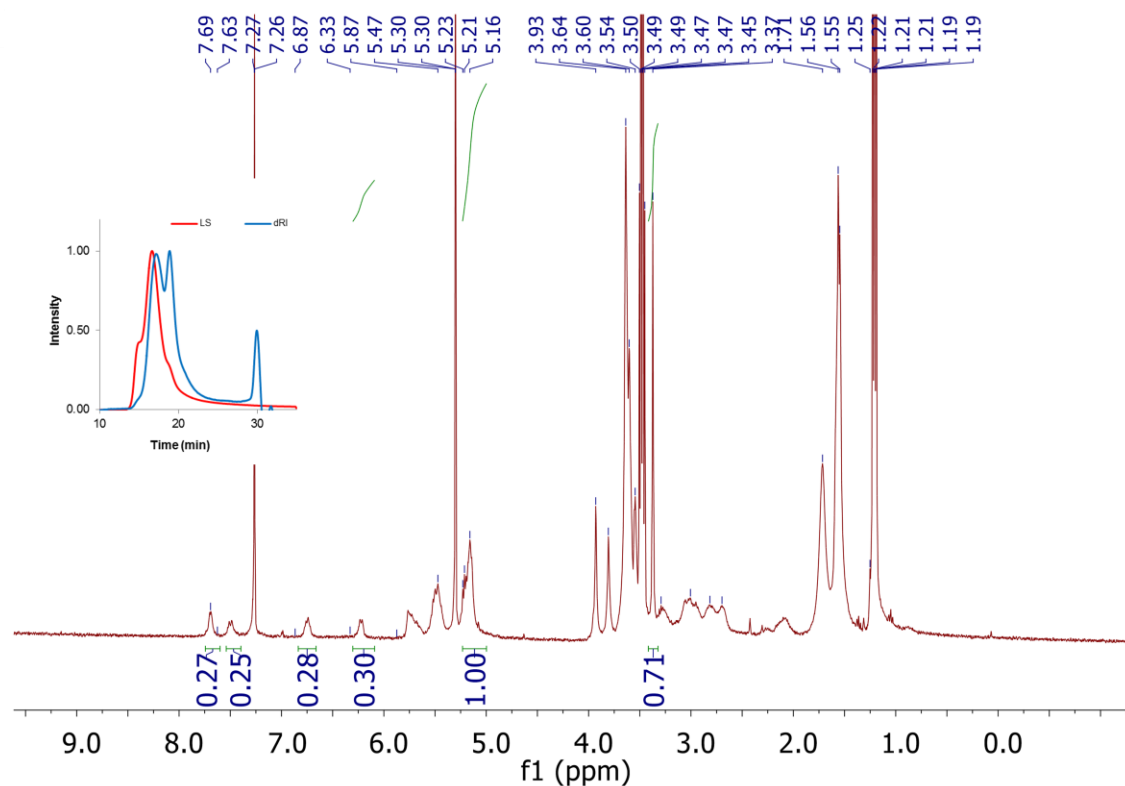
Figure 4.7: ¹H NMR and SEC-MALS in DMF as the eluent of polymer **4b**. Dispersity was not able to be determined since the polymer aggregates in the conditions used for SEC-MALS.

4. Morphology Studies of Polymer 4b

Nanoparticles of polymer **4b** were formulated by dialysis from DMSO into buffered water of and spherical nanoparticles of 100 nm diameter were formed at both pH 7.4 and 5.5 as evidenced by TEM (Figure 4.8 A, B) and DLS (Figure 4.9 A, B). Deprotection of the nitrobenzyl caged-imidazole via treatment of the nanoparticles with 350 nm UV light for six minutes at either pH 5.5 or 7.4. The cleavage of the nitrobenzyl group was monitered by by UV absorption spectra of polymer **4b**. Cleavage of the protecting group was complete after 6 min of UV light exposure indicated by the disappearance of the peak at 350 nm (Figure 4.10). After exposing to 350 nm UV light, particles in pH 7.4 buffer remained discrete nanostructures as evidenced by TEM (Figure 4.8 C) and DLS (Figure 4.9 C). At pH 5.5, we observed a change to micron-sized aggregates from discrete spherical structures as evidenced by TEM (Figure 4.8 D) and DLS (Figure 4.9 D).
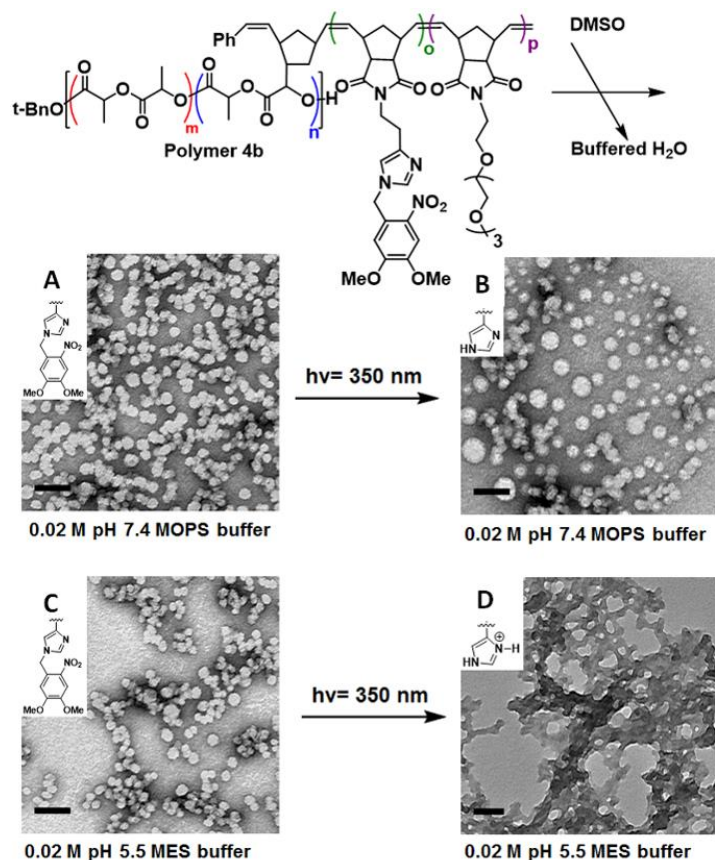
Figure 4.8. Responsive imidazole derivatized PLA nanoparticles. Polymers were dialyzed from DMSO to buffered water at a concentration of 1mg/mL. Spherical nanoparticles of 100 nm diameter were formed at both pH 7.4 (a) and 5.5 (c). After exposing to 350 nm UV light, particles in pH 7.4 buffer remained discrete nanostructures (b) and particles at pH 5.5 transformed from nanospheres to micron scale aggregates (d). This suggests that protonation of the liberated imidzaole moiety is necessary for the shape change, due to putative electrostatic repulsion of the positively charged imidazolium ions at low pH. Stained with 1% uranyl acetate. Scale bar = 200 nm.
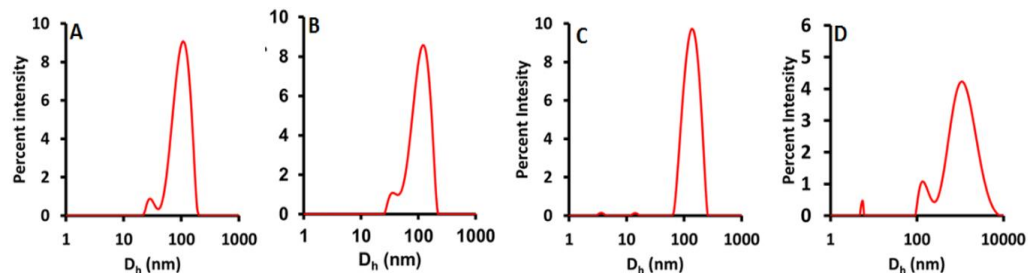
Figure 4.9. DLS of polymer **4b** (A) Before UV irradiation pH 7.4 in 0.02M MOPS buffer (B) After UV irradiation 3 min pH 7.4 in 0.02M MOPS buffer (C) Before UV irradiation pH 5.5 in 0.02M MES buffer and (D) After UV irradiation 3 min pH 5.5 in 0.02M MES buffer.

157
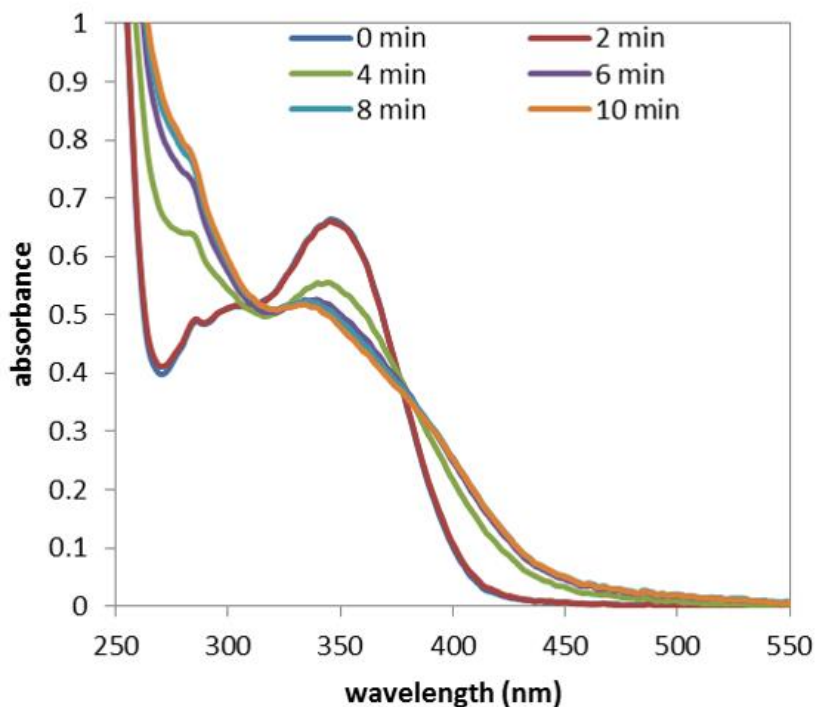
Figure 4.10. Absorbance spectra of polymer **4b** upon photolysis at 350 nm after 6 minutes the nitrobenzyl group is fully cleaved from polymer **4b**.

We attribute this change in shape of polymer **4b** to both removal of the bulky nitrobenzyl group and to protonation of the newly liberated imidazole moiety after exposure to UV light in an acidic environment. The disruption of the nanoparticle morphology of **4b** after exposure to UV light is likely due to electrostatic repulsion of the positively charged imidazolium groups and also to removal of the potentially self-associating 2-nitrobenzyl moieties. Imidazole-containing nanoparticles generated by removal of the 2-nitrobenzyl group from polymer **4b** in pH 7.4 buffered water (Figure 4.8 A) could be made to form the same aggregated structures as shown in Figure 4.8 D by decreasing the pH of the solution via slow addition of HCl to pH 5.5 (Figure 4.11), indicating the necessity of both stimuli, a reduction in pH and the application of UV light, to facilitate the morphology changed observed for polymer **4b**. Likewise, note that alkyl imidazoles, such as 2-nitrobenzyl protected polymer **4b**, should also be protonated at pH 5.5, however, this material does

158

not aggregate until exposed to UV-light, indicating that a decrease in pH is not alone sufficient for the morphology change.
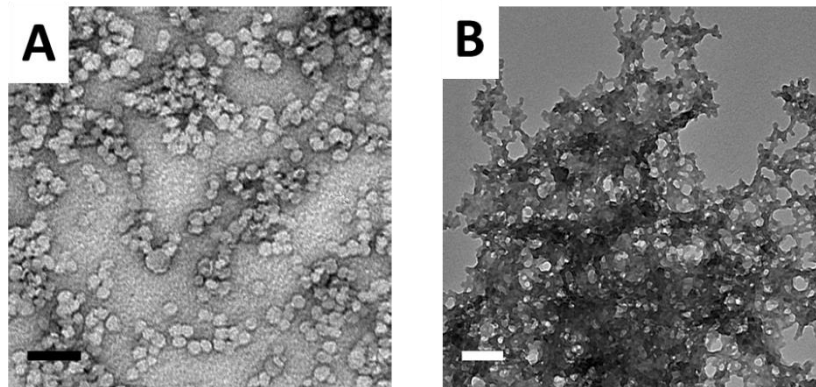
Figure 4.11. (A) Nanoparticles of polymer **4b** after UV exposure for 6 min in 0.02M pH 7.4 MOPS buffer. (B) Reduction of the pH from pH 7.4 to pH 5.5 with 0.1M HCl resulted in a morphology change to micron scale aggregates. Scale bar = 200 nm.

C. Conclusion

In summary, we have synthesized novel PLA-based materials via graft-from ROMP to install a high density of functionality from relativity low density branch points along the PLA backbone. As a proof-of-principle, we synthesized polynorbornyl grafts derivatized with a phenyl group along the PLA backbone and generated well-defined polymers and polymeric nanoparticles. We then synthesized 2-nitrobenzyl-protected imidazole graft variants to illustrate that chemical handles with increasing functionality can be incorporated into PLA via this method by capitalizing on the high functional group tolerance of the Grubbs' second generation modified catalyst. Photoprotected imidazole PLA polymers were formulated into nanoparticles and demonstrated a morphology change only in the presence of both the UV trigger and reduced pH as dual stimuli. This work represents a significant step toward highly functionalizable PLA materials that are potentially useful for a wide range of biomedical or materials applications.

D. Experimental

1. General Methods

All synthetic reagents were from Aldrich, Fisher Scientific, Alfa Aesar, or Fluka, and were used without further purification unless stated otherwise. All solvents used for reactions were obtained from Fisher scientific and dried on Alumina columns prior to use. Solvents used for chromatography were ACS technical grade and used without further purification. Water (18.2 $\mu\Omega$/cm) was filtered through a NANOPure Diamond™ (Barnstead) water purification system before use. All ^{1}HNMR spectra of all polymers and small molecule precursors were recorded on a Varian Mercury Plus 400 MHz NMR spectrometer in $CDCl_3$, CD_2Cl_2 or $(CD_3)_2NC(O)D$. ^{13}C NMR spectra of the products were obtained on a Varian VNMRS NMR spectrometer equipped with a 500MHz XSens Cold Probe in $CDCl_3$. Chemical shifts are reported as δ in units of parts per million (ppm) referenced to residue solvent peak. Coupling constants are reported as a J value in Hertz (Hz). Mass spec analysis was performed by the UCSD Chemistry and Biochemistry Molecular Mass Spectrometry Facility on a ThermoFinnigan LCQdeca mass spectrometer with an atmospheric pressure electrospray ionization (APCI) source or an electrospray ionization (ESI) source. Polymer dispersities and molecular weights were determined by size-exclusion chromatography (Phenomenex Phenogel 5u 10, 1K-75K, 300 x 7.80 mm in series with a Phenomex Phenogel 5u 10, 10K-1000K, 300 x 7.80 mm (0.05 M LiBr in DMF, 0.75 mL/min 60oC)) using a Hitachi-Elite LaChrom L-2130 pump equipped with a UV detector (Hitachi- Elite LaChrom L-2420), a multi-angle light scattering detector (DAWN-HELIOS: Wyatt Technology) and a refractive index detector (Optilab T-rEX: Wyatt Technology). Data analysis was performed using the ASTRA software package. TEM images were acquired on a carbon Formvar grid (Ted Pella,

Inc.) with 1% uranyl acetate stain on a FEI Tecnai G2 Sphera at 200 kV. The Grubbs' 2nd generation modified catalyst (IMesH$_2$)(C$_5$H$_5$N)$_2$(Cl)$_2$Ru=CHPh was prepared according to the published protocols.[1] Irradiation with 350 nm UV light was performed using a Rayonet photoreactor equipped with 8UV-A lamp (8W maximum intensity).

2. Synthesis of Lactide

Synthesis of exo-5-Norbornene-2-methanol (1.1): To flame dried 250 mL 3-neck flask, equipped with a stir bar, exo-5-norbornenecarboxylic acid (5.00 g, 36.0 mmol) was added. The flask was purge with N$_2$ and 125 mL of THF was added via a cannula to dissolve the exo-5-norbornenecarboxylic acid. The flask was cooled in a 0 °C ice bath. While still under N$_2$, in the ice bath the powdered LiAlH$_4$ (2.75 g, 72.3 mmol) was added slowly. After addition, the reaction was set to reflux for 2 hrs. The reaction was quenched with saturated NH$_4$Cl solution in an ice bath. The solution was filtered with ether and washed once with water. The organic layer was dried over sodium sulfate and concreted *in vacuo* to give the known alcohol as clear oil (4.49 g, quantitative yield). ^{1}H-NMR (400 MHz, CDCl$_3$) δ 6.09 (ddd, J = 14.5, 5.7, 3.0 Hz, 2H), 3.78 – 3.64 (m, 1H), 3.55 (d, J = 9.3 Hz, 1H), 2.82 (s, 1H), 2.75 (s, 1H), 1.61 (d, J = 6.3 Hz, 1H), 1.39 (s, 1H), 1.33 (dd, J = 6.1, 4.2 Hz, 1H), 1.31 – 1.27 (m, 1H), 1.27 – 1.22 (m, 1H), 1.15 – 1.06 (m, 1H).

Synthesis of 5-Norbornene-2-carboxaldehyde (1.2): *Exo*-5-Norbornene-2-methanol **1.1** (4.49 g, 36.2 mmol) was dissolved in 150 mL dichloromethane and allowed to stir in a 250 mL round bottom flask at 0 °C in an ice bath. Dess–Martin periodinane (18.42 g, 43.4 mmol) was added and the flask was purged with N$_2$. The solution was allowed to stir in the ice bath, under N$_2$, for 4 hrs. The reaction was filtered through a silica plug (100% EtOAc) to purify giving the known aldehyde as yellow oil (4.41 g 80%). ^{1}H NMR (400 MHz, CDCl$_3$) δ= 9.79 (d, J = 2.4 Hz, 1H), 6.16 (ddd, J

= 25.4, 5.6, 3.1 Hz, 2H), 3.17 – 3.08 (m, 1H), 2.98 (s, 1H), 2.34 – 2.20 (m, 1H), 1.96 (dt, J = 11.9, 4.0 Hz, 1H), 1.43 – 1.31 (m, 1H), 1.34 – 1.21 (m, 2H). ESI-MS (m/z) calculated for : $C_8H_{10}O$ [M]$^+$ 122.07; found [M+ Na]$^+$ 145.21

Synthesis of 2-(bicyclo[2.2.1]hept-5-en-2-yl)-2-hydroxy-1-(1H-indol-1-yl)ethan-1-one (**1.3**): To a 250 mL round bottom flask 1-(2,2-dimethoxyethyl)-2-isocyanobenzene (7.61g, 39.8 mmol), which was synthesized as previously reported[36], and **1.2** (5.84 g, 47.8 mmol) were dissolved in dichloromethane. While stirring, DI water was added (1.43 g, 79.6 mmol). After 5 min, the camphor sulfonic acid was added to the solution (1.99 g, 8.0 mmol). The solution was allowed to stir for 12 hr, then the reaction was concentrated *in vacuo* and immediately purified by column chromatography (6:4 DCM: hexanes) giving the desired N-acylindole as a white solid (4.33 g, 41%) . ^{1}H NMR (400 MHz, CDCl$_3$) δ 8.50 (t, J = 8.0 Hz, 1H), 7.59 (d, J = 7.7 Hz, 1H), 7.50 (d, J = 3.8 Hz, 1H), 7.46 – 7.36 (m, 1H), 7.33 (t, J = 7.1 Hz, 1H), 6.70 (t, J = 3.7 Hz, 1H), 6.16 – 6.01 (m, 2H), 4.94 (dd, J = 8.0, 5.5 Hz, 1H), 3.34 (d, J = 8.1 Hz, 1H), 2.81 (d, J = 62.0 Hz, 2H), 1.88-1.80 (m, Hz, 1H), 1.68 – 1.50 (m, 2H), 1.42 – 1.24 (m, 2H). ^{13}C NMR (100 MHz, CDCl$_3$) δ 173.43, 137.82, 137.57, 136.82, 130.60, 125.60, 124.48, 121.16, 117.00, 110.33, 74.40, 46.43, 43.93, 43.22, 42.05, 29.13. ESI-MS (m/z) calculated for $C_{17}H_{17}NO_2$ [M]$^+$ 267.13; found [M+H]$^+$ 268.11.

Synthesis of 2-(bicyclo[2.2.1]hept-5-en-2-yl)-2-hydroxyacetic acid (1.4): To a 250 mL round bottom flask a solution of **(1.3)** (4.33 g, 16. 2 mmol) in 150 mL of THF at 0 °C was added 1.0 M LiOH(aq) (32.1 mL, 32.1 mmol). After 2 hrs, 1.0M NaOH (10 mL) was added to the reaction to ensure a basic pH. The aqueous phase was washed with EtOAc (3 x 100 mL) to remove the indole byproduct. The combined organic layers were back-extracted with 1.0M NaOH (2 x 25 mL). The combined aqueous layers were acidified to pH 2 using 6M HCl and then extracted with ether (6 x

100 mL) The combined organic layers were dried with sodium sulfate and concentrated *in vacuo* to give the α-hydroxy acid as a tan solid (2.31 g, 86%). ^{1}H NMR (400 MHz, CDCl$_3$) δ 6.22 – 6.01 (m, 2H), 4.14 (dd, J = 73.4, 7.5 Hz, 1H), 3.02 – 2.77 (m, 2H), 1.84 – 1.70 (m, 1H), 1.58 (tdd, J = 16.1, 12.9, 4.1 Hz, 2H), 1.39 (dd, J = 37.0, 8.6 Hz, 2H). ^{13}C NMR (100 MHz, CDCl$_3$) δ 179.89, 137.47, 136.26, 74.06, 45.93,43.62, 43.44, 41.74, 28.79 ESI-MS (*m/z*) calc [M]$^+$ for C$_9$H$_{12}$O$_3$ 168.08; found [M-H]$^-$ 167.14

Synthesis of 3-(bicyclo[2.2.1]hept-5-en-2-yl)-6-methyl-1,4-dioxane-2,5-dione (1): Compound **1.4** (1.00 g, 5.94 mmol) and triethylamine (0.63 g, 0.87 mL, 0.062 mmol) were added to a 100 mL flask and dissolved in 50 mL dry acetonitrile and allowed to stir at 0 °C under nitrogen. After 5 min, 2-bromopropionyl bromide (1.4 g, 0.65 mL, 6.24 mmol) was added and the solution was allowed to stir at 0 °C for 30 min. Another equivalent of triethylamine (0.63 g, 0.87 mL, 0.062 mmol) was added and the reaction was allowed to stir at 70 °C for 3 hrs. The product was filtered through a silica plug in EtOAc and concentrated *in vacuo*. The product was recrystallized in toluene, giving the product as a white solid (760 mg, 42%). ^{1}H NMR (400 MHz, CDCl$_3$) δ 6.31 – 5.99 (m, 2H), 5.03 (q, J = 6.7 Hz, 1H), 4.75 (dd, J = 24.3, 8.7 Hz, 1H), 3.11 – 2.80 (m, 2H), 2.03 (d, J = 4.7 Hz, 1H), 1.66 (dt, J = 6.7, 3.4 Hz, 3H), 1.57 (dd, J = 12.1, 8.6 Hz, 1H), 1.50 – 1.43 (m, 1H), 1.37 (dd, J = 20.4, 9.0 Hz, 2H).^{13}C NMR (100 MHz, CDCl$_3$) δ 167.66, 166.55, 137.56, 135.84, 79.22, 72.14, 45.08, 42.25, 39.88, 30.31, 28.31, 15.81 ESI-MS (*m/z*) calc [M]$^+$ for C$_{12}$H$_{14}$O$_4$ [M]$^+$ 222.09; found [M-H]$^-$ 221.17 and [M+H$_2$O-H] 239.22.

3. Synthesis of Monomers:

Synthesis of (N-Benzyl)-5-norborene-exo-2,3-dicarboximide (phenyl monomer 3): To a stirred solution of N-benzylamine (2.85 g, 26.6 mmol) in dry toluene (125 mL) were added 5-norbornene-*exo*-2,3-dicarboxylic anhydride (4.10 g, 25.0 mmol) and triethylamine (3.83 mL, 27.5 mmol). The reaction was heated to reflux overnight under an atmosphere of N_2. The reaction was cooled to room temperature and washed with 10% HCl (3 x 50 mL) and brine (2 x 50 mL). The aqueous layers were combined and extracted with ethyl acetate (60 mL). The combined organic layers were dried with $MgSO_4$, filtered, and concentrated to dryness, yielding a pale yellow solid that was then recrystallized from ethyl acetate/hexanes to give the known product (4.98 g, 79%) as white crystals. ^{1}H NMR (CDCl$_3$): δ 7.25-7.40 (m, 5H), 6.28 (s, 2H), 4.61 (s, 2H), 3.26 (s, 2H), 2.69 (s, 2H), 1.42 (d, 1H, *J*=9.6 Hz), 1.07 (d, 1H, *J*=9.6 Hz).). ^{13}C NMR (100 MHz, CDCl$_3$) δ 177.94, 137.71, 135.02, 133.68, 117.20, 47.73, 45.01, 42.56, 38.18, 25.06.

Synthesis of 2-(2-(1H-imidazol-4-yl)ethyl)-3a,4,7,7a-tetrahydro-1H-4,7-methanoisoindole-1,3(2H)-dione (imidazole monomer 4a): To a flame dried 100 mL round bottom flask, cis-5-Norbornene-exo-2,3-dicarboxylic anhydride (200 mg, 1.21 mmol) and histamine dihydrochloride (336 mg, 1.82 mmol) were added. The flask was purged with nitrogen and dry DMF was added via a syringe. Triethylamine (1.19 mL, 8.52 mmol) was then added drop wise to the flask while stirring. A condenser was added to the flask and the flask was placed in a 130°C oil bath for 12 hrs. The reaction was concentrated *in vacuo* and purified by column chromatography (9:1:90 MeOH:Et$_3$N:DCM) giving the product as a brown solid (180 mg, 60%). ^{1}H NMR (400 MHz, CDCl$_3$) δ 11.54 (s, 1H), 7.63 (s, 1H), 6.83 (s, 1H), 6.20 (s, 2H), 3.73 (t, *J* = 7.4 Hz, 2H), 3.15 (s, 2H), 2.88 (t, *J* = 7.4 Hz, 2H), 2.59 (s, 2H), 1.38 (d, *J* = 9.8 Hz, 1H), 1.05 (d, *J* = 9.8 Hz, 1H). ^{13}C

NMR (100 MHz, CDCl$_3$) δ 177.94, 137.71, 135.02, 133.68, 117.20, 47.73, 45.01, 42.56, 38.18, 25.06. ESI-MS (*m/z*) calc [M]$^+$ for C$_{15}$H$_{17}$N$_3$O$_2$ [M]$^+$ 257.12; found [M+H]$^+$ 258.17 and [M+Na]$^+$ 280.16.

Synthesis of 2-(2-(1-(4,5-dimethoxy-2-nitrobenzyl)-1H-imidazol-4-yl)ethyl)-3a,4,7,7a-tetrahydro-1H-4,7-methanoisoindole-1,3(2H)-dione (photo-protected imidazole monomer 4): Imidazole monomer **(4a)** (100 mg, 0.38 mmol) and 4,5-Dimethoxy-2-nitrobenzyl bromide (128.8 mg, 0.47 mmol) were added to a flame dried 100 mL round bottom flask. The flask was then purged with N$_2$ and DMF was added via syringe. Potassium carbonate (64.5 mg, 0.47 mmol) was then added to the reaction. The reaction was allowed to stir for 24 hrs at room temperature under a nitrogen atmosphere. The reaction was then diluted with 200 mL DCM and washed with saturated sodium bicarbonate solution (3 x 100 mL), brine (100 mL) and dried over sodium sulfate. The reaction was then filtered, concentrated *in vacuo* and purified by column chromatography (100:0 → 100:3 DCM: MeOH) to yield the product as a pale yellow solid (45 mg, 25%). ^{1}H NMR (400 MHz, CD$_3$CN) δ 7.73 (d, *J* = 26.1 Hz, 1H), 7.50 (s, 1H), 6.82 (s, 1H), 6.60 (s, 1H), 6.28 (s, 2H), 5.42 (s, 2H), 3.90 (s, 3H), 3.85 (s, 3H), 3.63 (t, *J* = 7.3 Hz, 2H), 3.05 (s, 2H), 2.74 (t, J = 7.3 Hz, 2H), 2.58 (s, 2H), 1.29 (d, J = 9.6 Hz, 1H), 1.14 (d, *J* = 9.7 Hz, 1H).^{13}C NMR (100 MHz, CDCl$_3$) δ 177.63, 153.81, 148.17, 139.80, 137.57, 137.34, 127.43, 116.19, 109.57, 108.03, 56.20, 47.97, 47.53, 44.81, 42.43, 38.18. 26.19 ESI-MS (*m/z*) calc [M]$^+$ for C$_{24}$H$_{26}$N$_4$O$_6$ 452.17; found [M+H]$^+$ 453.14 and [M+Na]$^+$ 475.07

Synthesis of 2-(2,5,8,11-tetraoxatridecan-13-yl)-3a,4,7,7atetrahydro-1H-4,7-methanoisoindole-1,3(2H)-dione (tetra(ethylene glycol) norbornene monomer 5): A solution of *cis*-5-Norbornene-*exo*-2,3-dicarboxylic anhydride (1.5 g, 9.1 mmol) and 2,5,8,11-tetraoxatridecan-13-amine[3] (2.27 g, 11.0 mmol) in toluene (50 mL) was heated at reflux overnight under a nitrogen atmosphere. The reaction mixture was cooled to room temperature, concentrated to dryness and purified by flash chromatography (2% MeOH in CH_2Cl_2) to give the product as a light yellow oil, 3.12g (97%). ^{1}H NMR, 400MHz, $CDCl_3$, δ 6.26 (m, 2H), 3.5-3.7 (m, 16H), 3.36 (s, 3H), , 3.24 (m, 2H), 2.66 (s, 2H), 1.47, (m, 1H), 1.35 (m, 1H). ^{13}C NMR, 100MHz, $CDCl^3$, δ 177.91, 137.73, 71.83, 70.50, 69.77, 66.78,58.95, 47.73, 45.19, 42.63, 37.64 HRMS Calc $[M+Na]^+$ = 376.1736, Obs. = 376.1730.

4. Synthesis of Polymers

Procedure for ring opening polymerization (ROP) (Polymer 2): The polymerization was carried out with tin(II) 2-ethylhexanoate (stannous octoate, $Sn(Oct)_2$) (purchased from Alfa Aesar) and 4-tert-butylbenzyl alcohol (purchased from Acros) without further purification. The polymerization method is similar to that described by Baker and coworkers.[3] $Sn(Oct)_2$ (0.01M in anhydrous toluene, 7.76 mL) and 4-*tert*-butylbenzyl alcohol (0.01M in anhydrous toluene, 7.76 mL) were added to a small 20 mL pear shaped flask and the solution was concentrated *in vacuo*. To the flask was then added D,L-lactide (1.0 g, 9.7 mmol) (freshly recrystallized from toluene) and compound **(1)** (333.6 mg, 1.5 mmol). The flask was then equipped with a small stir bar and placed under vacuum. After 1 hour, the flask was flushed with nitrogen, tightly sealed and heated at 130 °C in a silicone oil bath for 2 hrs. After the reaction was complete, the flask was cooled in an ice bath, dissolved in CD_2Cl_2 and the crude was analyzed by ^{1}H NMR. A small aliquot of the

CD$_2$Cl$_2$ solution was concentrated *in vacuo*, redissolved in DMF, filtered through a Whatman Anontop 10 0.2 µm filter and analyzed by SEC-MALS to determine the molecular weight of the polymer. To purify, the polymer was dissolved in dichloromethane and precipitated with cold methanol. The degree of polymerization (conversion of monomer to polymer) calculated from ^{1}H NMR was 98%. The polymer was obtained as a light brown solid (1.55 g, 90%).

Procedure for graft-from ring opening metathesis polymerization of phenyl monomer (Polymer 3): Graft-from PLA polymers were polymerized using Grubbs' modified second generation catalyst [(H$_2$IMES)(pyr)$_2$(Cl)$_2$Ru=CHPh]. Polymer **2** (10 mg, 0.0026 mmol) was dissolved in in dry, degassed CH$_2$Cl$_2$ (8 mL) in a 10 mL vial under a nitrogen atmosphere. The catalyst (2.13 mg, 0.0029 mmol) 1.1 equivalents with respect to norbornene units, was also dissolved in dry, degassed CH$_2$Cl$_2$ in a separate vial (0.2 mL). The polymer solution was added to the Grubb's catalyst and the solution was allowed to stir for 10 min. Degassed cold MeOH was added to the vial via a syringe to precipitate out the catalyst loaded PLA polymer. The vial was centrifuged at 4000 rpm for 5 min. The supernatant was removed via syringe, to ensure that there was no free Grubbs' catalyst in solution. The polymer was resuspended in degassed dichloromethane and monomer **3** was added (3.36 mg, 0.013 mmol), 5 equivalents with respect to norbornene units. The reaction was left to stir for 1 hr before quenching with ethyl vinyl ether. The polymer was purified by precipitation into cold ether. ^{1}H-NMR, in CD$_2$Cl$_2$, was used to determine the degree of polymerization of the PLA-ROMP polymer. A small aliquot of the polymer was dissolved in DMF, filtered through a Whatman Anontop 10 0.2 µm filter and analyzed by SEC-MALS to determine the molecular weight and dispersity of the polymer.

Procedure for the negative control reaction: verification of precipitation step:
Unfunctionalized PLA (10 mg, 0.0030 mmol) is dissolved in 8 mL of degassed, dry CD_2Cl_2 and added to a solution of Grubb's catalyst (2.40 mg, 0.033 mmol), 1.1 equivalents with respect to the number of norbornene units on polymer **2** and was stirred for 10 min under a nitrogen atmophere. Degassed cold MeOH was added to the vial via a syringe to precipitate out the unfunctionalized PLA polymer. The vial was centrifuged at 4000 rpm for 5 min. The supernatant was removed via syringe, to ensure that there was no free Grubbs' catalyst in solution. The polymer was then resuspended in degassed CD_2Cl_2 and monomer 3 was added (3.80 mg, 0.150 mmol), 5 equivalents with respect to norbornene units on polymer **2**. The reaction was left to stir for 30 min before taking an ^1H NMR spectrum. None of the phenyl peaks in the NMR are broadened and olefin peak $\delta = 6.26$ ppm is still present which indicates no polymerization. After the reaction: the polymer was precipitated with cold MeOH, which yielded unfunctionalized PLA.

Procedure for graft-from ring opening metathesis polymerization of nitro benzyl protected imidazole monomer (Polymer 4): Graft-from PLA polymers were polymerized using Grubbs' modified second generation catalyst $[(H_2IMES)(pyr)_2(Cl)_2Ru=CHPh]$. Polymer **2** (10 mg, 0.0026 mmol) was dissolved in in dry, degassed CH_2Cl_2 (8 mL) in a 10 mL vial under a nitrogen atmosphere. The catalyst (2.13 mg, 0.0029 mmol), 1.1 equivalents with respect to norbornene units was also dissolved in dry, degassed CH_2Cl_2 in a separate vial (0.2 mL). The polymer solution was added to the Grubb's catalyst and the solution was allowed to stir for 10 min. Degassed cold MeOH was added to the vial via a syringe to precipitate out the catalyst loaded PLA polymer.. The vial was centrifuged at 4000 rpm for 5 min. The supernatant was removed via syringe, to ensure that

there was no free Grubbs' catalyst in solution. The polymer was resuspended in degassed dichloromethane and the imidazole ROMP monomer **4**, was added (6.03 mg, 0.013 mmol), 5 equivalents with respect to norbornene units on PLA polymer **2**. The reaction was left to stir for 6 hrs before quenching with ethyl vinyl ether. The polymer was purified by precipitation into cold ether. ^{1}H-NMR, in CDCl$_3$ was used to determine the degree of polymerization of the PLA-ROMP polymer and molecular weight (M_n). Dispersity (Đ) was not able to be determined since the polymer aggregates in the conditions used for SEC-MALS.

Procedure for graft-from ring opening metathesis polymerization of nitro benzyl protected imidazole monomer 4 with tetra(ethylene glycol) norbornene monomer 5 (Polymer 4b):
Graft-from PLA polymers were polymerized using Grubbs' modified second generation catalyst [(H$_2$IMES)(pyr)$_2$(Cl)$_2$Ru=CHPh]. The PLA polymer (10 mg, 0.0026 mmol) was dissolved in in dry, degassed CH$_2$Cl$_2$ in a 10 mL vial under a nitrogen atmosphere. The catalyst (2.13 mg, 0.0029 mmol), 1 equivalent with respect to norbornene units on the PLA backbone, was also dissolved in dry, degassed CH$_2$Cl$_2$. Polymer **2** was added to the Grubb's catalyst solution and the solution was allowed to stir for 10 min. Degassed cold MeOH was added to the vial via a syringe to precipitate out the catalyst loaded PLA polymer. The vial was centrifuged at 4000 rpm for 5 min. The supernatant was removed via syringe, to ensure that there was no free Grubbs' catalyst in solution. The polymer was resuspended in degassed dichloromethane and the imidazole ROMP monomer **4**, was added (6.03 mg, 0.013 mmol), 5 equivalents with respect to the norbornene units. The reaction was left to stir for 6 hrs before the tetra(ethylene glycol) norbornene monomer **5**, (4.17 mg, 0013 mmol), 5 equivalents with respect to norbornene units, was added. The reaction was left to stir for another 3 hrs before quenching with ethyl vinyl ether. The polymer was purified by

precipitation into cold ether. ^{1}H-NMR, in CDCl$_3$ was used to determine the degree of polymerization of the PLA-ROMP polymer and molecular weight (M$_n$). Dispersity (Đ) was not able to be determined since the polymer aggregates in the conditions used for SEC-MALS.

5. Procedure for Nanoparticle Synthesis

Procedure for nanoparticle formation via the solvent evaporation*: 2 mg of **polymer 2** or unfunctionalized PLA was dissolved into 2 mL of THF. This solution was added to 2 mL of DI H$_2$O via syringe pump at a rate of 8 mL/hr. The solution was allowed to stir for 30 min and was subsequently concentrated *in vacuo* to remove the THF. Nanoparticles were analyzed by DLS and TEM.

Procedure for nanoparticle formation via the dialysis method: Unsuccessful attempts with polymer 4: Many solvents were screened to attempt to formulate nanoparticles of **polymer 4** via the solvent evaporation method. The polymer was only soluble in methylene chloride, THF, DMF and DMSO. Methylene chloride is not soluble in water thus 2 mg of the polymer was added to 2 mL of DI H$_2$O and 2 mL of methylene chloride and sonicated attempting formulation of nanoparticles via the nanoprecipitation method, but the only result was large aggregated polymers, not well defined nanostructures. **Polymer 4** was only sparingly soluble in THF, even with heating. When nanoparticle formation was attempted at the same concentrations as above, the polymer crashed out of solution. Luckily the polymers were very soluble in DMF and DMSO, however both solvents have a higher boiling point than water so the solvent evaporation method was not possible. Therefore the dialysis method was used to formulate nanostructures of **polymer 4**. 1 mg

of **polymer 4** was dissolved in 900 μL of DMSO. 100 μL of DI H$_2$O was added to the solution over 10 min while stirring. The solution was allowed to stir for 12 hrs. The solution was transferred to a MWCO 3,500 Slide-A-Lyzer™ MINI Dialysis Device, 2 mL and placed in 1 L of 0.02M pH 7.4 MOPS buffer or 0.02M pH 5.5 MES buffer. The dialysis water was changed 3 times over 24 hrs. This procedure yielded only large aggregates and not well-dispersed spherical particles. Thus in an attempt to create spherical nanoparticles **polymer 2** was polymerized with monomer **4** and the tetra(ethylene glycol) norbornene monomer **5** to increase water solubility(yielding **polymer 4b**.) Dialysis conditions (DMSO into water or buffer) was utilized to create well-defined nanostructures. Dialyzing from DMSO gave more uniform nanostructures than dialyzing from DMF into water or buffer.

Procedure for nanoparticle formation via the dialysis method: Successful attempts with polymer 4b: 1 mg of **polymer 4b** was dissolved in 900 μL of DMSO. 100 μL of DI H$_2$O was added to the solution over 10 min while stirring. The solution was allowed to stir for 12 hrs. The solution was transferred to a MWCO 3,500 Slide-A-Lyzer™ MINI Dialysis Device, 2 mL and placed in 1 L of 0.02M pH 7.4 MOPS buffer or 0.02M pH 5.5 MES buffer. The dialysis water was changed 3 times over 24 hrs. Nanoparticles were transferred to a small Eppendorf tube for TEM and DLS analysis.
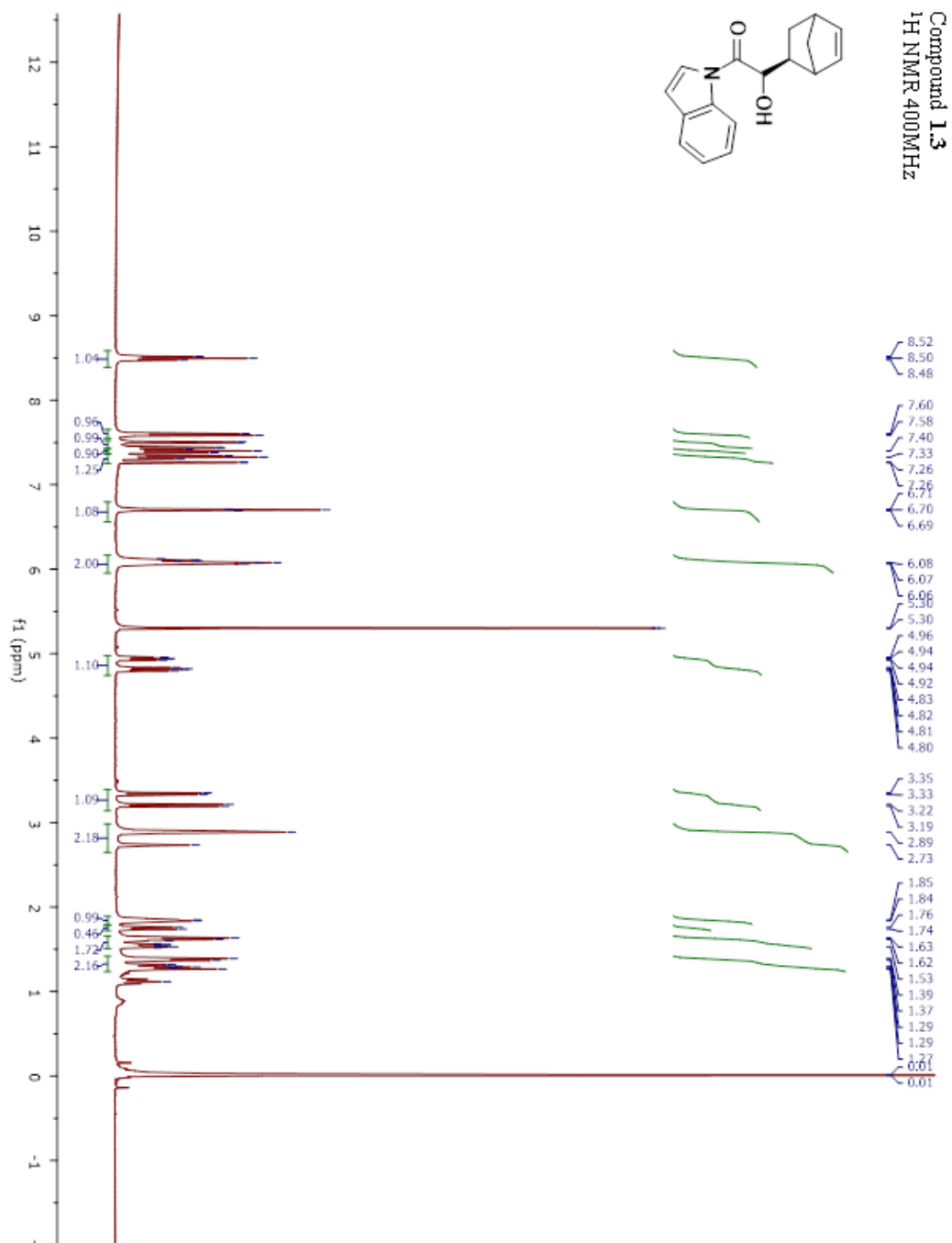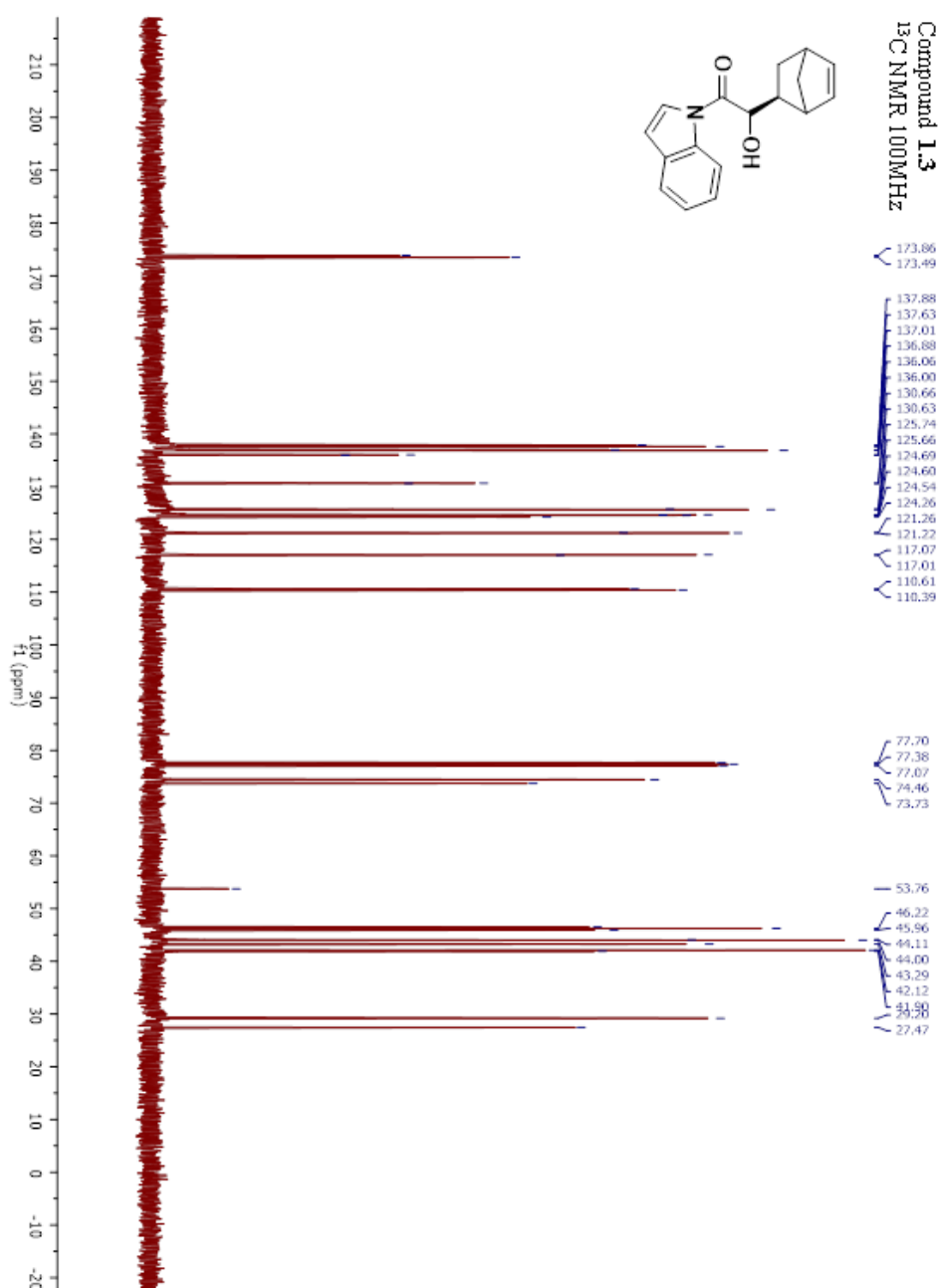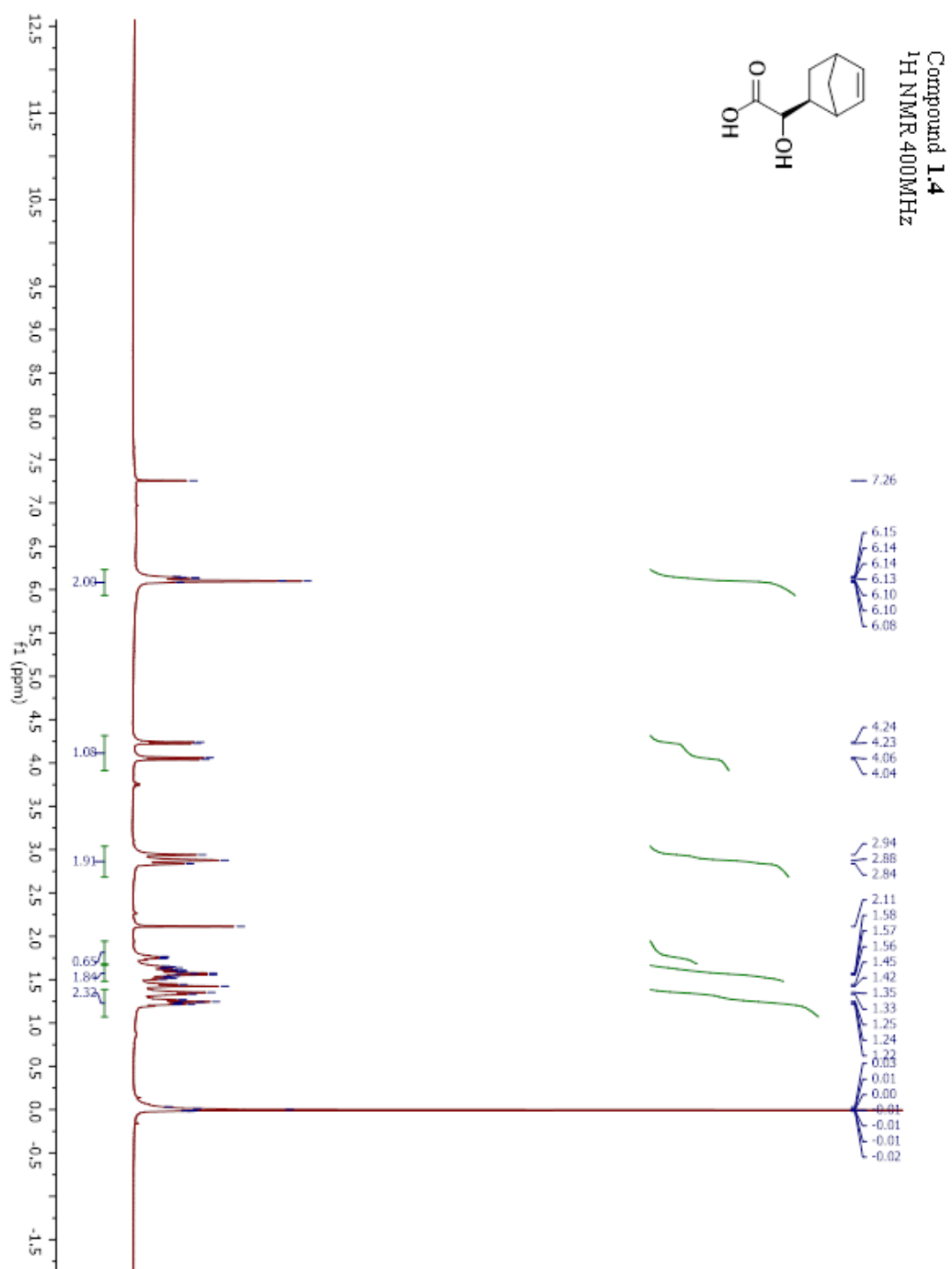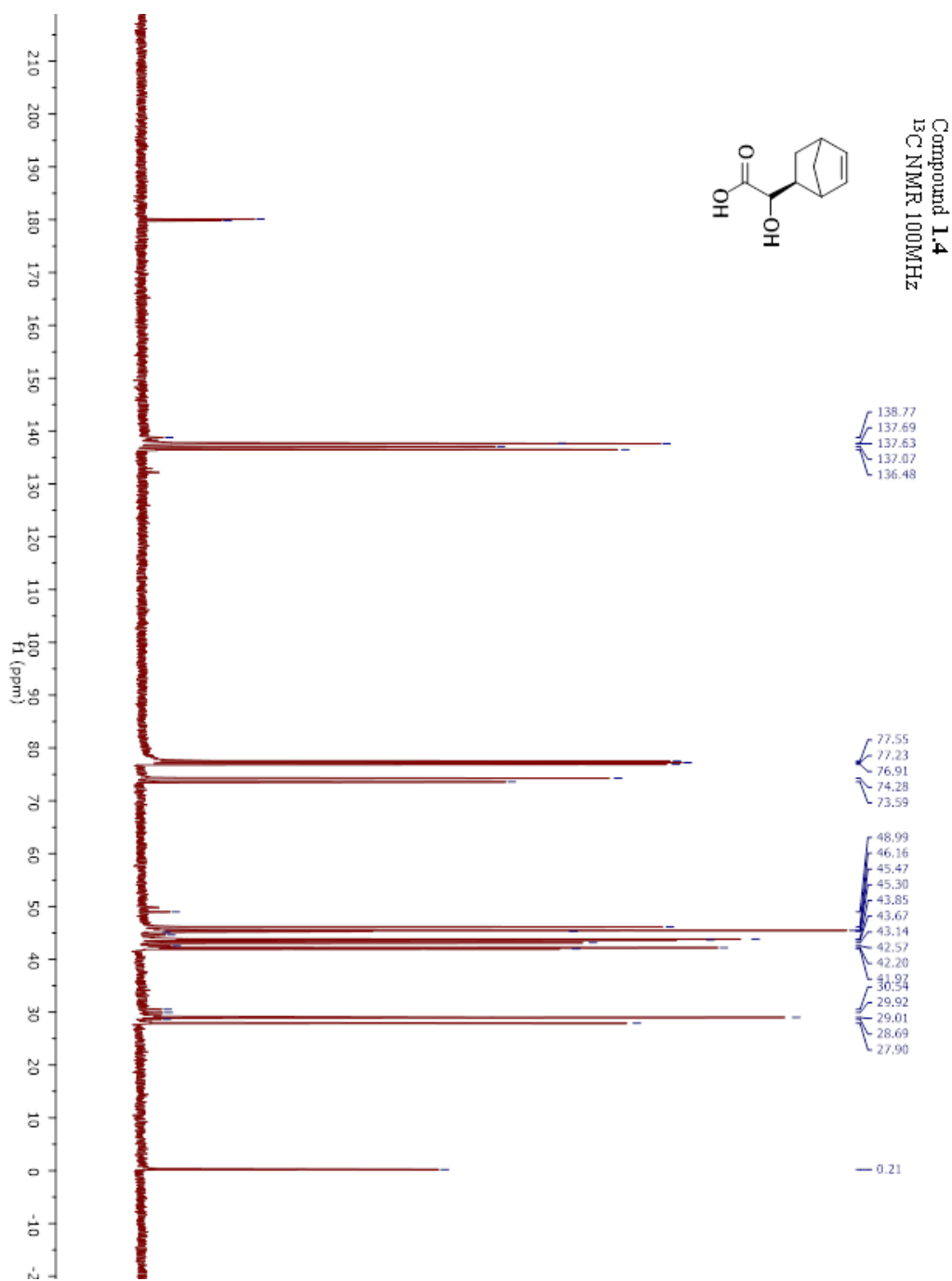
E. Appendix

Figure 4.12. ^{1}H NMR spectrum of compound **1.3**.

Figure 4.13. $^{13}C\{^{1}H\}$ NMR spectrum of compound **1.3**.

Figure 4.14. ^{1}H NMR spectrum of compound **1.4**

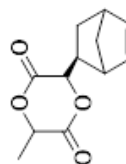**Figure 4.15.** $^{13}C\{^1H\}$ NMR spectrum of compound **1.4**.
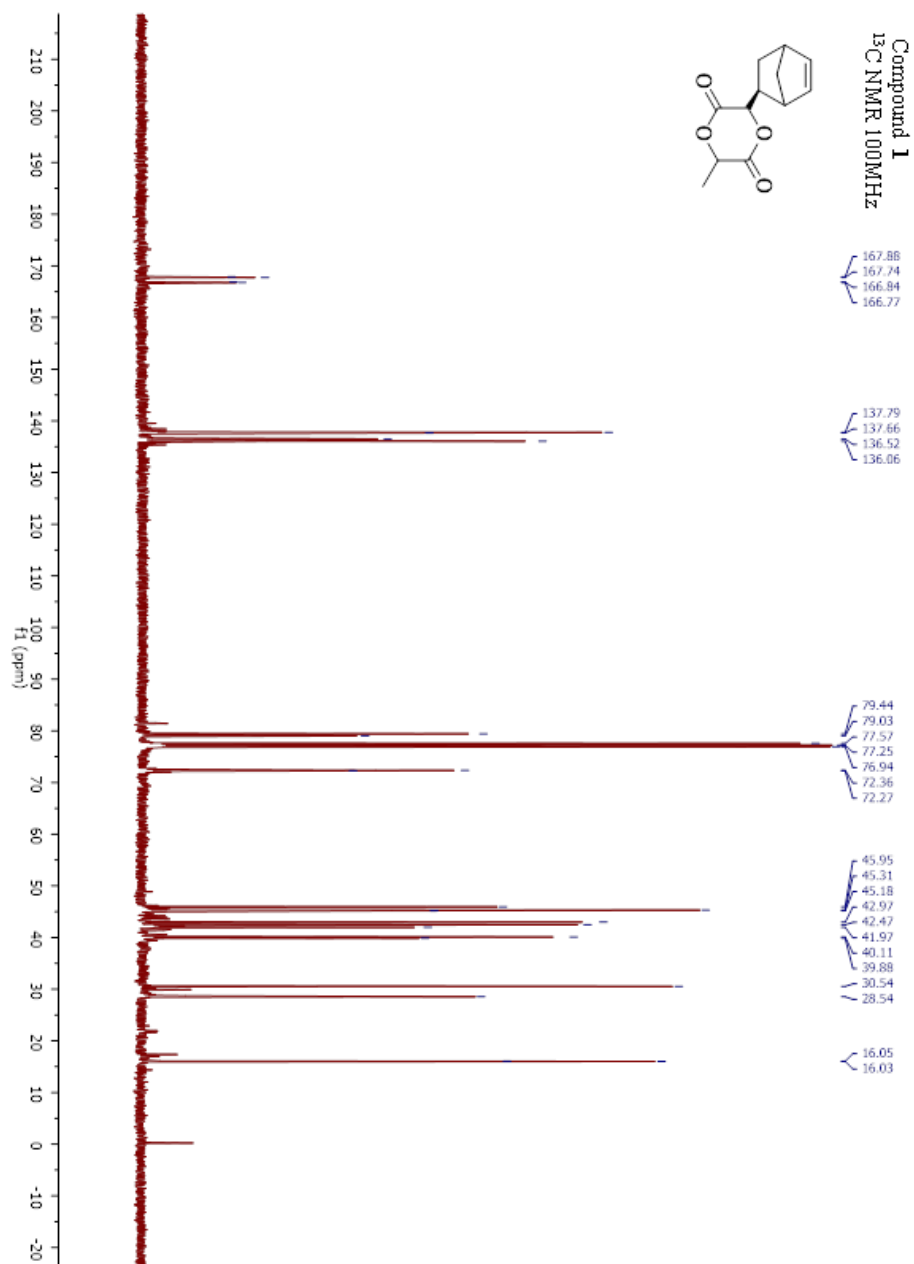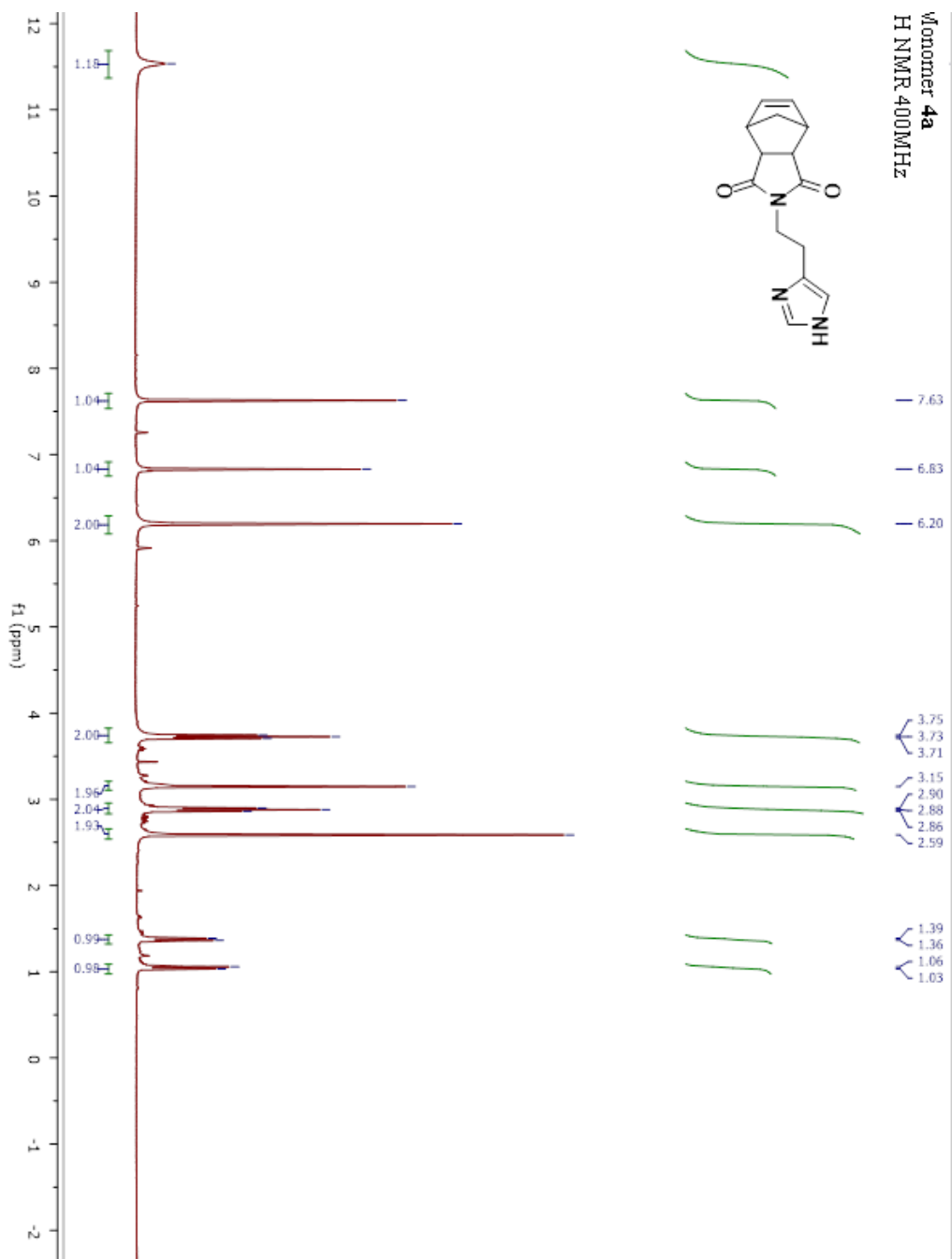
175
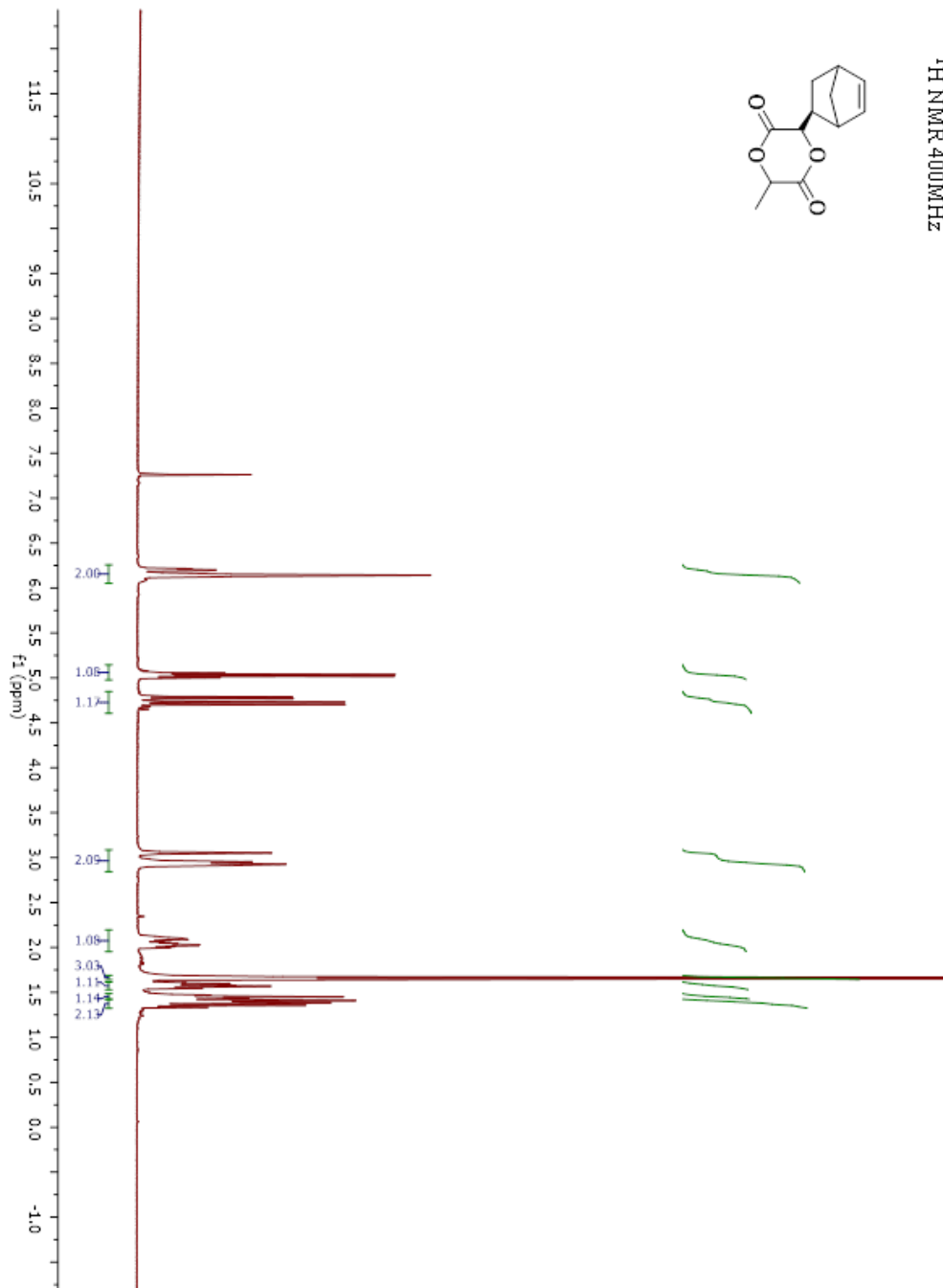
Figure 4.16. ¹H NMR spectrum of compound **1**.

Figure 4.17. ^{13}C{^{1}H} NMR spectrum of compound **1**.

Figure 4.18. ^{1}H NMR spectrum of compound **4a**.

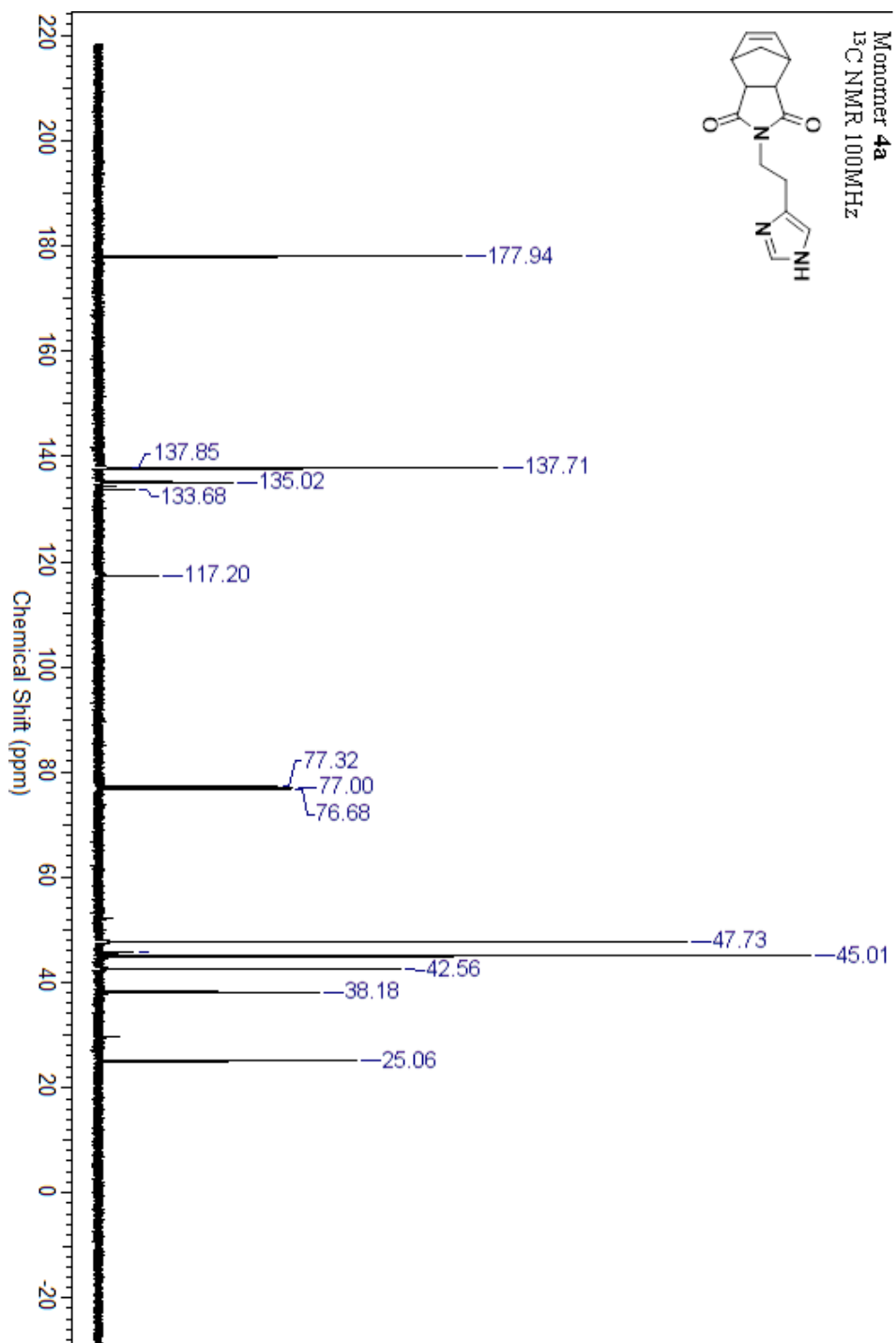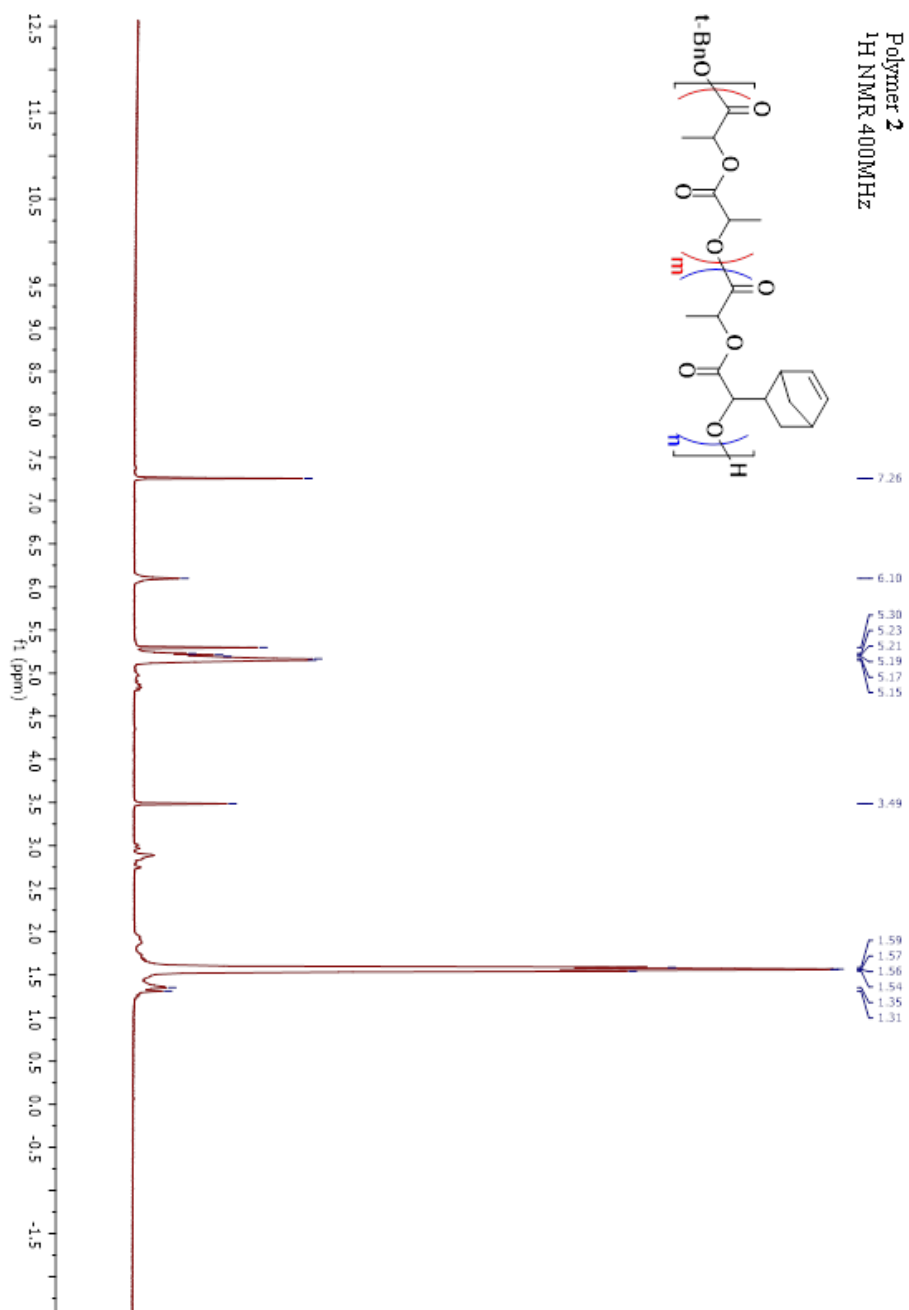**Figure 4.19.** $^{13}C\{^1H\}$ NMR spectrum of compound **4a**.

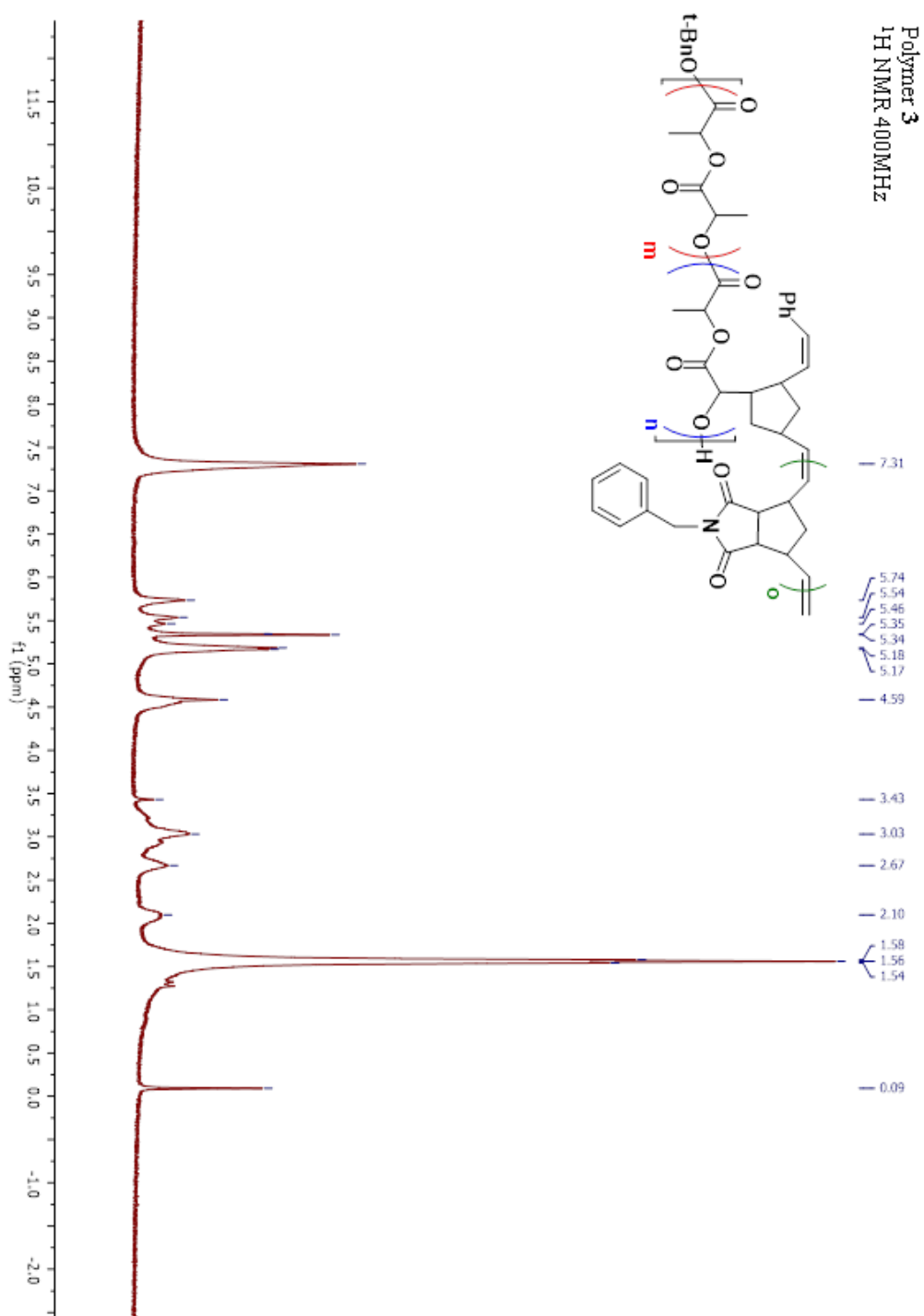**Figure 4.20.** ¹H NMR spectrum of polymer **2**.

Figure 4.21: ^{1}H NMR spectrum of polymer **3**.

F. Acknowledgments

Chapter 4, is a full reprint of the publication "Dual Responsive Polymeric Nanoparticles Prepared by Direct Functionalization of Polylactic Acid-based Polymers via Graft-from Ring Opening Metathesis Polymerization" Veccharelli, K. M.; Tong, V. K.; Young, J. L.; Yang, J. Gianneschi, N. C. *Chem. Commun.*, **2016**, 52, 567. The dissertation author was the primary investigator and author of this material.

G. References

(1)   A.-C. Albertsson and I. K. Varma, *Biomacromolecules*, 2003, **4**, 1466–86.

(2)   A. M. Reed and D. K. Gilding, *Polymer (Guildf).*, 1981, **22**, 494–498.

(3)   C. E. Holy, J. A. Fialkov, J. E. Davies and M. S. Shoichet, *J. Biomed. Mater. Res. A*, 2003, **65**, 447–53.

(4)   T.-Y. Kim, D.-W. Kim, J.-Y. Chung, S. G. Shin, S.-C. Kim, D. S. Heo, N. K. Kim and Y.-J. Bang, *Clin. Cancer Res.*, 2004, **10**, 3708–16.

(5)   K. S. Lee, H. C. Chung, S. A. Im, Y. H. Park, C. S. Kim, S.-B. Kim, S. Y. Rha, M. Y. Lee and J. Ro, *Breast Cancer Res. Treat.*, 2008, **108**, 241–50.

(6)   D. Bourissou, S. Moebs-Sanchez and B. Martín-Vaca, *Comptes Rendus Chim.*, 2007, **10**, 775–794.

(7)   Y. Yu, J. Zou and C. Cheng, *Polym. Chem.*, 2014, **5**, 5854–5872.

(8)   T. Trimaille, M. Möller and R. Gurny, *J. Polym. Sci. Part A Polym. Chem.*, 2004, **42**, 4379–4391.

(9)   J. A. Castillo, D. E. Borchmann, A. Y. Cheng, Y. Wang, C. Hu, A. J. García and M. Weck, *Macromolecules*, 2012, **45**, 62–69.

(10) R. E. Drumright, P. R. Gruber and D. E. Henton, *Adv. Mater.*, 2000, **12**, 1841–1846.

(11) M. Yin and G. L. Baker, *Macromolecules*, 1999, **32**, 7711–7718.

(12) X. Jiang, E. B. Vogel, M. R. Smith and G. L. Baker, *Macromolecules*, 2008, **41**, 1937–1944.

(13) W. W. Gerhardt, D. E. Noga, K. I. Hardcastle, A. J. García, D. M. Collard and M. Weck, *Biomacromolecules*, 2006, **7**, 1735–42.

(14) M. Leemhuis, J. H. van Steenis, M. J. van Uxem, C. F. van Nostrum and W. E. Hennink, *European J. Org. Chem.*, 2003, **2003**, 3344–3349.

(15) M. Rubinshtein, C. R. James, J. L. Young, Y. J. Ma, Y. Kobayashi, N. C. Gianneschi and J. Yang, *Org. Lett.*, 2010, **12**, 3560–3.

(16) H. K. Hall and A. K. Schneider, *J. Am. Chem. Soc.*, 1958, **80**, 6409–6412.

(17) I. A. Barker, D. J. Hall, C. F. Hansell, F. E. Du Prez, R. K. O'Reilly and A. P. Dove, *Macromol. Rapid Commun.*, 2011, **32**, 1362–1366.

(18) Y. Yu, J. Zou, L. Yu, W. Ji, Y. Li, W.-C. Law and C. Cheng, *Macromolecules*, 2011, **44**, 4793–4800.

(19) J. Zou, C. C. Hew, E. Themistou, Y. Li, C.-K. Chen, P. Alexandridis and C. Cheng, *Adv. Mater.*, 2011, **23**, 4274–4277.

(20) R. J. Williams, I. A. Barker, R. K. O'Reilly and A. P. Dove, *ACS Macro Lett.*, 2012, **1**, 1285–1290.

(21) C. Feng, Y. Li, D. Yang, J. Hu, X. Zhang and X. Huang, *Chem. Soc. Rev.*, 2011, **40**, 1282–95.

(22) M. Zhang and A. H. E. Müller, *J. Polym. Sci. Part A Polym. Chem.*, 2005, **43**, 3461–3481.

(23) H. Lee, J. Pietrasik, S. S. Sheiko and K. Matyjaszewski, *Prog. Polym. Sci.*, 2010, **35**, 24–44.

(24) S. S. Sheiko, B. S. Sumerlin and K. Matyjaszewski, *Prog. Polym. Sci.*, 2008, **33**, 759–785.

(25) Y. Xia, B. D. Olsen, J. A. Kornfield and R. H. Grubbs, *J. Am. Chem. Soc.*, 2009, **131**, 18525–32.

(26) I. Czelusniak, E. Khosravi, A. M. Kenwright and C. W. G. Ansell, *Macromolecules*, 2007, **40**, 1444–1452.

(27) F. Leroux, V. Montembault, S. Pascual, W. Guerin, S. M. Guillaume and L. Fontaine, *Polym. Chem.*, 2014, **5**, 3476.

(28) S. Jha, S. Dutta and N. B. Bowden, *Macromolecules*, 2004, **37**, 4365–4374.

(29) D. Mecerreyes, B. Atthoff, K. A. Boduch, M. Trollsås and J. L. Hedrick, *Macromolecules*, 1999, **32**, 5175–5182.

(30)   F. Tasaka, Y. Ohya and T. Ouchi, *Macromolecules*, 2001, **34**, 5494–5500.

(31)   K. Fukushima, R. C. Pratt, F. Nederberg, J. P. K. Tan, Y. Y. Yang, R. M. Waymouth and J. L. Hedrick, *Biomacromolecules*, 2008, **9**, 3051–6.

(32)   W. Dai, J. Zhu, A. Shangguan and M. Lang, *Eur. Polym. J.*, 2009, **45**, 1659–1667.

(33)   R. J. Williams, R. K. O'Reilly and A. P. Dove, *Polym. Chem.*, 2012, **3**, 2156.

(34)   M. S. Sanford, J. A. Love and R. H. Grubbs, *J. Am. Chem. Soc.*, 2001, **123**, 6543–6554.

(35)   J. A. Love, J. P. Morgan, T. M. Trnka and R. H. Grubbs, *Angew. Chem. Int. Ed. Engl.*, 2002, **41**, 4035–7.

(36)   Gilley, C. B.; Buller, M. J.; Kobayashi, Y. *Org. Lett.* **2007**, *9* (18), 3631.